FRIEDA RIVER

Frieda River Limited
Sepik Development Project
Environmental Impact Statement

Appendix 2b – Frieda River Hydroelectric Project Limnology Study, Phase 2

FRP-2-D-00-01-D-084-003

coffey
A TETRA TECH COMPANY

HydroNumerics

HydroNumerics

Frieda River Hydroelectric Project

Limnology Study

Phase 2

Final Report

3 July 2018

Prepared for SRK (Australasia) Pty Ltd

HydroNumerics Pty Ltd
ABN 87 142 999 246
www.hydronumerics.com.au

DOCUMENT SUMMARY

GENERAL INFORMATION	
Project Title	Frieda River Hydroelectric Project
Project Manager	Peter Yeates (Mb +61 400 750 980) peter.yeates@hydronumerics.com.au
Document Title	Limnology Study, Phase 2.
Document Type	Final Report
Authors	Peter Yeates
Document ID	HN_SRK_FRHEPPhase2_Final.docx

CLIENT INFORMATION	
Client	SRK Australasia Pty Ltd
Contact	Claude Prinsloo
Details	cprinsloo@srk.com.au

DOCUMENT HISTORY			
Prepared by	Peter Yeates	Hydronumerics	03/07/2018
	Patricia Okely	Hydronumerics	
Reviewed by	Chris Dallimore (v4)	Hydronumerics	08/05/2018
	Chris O'Neill (v4)	Hydronumerics	08/05/2018
	Kevin Boland (v3)	TWS	26/02/2018
	John Chapman (v3)	SRK	09/03/2018
	Coffey (v4)	Coffey	29/05/2018
Submitted to	Claude Prinsloo	SRK	01/06/2018

NOTICE

DISCLAIMER

The accuracy of information presented in this document is entirely dependent on the accuracy and completeness of supplied information. Hydronumerics Pty Ltd makes no warranty, representation or guarantee with respect to the accuracy and completeness of supplied information, shall have no liability to any person for any errors or omissions in the supplied information, and shall have no liability for loss or damage of any kind suffered or incurred by any person acting in reliance on the information in this document where the loss or damage arises from errors or omissions in the supplied information.

EXECUTIVE SUMMARY

Frieda River Limited (FRL) is undertaking a feasibility study of a Frieda River Hydroelectric Project (FRHEP) to support the proposed Frieda River Copper-Gold Project (FRCGP) in the Sandaun Province of Papua New Guinea (PNG).

A component of the FRHEP feasibility study is to investigate the limnology of the proposed FRHEP reservoir, formed by the construction of an embankment downstream of the junction of the Frieda and Nena rivers. The FRHEP embankment will impound a reservoir of more than 10000 GL at probable maximum flood level.

The reservoir will inundate three major river courses that form the primary reservoir branches: the Nena River to the west of the embankment; the Ok Binai, which flows from the southwest and converges mid-way along the Nena branch; and the Niar (Upper Frieda), River which carries converged flow from numerous dendritic sub-branches that flow up from the south towards the embankment.

The FRHEP facility is designed for hydropower generation to supply the FRCGP activities with a secondary function to store waste rock and tailings. Waste rock generated by FRCGP mining activities will be deposited into the reservoir via barges that release the material from the surface. Tailings will be deposited at the bottom of the FRHEP through a floating pipeline, a series of floating pontoons and tremie pipe system with diffuser. The tremie pipe system aims to minimise suspension of the tailings.

As part of the project scoping phase study a three-dimensional model has been applied to simulate the hydrodynamics and sediment transport that are likely to occur in the FRHEP reservoir. The model has been applied to three periods: (a) a 10-year period that includes filling for the reservoir then operations; (b) a 10-year period that includes operations and (for the last 2 years of the simulation) the closure of the HEP; and (c) an extended HEP closure simulation. Simulations (b) and (c) included the planned final distribution of mine waste rock and tailings to be stored in the reservoir. Meteorological data collected from site and flow and sediment load data generated by concurrent studies have been applied to force the model. In the absence the data that is typically required to run and calibrate limnological models, a series of sensitivity simulations were performed to test the assumptions that have been made. Simulations of the operational period with the inclusion of the stored waste rock and tailings material have been undertaken to assess the potential mobility of the stored material and subsequent contribution to the downstream releases.

Model results suggest that the FRHEP reservoir is likely to be persistently stratified with no regular periods of complete mixing, and that the addition of waste rock and tailings to the reservoir beneath the epilimnion is unlikely to alter the top-down stratification structure. Modelled inflows from the major rivers form intrusions through the reservoir at a depth of neutral buoyancy following an initial plunge near their headwaters. In addition to the inflows, the HEP intake rate and depth play an important role in shaping the stratification and promoting short-circuiting of inflow waters through the reservoir. Despite the preferential flow paths of the catchment inflows (which carry high sediment loads) a large portion of the natural catchment sediments settle to the bottom during the time is takes for the inflows to travel through the body of the reservoir. The settled material falls into the deeper waters of the reservoir that are beneath the HEP intake and deposit at the bed. Whilst resuspension of the settled catchment material will occur to some extent, this is likely to occur only periodically in the upper reaches when flow events of sufficient size create enough bed stress to mobilise the settled material. Bed stress declines in deeper areas away from the

headwaters so that mobilisation after settling at locations away from the headwaters decreases.

Sub-aqueous storage of waste rock and tailings in the reservoir carries with it the potential risk of resuspension and subsequent downstream release of stored waste rock and tailings material. Model results suggest that under base case flow conditions (with flow rates less than 10 year ARI) and during typical weather conditions some erosion of the stored waste rock and tailings is likely to occur, and most extensively if fine material is deposited near the headwaters or migrates upstream (from their designated storage locations in the project description) towards the headwaters of the major inflows. Model results show that mobilisation is more frequent and widespread if the finer fractions of waste rock and tailings deposits are not protected from bed stress by sheltering or cohesion within the particle size mix, which can increase resistance to bed stress. The actual critical bed stress at which mobilisation of waste rock and tailings will occur is not known. However, when resuspension is modelled, the resuspended plume is typically confined to waters near the bottom (above the stored material) and the portion that is entrained into the flow above (and out through the HEP intake) is significantly diluted so that the contribution to downstream TSS concentrations is small.

Modelling indicates that any proposed deposition near to the embankment (1 to 2 km upstream) is likely to have a significant impact on TSS at the embankment (and inflow into the HEP) due to the slow settling rate of the fine fraction that contributes to the barged waste rock material.

The water quality in the reservoir will likely go through a period of early adjustment to filling that is dominated by decomposition of inundated vegetation. Over time the establishment of macrophyte growth will then stabilise the water quality. Greenhouse gas (GHG) emissions from the FRHEP reservoir are estimated to be up to approximately 6000 mg CO_2-equivalent $m^{-2}d^{-1}$ in the initial stages after filling, which is likely to be followed by a slow down of decomposition of inundated vegetation and burial of that vegetation under stored waste rock and tailings leading to a decline in emissions over time.

There is uncertainty associated with all elements of the scoping phase study presented in this report given that the model cannot be calibrated and validated; however, there are some uncertainties that can potentially be addressed (those related to the work undertaken herein) and are likely to carry some level of risk to the project outcomes. These should be considered in further, more detailed studies. The first is to investigate the critical shear stress at which the waste rock and tailings mobilise and the rate of erosion that results.

The second is to consider further sensitivity tests of the model that focus on remaining uncertainties when a final project description has been issued. There are key uncertainties associated with the mobility of the waste rock and tailings that are stored in the reservoir; addressing these uncertainties will require additional information about the potential mobility of the waste rock and tailings particles (from laboratory analysis) and re-simulation of their mobility in the FRHEP using the additional information under a range of environmental conditions. Additional modelling sensitivity analysis in forward works should include broadening the study of wind related limnological processes, further testing of a finer resolution model to determine the effects of grid

resolution on modelling outcomes, and investigating extreme conditions (such as high flows and storms) to provide information about worst-case scenarios.

Thirdly, improving (decreasing) the detection limit of some water quality sampling (most critically for FRP) should be considered to better understand the likely water quality response.

Additional scenarios to assess the potential in-reservoir and downstream impact of a failure of the tailings pipes should also be considered in future modelling works. The extent of the

impact will depend on the size of failure, the location of the failure in the reservoir (most critically the distance from the embankment) and the depth of the failure.

Long-term changes (e.g. up to 100 years) in the limnological behaviour that occur in response to changes in flow and meteorology have not been considered in this report, but should be given consideration in future investigations.

In terms of recommendations that relate to the current project description, careful consideration needs to be given to the risks associated with the storage of waste rock and tailings in the upper reaches of the Nena arm (as indicated in the current project description) due to the exposure of these areas to bed stress that is likely to be sufficient to trigger resuspension of the stored material and transportation of the fine fractions towards the embankment.

Consideration should also be given to the operational rules of the FRHEP reservoir to avoid large and frequent fluctuations in water level that put strain on littoral habitats and potentially reduce the likelihood of establishing a reservoir with good water quality.

TABLE OF CONTENTS

LIST OF FIGURES

LIST OF TABLES

GLOSSARY OF TERMS

Anoxic water	Water with zero oxygen concentration.
Blue-green algae	See Cyanobacteria below.
Chlorophyll 'a'	A pigment common to all algae, the concentration of which is an indicator of total phytoplankton biomass in a lake or reservoir.
CO_2	Carbon dioxide.
Cyanobacteria	A unique group of prokaryotic phytoplankton often described as 'blue-green algae'. Various species of this group are toxic to humans and animals.
Diurnal	Occurring within the cycle of a day.
DO	Dissolved oxygen. The partial pressure of the oxygen molecules dissolved in a liquid - here water - is also referred to as oxygen tension.
DOC	Dissolved organic carbon.
Epilimnion	Top-most layer in a stratified lake or reservoir, occurring above the metalimnion and deeper hypolimnion.
Euphotic zone	Region in a water column where light can penetrate and photosynthesis can occur.
FRP	Filterable reactive phosphorus. That part of the total phosphorus in a water body that is assumed as biologically available.
Hypolimnion	Dense, bottom layer of water in a stratified lake or reservoir. It is the layer that lies below the thermocline.
Meromictic	Water body that undergoes only partial vertical mixing and the primary circulating water mass does not mix with a lower portion.
Metalimnion	Layer in which density changes more rapidly with depth than it does in the layers above (epilimnion) or below (hypolimnion).
Oligomictic	Water body with poor (oligo) vertical mixing. The mixing is irregular, or sporadic and usually of short duration.
Oligotrophic	Water body with low primary productivity, the result of low nutrient content.
Oxycline	Region of high dissolved oxygen gradients.
Polymictic	Water body with many periods of vertical mixing even to the extent that it is mixed nearly continuously throughout the year.
Seiche	Oscillation of the density interface in a stratified water body.
Thalweg	The line defining the lowest points along the length of a river bed or valley.
Thermocline	Region in a stratified water body where vertical temperature gradients are highest.
TOC	Total organic carbon.
Wind Fetch	An uninterrupted distance over which wind blows without a significant change in direction.

1 Introduction

1.1 Study Overview

Frieda River Limited (FRL) is undertaking a feasibility study of a Frieda River Hydroelectric Project (FRHEP) to support the proposed Frieda River Copper-Gold Project (FRCGP) in the Sandaun Province of Papua New Guinea (PNG).

A component of the FRHEP feasibility study is to investigate the limnology of the proposed FRHEP reservoir. In July 2017, Hydronumerics Pty Ltd was commissioned by SRK Consulting (Australasia) Pty Ltd (SRK) to undertake an initial scoping study (Phase 1) of the limnology. The scoping study was focussed on identifying potential key risks and fatal flaws (Hydronumerics, 2017) based on the findings of an earlier FRHEP limnology study completed in 2011 (Hydronumerics, 2011), with consideration given to a series of project updates. The project updates include an increased FRHEP embankment height and subaqueous storage of tailings and waste rock from the FRCGP within the FRHEP reservoir.

A second (Phase 2) more detailed limnology study was commissioned in October 2017. The findings of this study are documented in this report.

1.2 Site Description

1.2.1 Location and Topography

The FRHEP reservoir is to be formed by the construction of an embankment on the upper Frieda River in the Sandaun Province of PNG (Figure 1.1). The site is located in the Frieda River catchment in the mountainous Bismarck Range. Elevations in the range extend from 60 m ASL (above sea level) at the embankment site to 2800 m ASL at Mount Stolle. The Frieda River catchment covers a total area of 1036 km^2 (Figure 1.2)

At Iniok, 40 km downstream of the proposed embankment, the Frieda River feeds into the Sepik River, which runs from the central mountains into a meandering lower reach that consists of a network of swamps and lagoons prior to reaching the Bismarck Sea.

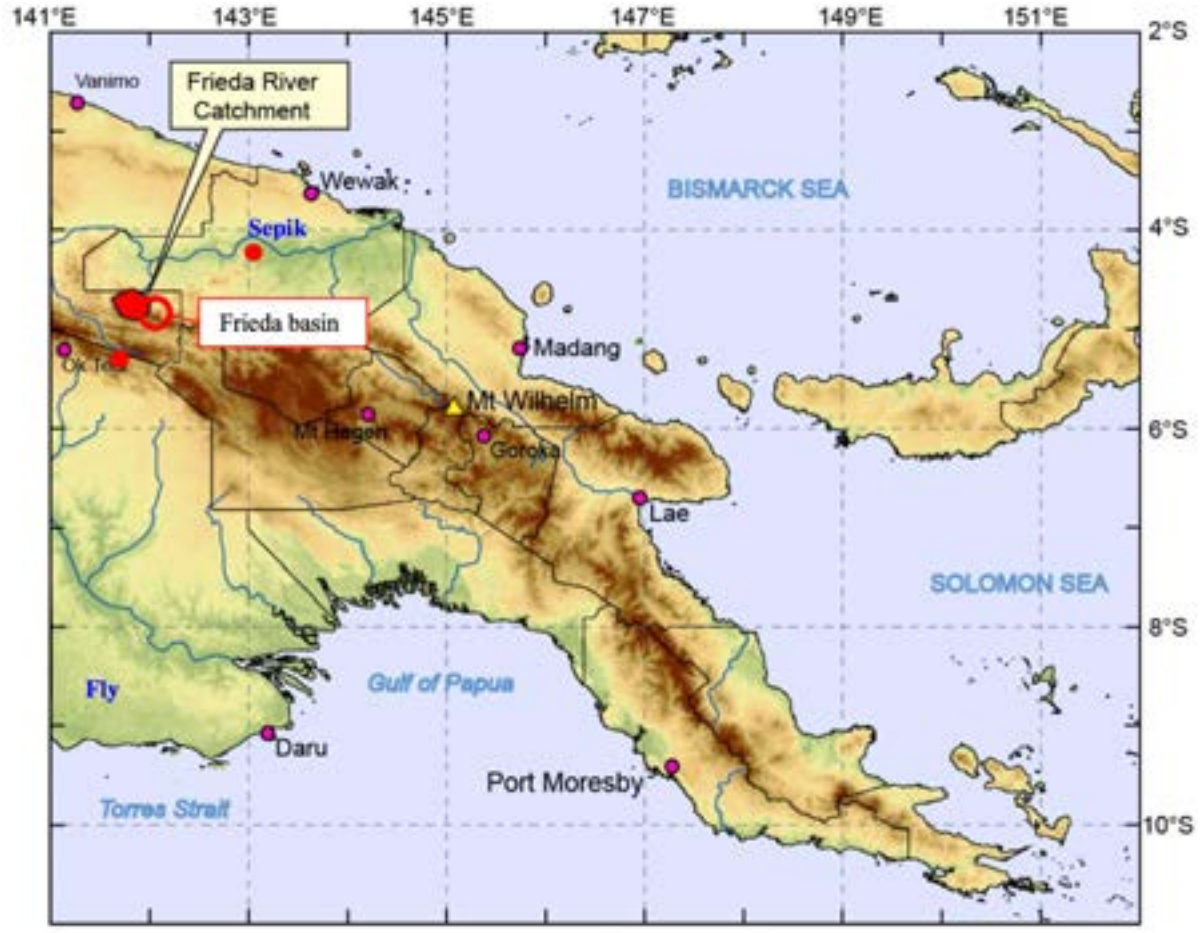

Figure 1.1 Location of the Frieda River Catchment (SKM, 2011).

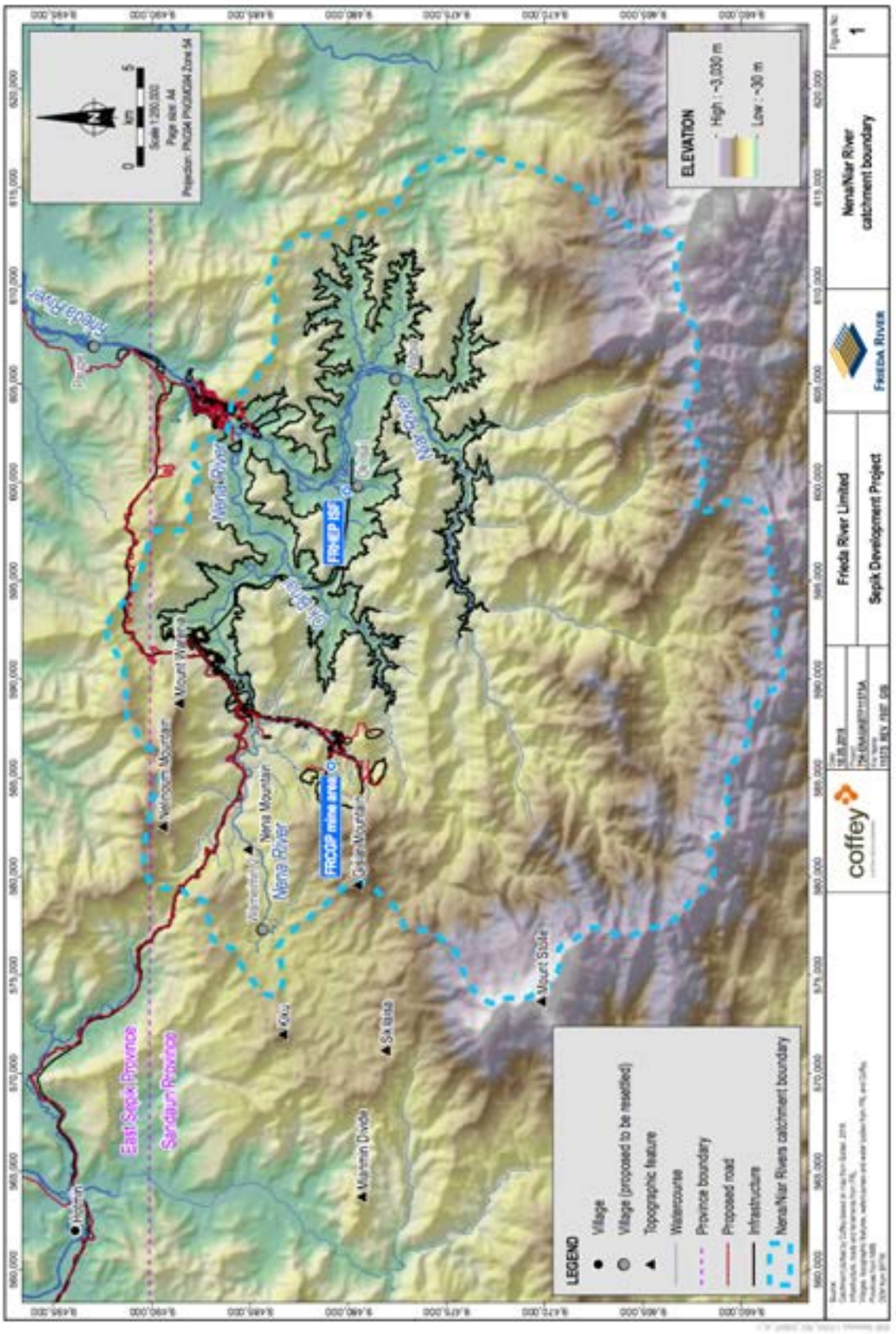

Figure 1.2 Frieda River catchment topography and major waterways (Coffey, pers. comm. 2018).

1.2.2 Meteorology

Climate in PNG is tropical and consists of a northwesterly monsoon from December to March and a southeasterly monsoon from May to October. Annual average rainfall ranges from 2500 to 3500 mm. Mean maximum temperatures range from 32°C at the coast to 15°C to 25°C in the mountainous regions. Seasonal variation in maximum temperatures is typically low.

The Bismarck Range influences the climate experienced at the Frieda River project site. An analysis of available meteorological data from site (SRK, 2016) reports annual average rainfall ranging from 7800 to 8800 mm, with the highest rainfall occurring in March. Average monthly relative humidity is consistently high (81 to 84%) during all months of the year. Average air temperatures are between 26.7 and 27.1 ^{o}C and diurnal variation of air temperature exceeds the annual variation, with night time temperatures of 19 to 21 °C and daytime temperatures of 24 to 30 °C (Hydronumerics, 2011).

Monthly average solar radiation is between 171 and 195 W m^{-2} and pan evaporation rates are less than 170 mm per month (~ 2000 mm per year), which is significantly less than precipitation rates. Daily average wind speeds are less than 1.5 m s^{-1}.

1.3 Project Description

1.3.1 Embankment

The FRHEP embankment will be situated approximately 1 km downstream of the junction of the Nena and Niar (Upper Frieda) rivers (Figure 1.3) at the Frieda River catchment boundary in the northeast of the Frieda River catchment (see Figure 1.2). This study is based on the schematic of the embankment illustrated in Figure 1.4 below.

The embankment features are as follows (Pers. Comm. Claude Prinsloo, 9 Feb 2018):

- Deep diversion tunnel at 56.3 m RL;
- Low-level HEP intake at 143.3 m RL;
- Operational-level HEP intake (final level) at 185.6 m RL; and
- Spillway at 226.1 m RL.

Figure 1.3 Aerial photograph with labelling of embankment site features (adapted from Sinohydro, 2017)

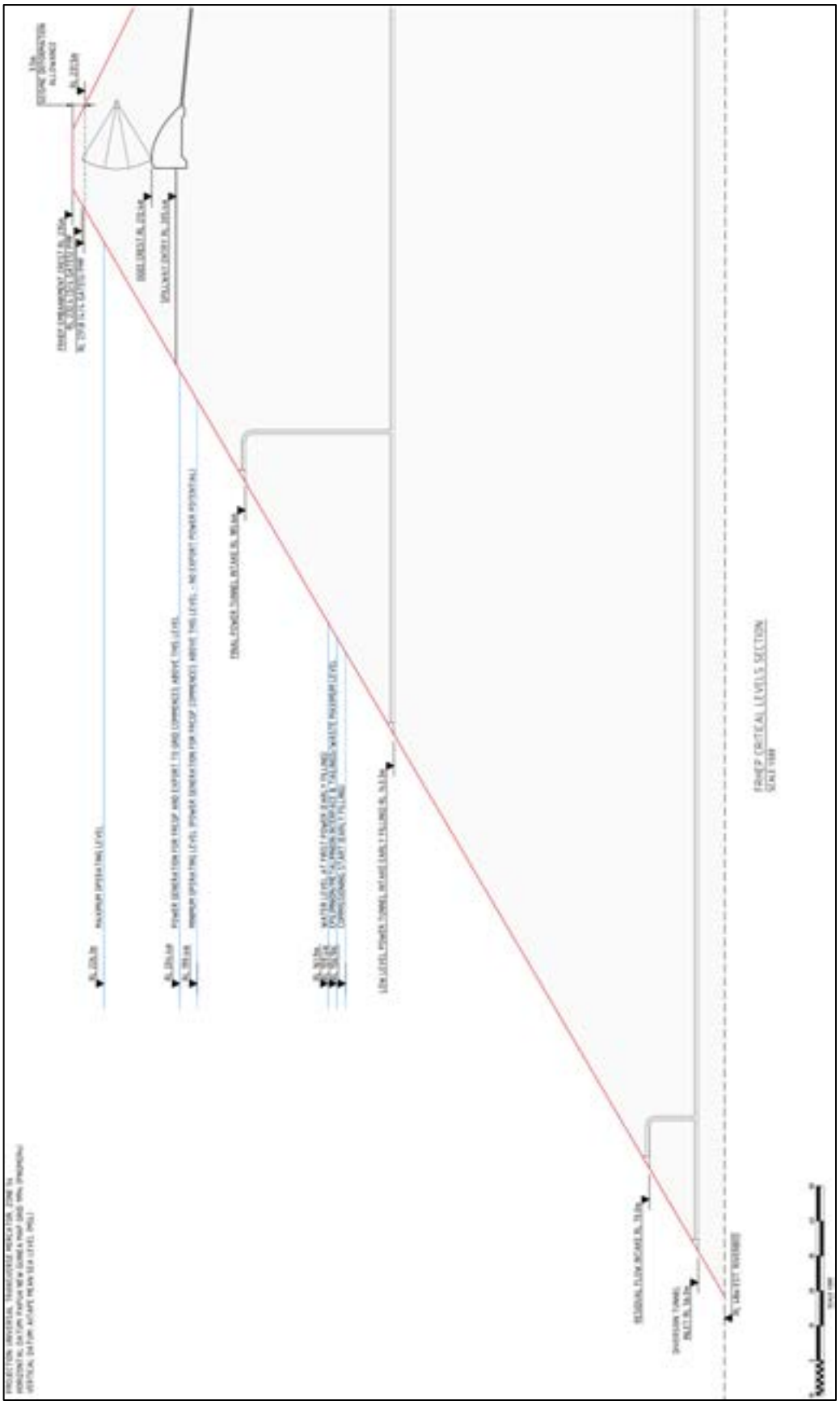

Figure 1.4 Embankment design schematic (SRK, Pers. Comm. Claude Prinsloo, 9 Feb 2018)

1.3.2 FRHEP Reservoir

The FRHEP embankment will impound a reservoir of approximately 10000 GL with a footprint as illustrated in Figure 1.5. The reservoir will inundate three major river courses that form the primary reservoir branches: the Nena to the west of the embankment; the Ok Binai, which flows from the southwest and converges mid-way along the Nena branch; and the Niar (Upper Frieda) River, which carries converged flow from numerous dendritic sub-branches that flow up from the south towards the embankment.

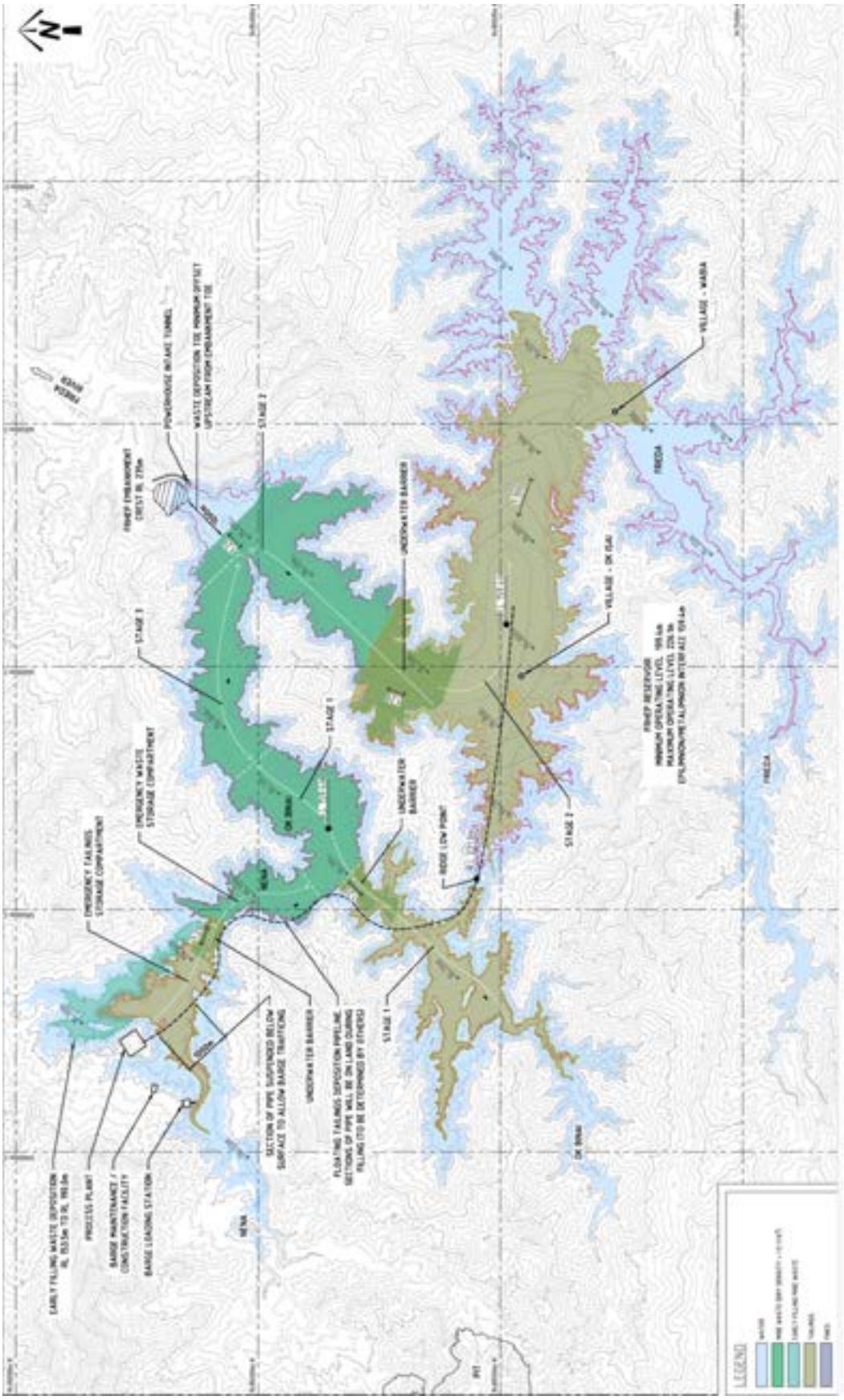

Figure 1.5 Footprint of FRHEP reservoir illustrating proposed Option 2 waste rock (coloured in green) and tailings (coloured in brown) storage areas (SRK, 2018).

1.3.3 Waste Rock and Tailings Storage

The FRHEP facility is designed for hydropower generation to supply the FRCGP activities. A secondary function will be to store waste rock and tailings, as illustrated in Figure 1.5 (Option 2 from SRK Project Memo: PNA009_MEMO_Tailings and Mine Waste rock Management - FRHEP_Rev2.pdf). Waste rock at tailings will be deposited up to 159.4 m RL, which is 26.2 m below height of final level HEP intake at 185.6 m RL.

Waste rock generated by FRCGP mining activities will be deposited from the reservoir (water) surface by barge.

Tailings will be deposited at the bottom of the FRHEP through a floating pipeline, a series of floating pontoons and tremie pipe system with diffuser (Figure 1.6). The tremie pipe system aims to minimize suspension of the tailings. The disposal of tailings at the headwaters of the FRHEP will be avoided to minimise tailings suspension by inflows.

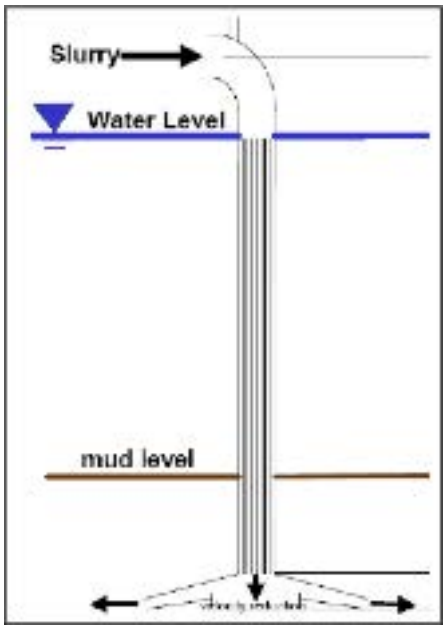

Figure 1.6 Tremie diffuser (SRK, 2017b)

1.3.4 Closure

The FRHEP embankment will remain a permanent landform. The preliminary closure plan is to seal all FRHEP inlets, channels and tunnels and lower the spillway. The embankment will remain a discharge facility.

1.4 Phase 2 Limnology Study

1.4.1 Scope of Work

Hydronumerics was engaged to undertake the services summarized in Table 1.1 as part of a Phase 2 Limnology Study.

Table 1.1 Services undertaken by Hydronumerics as part of the Phase 2 FRHEP Limnology Study.

Task	Description
1. Hydrodynamic Modelling	
a. Model configuration	Identify model requirements to provide information to in-reservoir and downstream water quality assessments.
b. Collate data	Collate data in preparation for hydrodynamic model of the proposed hydroelectric reservoir.
c. Build hydrodynamic model	Build updated hydrodynamic model of the proposed hydro hydroelectric reservoir.
d. Performance testing	Performance testing of be model against expected behaviour (from Phase 1) and identify key uncertainties and sensitivities.
e. Uncertainty analysis	Uncertainty and sensitivity analysis to assess confidence in model predictions.
f. Output analysis	Output analysis to match requirements identified in task (a).
g. Report on hydrodynamics	Reporting flow dynamic, mixing, stratification and turnover and recommendations for addressing gaps and uncertainties in further work.
2. Sediment Modelling	
a. Model configuration	Configure sediment classes and their physical properties.
b. Collate data	Collate data from the field and sediment transport models to provide input into the FRHEP reservoir model.
c. Build model	Update hydrodynamic model to include sediment modelling components and outputs that include deposition rates, resuspension and downstream release.
d. Performance testing	Test and adjust the model set-up and inputs and check against expected conditions.
e. Uncertainty analysis	Uncertainty and sensitivity analysis to assess confidence in model predictions. This is done by modelling a matrix of model configurations that incorporate the ranges of key variables that are not known to identify whether the uncertainties have a substantial impact on the modelling result.
f. Output analysis	Sediment modelling output analysis to meet EIS requirements – e.g. graphical, time series, statistical
g. Report on HEP Water Quality	Reporting on FRHEP Sediment Modelling
3. Water Quality Assessment	
a. Literature Review	Review of literature of water quality in tropical reservoirs that relates to processes that are likely to occur in FRHEP.
b. Collate Water Quality data	Determine inputs into the reservoir from existing data and models.
c. Estimate Water Quality variables	Describe the different stages of development of water quality in terms of turbidity, oxygen, nutrients, primary production and organic matter and how they relate to the physical limnology. Estimate likely concentrations of these water quality these variables in release waters and compare to guidelines.
d. Inform SRK Chemistry assessment	Provide information from the hydrodynamic modelling and Water Quality assessment that assists with SRK's assessment of metals, sulphate, pH and alkalinity
e. Report on HEP Water	Reporting on Water Quality Assessment

	Quality	
4.	**Greenhouse Gas Emissions**	
a.	Methods	Identify appropriate method for emissions assessment using combination of model predictions (where possible) and reported values
b.	Application	Apply method to produce assessment of likely emissions rates
c.	Report of GG emissions	
5.	**Downstream Water Quality Assessment**	
a.	Support SRK's assessment	Use hydrodynamic and sediment modelling and water quality estimates to support SRK's assessment of the downstream water quality

1.4.2 Limitations

This assessment is based on the application of a fit-for-purpose limnological model that has been applied to numerous aquatic systems and published in peer-reviewed literature (see Section 3.1). However, there are some important limitations in the application to FRHEP that need to be noted. Firstly, the FRHEP reservoir is hypothetical and therefore data does not exist to calibrate and validate the model, which is a normal procedure when developing limnological models of existing water bodies. As a result, the accuracy of the model cannot be assessed.

Secondly the modelling undertaken in this study relies on inputs from a number of sources: measured (i.e. limited riverine water quality), derived from other models that have been applied in concurrent studies (as is the case with the hydrological and sediment inputs into the FRHEP), or, if no information from the project site exists, inputs have been derived or assumed from literature. There is uncertainty associated with each form of input. In addition, where the spatial and temporal coverage of information from site is limited, assumptions are required regarding the spatial representativeness of monitoring sites (as is the case for meteorological data) and the filling of gaps when data records are incomplete.

Thirdly, there are no available reference studies of reservoirs with comparable dimensions, hydrology, climatic setting or operations to FRHEP. This is compounded by the fact that there is a paucity of information on tropical lakes and reservoirs in general, particularly in PNG.

As a consequence, the results in this study must be considered in the light of the uncertainties. A sensitivity analysis has been undertaken (see Appendix) to identify the likely impact of key uncertainties on model outputs.

1.4.3 Structure of this Report

This report describes the finding of the Phase 2 limnology study. Chapter 2 provides background information on the tropical limnology, lakes and reservoirs in PNG and previous studies that have been undertaken for the FRHEP reservoir.

Chapter 3 describes the application of a hydrodynamic and sediment transport model to assess the likely limnology of the FRHEP reservoir during filling, operations and closure and the impacts of waste rock and tailings additions to the reservoir.

Chapter 4 considers the behaviour of water quality variables in the FRHEP reservoir (dissolved oxygen, nutrients and primary production) in the early stages of filling and stabilisation and in the long term. Chapter 5 discusses the potential green house gas emissions from the FRHEP reservoir.

A summary of the findings and recommendations is provided in Chapter 6.

2 Background

2.1 Basic Limnology

The limnology of tropical lakes and reservoirs is distinctive due to the small seasonal climatic variation experienced at low latitudes (Lewis 1995). In tropical lakes and reservoirs that are sufficiently deep, a vertical temperature gradient develops, in response to surface heating, to produce a density-stable layered (i.e. stratified) water column with warm water near the surface (the epilimnion) overlaying cooler water near the bottom (the hypolimnion). A region marked by temperature gradients, the metalimnion, separates the epilimnion and hypolimnion and the buoyancy effects in the metalimnion inhibit mixing, therefore limiting the vertical exchange of dissolved and suspended constituents between the epilimnion and hypolimnion (and in some cases reducing the rate of exchange down towards the rate of molecular diffusion). The extent of mixing that takes place will depend on the strength of the stratification (i.e. it's potential energy) relative to the energy input and mixing efficiency of destabilising forces such as surface cooling, surface wind stress and inflows, which initiate turbulent mixing.

Vertical gradients in the concentrations of dissolved and suspended constituents (such as salts or suspended solids) can either strengthen (when there are higher concentrations in the hypolimnion) or weaken (when there are higher concentrations in the epilimnion) the density gradients produced by temperature differences.

The temperature difference from top-to-bottom in tropical reservoirs may be as little as 3 to 5 ^{o}C, which is small compared to temperate lakes and reservoirs, where during summer the top-to-bottom temperature difference may be as much as 15 to 20 ^{o}C. However, the relationship between water temperature and density is non-linear and water with higher temperatures, as experienced in the tropics, has a greater density difference per degree of temperature change compared to water at lower temperatures. This means that a smaller temperature difference between the epilimnion and hypolimnion in warm tropical lakes and reservoirs will impose a significant density difference that is able to maintain stable stratification.

In the absence of the changes that are induced by a cool winter that is typically experienced in temperate lakes and reservoirs, stratification in tropical lakes and reservoirs may persist indefinitely, as is the case in a meromictic lake, or mixing may be irregular (either full or partial) and infrequent, as is the case in an oligomictic lake (Vyverman 1994). In oligomictic lakes and reservoirs, a mixing cycle is often induced by unusual changes in meteorology, such as storms combined with cold air temperatures, rather than regular seasonal changes (Beadle 1974).

Partial mixing may occur in meromictic lakes and reservoirs, and more frequently (than full mixing) in oligomictic lakes, which creates an important pathway for exchange between the hypolimnion and epilimnion that occurs in the absence of complete top-to-bottom mixing (often referred to as 'turnover'). Moreover, the description of "top-to-bottom mixing" as a "turnover" event is inaccurate, because the mixing typically occurs as a top-to-bottom erosive process that entrains and dilutes hypolimnetic water into the epilimnion as it deepens, and not as a turning over of the waters. In the event of large internal waves, titling of the thermal structure and subsequent upwelling may lift hypolimnion waters to the surface and encourage some mixing, but may not necessarily lead to complete mixing that dismantles the stratification. In contrast to meromictic and oligomictic lakes, temperate lakes typically exhibit monomictic behaviour by mixing vertically every winter from top to bottom followed by a return of thermal stratification in spring. The stratification strengthens through spring, reaching a peak in summer, and then erodes during autumn before complete mixing in winter.

In tropical climates, shallow lakes often have insufficient depth to persistently stratify and therefore mix multiple times during the year, or as frequently as each night during night-time cooling (Barbosa and Padisak 2002). Tropical lakes and reservoirs at high altitudes (above 3,000 m ASL) may mix regularly regardless of their depth because they are exposed to cold

night time air temperatures that cool the surface sufficiently to induce frequent convective mixing (Umana 2001).

Mixing of tropical lakes and reservoirs typically occurs in response to one, or a combination of up to three processes: i) the action of surface wind stress that mixes the water from the surface down; ii) convective mixing due to cooling of the epilimnion; or iii) erosion of gradients by shear mixing from inflows. For example, the African Great Lakes mix during the slightly cooler months in the middle of the year that coincide with exposure to persistent trade winds (Talling 1966). These findings are not directly transferable to FRHEP, because reservoirs formed by the impoundment of rivers tend to be significantly more wind-sheltered by the surrounding terrain and have large aspect ratios that require persistent winds to blow along their main axis to maximise wind-induced mixing. Talling and Lemoalle (1998) clearly illustrated a strong positive correlation between wind fetch and increased mixing depth in tropical lakes.

Inflows tend to be more important to mixing in reservoirs than lakes, and small reservoirs with large inflows experience more frequent mixing (Lewis 1995). Inflows are typically cooler than the epilimnion and form underflows or intrusions that entrain the hypolimnetic and/or metalimnetic water on passage through the reservoir and therefore can weaken temperature gradients. The action of inflows in some tropical reservoirs may have the reverse effect by maintaining stratification (Mtada 1986). This is due to the presence of a selective withdrawal layer than can lead to be formation of step-gradients at the upper and lower boundaries of the withdrawal layer.

Deep tropical lakes at low latitudes, with sheltered wind conditions therefore have little tendency to mix regularly, either partially or completely, and can be broadly classified as oligomictic. Extremely deep tropical lakes, such as Lake Tanganyika in central Africa (with a mean depth of 563 m) experience stratification that is effectively permanent (Talling and Lemoalle 1998) and are better classified as meromictic.

2.2 Lakes and Reservoirs in Papua New Guinea

The climate of PNG is characteristically tropical. Air temperatures are high (20 to 32 °C) throughout the year with little seasonal variation (Osborne 1989). Rainfall is high (more than 2500 mm yr^{-1}) and can be extremely high in some regions (up to 10000 mm yr^{-1}). A combination of mountainous terrain and high intensity rainfall in many regions leads to high flow rates in rivers. High rainfall and temperatures maintains humid, cloudy conditions with moderate evaporation.

Few studies on the limnology of lakes and reservoirs in PNG are available; none of which consider a water body similar to FRHEP reservoir in all key regards. We examine here selected examples from the literature that provide an indication of the likely limnology of the FRHEP reservoir.

Most lakes in PNG are small, shallow, and tend to be polymictic and oligotrophic (Chambers 1987). Lake Murray in the Western Province (with a surface area of 647 km^2) and Chambri Lake in the East Sepik Province (200 km^2) of the PNG lowlands are the largest lakes, however, like many smaller lowlands lakes, they are shallow. Lewis (1995) hypothesised that all lowland lakes in PNG shallower than 40 m would be polymictic, following a diurnal pattern that sees complete mixing occur during the cooler night-time temperatures, with day-time water column temperature differences from top-to-bottom in the range of 1 to 3 °C.

The deeper Lake Wisdom in the Madang Province (86 km^2) and Lake Dakataua in the West New Britain Province (49 km^2) have comparable altitude to the proposed hydro-power reservoir; however, these lakes are volcanic crater lakes located on islands off the PNG mainland and are exposed to higher oceanic wind conditions and have comparably small inflows. Despite this, temperatures observations indicate that these lakes, particularly Lake Dakataua, stratify for long periods (Ball and Glucksman 1980); however, seasonal temperature

records are not available to confirm the periodicity of stratification and mixing cycles in these lakes.

Lake Kutubu (49 km^2) in the Southern Highlands Province of PNG is the most similar, albeit natural, lake to the proposed FRHEP reservoir and was formed by natural impoundment of a river valley. Lake Kutubu is located at an altitude of 808 m ASL, has a maximum depth of 70 m and a mean depth of 36 m. Limited observations of surface temperature indicate that Lake Kutubu is approximately 26 to 30 °C near the surface, stratified below 16 m (Chambers 1987) and oligomictic, with irregular mixing events that occur during abnormally cold or stormy weather (Bayly et al. 1970). These mixing events are estimated to occur only once or twice a decade, after which the surface waters experience a rapid decrease in oxygen (leading to fish asphyxiation) and increased nutrient concentrations that support algal blooms (D'Cruz 2008).

During stratification the epilimnion of Lake Kutubu is 3 to 4 °C warmer than the hypolimnion, has high clarity (Secchi depth measurements of 6.5 to 8 m), is well oxygenated, low in nutrients and metals, and slightly alkaline. In contrast, the hypolimnion is typically anoxic and has elevated concentrations of sulphide, nutrients, and metals, and lower pH. Inflows into the lake are cooler than the epilimnion and therefore underflow into the hypolimnion, transporting dissolved and particulate organic matter deep into the lake. The stratification, sub-surface inflow intrusions and shallow outflow ensure that Lake Kutubu acts as a sink for fluvial loads by delivering sediments loads deep into the water column with limited removal near the surface.

Two examples of artificially constructed reservoirs in PNG are Yonki Reservoir and Lake Sirinumu. Yonki Reservoir in Eastern Highlands Province was commissioned in 1991 and is 60 m deep, 10 km^2 and situated at 1,200 m ASL. However, there is no detailed information available on the limnology of Yonki Reservoir. Lake Sirinumu, located at a lower altitude of approximately 540 m ASL is a 34 m deep hydropower reservoir on the Laloki River in the Central Province that was commissioned in 1971 as the first major reservoir in PNG. In contrast to Yonki Reservoir, Sirinumu Reservoir is significantly shallower and given that its depth is less than 40 m, it is likely to be polymictic based on the classification scheme of Lewis (1995).

The limnological information available suggests that a majority of PNG's lakes are unproductive and oligotrophic, due to low nutrient status and high flushing rates (Chambers 1987); however, the majority are also small (surface area of less than 1 km^2), shallow (less than 10 m deep) and most likely polymictic. Given the size, altitude and depth of the proposed FRHEP reservoir, it is likely that the basic limnology of the reservoir will be similar to that of the deeper Lake Kutubu.

There are however some unique features of the FRHEP reservoir that make it difficult to develop a conceptual understanding (without modelling) of the likely limnological behaviour of FRHEP reservoir on the basis of available studies of existing lakes and reservoirs in PNG (most notably Lake Kutubu) and tropical regions more generally. Firstly, the proposed reservoir is deep and has a complex bathymetry that includes the junction of two major rivers and contributions from numerous smaller tributaries, giving it a highly dendritic shape (i.e. tree branch like footprint). Secondly, the average annual rainfall in the Frieda River catchment is 7,700 mm, as opposed to 4,500 mm in the Lake Kutubu catchment, and therefore a more energetic inflow regime is expected, particularly when considered in the context of the complex morphometry. Finally, the operation of the hydropower plant will influence the hydrodynamics in a way that is considerably different from the natural overflow observed in Lake Kutubu, at least during the operational period of the FREHP.

2.3 Previous Studies

2.3.1 Overview

A previous study of the limnology of an earlier FRHEP description was undertaken in 2011 (Hydronumerics, 2011). As part of a first phase of this study the earlier study of 2011 was reviewed and the impacts of the updated project description were considered – this included a higher embankment and subaqueous storage of waste rock and tailing in the reservoir (see Hydronumerics, 2017). The Phase 1 report identified key risks, knowledge gaps and fatal flaws that have been summarised in the sub-sections that follow.

2.3.2 Key Risks

The key risks identified in Phase 1, in the absence of waste rock and tailings storage are:

- High organic matter, biological oxygen demand, low oxygen concentrations (and potential fish kills) and methane release associated with the decay of flooded vegetation during, and for some time after, filling;
- Potential for generation of H_2S in the anoxic hypolimnetic region of the reservoir which, if significant, could be corrosive to FRHEP turbines (note that H_2S will react with divalent metals to form insoluble metal sulphides which will strip dissolved metals from the water column and consume available H_2S);
- Nutrient enrichment from the decay of flooded vegetation and soils and external inputs that leads to high algal productivity with the potential for growth of nuisance algae such as Cyanobacteria (commonly called ‘blue green algae’);
- Development of a strong and persistent chemocline with hypolimnetic oxygen depletion leading to poor surface (and release) water quality (including temperature change) during partial or complete mixing; and
- Bioaccumulation of metals in the food chain.

The subaqueous storage of waste rock and tailings introduces additional considerations that have the potential to alter the findings of previous studies and may increase the risk to in-situ and release discharge water quality. These additional risks include:

- Release of tailings (or fine waste rock) into the water column during the deposition process;
- Scouring of fine tailings from bottom storage during inflows and transport of the suspended material towards the embankment with the potential for downstream release; and
- Release of metals from waste rock and tailings during hypolimnetic anoxia and the subsequent mixing of these metals into the surface and discharge waters.

The current FRHEP design aims to minimise the risks associated with the release of tailings solids as suspended solids during deposition by using a tremie diffuser beneath the surface of the deposits. The temperature of the slurry delivered by the diffuser should be controlled to prevent buoyant thermal currents that may destabilise the mud.

The release of dissolved metals from waste rock and tailings under persistent or intermittent anoxia should be assessed and impacts evaluated; if required, mitigation measures should be identified.

2.3.3 Knowledge Gaps

In the previous limnology study, in the absence of calibration and validation steps usually employed to verify model performance, numerous assumptions were required. While the modelling outcomes were consistent with available scientific literature, no single example in the literature could be used as an analogue for the FRHEP reservoir.

The key areas of uncertainty identified in the previous study include:

- Spatially limited and sporadic meteorological, hydrological and water quality data from the project site. Note that since 2011 there has been ongoing additional data collection on site that has been used in this updated study;
- Uncertainty associated with persistence of stratification and the potential for and/or frequency of partial or complete mixing – this relates most closely to limited records of meteorological data;
- Limited understanding of the availability of nutrients and metals, and release rates of nutrients and metals from sources in the reservoir footprint under changing oxygen concentrations; and
- No prior knowledge of the characteristics of the phytoplankton community, or higher organisms, that will colonise the reservoir and the role they will play in cycling of nutrient and metals.

Additional knowledge gaps that were identified and arise out of subaqueous storage of waste rock and tailings in the reservoir include:

- Mobility of fine particulate tailings and waste rock and the transport of these through the reservoir;
- Impact of bathymetric changes on the flushing of the hypolimnion and frequency of partial or complete mixing; and
- Potential for metal release from waste rock and tailings under anoxic conditions.

2.3.4 Fatal Flaws

The Phase 1 Limnology study extrapolates the findings from the previous limnology study in 2011 to conclude there did not appear to be any ‘fatal flaws’ with respect to the limnology of the updated FRHEP reservoir. However, there are key potential risks, which have been identified above, and a series of knowledge gaps that should be addressed as the project investigations progress.

It is our opinion that the most significant risks (as identified in Phase 1) are associated with the uncertainty of the behaviour of the waste rock and tailings material when exposed to the physical and chemical conditions that are likely to arise in the FRHEP reservoir.

3 Hydrodynamics and Sediments Model

3.1 Model Description

The three-dimensional Aquatic Ecosystem Model (AEM3D, see http://www.hydronumerics.com.au/software/aquatic-ecosystem-model-3d) was applied to simulate the hydrodynamics and sediment transport in the FRHEP reservoir. The transport equations in AEM3D are unsteady Reynolds-averaged Navier-Stokes equations and scalar transport equations with the Boussinesq approximation with no non-hydrostatic pressure terms. The free surface evolution is governed by an evolution equation developed by a vertical integration of the continuity equation applied to the Reynolds-averaged kinematic boundary condition.

The equations are solved using the TRIM numerical scheme (Casulli and Cheng 1992), with modifications to improve accuracy, scalar conservation, numerical diffusion, and implementation of a mixed-layer turbulence closure scheme. Solutions are made on an Arakawa C-grid (orthogonal with option of varying width) in which flow velocity is defined on the cell faces and the free-surface height and scalar concentrations are solved at the cell centre. The free-surface height in each column of grid cells moves vertically through the grid to improve computational efficiency and allows sharper vertical gradients to be maintained with coarse grid resolutions.

AEM3D is a deterministic model based on generic algorithms that describe observed physical processes with mathematic form and coefficients (generally for efficiency of processes such as mixing rates) that are known (within an acceptable range) from laboratory work presented in the literature. The model does not rely on empirical derivations and does not require extensive calibration of parameters to tune the hydrodynamics.

AEM3D computes solutions to the following processes (in the order shown) at time steps of the order of minutes:

- Surface heating/cooling in the surface layer;
- Mixing of scalar concentrations (i.e. dissolved and suspended constituents) and momentum using a mixed-layer turbulent kinetic energy model;
- Introduce wind energy as a momentum source in to the surface mixed-layer;
- Solve the free-surface (water level) evolution and velocity field;
- Apply horizontal diffusion of momentum;
- Advection of scalars in the velocity field; and
- Horizontal diffusion of scalars.

Heat exchange through the surface of the water is governed by the bulk transfer models documented Amorocho and Devries (1980), Imberger and Patterson (1981) and Jacquet (1983). The energy transfer across the free surface is separated into non-penetrative components of long-wave radiation, sensible heat transfer, and evaporative heat loss, complemented by penetrative shortwave radiation. Non-penetrative effects are introduced as sources of temperature in the surface-mixed layer, whereas penetrative effects are introduced as source terms in one or more grid layers on the basis of an exponential decay and a light extinction coefficient in accordance with Beer's Law. Salt is conserved on the basis of advective, diffusive and evaporative processes.

Sediment dynamics in AEM3D are modelled concurrently with the hydrodynamics. Sediments are treated as a concentration of inert particles with user-prescribed diameter and density. The choice of the number of different particle sizes and the properties of the particle is not limited

and depends on the type of aquatic ecosystem and the availability of data. The model set-up will typically include a combination of clay, silt, fine sand and coarse sand, which are potentially mobile in terrestrial and coastal surface water bodies that are not fast flowing.

The particles are introduced within terrestrial flow or resuspended from an initialised bed load and undergo settling based on a Stokes settling derivation. Resuspension rates are determined for each particle size based on the particle density, bottom shear stress (above a critical shear stress) and a user-defined erosion rate. Bottom shear is determined from currents resolved by the hydrodynamic solver AEM3D in response to winds, tides, river inputs and internal waves. The resuspension and deposition of the sediments changes the bottom morphology.

AEM3D is a recent update (released in 2016) of ELCOM-CAEDYM that was previously developed by the Centre for Water Research, University of Western Australia, and has been extensively published in peer-reviewed scientific literature (Trolle et al. 2012).

3.2 Model Set-up

3.2.1 Simulation Periods

The time-stamps used in this report were assigned based on the time periods of SRK rainfall and runoff realisations (SRK, 2017c), which start at year 2000. In terms of project timeline the filling of the reservoir begins at the start of the realisation time series on 1 January 2000.

The time series of TSS inputs into the model takes into account estimates of catchment runoff and contributions from project activities upstream of the reservoir that were provided by Golder Associates (2018). See Section 3.2.4 for further details.

The simulations described below do not include the potential impacts of barge deposition of waste rock, which was examined separately as described in Section 3.3.6.

The model was configured to simulate three separate periods:

Filling - a ten-year period from 2000 to 2009 that starts with filling of the reservoir. In this simulation there are no waste rock and tailings stored in the reservoir. This has been undertaken to assess the behaviour of the reservoir and the downstream release of sediments during the filling and construction phase and continuing through to an operational phase.

Operations - a ten-year period from 2028 to 2037 when the reservoir starts at operational level (225 m RL) and includes the final storage plan for waste rock and tailings. In the final 2 years of this simulation the operation of the reservoir shifts to HEP closure, during which there is only spillway release. This simulation has been designed to assess the impact of the waste rock and tailings storage in the reservoir and the change in behaviour when the operation of the HEP ceases.

HEP Closure – This simulation is an extension of the operations simulation (from 2038 to 2043) to assess the change in limnology after the HEP operations cease.

The bathymetry, meteorology and hydrology used to configure these simulations are described below.

3.2.2 Bathymetry

LIDAR data (provided by SRK) with a 10 x 10 m horizontal resolution was used to generate two sets of orthogonal model grids with a 100 x 100 m and a 200 x 200m horizontal resolution. The vertical resolution for both was set to 2 m. The cell structure of the 200 x 200 m resolution bathymetry is illustrated in Figure 3.1.

The time step of the model was set to 120 seconds and the real-time to run-time ratio was approximately 1000:1 for a 200 x 200 m grid, so that each decadal simulation takes approximately 4 days to complete. The real-time to run-time ratio reduced to approximately 150:1 for the 100 x 100 m grid, making the simulation time for the finer grid prohibitive in the timeframe of the project.

The surface area and storage curves are illustrated in the Appendix.

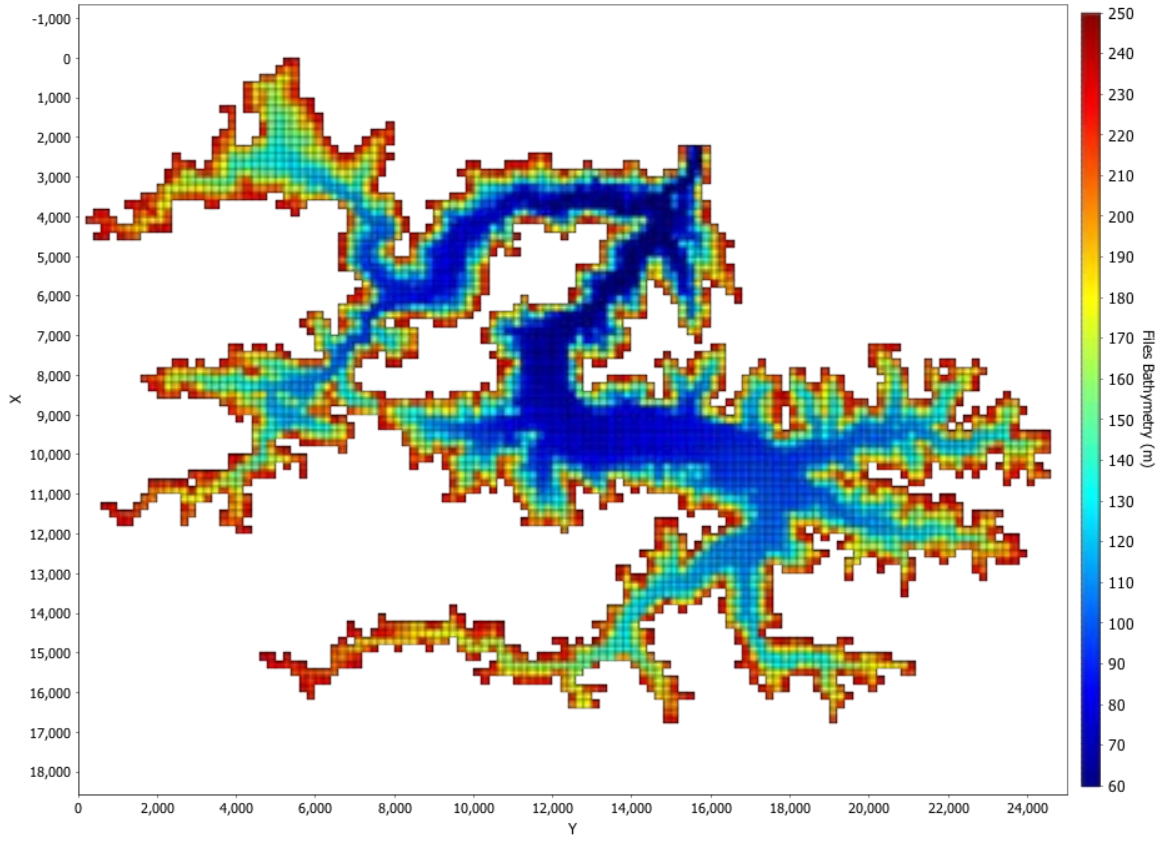

Figure 3.1 Model grid bathymetry with 200 x 200 m horizontal resolution. Horizontal axes and vertical scale are in metres.

3.2.3 Meteorology

Meteorological data recorded at 15-minute intervals at Nena, Moraupi and Iniok weather stations (Table 1.1, Figure 3.2) were used for the FRHEP reservoir model. Nena AWS temperature (AT), relative humidity (RH), solar radiation (SR), and wind speed (WS) and direction (WD) data from January 2009 to December 2014 were used to develop a time series for the model. Data from Moraupi AWS was used to fill gaps in the Nena AWS record, allowing for a continuous time series (as required by the model).

Daily average cloud cover was approximated by comparing solar radiation records at Nena AWS to theoretical estimates of clear-sky incoming solar radiation at the edge of the earth's atmosphere. Synthesised rainfall data for the lower Frieda River catchment was provided by SRK (2017c, realisation #88) and applied as precipitation on the reservoir surface. The temperature of the rainfall was set to the temperature of the reservoir surface.

Table 3.2 documents how the six years of continuous meteorological data was used to synthesize a 10-year time series for the baseline simulations. The selection of meteorological

data begins with an initial year of observed data in 2012 followed by a continuous series from 2009 to 2014 and then a repeat of 2011 to 2013 to complete a 10-year time series.

Some basic statistical properties of the meteorological data in the simulations years are shown in Table 3.3. Simulation years 2005-6 and 2009 in the filling simulation and 2033-34 and 2037 in the operation simulation have both cooler maximum temperatures and lower solar radiation compared to the 10-year average. Wind speeds are typically low and there is little variation in the average maximum daily wind speed between the years.

The meteorological data used for the filling and operations simulations are plotted in the Appendix.

Table 3.1 Summary of data availability from meteorological stations, and application to limnological model.

Station	Records	Application to model
Nena AWS	1994-1999 (WD, SR only) 2008-2017 (significant data gaps from 2015 onwards)	2009-2014 (6yrs) AT, RH, SR, WS, WD WS from 2015-2016 used to fill data gaps in previous years
Moraupi AWS	2009-2017 (significant data gaps from 2014 onwards)	AT, RH, SR, WD for Nena gaps (see notes above)
Iniok AWS	2008-2015 (significant data gaps from 2013 onwards)	Not used at this stage

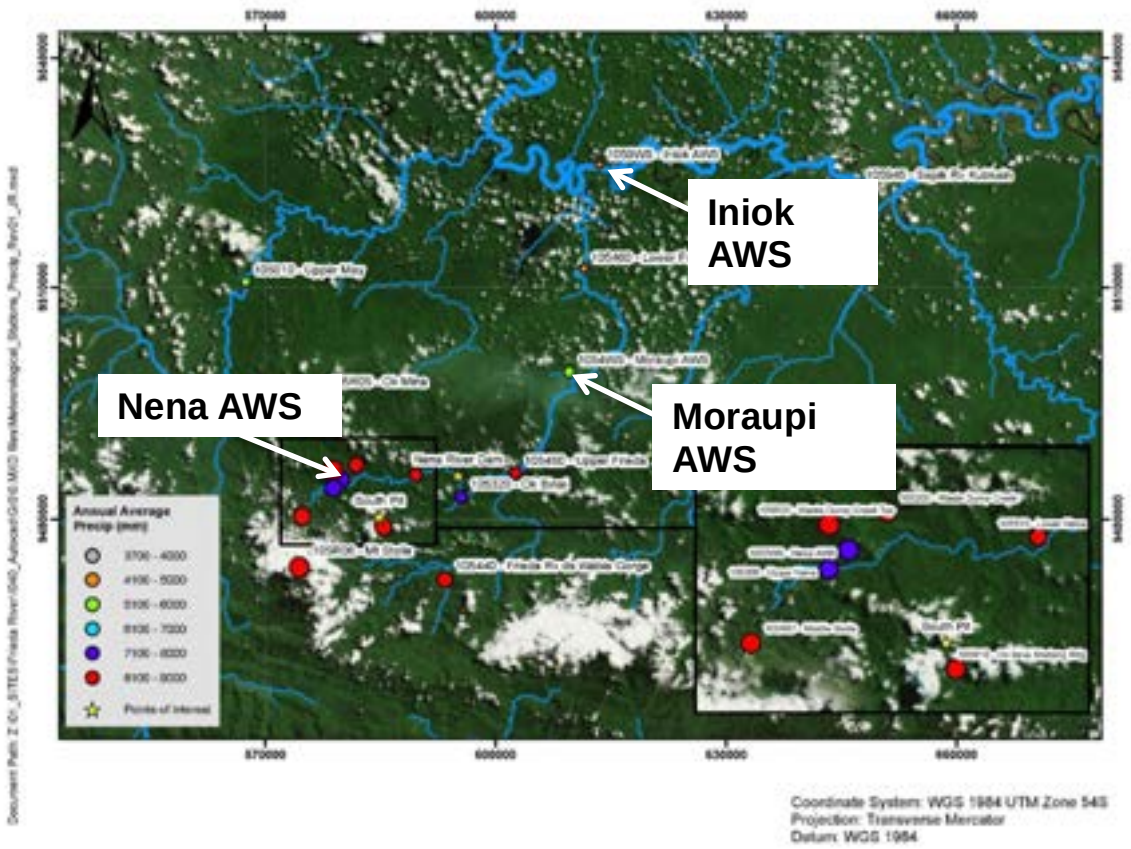

Figure 3.2 Location of weather stations that provided meteorological data for the study (SRK, 2016).

Table 3.2 Application of Nena AWS meteorological data to generate 10-year model forcing periods.

Year of Nena AWS record	Hydrograph year (SRK, realisation #88)	
	Filling	Operations
2012	2000	2028
2009-14	2001-06	2029-34
2011-13	2007-9	2035-37

Table 3.3 Basic statistics of meteorological series used to force the model. Shading indicates a negative (blue shade) or positive (red shade) anomaly from the 10-year average.

Base case model year		**Mean Daily Max. Air Temp. (^oC)**	**Mean Daily Min. Air Temp. (^oC)**	**Mean Daily Solar Rad. (Wm^{-2})**
Filling	**Op.**			
2000	2028	27.8	19.5	4081.5
2001	2029	28.2	19.7	3581.7
2002	2030	27.9	19.9	4233.8
2003	2031	27.8	19.5	4548.1
2004	2032	27.8	19.5	4083.3
2005	2033	27.2	19.7	3686.4
2006	2034	27.5	19.6	3480.4
2007	2035	27.8	19.5	4548.1
2008	2036	27.8	19.5	4083.3
2009	2037	27.2	19.7	3686.4
10yr average		*27.70*	*27.7*	*19.6*
Annual Mean Anomaly from 10yr average				
2000	2028	0.1	-0.1	80.2
2001	2029	0.5	0.1	-419.6
2002	2030	0.2	0.3	232.5

2003	2031	0.1	-0.1	546.8
2004	2032	0.1	-0.1	82.0
2005	2033	-0.5	0.1	-314.9
2006	2034	-0.2	0.0	-520.9
2007	2035	0.1	-0.1	546.8
2008	2036	0.1	-0.1	82.0
2009	2037	-0.5	0.1	-314.9

3.2.4 Inflows

The model was configured to account for 16 inflow entry points (Figure 3.3, Table 3.4) into the FRHEP reservoir with flow rates and sediment concentrations consistent with the sediment transport provided by Golder Associates using daily flow rates for each tributary based on flow realisation number 88 (SRK, 2017c). Daily inflow rates were compressed into 6-hour hydrographs (see Appendix for further details). The shape of each daily hydrograph was extracted from the peak flow assessments (SRK, 2017c).

The temperature of the inflows was assigned using a relationship between stream flow temperature and air temperature (Hydronumerics, 2011) given by $T_{inflow} = 0.232T_{air} + 14.21$. This relationship was derived using a least-squares fit between water temperature recorded in the Upper Nena River and air temperature at the Nena AWS during 2008. The calculated inflow temperatures include a diurnal variation that follows air temperature and range between 20.1-23.5 ^{o}C (mean of 21.4 ^{o}C).

Salinity of the inflows was assigned zero, as the observed concentrations in the streams is sufficiently small to have negligible impact on the water density.

The major inflows have been traced in the model using a mass conservative inert tracer that provides a means to assess transport and dilution of the inflows during passage through the reservoir. Tracer concentrations were assigned a value of one in the inflows.

The total suspended sediments in each inflow consist of four particle size groups (Table 3.5), which have been derived from Golder Associates (2018). A specific gravity of 2.65 was assigned to each group.

Figures that illustrate flow rates, temperature and sediment loads of the inflows are included in the Appendix.

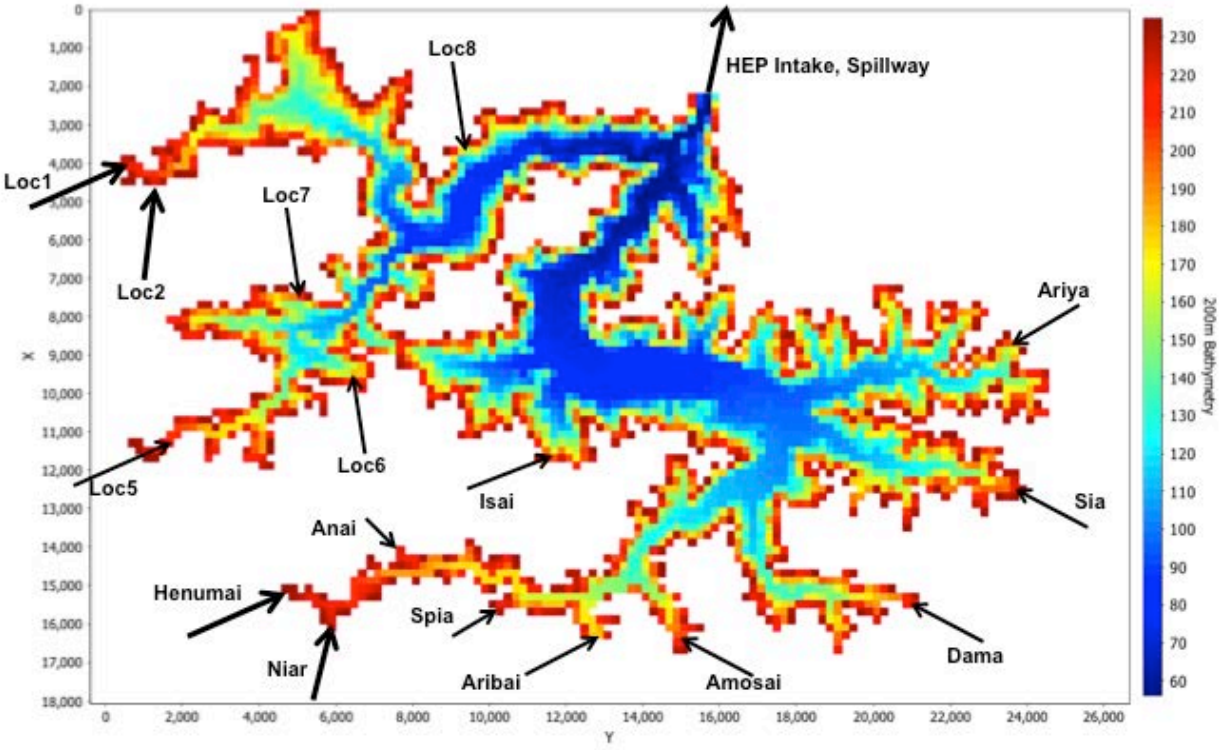

Figure 3.3 Location of modelled inflows.

Table 3.4 Mean inflow properties of mean flow rate ($m^3 s^{-1}$) and TSS concentration (mg L^{-1}) over a 44-year time series.

Inflow	**Mean Flow rate ($m^3 s^{-1}$)**	**Mean TSS concentration* (mg L^{-1})**
Henumai	37.1	124.1
Niar	25.6	124.1
Anai	2.6	124.1
Spia	2.6	124.1
Aribai	12.8	124.1
Amosai	10.2	124.1
Dama	12.8	124.1
Sia	3.8	124.1
Ariya	7.7	124.1
Isai	11.5	124.1
Loc1 - Nena	43.2	295.5
Loc2	9.1	535.2

Loc5 – Ok Binai	3.6	172.6
Loc6	7.1	57.2
Loc7	1.5	68.9
Loc8	5.7	110.8

Table 3.5 Properties of catchment particle size groups.

Sediment Origin	**Size (microns)**	**% Distribution**	**Critical Shear Stress (Pa)**	**Erosion Rate (g/m2/day)**
Catchment	2	Variable*	1.3E-02	1.7E+07
Catchment	4	Variable	2.0E-02	1.1E+07
Catchment	8	Variable	3.1E-02	6.9E+06
Catchment	16	Variable	4.9E-02	4.4E+06

* The PSD's for catchment contributions are variable and provided as part of the outputs from Golder Associates (2018) catchment modelling.

3.2.5 Outflows

The outflow sequence is based on the modelled water level, with the following embankment operations:

- Extraction via deep diversion tunnel of 50 m^3s^{-1} occurs until 9 August 2000 when water level reaches 161.9 m RL;
- On 9 August 2000 extraction from a low-level HEP intake (at 143.5 m RL) commences. The extraction rates follow a time series provided in "FRHEP_MonthlyFlows_Limnology_RevB.xlsx", which increased from 50 to 148.3 m^3s^{-1} on 27 September 2000.
- On 15 May 2003, extraction switches from the low-level intake to the final level HEP intake at 185.6 m RL. Intake rates are between 148.3 to 229.9 m^3s^{-1} until 3 Jan 2036, and then HEP intakes cease.

3.2.6 Waste Rock and Tailings

The assessment of the mobility of stored waste rock and tailings is based on the final in-filled storage condition (Figure 1.5). Both the waste rock and tailings size distributions were discretised as per Table 3.6 based on the particle size distribution curves for waste rock and tailings that were provided by SRK.

Sediment resuspension in the AEM3D model uses a simple expression given by (Bengtsson et al., 1990) $E = C_e(\tau/\tau_c - 1)$, where E is erosion rate (g m^{-2} day^{-1}), C_e is an erosion rate coefficient (g m^{-2} day^{-1}), τ is the bottom shear (Pa, determined by the hydrodynamic model) and τ_c is the critical shear stress (Pa) required to resuspend the particles.

Following Chung et. al. (2009) the critical shear stress τ_c can be estimated from the equation $\tau_c = \tau_c^* \rho R g D$, where τ_c^* is the is the non-dimensional Shields' parameter, R is the submerged specific gravity (i.e. assumed as S.G. - 1 = 1.65), g is acceleration of gravity and D is the

sediment grain size. Cao et al. (2006) offers an explicit formulation for τ_c^* suitable for non-cohesive grain sizes, which has been applied here to yield critical shear stress (following Geremew and Yanful 2011, see Table 3.6, Figure 3.4 and Figure 3.5). Estimates of erosion rate coefficient were also derived from particle size based on Geremew and Yanful (2011).

A bulk density of 1600 kg m^{-3} for the waste rock and 1300 kg m^{-3} for the tailings has been assumed (John Chapman, SRK, pers. comms.). The resuspension model does not explicitly account for shielding, cohesion and flocculation of the sediments and erosion rate calculation assumes that the availability of waste rock and tailings material is not limiting.

The laboratory experiments of Gerenew and Yanful (2011) suggest that the theoretical estimates of critical shear stress are likely to be conservative and that the effects of sheltering and cohesion of fine fractions in mixed sediment sizes (as in the case of the waste rock and tailings) are likely to lead to some extent of equal mobility, whereby the sediment mix exhibits a single critical stress across a range of particle sizes within the sediment mix. Gerenew and Yanful (2011) measured critical shear stresses in the laboratory from 0.09 to 0.23 for a range of particle size mixtures of re-constituted tailings with differing ranges of fine contents. Results suggested that tailings with 50 to 55% or more fines (< 63 microns and with clay content less than 5%) were cohesive with significantly increased resistance to surface erosion. Lamb et al. (2008) suggests incipient motion for mixtures can be reasonably determined by a single critical stress by using the median particle size of the mixture in the derivation of critical stress. For the waste rock and tailings this estimate yields 1.3 and 0.1 Pa respectively.

In addition to the derived critical shear stress a single critical shear stress (referred to as the equal mobility case) of 0.12 Pa (following Mian and Yanful, 2003) has been applied to both waste rock and tailings sediments to account for potential shielding and cohesion. There is further discussion of critical shear stress provided in the Appendix.

Settling rates of resuspended waste rock and tailings is determined in the model from Stokes settling velocity for singular particles without flocculation. Because the waste rock and tailings storage excludes the shallow waters of the reservoir, it has been assumed (after Lick, 1986) that currents dominate resuspension stress and the effects of bed stress from wind-generated surface shear have been omitted.

Simulations of the process of barge deposition of waste rock material are discussed in Section 3.3.6.

Table 3.6 Waste rock and tailings particle properties.

Sediment Origin	**Size (microns)**	**% Distribution**	**Critical Shear Stress (Pa)**	**Erosion Rate (g m^{-2} day^{-1})**
Tailings	1.6	12.1 %	1.1E-02	2.0E+07
Tailings	5.4	7.7 %	2.4E-02	8.9E+06
Tailings	14.8	11.4%	4.7E-02	4.6E+06
Tailings	50	68.8%	1.0E-01	2.1E+06
Waste rock	1.6	0.44%	1.1E-02	2.0E+07
Waste rock	5.4	0.12%	2.4E-02	8.9E+06
Waste rock	14.8	4.43%	4.7E-02	4.6E+06

Waste rock	40	5%	9.0E-02	2.4E+06
Waste rock	300	10%	2.0E-01	1.1E+06
Waste rock	1000	20%	5.8E-01	3.7E+05
Waste rock	3000	60%	2.2E+00	9.9E+04

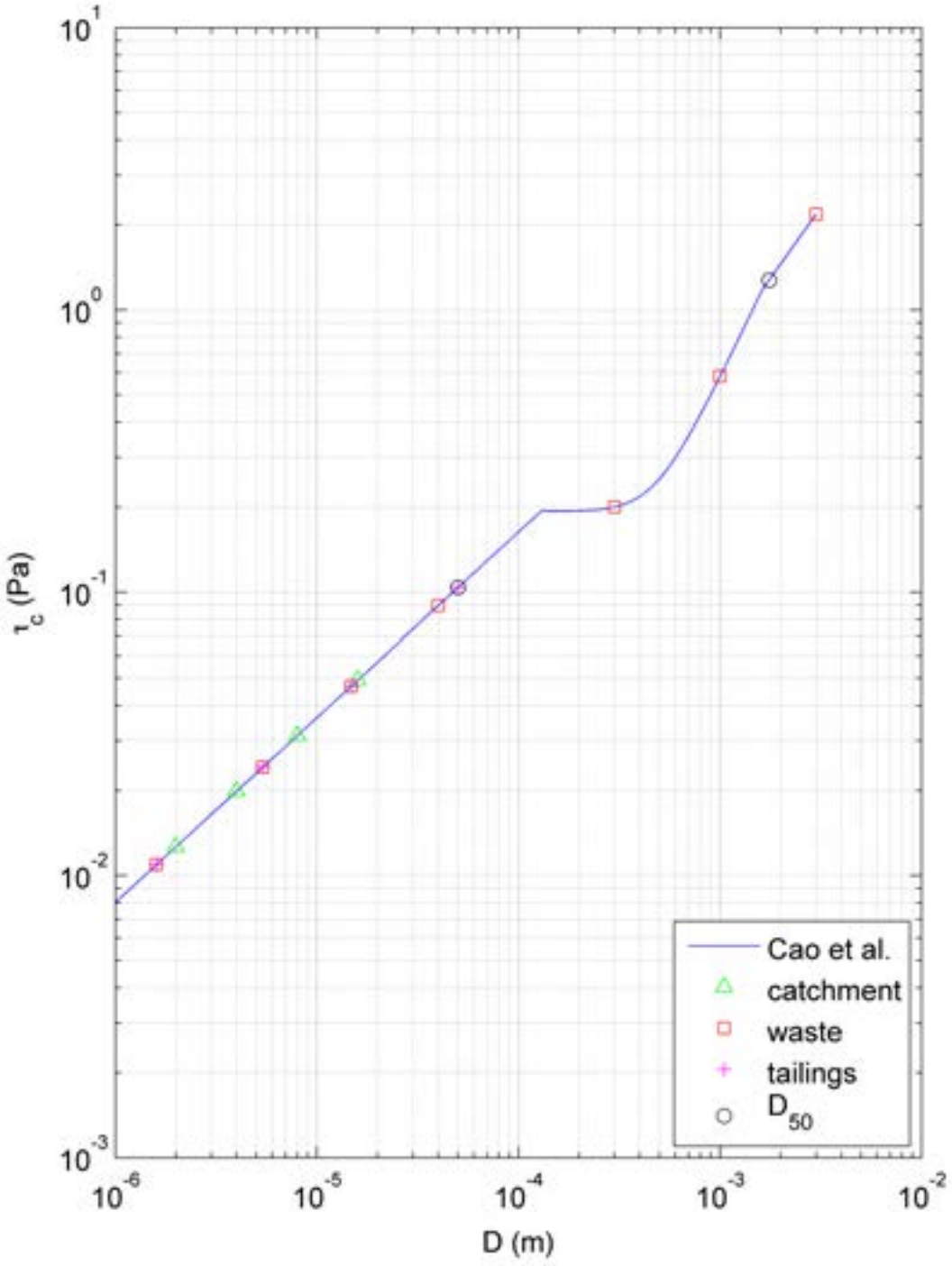

Figure 3.4 Critical shear stress as a function of particle diameter following derivation of Shields' Curve from Cao et al. 2006 (cited in Geremew and Yanful 2011 Eq. 4.). Markers indicate location on the critical shear stress curve for the different sizes and median size (D_{50}) for waste rock and tailings.

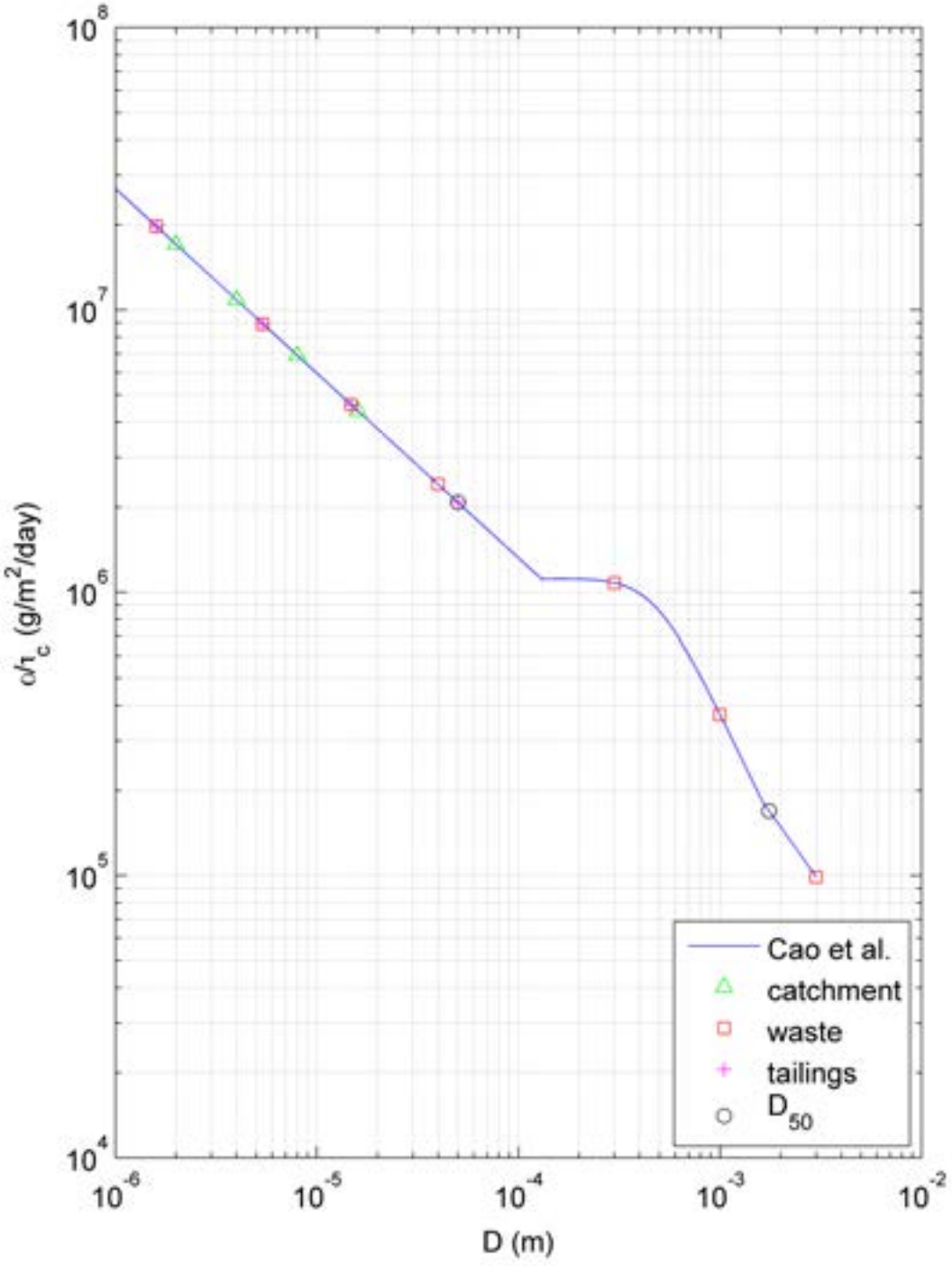

Figure 3.5 Erosion rate coefficient (variable C_e) as a function of particle diameter following derivation of Geremew and Yanful 2011. Markers indicate location on the erosion rate curve for the different sizes and median size (D_{50}) for waste rock and tailings.

3.2.7 Model Sensitivity

A series of sensitivity simulations were undertaken using a preliminary model that was applied on an earlier description of the project and prior to selection of the preferred project description.

The difference between the model results using the earlier and updated project description and the results of the sensitivity tests are described in the Appendix.

The sensitivity tests include changes to the hydrograph period, inflow temperature, meteorological data and HEP operations. Each test was performed over a sub-period of the operational simulation with the HEP operating. Whilst the sensitivity simulations were not repeated for the updated project description (due to project timeframes), the findings from the analyses that were performed with the preliminary model still provide an important indication of the model inputs and parameters that are likely to have the largest impact on the model results

Although the tests demonstrate changes to the results they also suggest that, with the exception of modifications to the HEP operation, the changes to the results are small. This indicates that the simulated persistent thermal stratification is resilient when challenged with systematic changes in model forcing and only subject to significant change in the event of large environmental and operational changes.

A series of scenario simulations were also undertaken using the preliminary model and are reported in the Appendix. The scenarios were designed to assess the changes to the limnology that may occur under different environmental and operational conditions. These include flow events, storm conditions, low water level and leachate release from the stored waste rock and tailings.

3.3 Model Results and Discussion

3.3.1 Filling

A ten-year period from 2000 to 2009 was simulated with no waste rock and tailings stored in the reservoir. This simulation was undertaken to assess the behaviour of the reservoir and the downstream release of catchment sediments during the filling and construction phase and continuing through to an operational phase.

Calculated temperature at the embankment (Figure 3.6) illustrates a filling period of approximately 3 years and 4 months over which time a thermal stratification develops and persists for the remainder of the simulation. Temperatures reach 26 to 32 ^{o}C in the surface layer of about 10 m, separated from cooler waters beneath (22 to 24 ^{o}C) characterised by a strong temperature gradient from 10 to 30 m deep that weakens below 30 m. The temperatures of the inflows control the temperature of the underlying waters during the filling stage.

The height of the HEP intake impacts on the temperature profiles as indicated when the low-level HEP intake at 143.3 m RL ceases and HEP intake moves up to 185.6 m RL in May 2003 (Figure 3.7). When operating at a water level of 226 m RL, and after a period of adjustment over 4 years, the stratification consists of a warm, mixed epilimnion above approximately 215 m RL. Underneath the epilimnion, the upper portion of the metalimnion is defined by gradients from 215 m RL down to 185 m RL that weaken in the lower metalimnion from 185 m RL down to 160 m RL before reaching the hypolimnion where temperature gradients are weak and near linear.

There are fluctuations in simulated epilimnion temperatures over time as the surface waters equilibrate to warm and cool weather. Whilst the epilimnion and upper metalimnion temperatures and temperature gradients decrease during cooler periods, the model results suggest that this process alone is insufficient to induce significant mixing and the stratification remains intact.

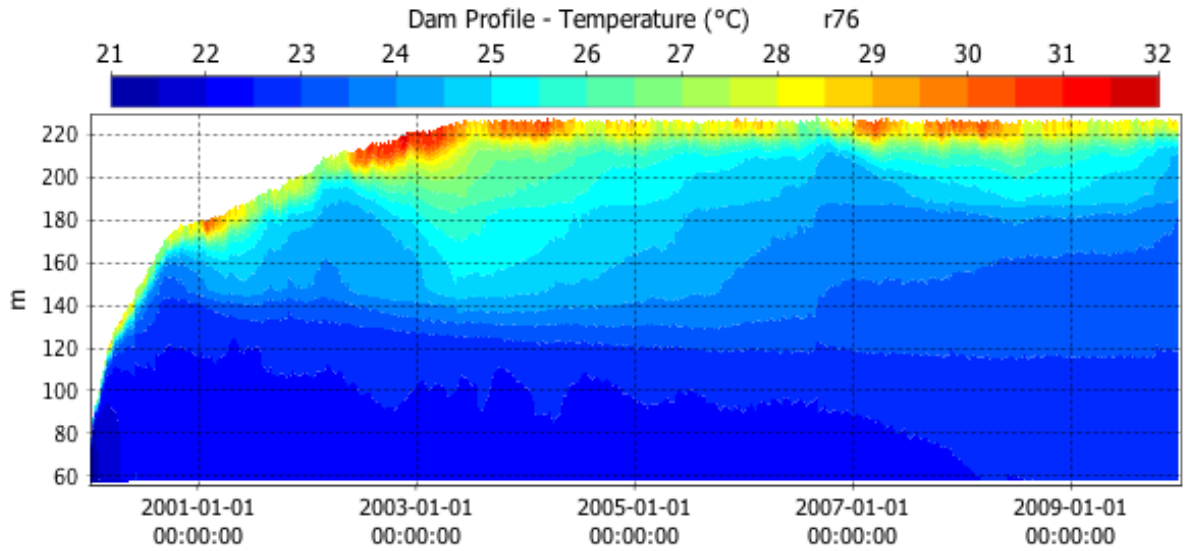

Figure 3.6 Temperature profiles over time at the embankment during the filling simulation.

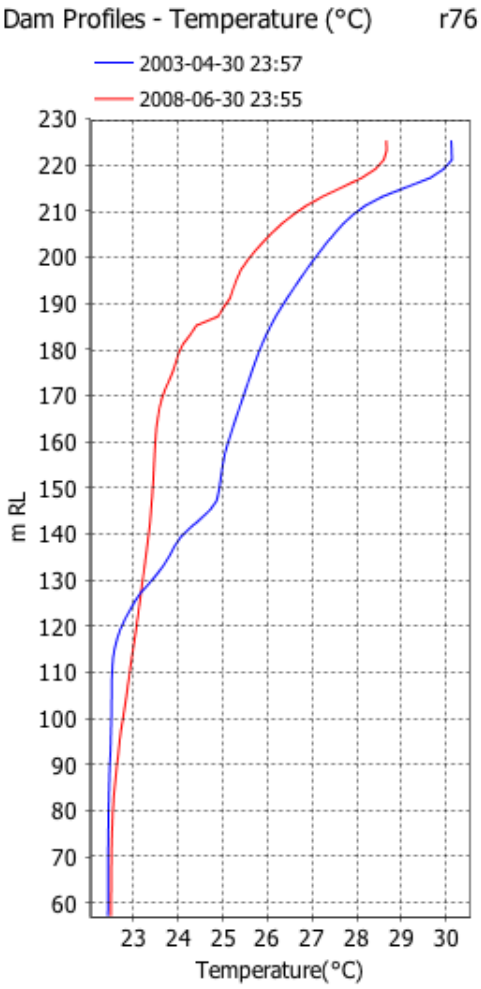

Figure 3.7 Temperature profile at the embankment during low-level HEP intake (blue) and operation level HEP intake (red).

Simulated temperatures along the Nena and Niar arms to the embankment (see Figure 3.8 and Figure 3.9) illustrate that the stratification observed at the embankment (deepest point of the reservoir) persists over much of the reservoir expanse with the exception of shallow regions

within 5 to 10 km of the headwaters of the main rivers. In these upper reaches inflow intrusions modify local stratification but the water column does not homogenise and temperature gradients remain. The local stratification is at times strengthened by the sub-surface intrusion of cooler inflows.

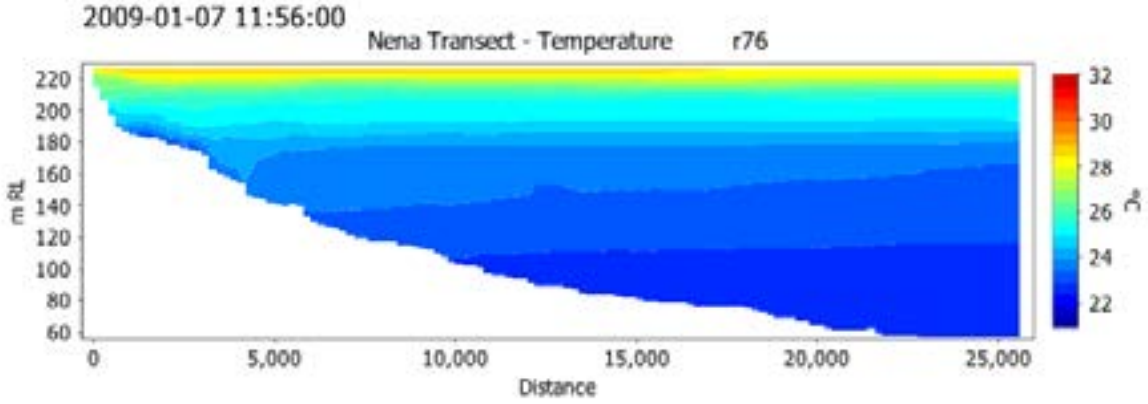

Figure 3.8 Simulated temperature from the headwaters of the Nena River (on the left of the figure) to the embankment (on the right) on 7 January 2009.

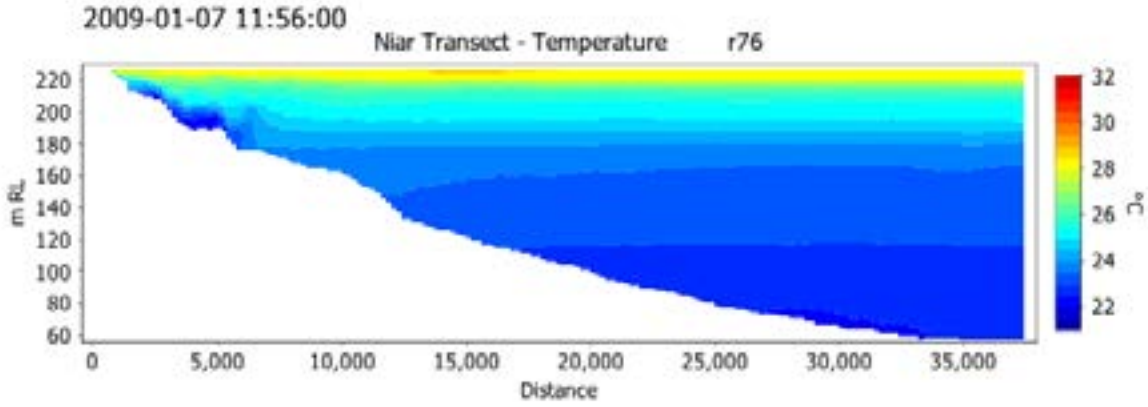

Figure 3.9 Simulated temperature from the headwaters of the Niar River (on the left of the figure) to the embankment (on the right) on 7 January 2009.

Lateral heterogeneity in the temperature was simulated across the expanse of the reservoir (see Figure 3.10). The differences in temperature can be attributed to proximity, number and size of inflows (which enter the reservoir at temperatures below the epilimnion temperatures) and local shallow dendritic reaches (such as the Ok Binai, Upper Nena and bend in the mid-Niar) that act to trap more heat from solar radiation near the surface than in the deeper expanses. The net effect is that the Niar River arm of the reservoir is slightly cooler than the Nena and Ok Binai arms (on average by less than 0.5 ^{o}C). Whilst small, this difference contributes to the vertical layer arrangement of the inflow contributions as they flow towards the embankment (see discussions below).

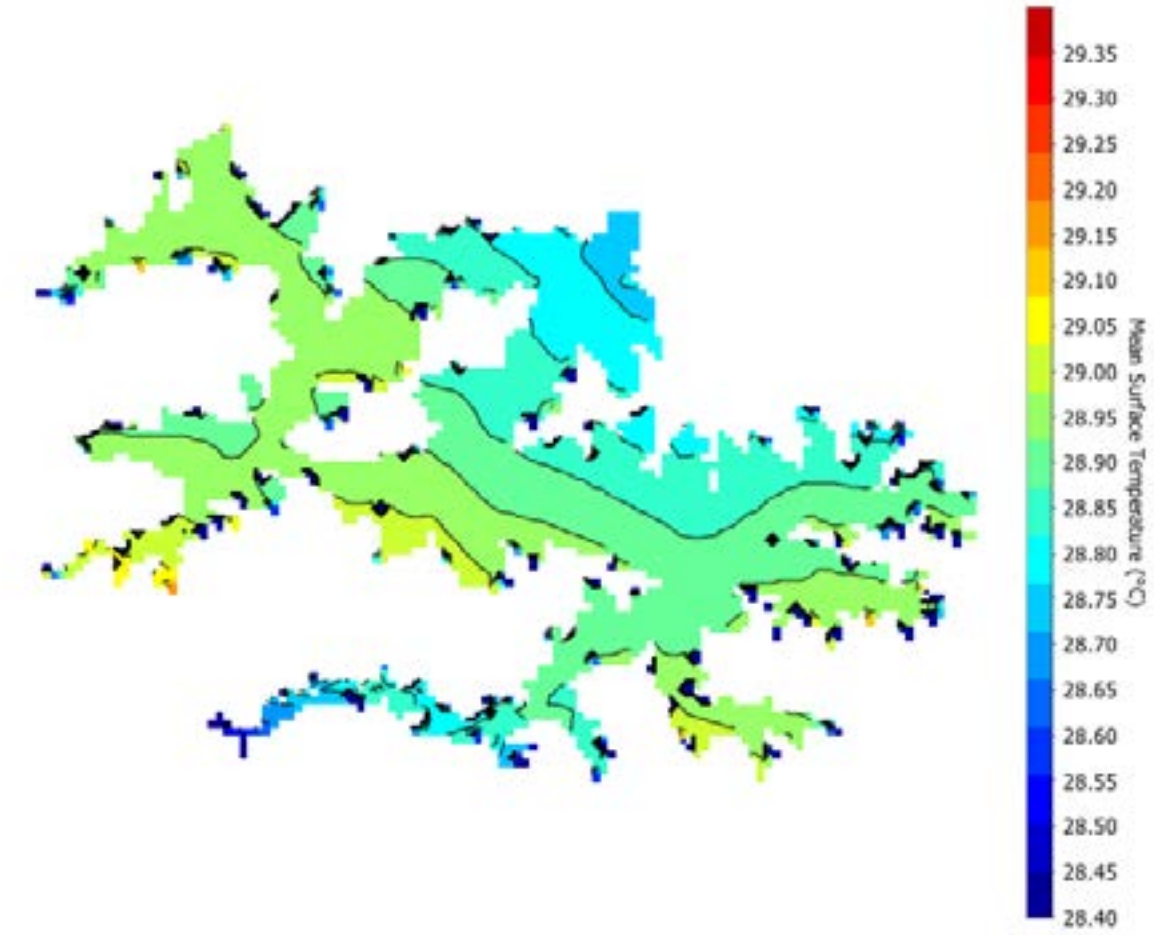

Figure 3.10 Mean surface temperature during operations simulation.

Overall the model results suggest that, under conditions of median flow (used for the simulations) and over the available range of observed meteorological conditions, the FRHEP reservoir is likely to be persistently stratified with no regular periods of significant vertical mixing. Extracting the simulated average age of the water from the model (see Figure 3.11) clearly illustrates that beneath 140 m RL there is a continual aging of the water due to a lack of mixing with the younger waters above (inflows arrive with an age of zero days). Between 140 m RL and 185 m RL in the lower metalimnion there is an age gradient that indicates a region of mixing between younger incoming waters with older waters in the hypolimnion below. Above 185 m RL the upper metalimnion and epilimnion waters reach an equilibrium whereby the average age (which can be considered a residence time) is less than one year.

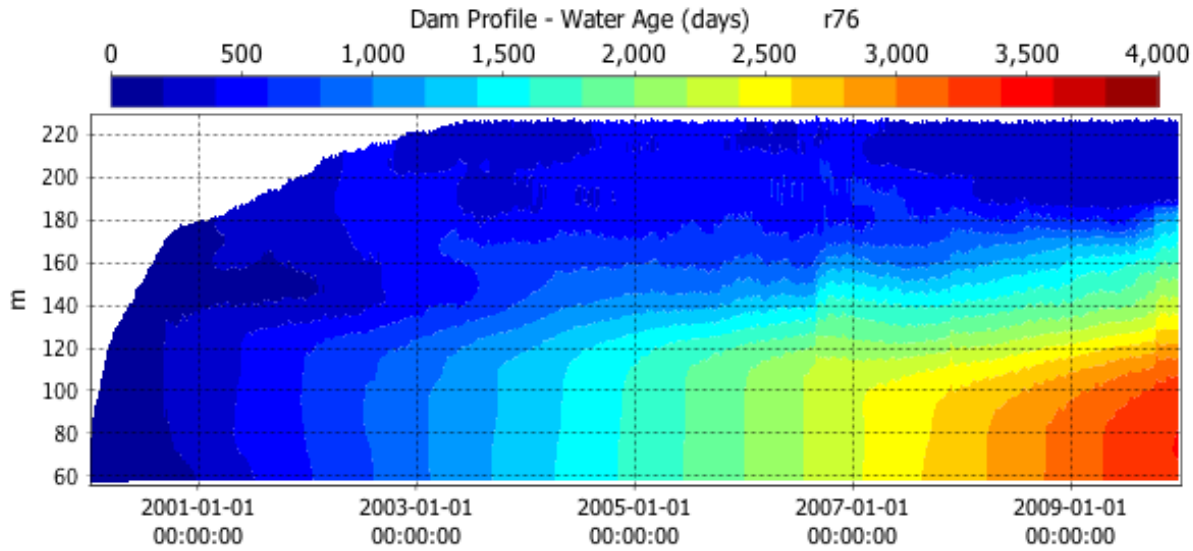

Figure 3.11 Simulated water age (in days) at the embankment during filling.

Model results show that inflows into the reservoir traverse the upper reaches as underflows that entrain warmer ambient water before peeling off the reservoir bed as lateral intrusions (see for example intrusions in Figure 3.12 and Figure 3.13) at a depth of neutral buoyancy within the thermal structure. Whilst the mechanism of entrainment followed by insertion is complex, the vertically layered result at the embankment consists of Nena arm tributaries overlying Niar arm tributaries. This will, to some extent, be caused by the warmer temperatures in the Nena arm of the reservoir resulting in less dense intrusions.

The depth of the FRHEP extraction within the stratified metalimnion leads to a thinned selective withdrawal layer (Anohin et al. 2006) over which extraction takes place. Furthermore, the withdrawal layer itself contributes to the development of steps in temperature profile that increase the strength of local vertical stratification, as suggested by Mtada (1986) and Casamitjana et al. (2003). Time series of profiles of the tracers from the Nena and Niar Rivers at the embankment (see Figure 3.14 and Figure 3.15) show a shift in intrusion depth when the low-level HEP is switched off, whereby the intrusion depths lift to be typically above (for the Nena arm tributaries) and below (for the Niar arm tributaries) the level of the operational HEP intake at 185 m RL.

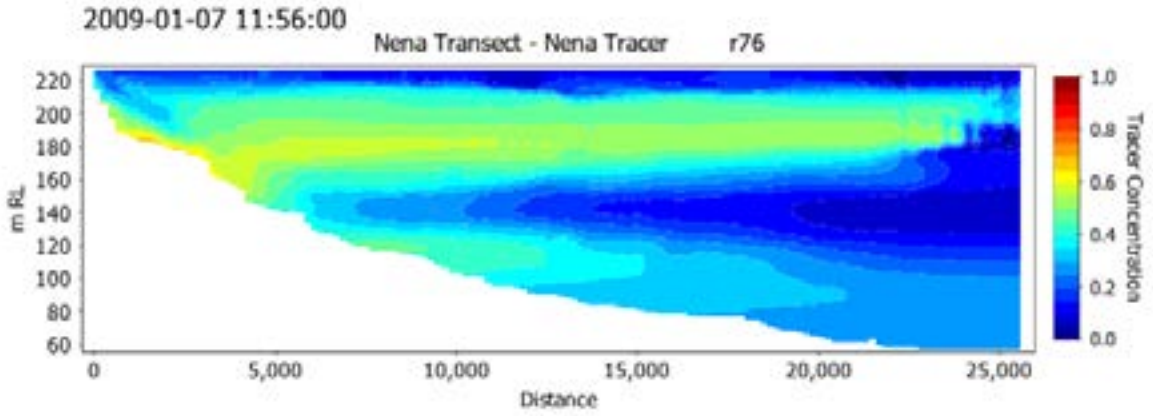

Figure 3.12 Model output from Nena River headwaters (on the left) to the embankment (on the right) on 1/7/2009 showing tracer concentrations from the Nena River as an intrusion across the reservoir.

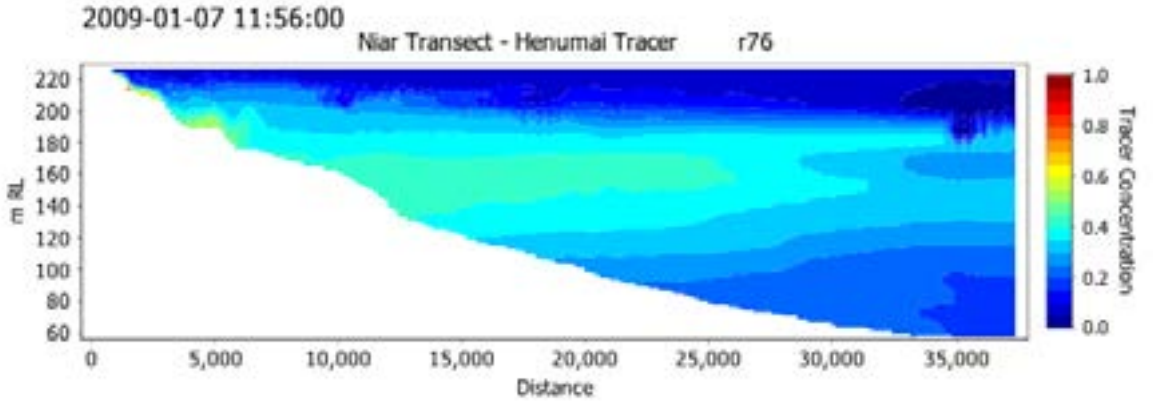

Figure 3.13 Model output from Henumai River headwaters (on the left) to the embankment (on the right) on 1/7/2009 showing tracer concentrations from the Henumai River as an intrusion across the reservoir.

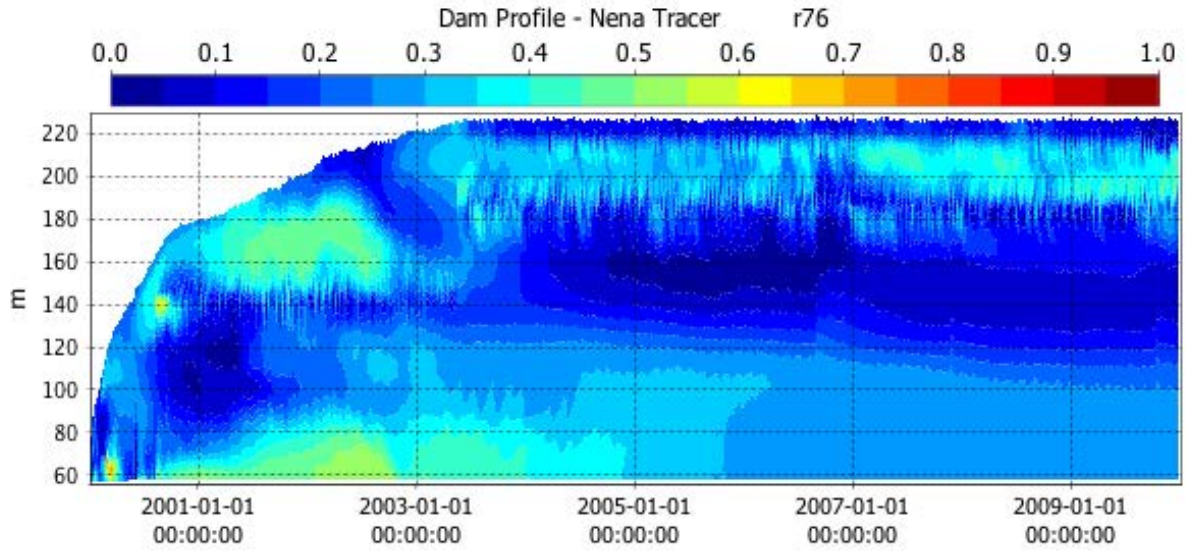

Figure 3.14 Simulated Nena inflow tracer during filling.

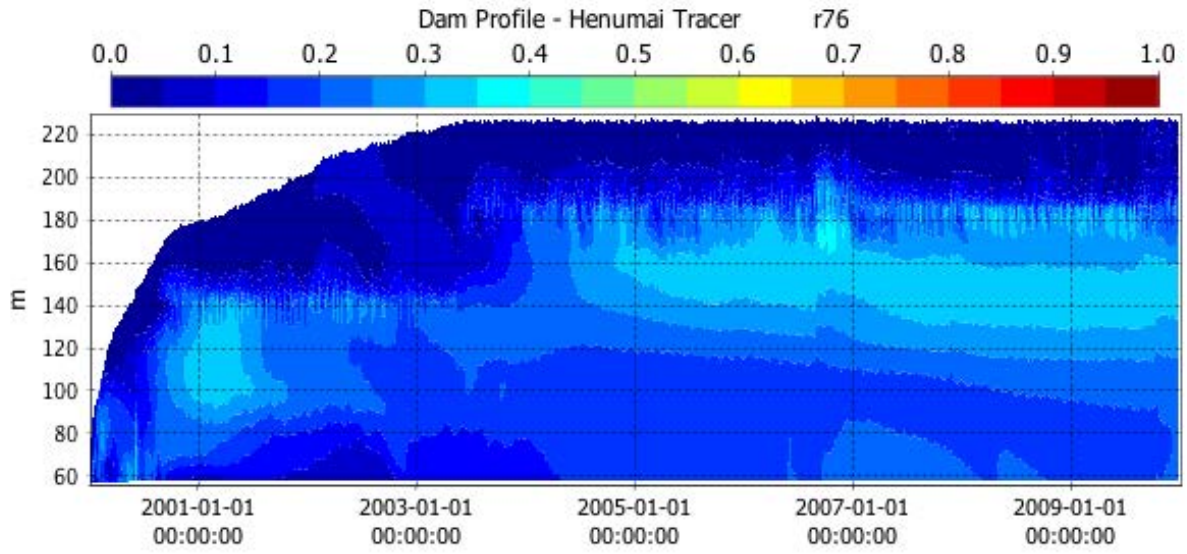

Figure 3.15 Simulated Henumai inflow tracer during filling.

Suspended sediments entering the reservoir from the tributaries follow the trajectory of the inflow tracers described above; however, as the particles settle over time, the extent over which the concentrations are elevated thickens (downwards) (see illustrations in Figure 3.16 to Figure 3.18). The attributes of the particles dictate settling velocity; the 2-micron particles take approximately 12 months to settle from the metalimnion to the bed once they reach the embankment (a vertical travel distance of 120 m). Larger particles (see illustrations of 4-micron particle concentrations in Figure 3.17) settle significantly faster (approximately 3-4 months). The TSS in the reservoir therefore consists mostly of the finest particle fractions that remain in suspension longer, reaching up to approximately 80 mg L^{-1} at the embankment.

On passage from the headwaters to the embankment the particle sizes in the inflows will settle at different rates leading to deposition maps that show smaller particles reaching the reservoir bed further towards the embankment (Figure 3.19). The in-reservoir deposition and downstream release of sediments from the reservoir is discussed in Section 3.3.5.

Deposited particles may be resuspended if there is sufficient bottom shear to overcome the critical shear required for suspension. This typically takes place during high flow events that scour the bottom of the reservoir near the headwaters and due to bottom shear from surface wind-waves in the shallows. Whilst resuspension and re-deposition processes included in the model determine to some extent the deposition maps and suspended solid concentrations, a detailed analysis of the resuspension of natural catchment sediments has not been undertaken. Resuspension of waste rock and tailings is discussed in Section 3.3.3.

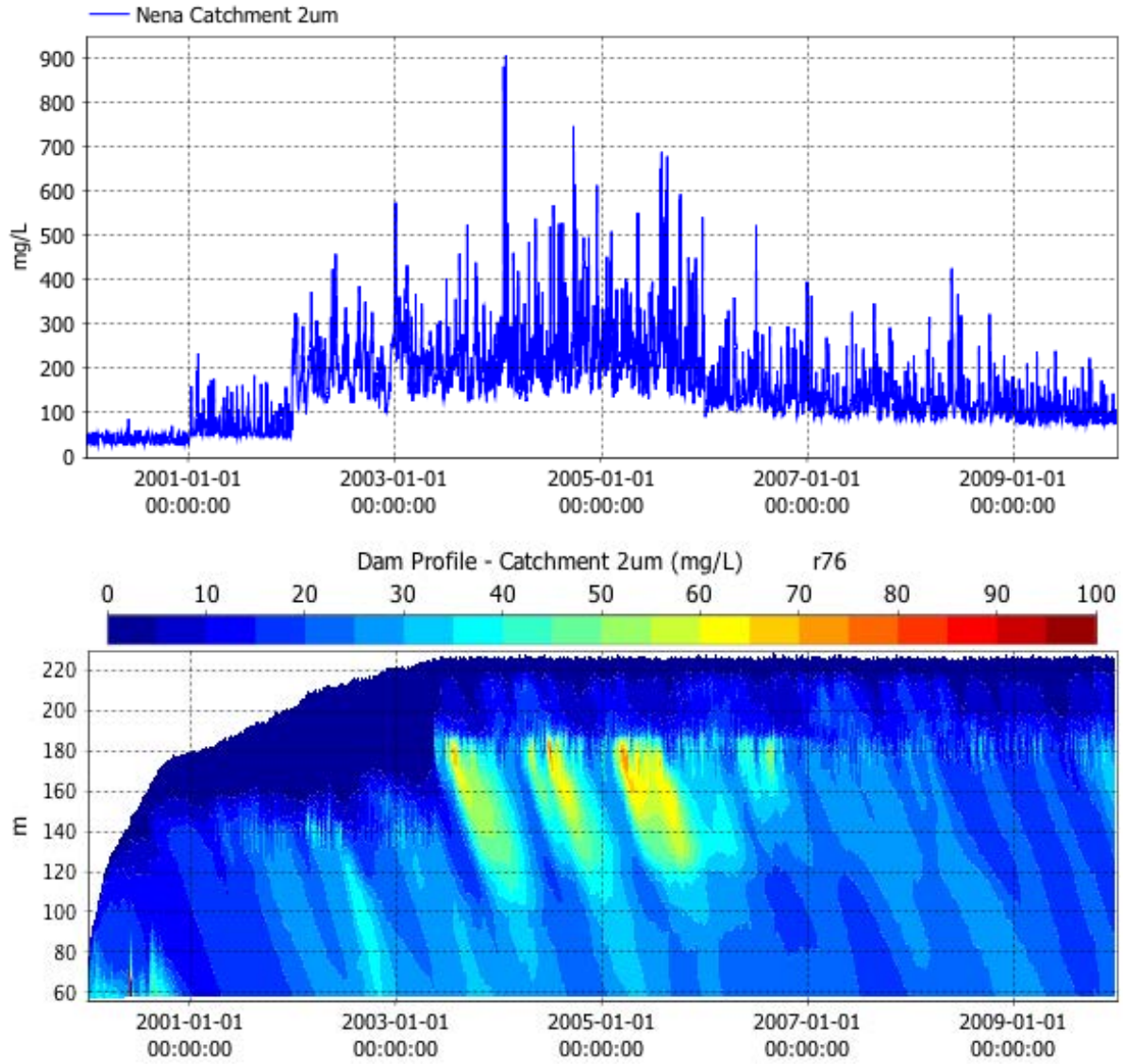

Figure 3.16 Simulated concentration (in mg L^{-1}) of 2-micron particles from catchment loads at the embankment during filling. The top panel illustrates the change in catchment loads of 2-micron particles that lead to increases in concentration at the embankment.

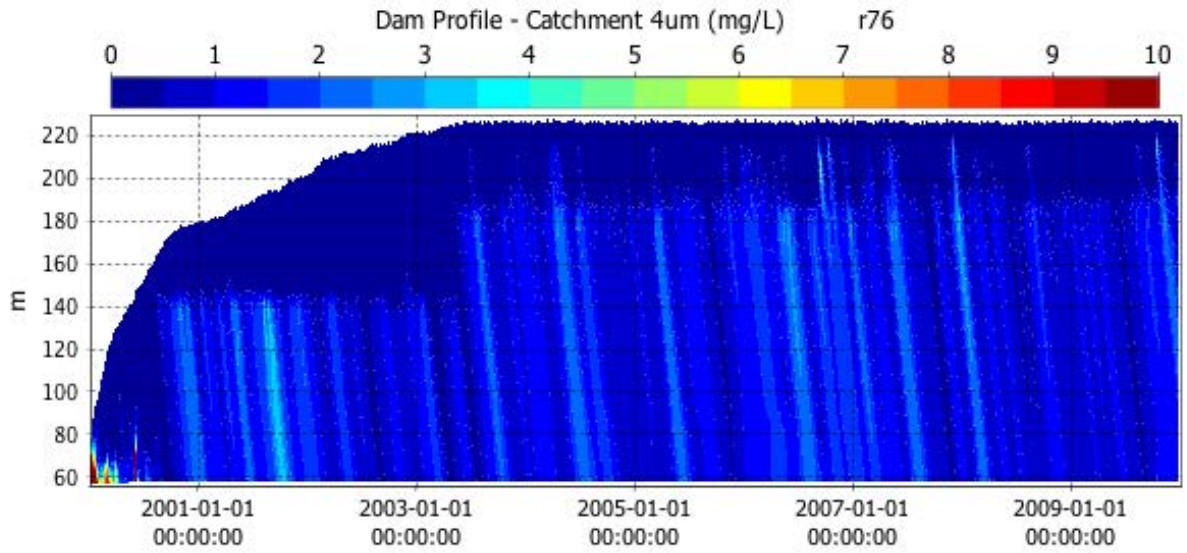

Figure 3.17 Simulated concentration (in mg L^{-1}) of 4-micron particles from catchment loads at the embankment during filling.

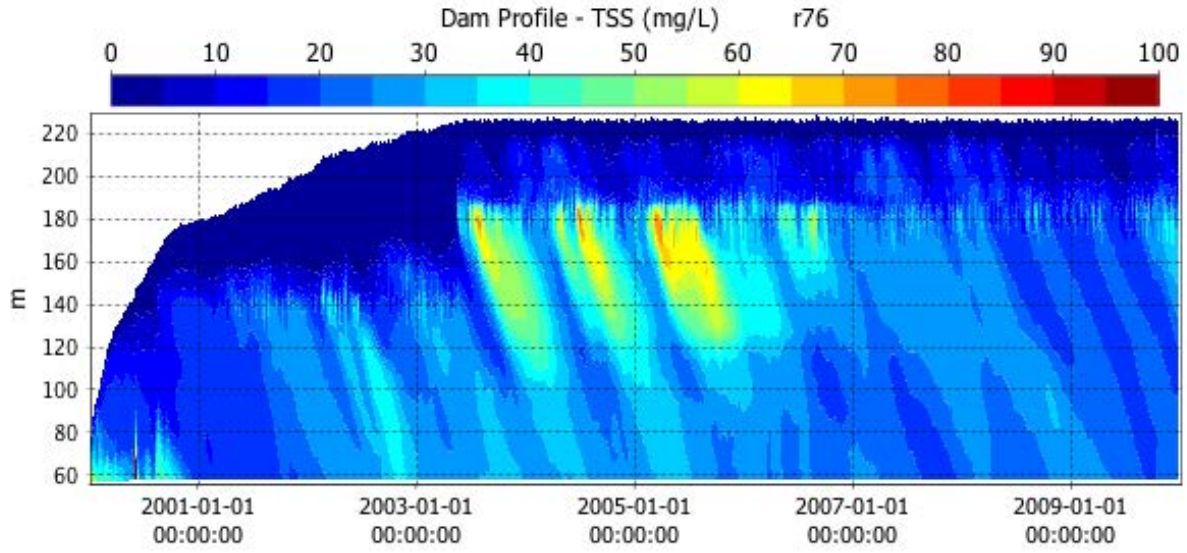

Figure 3.18 Simulated concentration (in mg L-1) of TSS from catchment loads at the embankment during filling.

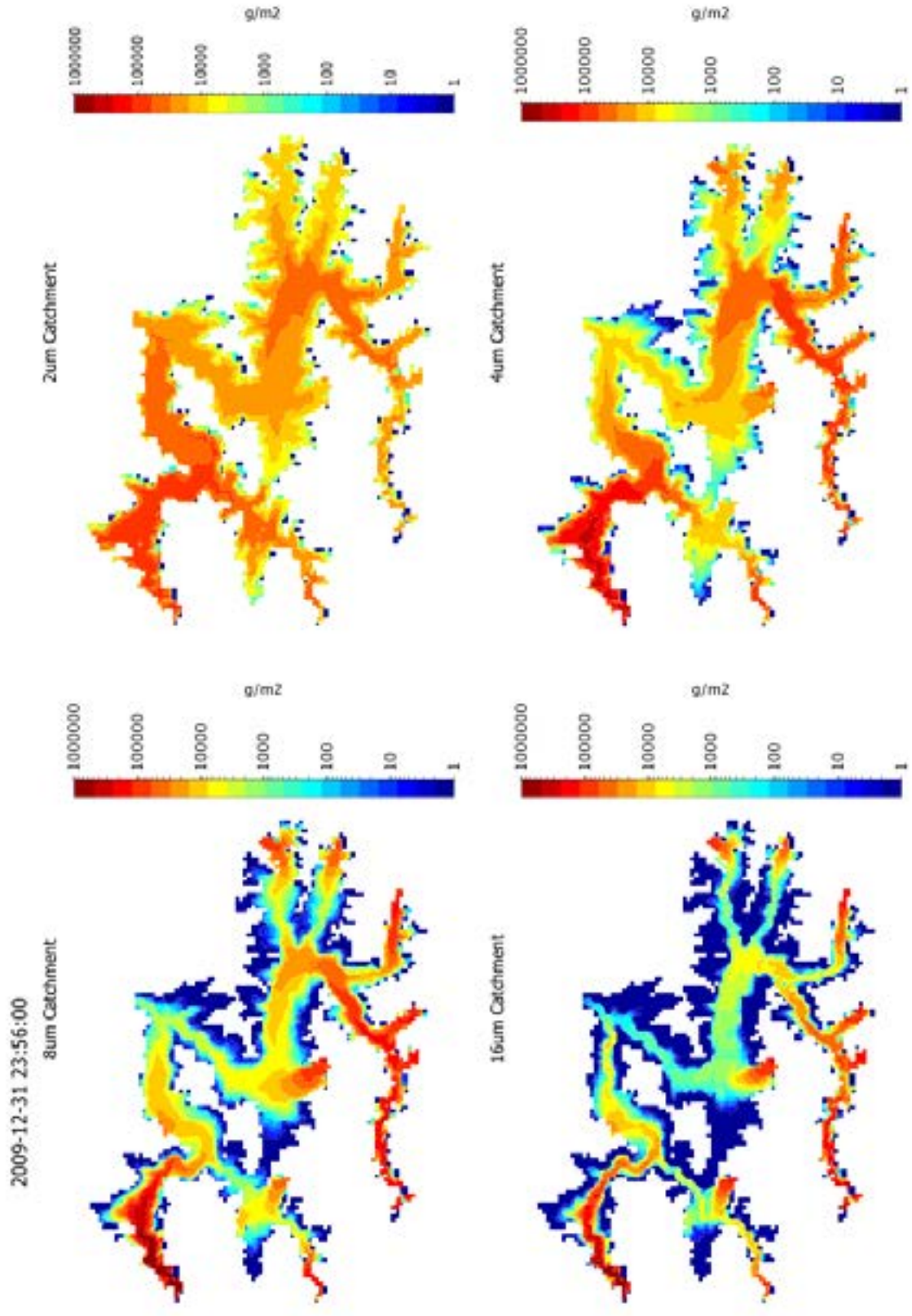

Figure 3.19 Simulated catchment sediment deposition maps (in g m^{-2}) of the four particle sizes in the inflowing waters at the end of the filling simulation. Note that the colour bar is on a log scale.

3.3.2 Operations

A ten-year simulation period from 2028 to 2037 starting at an operational level of 225 m RL was simulated with and final storage plan for waste rock and tailings included in the model. In the final 2 years of this simulation the operation of the reservoir shifts to post-HEP closure, during which there is only spillway release. This simulation has been designed to assess the impact of the waste rock and tailings storage in the reservoir and the change in behaviour when the operation of the HEP ceases. Note that the simulations described below do not include the potential impacts of barge deposition of waste rock, which was examined separately as described in Section 3.3.6.

The operations simulation was initialised using the simulated temperature profile at the embankment extracted after 5 years of the filling simulation (i.e. 2 years after the reservoir filled and the HEP intake shifted from 143.3 to 185.6 m RL). The selection of initial condition was tested (see Appendix) and the results indicate that when compared to the selection of an initial temperature profile produced after 10 years of the filling simulation (which was cooler below 180 m RL) the initial condition that as selected predicted higher concentrations of mobilised waste rock and tailings in the release waters. This occurred because there was an increase in the plunge depth of the catchment inflows into the warmer water column (i.e. that which was simulated after 5 years), which resulted in higher bed stress over the stored waste rock and tailings and therefore higher rates of resuspension.

It is expected that the HEP will remain operational for more than 100 years, so the period of the simulation to 2036 is representative of the likely behaviour of the reservoir during this period (based on flow realisation number 88 from SRK, 2017c) and the range of meteorological data available from site records (see Section 3.2.3). Long-term changes in the limnological behaviour that occur in response to changes in flow and meteorology have not been considered in this report, but should be given consideration in future investigations.

During the operations simulation the post-filling temperature structure is maintained until 2036, when HEP intakes cease (closure condition) and reservoir outflow occurs only via the spillway (see Figure 3.20). Prior to 2036 there are fluctuations in simulated epilimnion temperatures over time as the surface waters equilibrate to warm and cool weather but the stratification remains intact (see Figure 3.21). The simulated retention time during operations illustrates the continual aging of waters below 120 m RL, indicative of a lack of refreshment of the hypolimnion waters via inflow intrusions or mixing with the water column above (Figure 3.22).

From 2036 the temperature structure changes when the HEP intake is switched off and after a approximately 10 months of adjustment the temperature profile consists of a thin warm epilimnion to 10 m deep, sharp temperature gradients in a metalimnion from 10 to 20 m deep, and a very weak temperature gradients in the hypolimnion beneath (Figure 3.23). The response of the reservoir to the HEP closure period after 2036 is discussed further in Section 3.3.4.

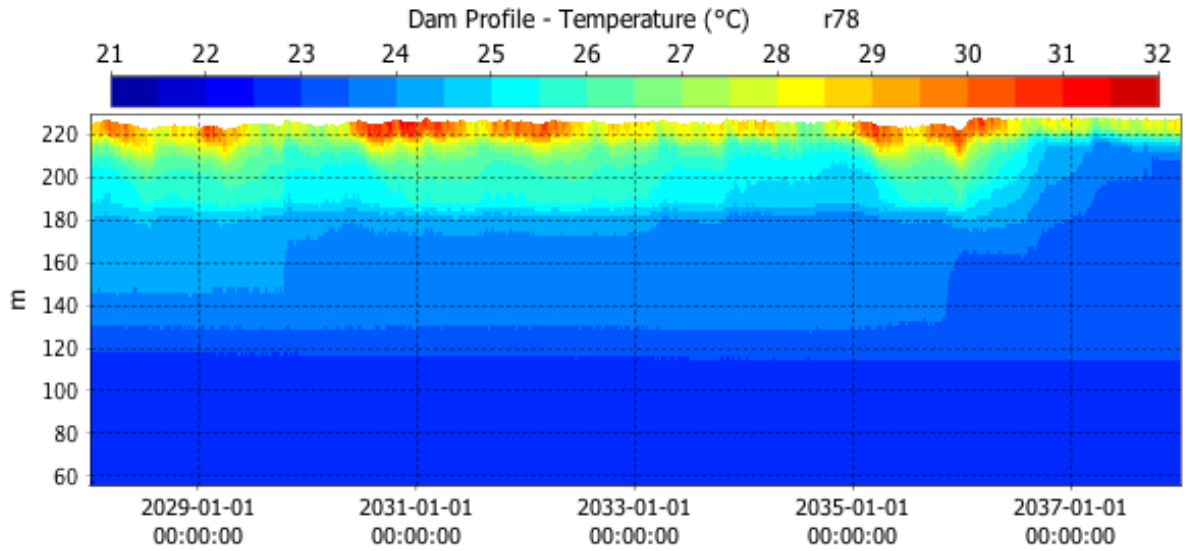

Figure 3.20 Temperature at the embankment during operations.

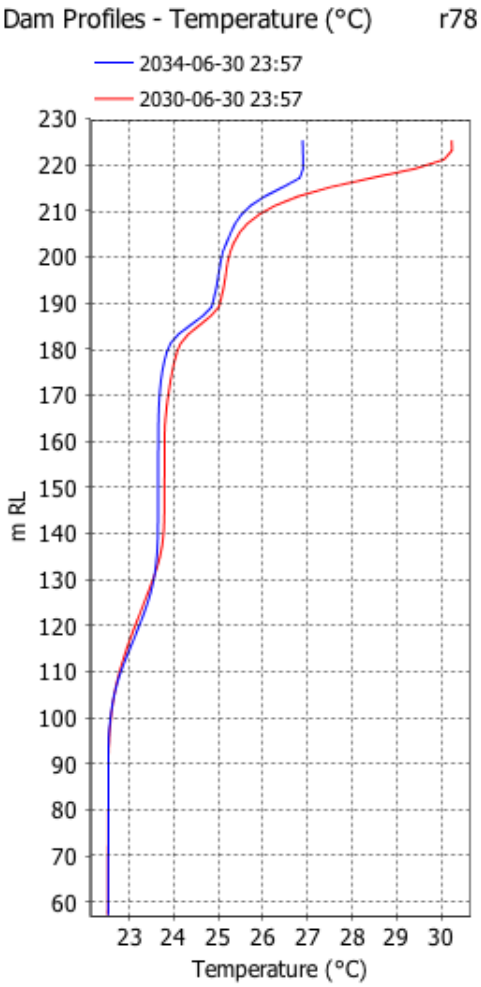

Figure 3.21 Temperature profile at the embankment during operations.

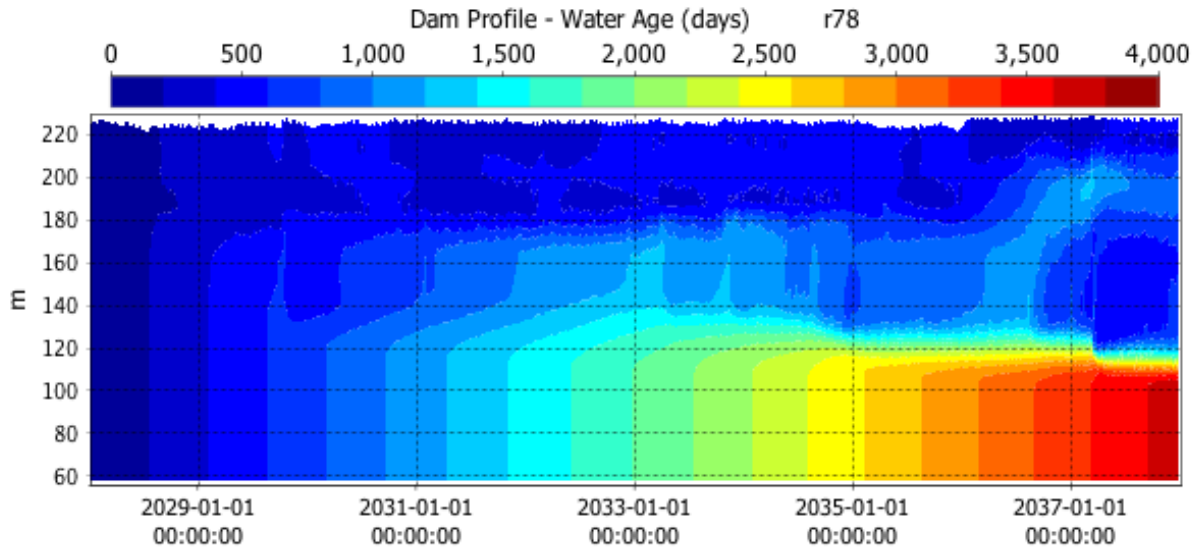

Figure 3.22 Simulated water age (in days) at the embankment during operations.

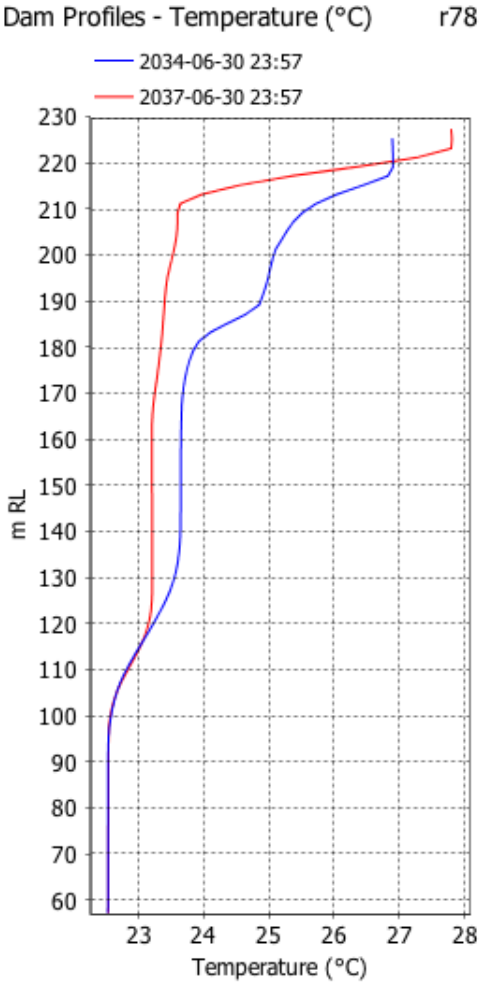

Figure 3.23 Temperature profile at the embankment during operations (blue) and closure (red).

Simulated temperatures along the Nena and Niar arms to the embankment (see Figure 3.24 and Figure 3.25) illustrate that the stratification observed at the embankment (deepest point of the reservoir) persists over much of the reservoir expanse as observed in the filing simulations. As a result the flow paths of the inflows and associated catchment sediment loads remain similar to the filling simulation after the adjustment from low to high elevation HEP intake (see Figure 3.26 to Figure 3.29), even with the inclusion of waste rock and tailings storage. The similarities between the hydrodynamics and sediment transport between the simulations with and without waste rock and tailings storage relates to the lack of mixing that takes place below the height of the waste rock and tailings storage (up to 159.4 m RL).

The persistent temperature stratification and lack of vertical mixing, coupled with inflow intrusions, results in the establishment of a preferential flow path whereby large tributary inflows intrude without extensive dilution with the ambient waters (particularly those of the hypolimnion). As illustrated in Figure 3.26, this leads to peaks in the concentration of Nena inflow tributaries overlying peaks in the Niar river tributaries at the height of the HEP intake at the embankment. The catchment sediment loads reaching the embankment peak below the height of the HEP intake and settle into the deeper waters (Figure 3.27 to Figure 3.29)

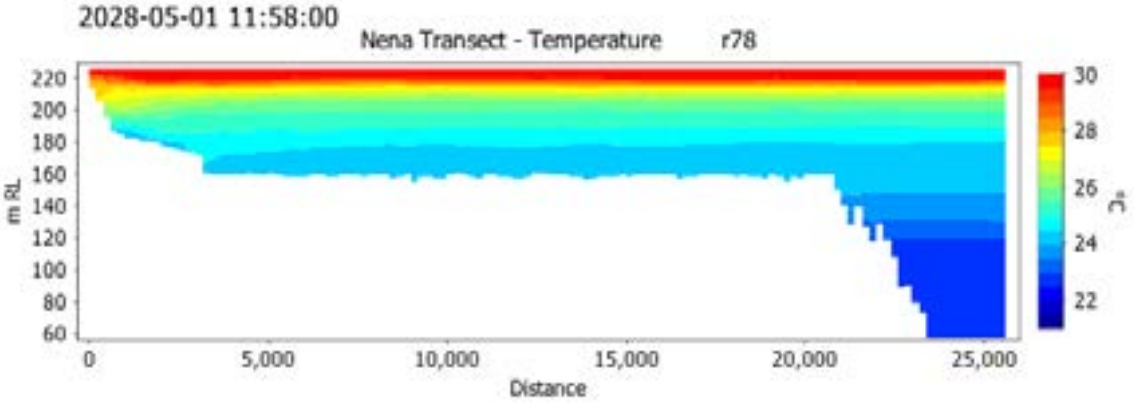

Figure 3.24 Simulated temperature from the headwaters of the Nena River (on the left of the figure) to the embankment (on the right) in May 2028.

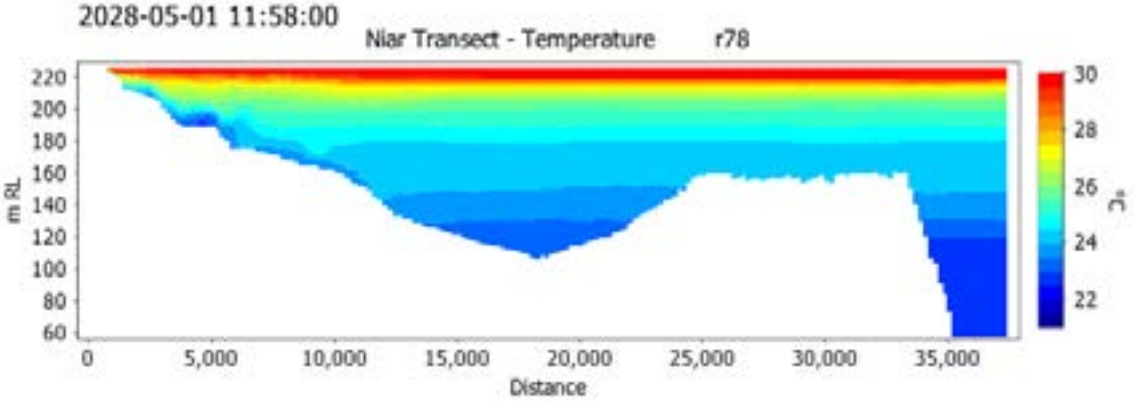

Figure 3.25 Simulated temperature from the headwaters of the Niar River (on the left of the figure) to the embankment (on the right) in May 2028.

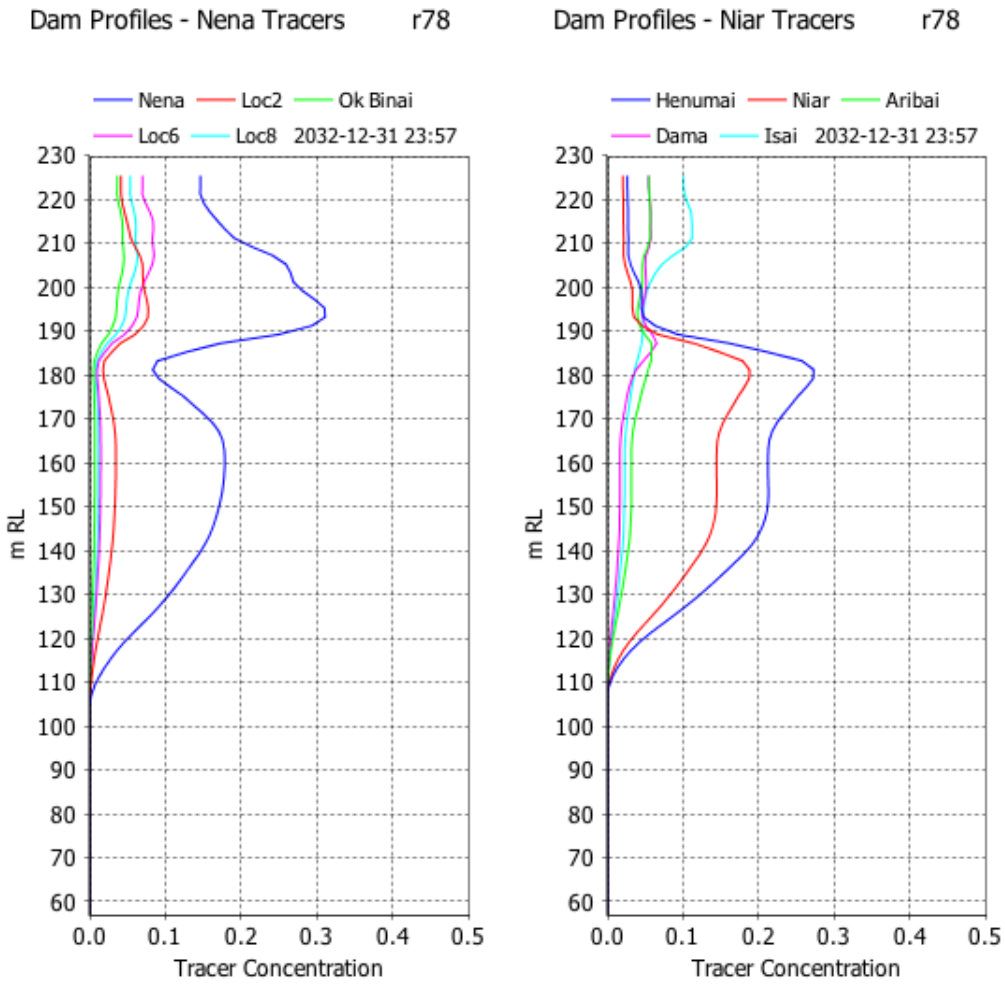

Figure 3.26 Simulated inflow fractions (0 to 1) in the waters at the embankment from inflows in the Nena/Ok Binai arm (left panel) and the Niar arm (right panel) of the reservoir. Simulation begins with no tracers in the profile.

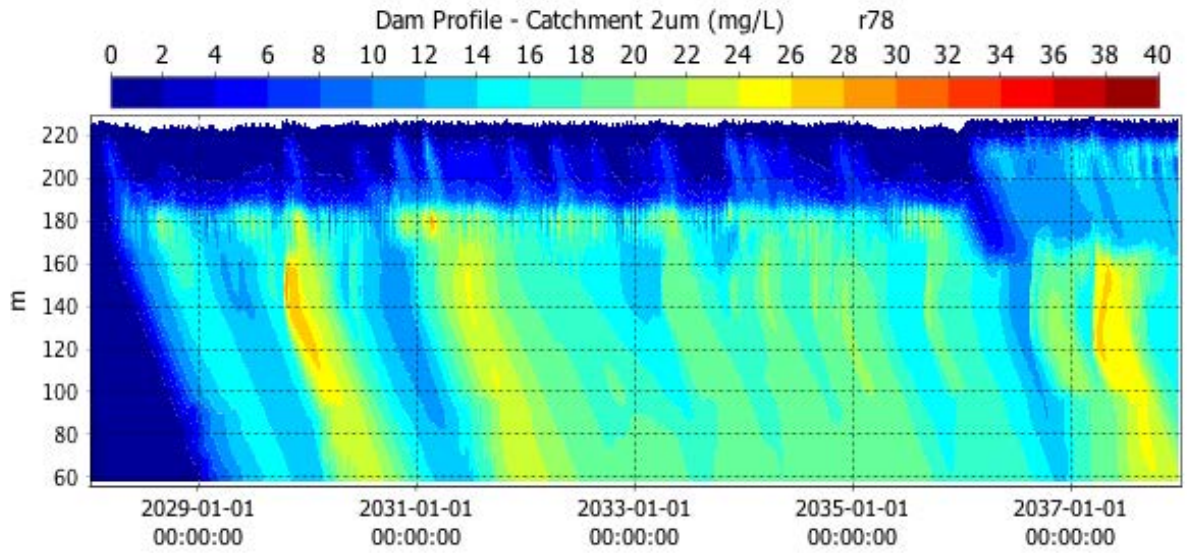

Figure 3.27 Simulated concentration (in mg L^{-1}) of 2-micron particles from catchment loads at the embankment.

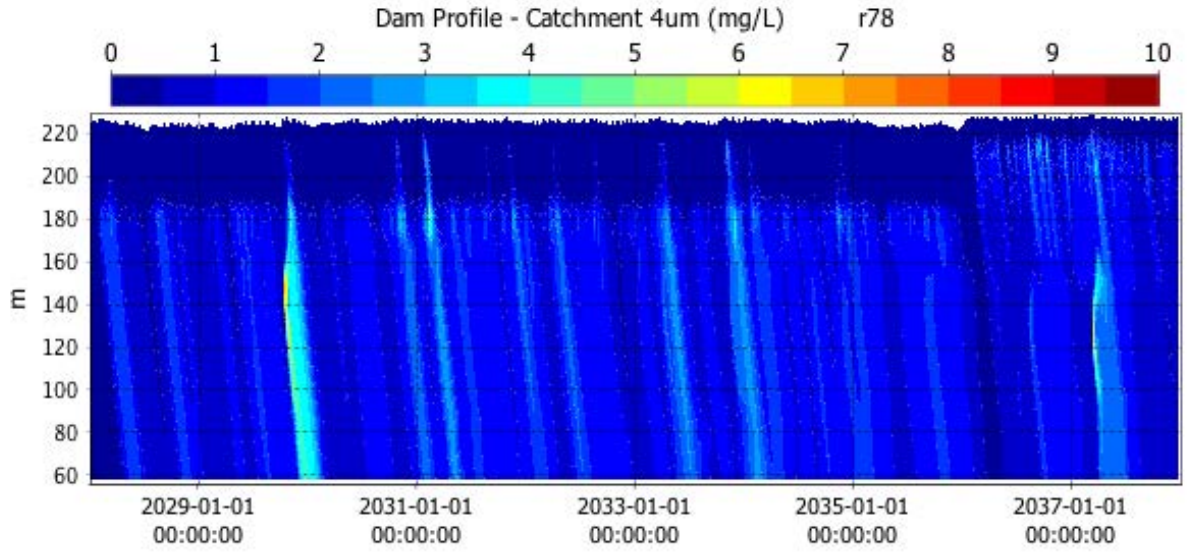

Figure 3.28 Simulated concentration (in mg L-1) of 4-micron particles from catchment loads at the embankment.

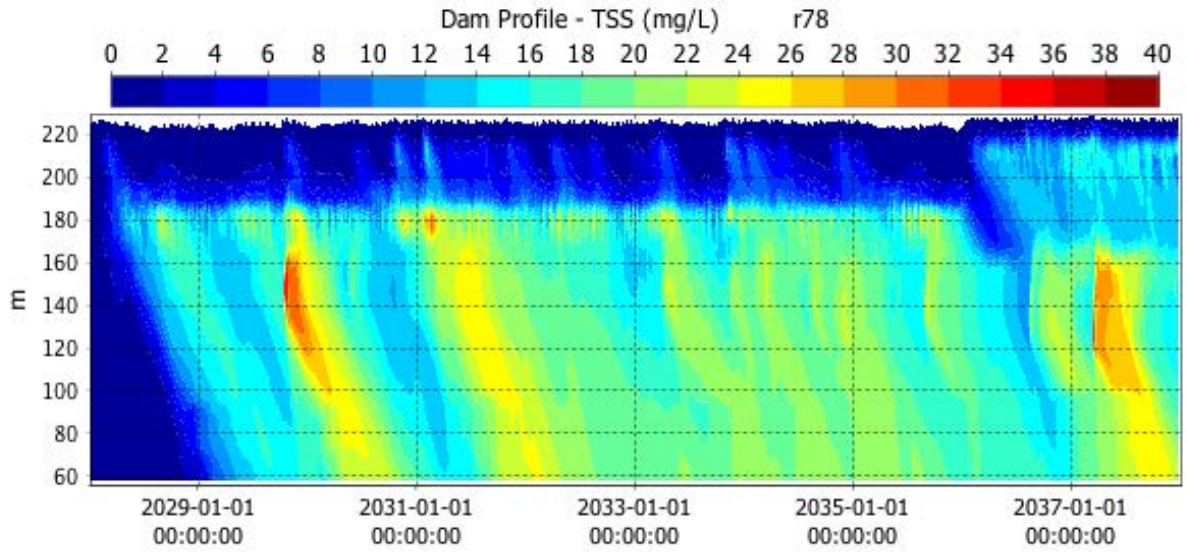

Figure 3.29 Simulated concentration (in mg L^{-1}) of TSS at the embankment.

3.3.3 Waste Rock and Tailings Mobility

Waste rock and tailings mobility was assessed for two cases using the operational HEP simulation and HEP closure simulation. The first, an equal mobility case, in which a single bed critical bed stress of 0.12 Pa is required to trigger suspension of waste rock and tailings regardless of the particle size. The second, derived mobility case, used estimates of critical shear stress derived as a function of particle size (see Table 3.6). The latter case is more conservative in that the fine sediments are more mobile under bed stress, when compared to the former case. The implications for the uncertainty associated with the estimates of resuspension are discussed in detail in the Appendix.

For the first case of equal mobility the resuspension of tailings from the upper Nena occurred during large flow events and the smallest sizes (which stay in suspension longer) reached the embankment (Figure 3.30) and exited the reservoir through the HEP intake in very low concentrations of less than 0.005 mg L^{-1} (Figure 3.31). For the equal mobility simulation there is no waste rock material that is resuspended and transported to the embankment because there is insufficient bed stress over the waste rock storage area to trigger resuspension.

Resuspension occurs in the upper Nena and the resuspended tailings are transported to the embankment along the Nena arm as illustrated in Figure 3.32 during the large inflows event on 6-8 October 2029 (flows in the Nena of 18-25 GL/day). At the peak of the event in on 8 October 2029, the 6-hour hydrographs have a lower flow than the 10 year ARI 6 hour hydrograph, based on the hydrology information provided by SRK (it is below the 10 year ARI event but could not be compared to the 5 year ARI as a corresponding flow was not provided). However, from visual inspection, 8 events of similar size occur over a 40-year time series, consistent with an approximately 5 year ARI. The results in Figure 3.30 indicate three similar events of tailings resuspension during the 10-year simulation.

Over time, some of the resuspended tailings settle into the deeper regions of the reservoir and some of the tailings are entrained into flow that propagates towards the embankment. The specific patterns of dilution and transport for each resuspension plume will depend on the broader hydrodynamics in the reservoir during and after resuspension, including the influence of inflow currents, counter-currents and vertical mixing rates.

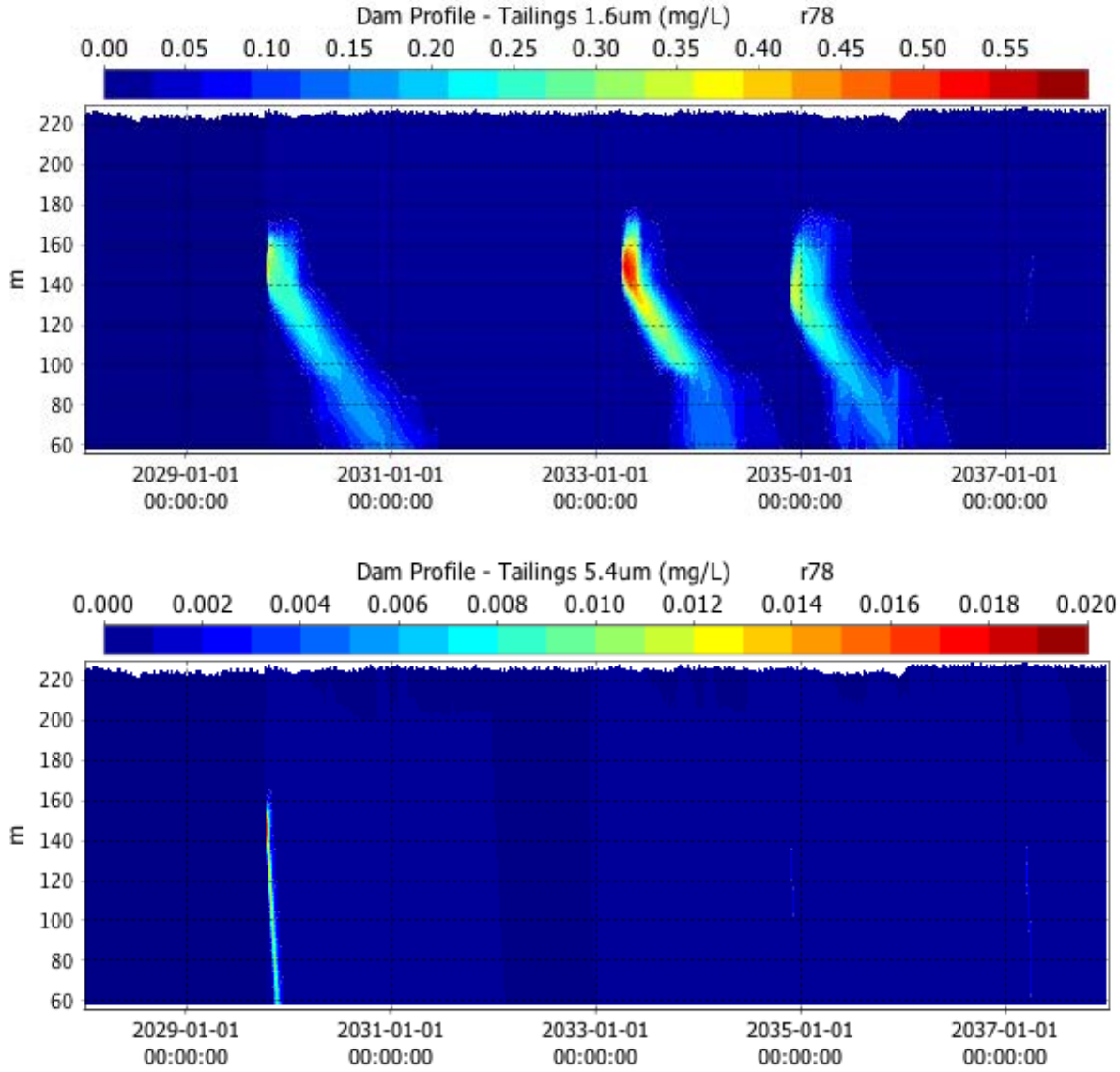

Figure 3.30 Concentrations of 1.6-micron (top panel) and 5.4-micron (bottom panel) tailings at the embankment during the equal mobility simulation.

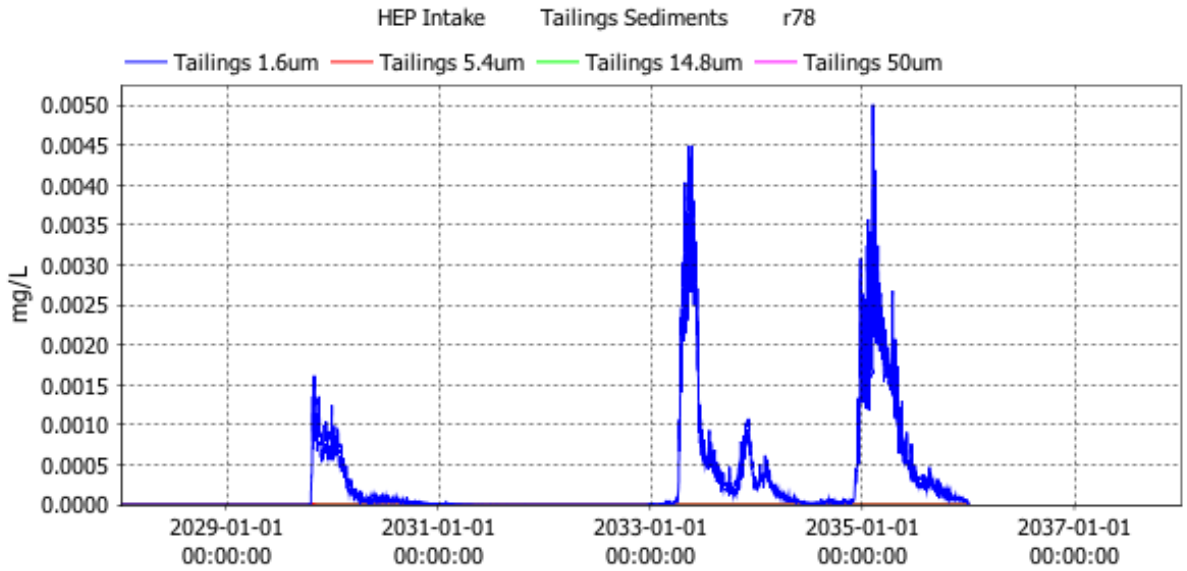

Figure 3.31 Concentrations of tailings in HEP intake water during the equal mobility simulation.

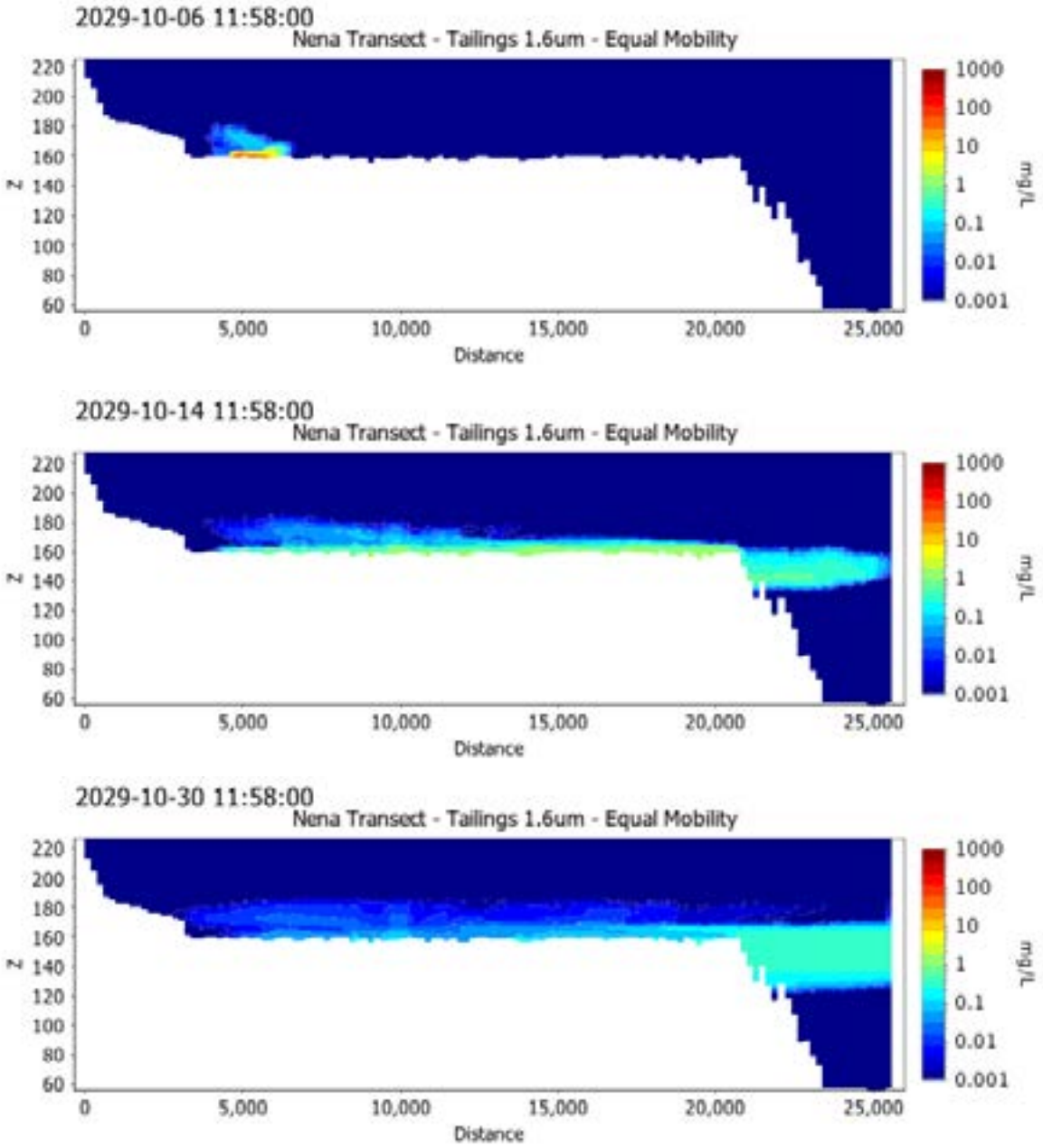

Figure 3.32 Series of contour figures showing the concentrations of re-suspended tailings (1.6 micron fraction) in transect from the Nena River headwaters to the embankment during October 2029 for the equal mobility case.

For the second case with derived critical shear stress the finer waste rock and tailings material resuspends at a lower critical shear stress which leads to a more concentrated resuspension plume (see Figure 3.33) and higher concentrations of resuspended material reaching the embankment and exiting with the HEP intake waters, including contributions from resuspended waste rock (see Figure 3.34 and Figure 3.35). The results also indicate a far greater frequency (on average approximately 1-2 times per year) of events that resuspended the fine fraction of waste rock and tailings and transport the resuspended material to the embankment.

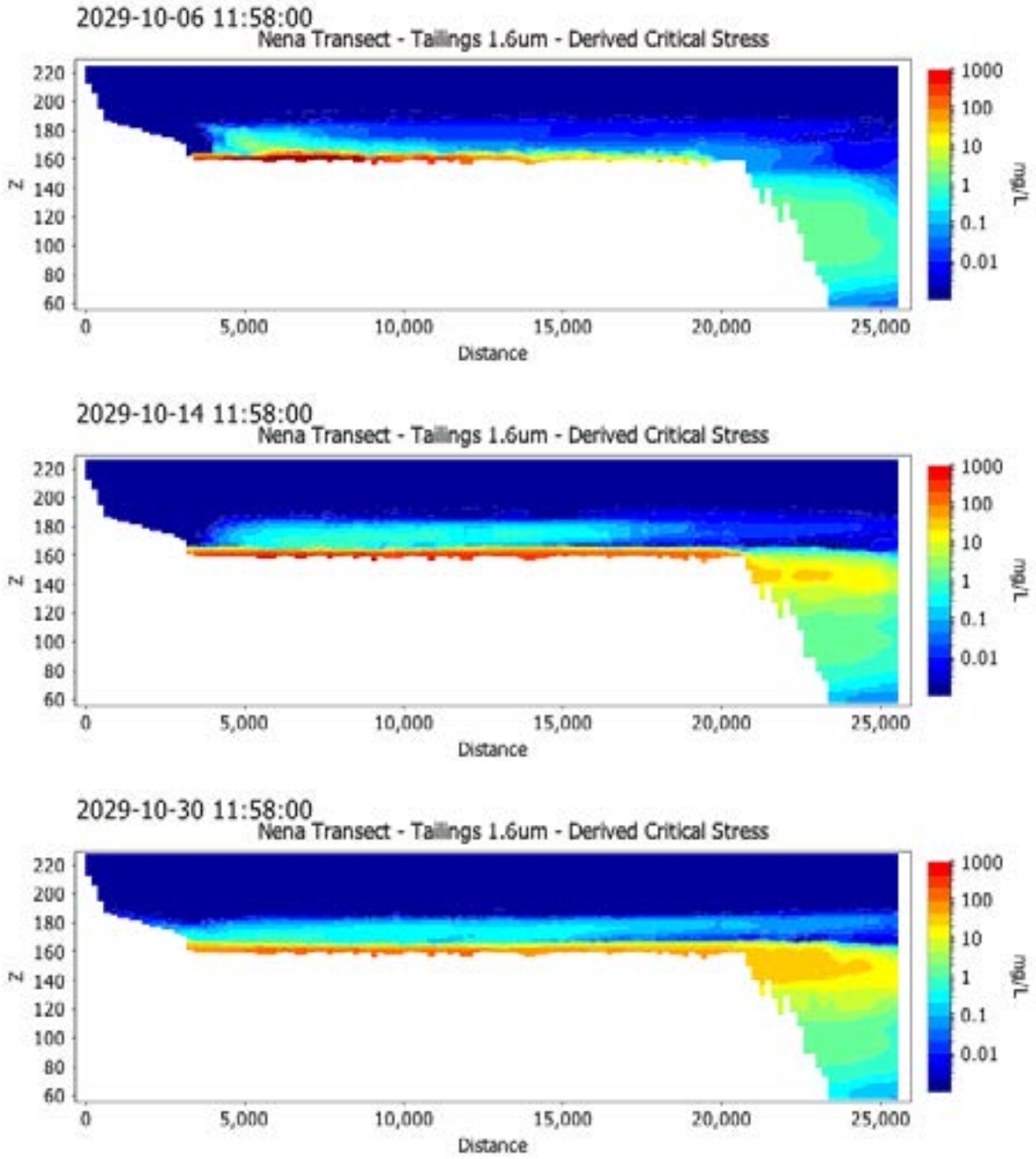

Figure 3.33 Series of contour figures showing the concentrations of re-suspended tailings (1.6 micron fraction) in transect from the Nena River headwaters to the embankment during October 2029 for the derived mobility case.

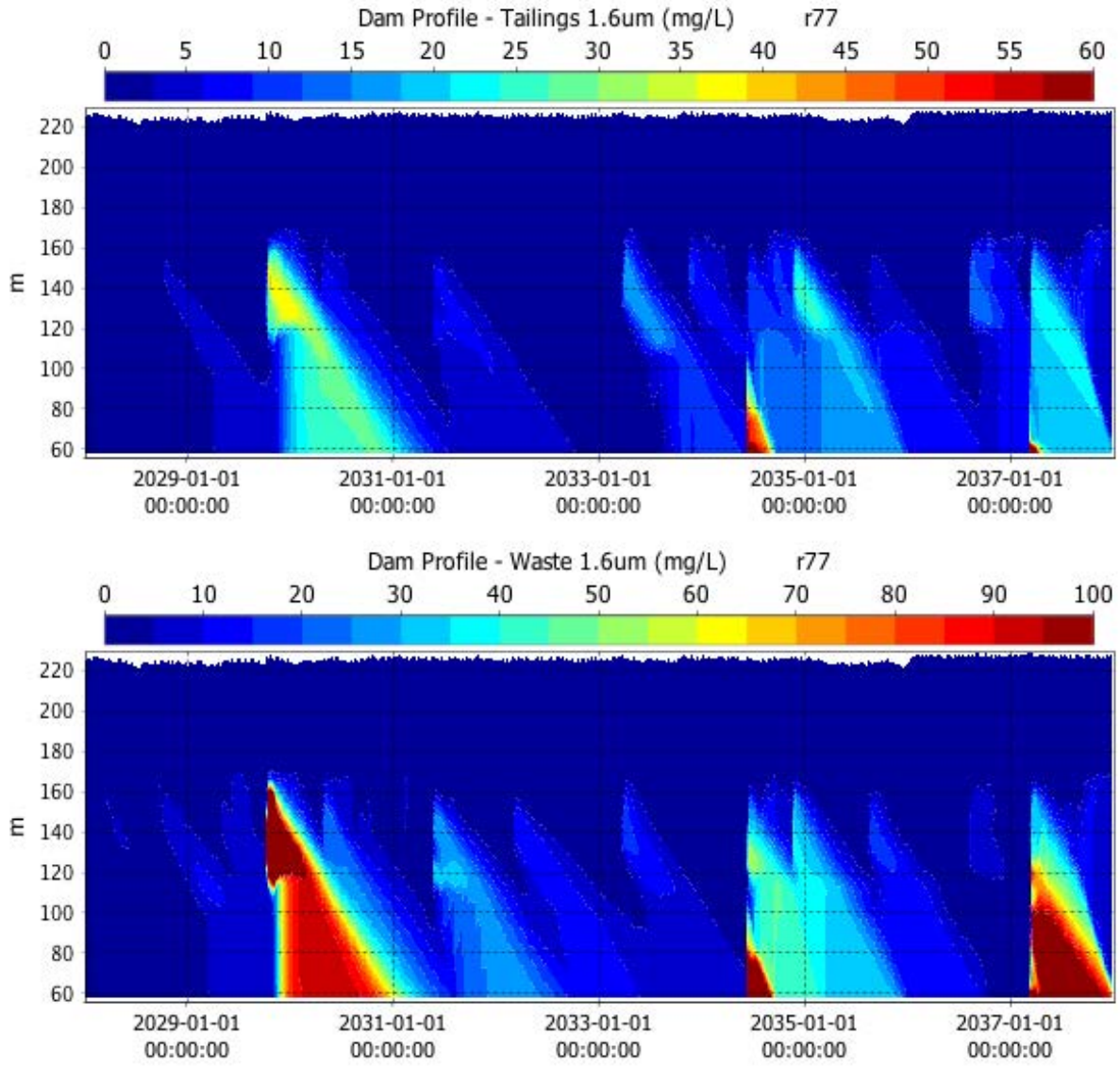

Figure 3.34 Concentrations of 1.6-micron tailings (top panel) and 1.6-micron waste rock (bottom panel) at the embankment during the derived mobility simulation.

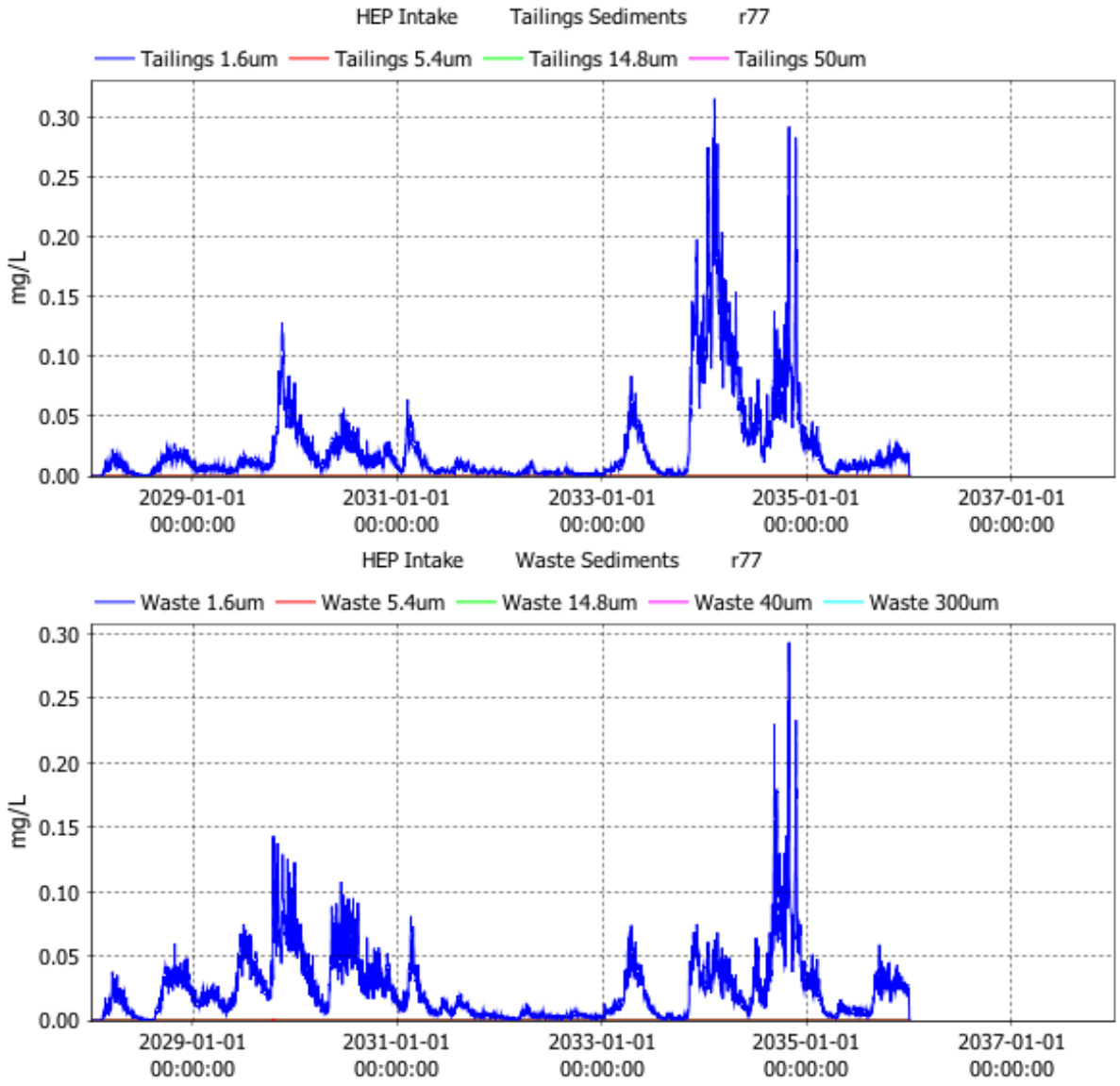

Figure 3.35 Concentrations of tailings (top panel) and waste rock (bottom panel) in HEP intake water during the derived mobility simulation.

When the derived mobility is applied resuspension of stored tailings also occurs in the Niar arm of the reservoir. There is resuspension of the stored tailings near the bottom; however, much of the localised resuspension is trapped in the bathymetric depression in the mid-Niar (see Figure 3.36).

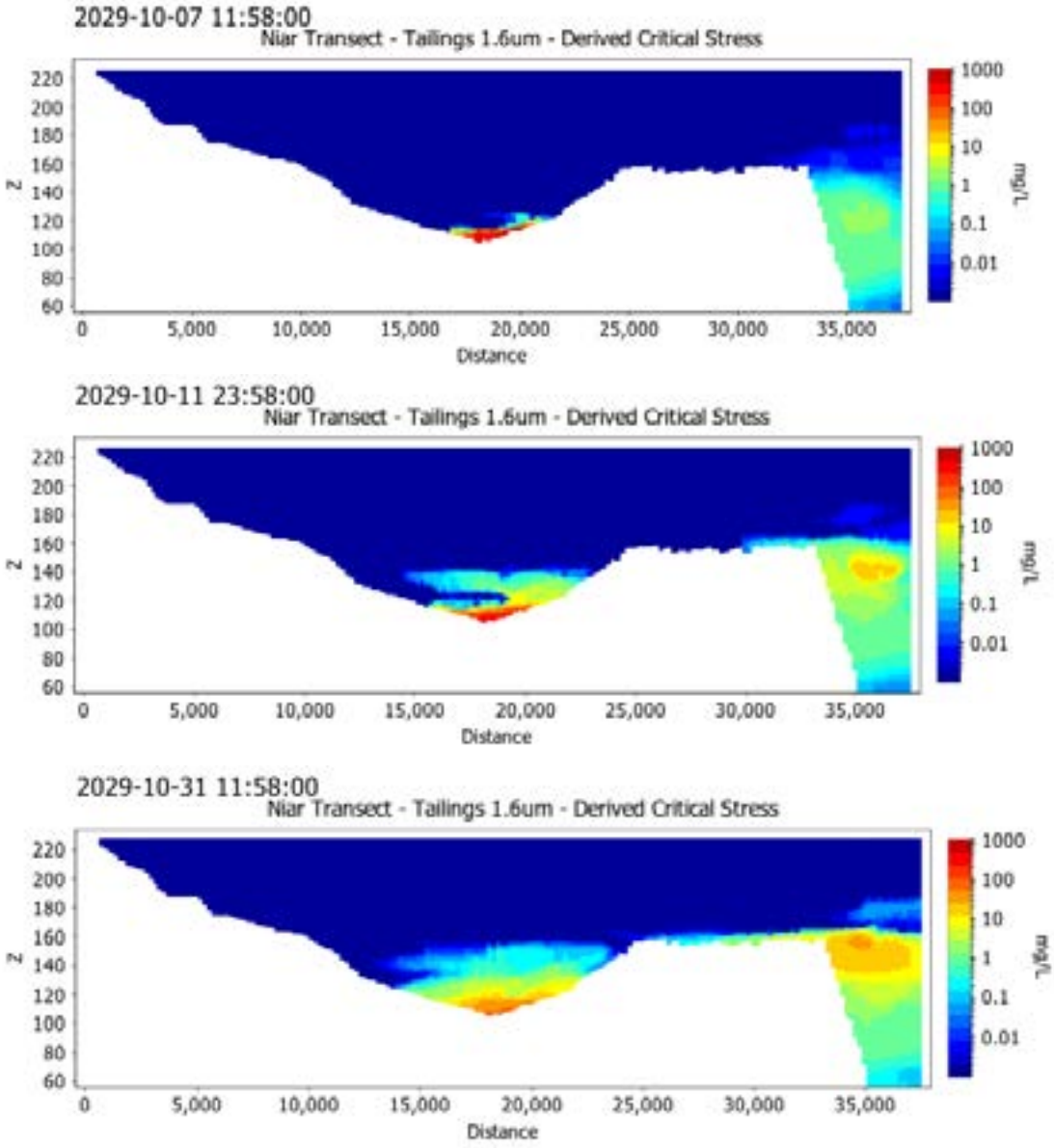

Figure 3.36 Series of contour figures showing the concentrations of re-suspended tailings (1.6 micron fraction) in transect from the Niar River headwaters to the embankment during October 2029.

The Nena and Niar arm resuspension features are illustrated in plan view in Figure 3.37 and Figure 3.38, which show initial resuspension and subsequent transport of the resuspended material. The suspended fine tailings in the lower Niar arm are the result of resuspension in the Upper Nena that has been transported downstream to the junction of the arms and upstream into the Niar arm. The localised resuspension in the mid-Niar spreads into the bathymetric depression but is contained within the depression.

The plan view of bottom concentrations of waste rock and tailings fractions after 10 years of simulation (see Figure 3.39 and Figure 3.40) illustrate the increased re-distribution of waste rock and tailings that occurs for the smaller sizes. The results indicate that for the derived mobility case the finest portions of the waste rock and tailings are likely to spread and re-settle throughout much of the reservoir.

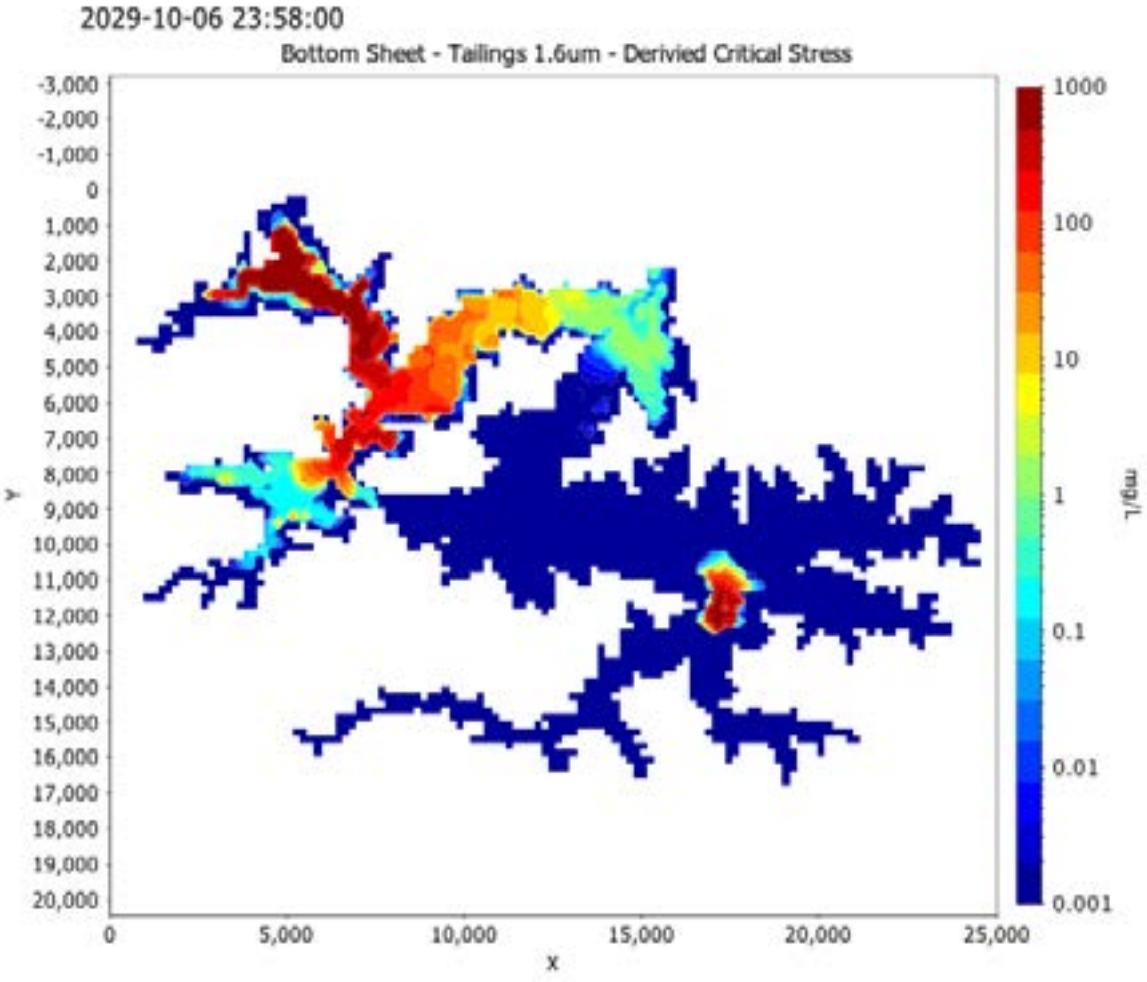

Figure 3.37 Plan view of re-suspended 1.6-micron tailings material showing concentrations at the bottom at the beginning of the large flow events in early October 2029.

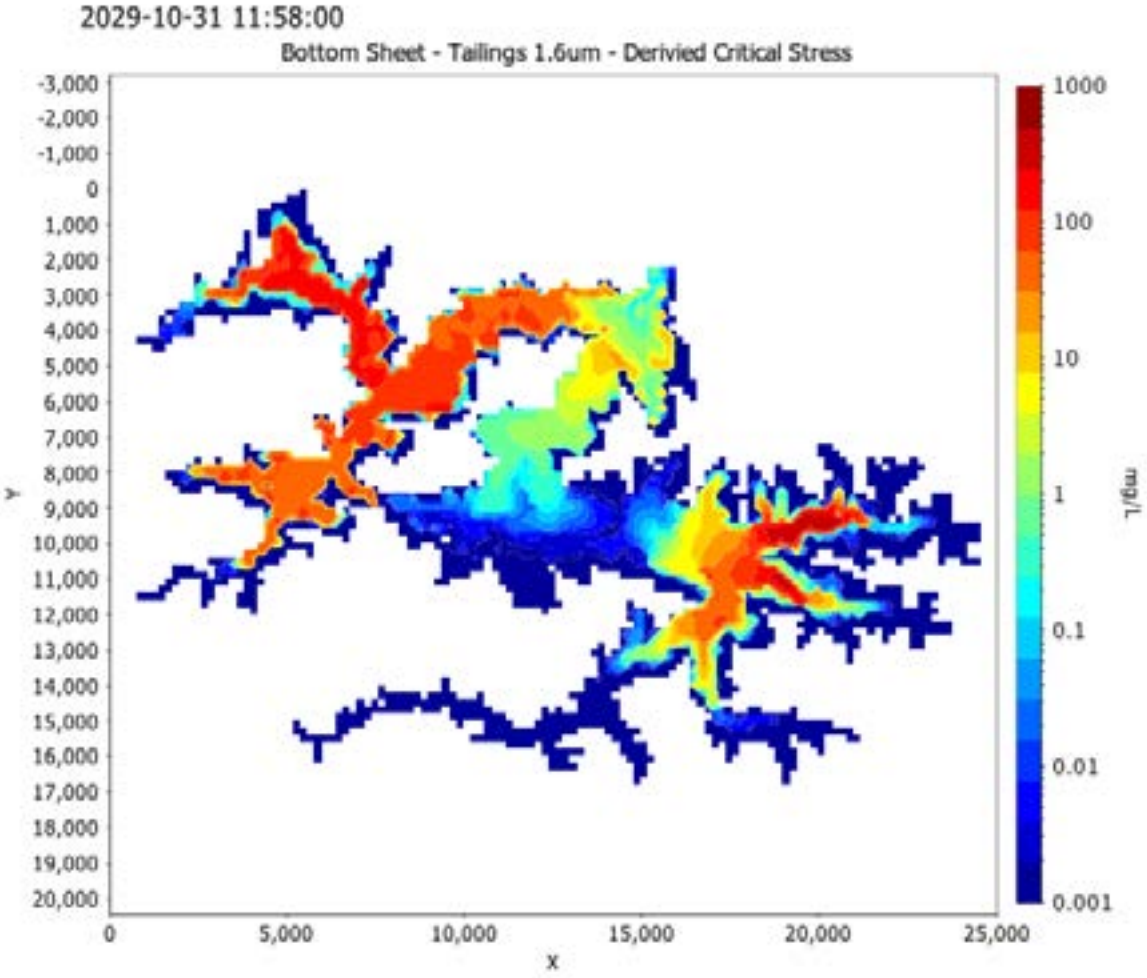

Figure 3.38 Plan view of re-suspended 1.6-micron tailings material showing concentrations at the bottom at the end of October 2029.

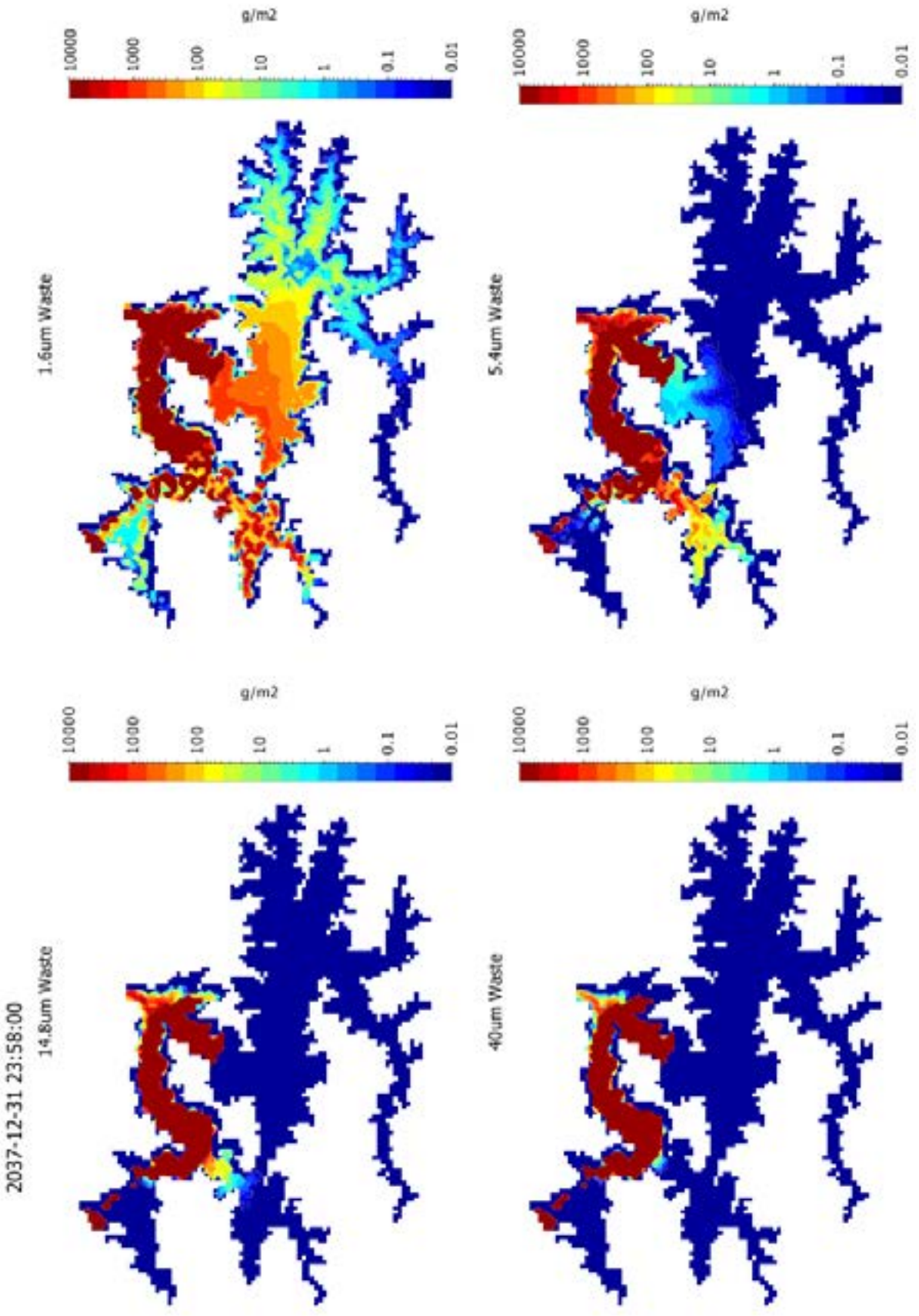

Figure 3.39 Plan view of area concentrations of waste rock at the bottom of the reservoir after 10 years of simulation.

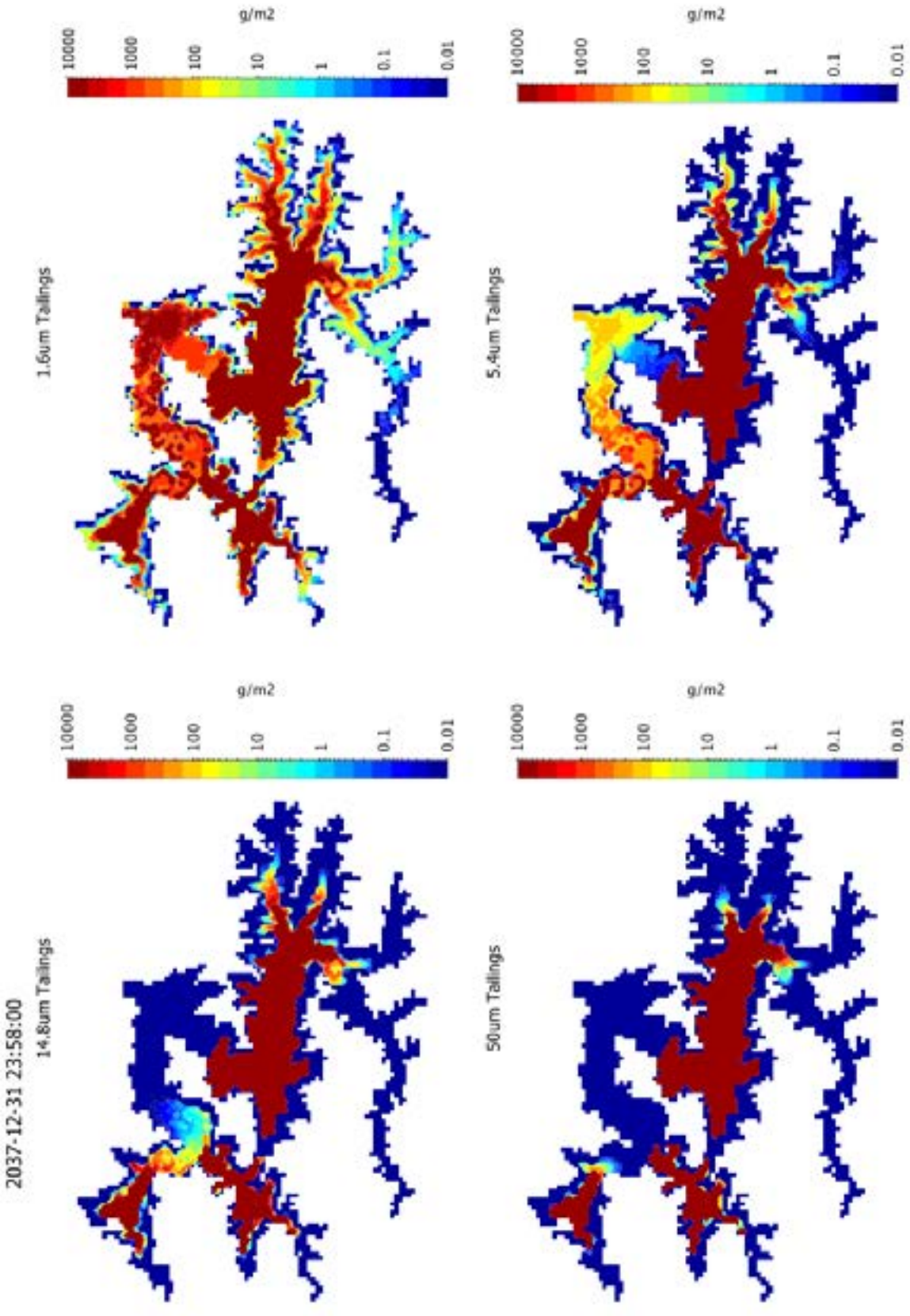

Figure 3.40 Plan view of areal concentrations of tailings at the bottom of the reservoir after 10 years of simulation.

3.3.4 HEP Closure

HEP closure (i.e. spillway only outflow) in the last years of the operations simulations shows that there is likely to be a significant shift in the temperature stratification (see Figure 3.23) compared to when the HEP is operating. The simulations of equal mobility and derived mobility for the stored waste rock and tailings were extended to assess potential long-term change in the physical limnology.

For the case with equal mobility of stored waste rock and tailings the simulated water age at embankment (illustrated in Figure 3.41) shows that whilst there is there is continued isolation of the deepest waters, there is a slow deepening of the water-age gradient. This indicates that over time new inflow waters are penetrating deeper into the water column as the temperature homogenises in the hypolimnion below 210 m RL (Figure 3.42). This in turn increases the plunging depth of the Niar-arm tributaries (and occasionally the Nena) (see Figure 3.43 and Figure 3.44). Large and plunging Nena flows, as is simulated in early 2040, are associated with the delivery of fine tailings material to the embankment (Figure 3.45). However, the concentrations that are released downstream from the spillway in response to these events are very low (Figure 3.46) because the rates of mixing and exchange between the epilimnion waters (that exit the spillway) and the water beneath remains very small.

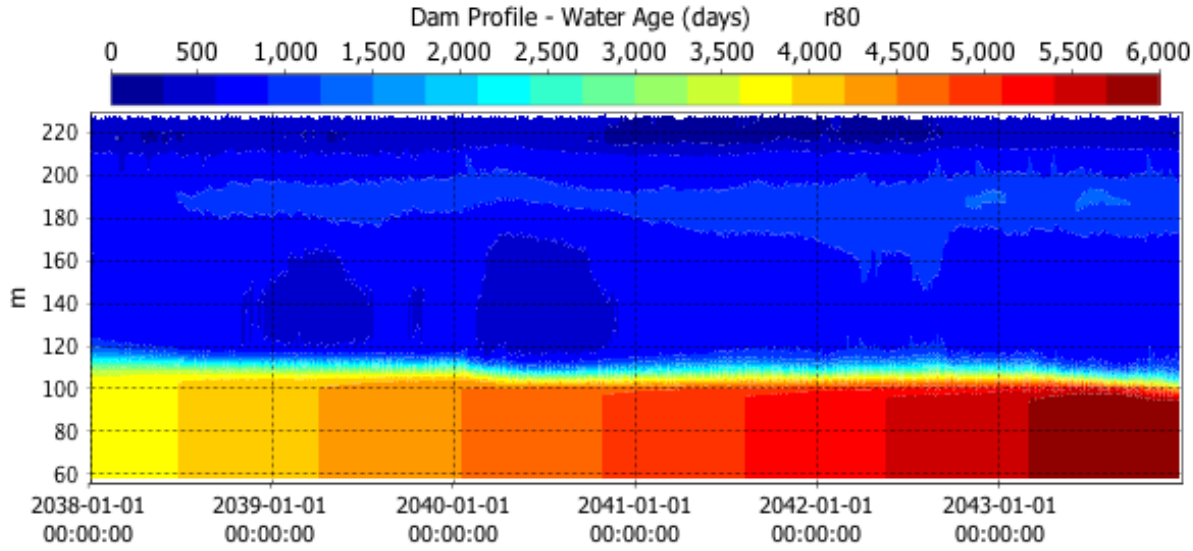

Figure 3.41 Simulated water age at the embankment for the extended HEP closure simulation with equal mobility.

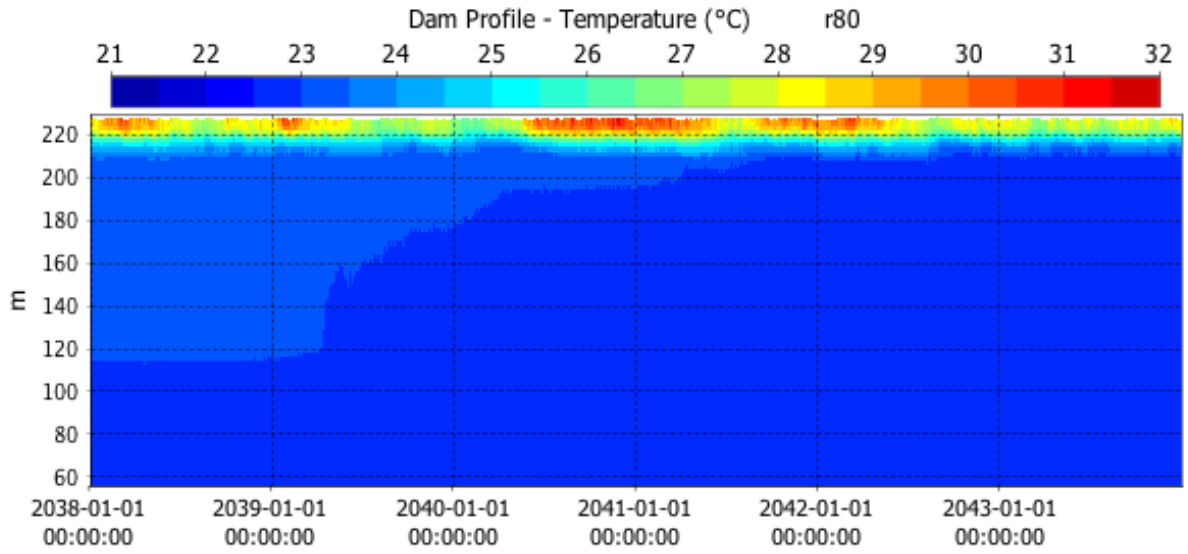

Figure 3.42 Simulated temperature at the embankment for the extended HEP closure simulation with equal mobility.

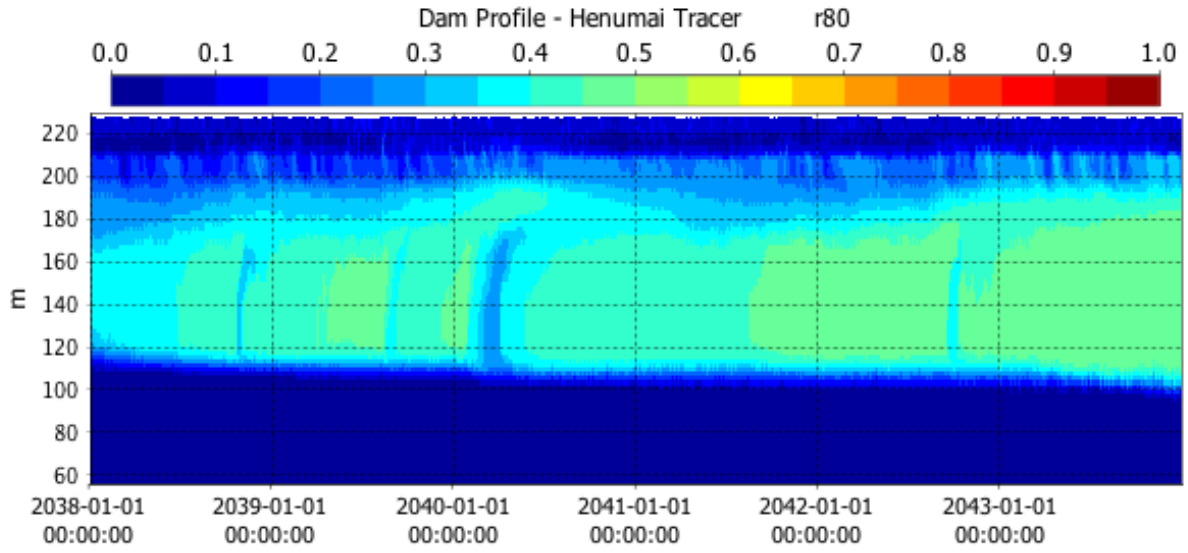

Figure 3.43 Simulated Henumai tracer at the embankment for the extended HEP closure simulation with equal mobility.

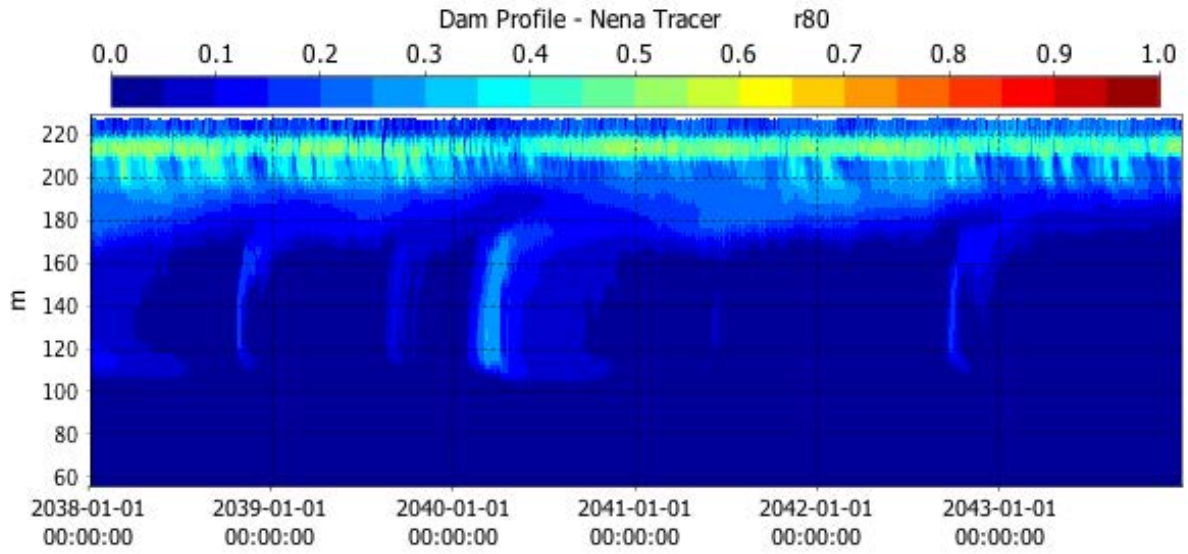

Figure 3.44 Simulated Nena Tracer at the embankment for the extended HEP closure simulation with equal mobility.

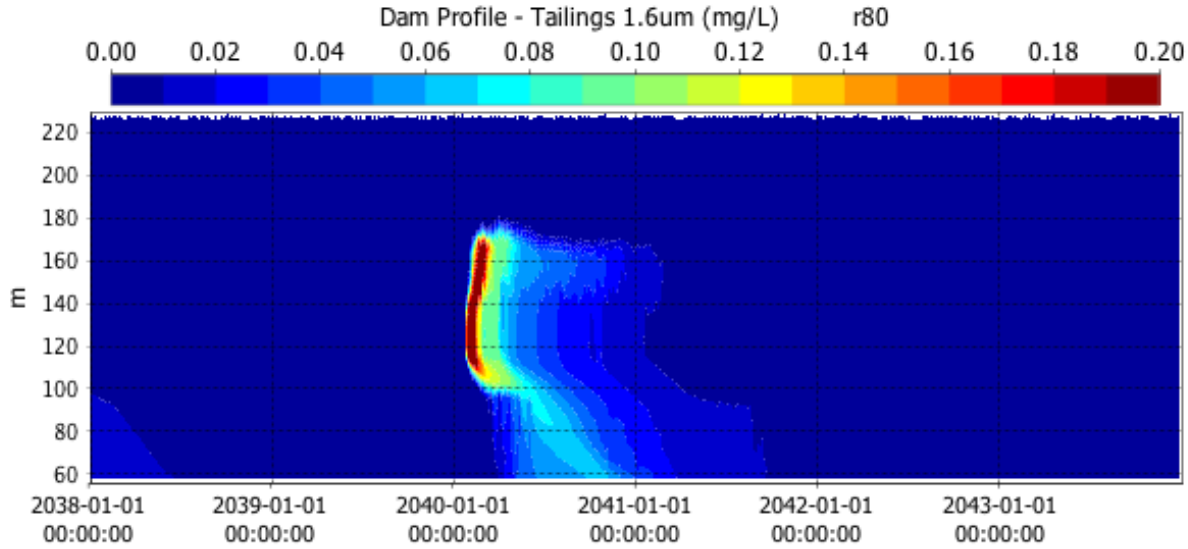

Figure 3.45 Simulated 1.6-micron tailings at the embankment for the extended HEP closure simulation with equal mobility.

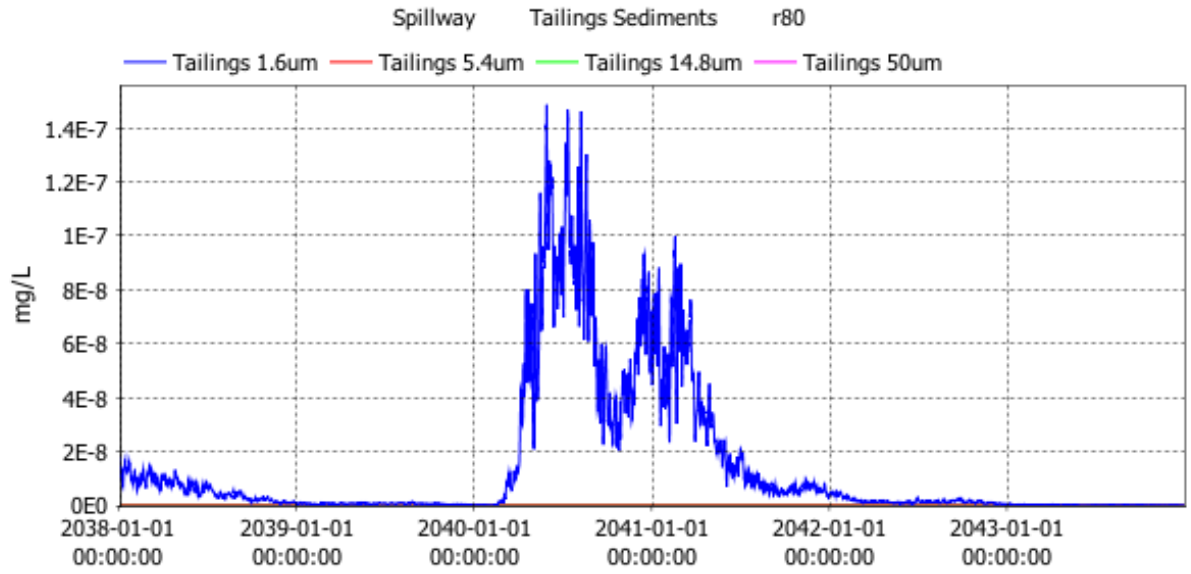

Figure 3.46 Simulated tailings concentrations in water running over the spillway during the extended HEP closure simulation with equal mobility.

For the derived mobility simulations there is a distinct change in the limnology after the HEP closure. The higher frequency and rates of suspension of sediments (catchment, waste rock and tailings) leads to an increase in the density of the inflow intrusions as they pass through the reservoir (see for example Figure 3.47). As a consequence the inflows plunge into the deeper waters leading to a refreshment of the hypolimnion that is clearly indicated in the water age at the embankment (Figure 3.48) and penetration of inflows to the bottom of the reservoir (Figure 3.49 and Figure 3.50). Despite changes to the basic mixing regime in the deeper waters the concentrations of waste rock and tailings material released from the spillway remain less than 0.001 mg/L (Figure 3.51).

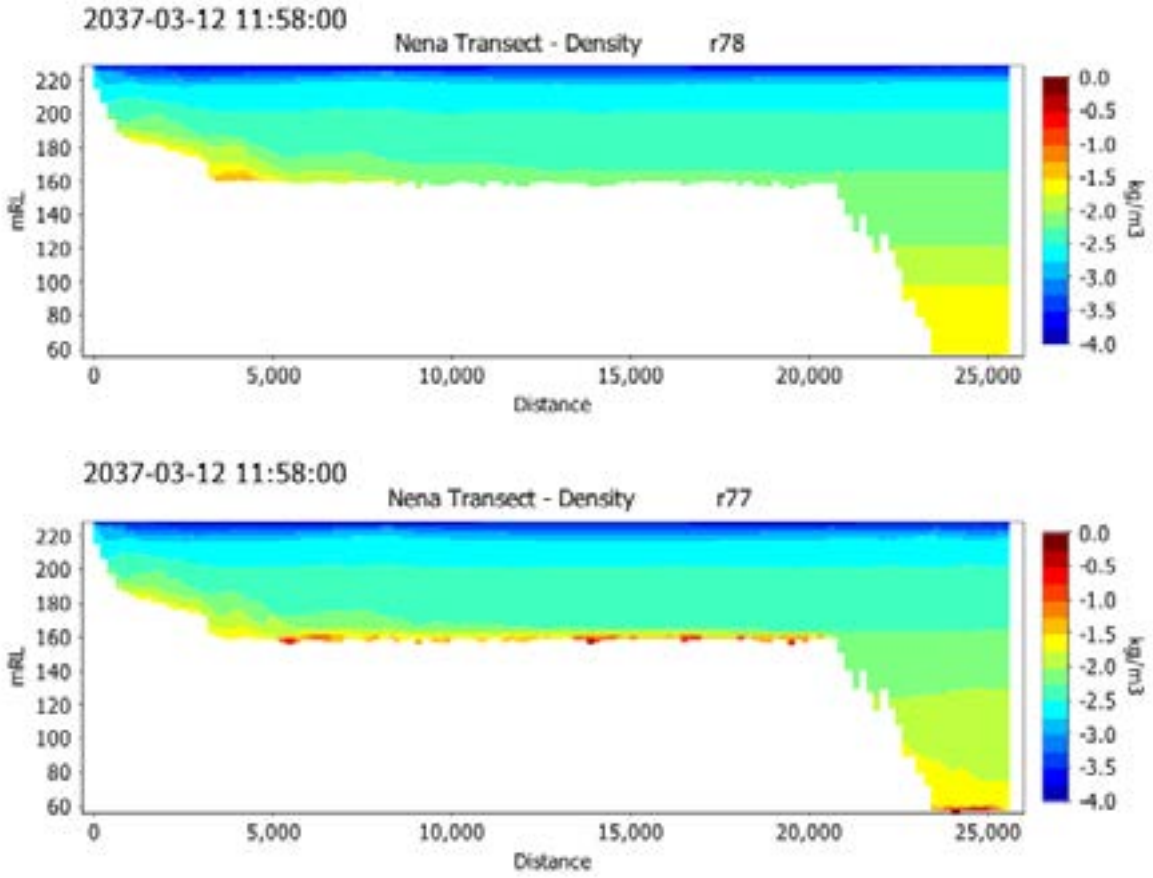

Figure 3.47 Density anomaly (from 1000 kg m^{-3}) in the Nena arm transect during an inflow event after HEP-closure for the equal mobility case (upper panel) and derived mobility case (lower panel).

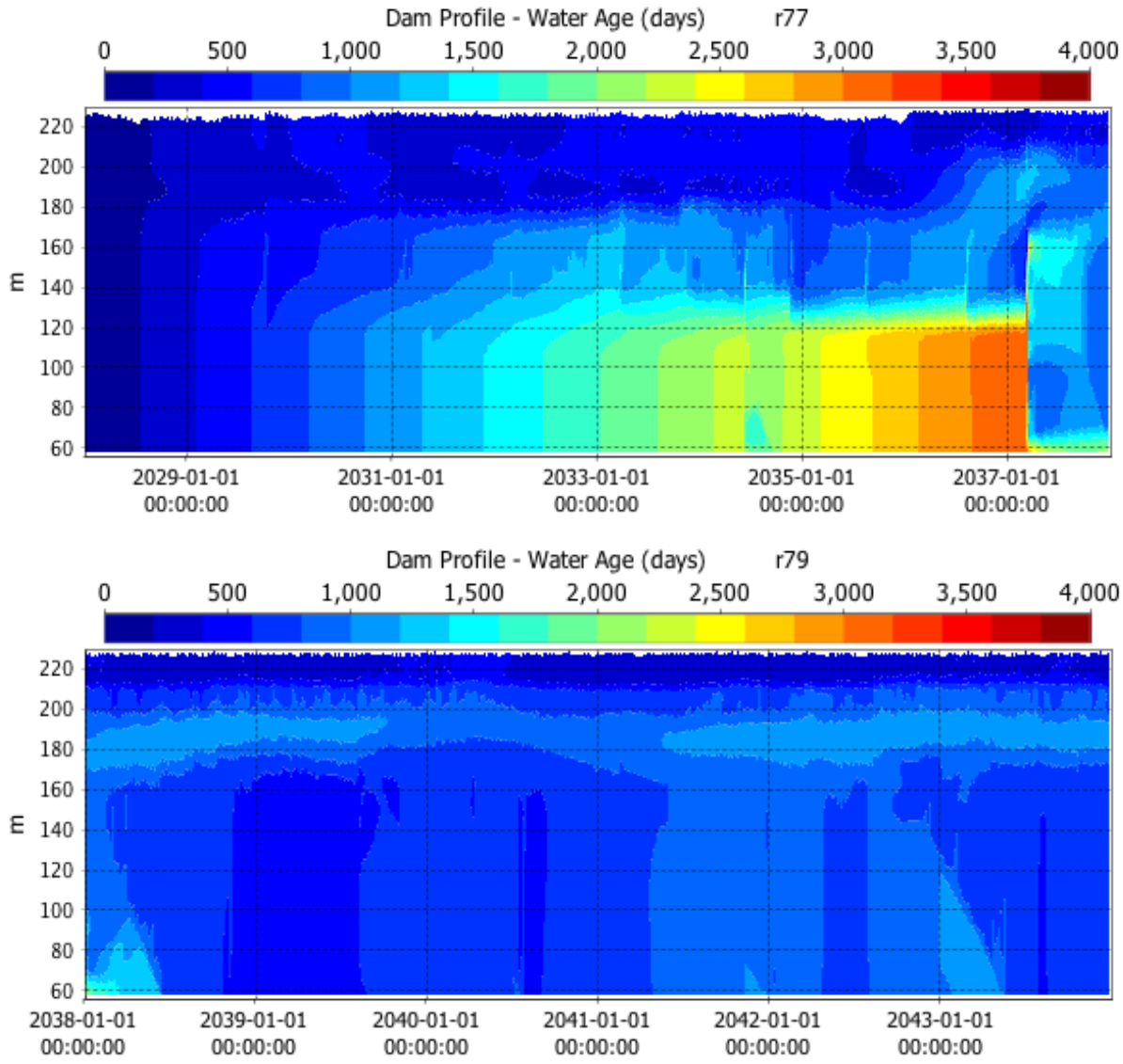

Figure 3.48 Simulated water age at the embankment during shift from HEP operations to HEP closure for derived mobility case (see 2037 in top panel) and continued HEP closure simulation (bottom panel).

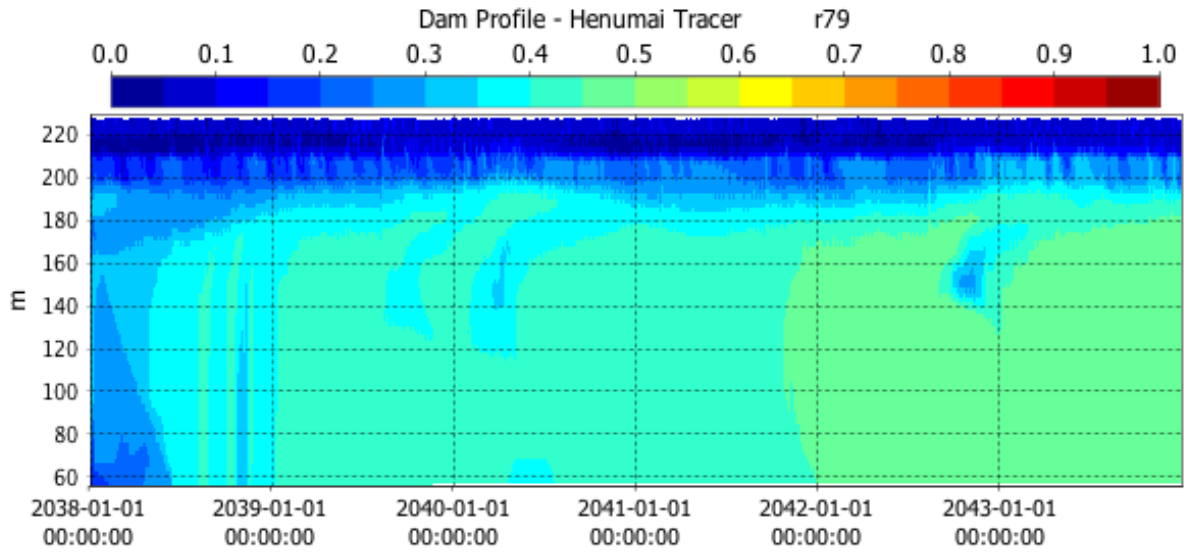

Figure 3.49 Simulated Henumai Tracer at the embankment for the extended HEP closure simulation with derived mobility.

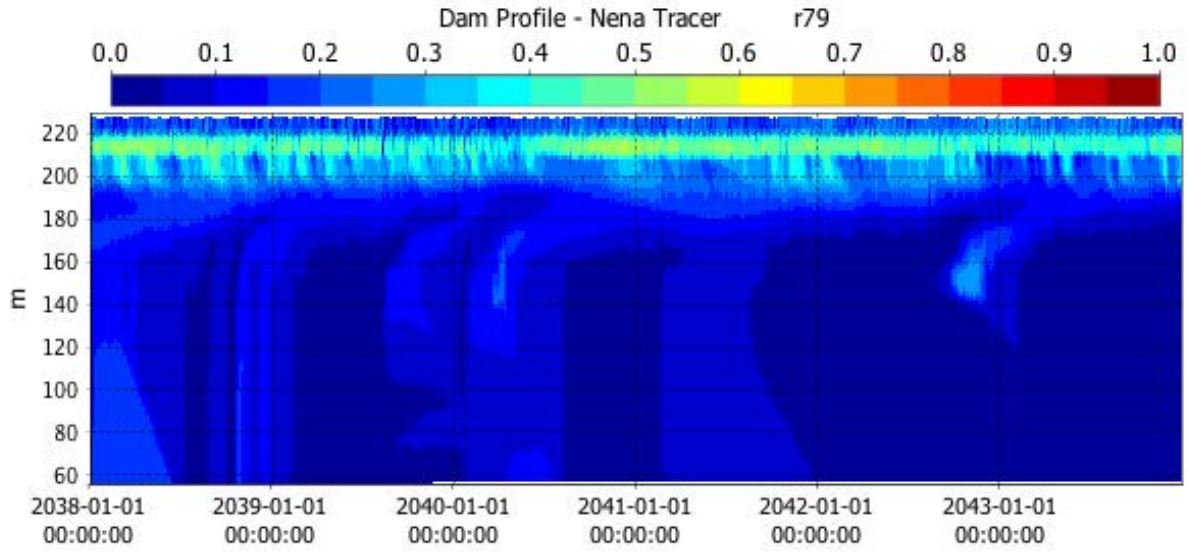

Figure 3.50 Simulated Nena Tracer at the embankment for the extended HEP closure simulation with derived mobility.

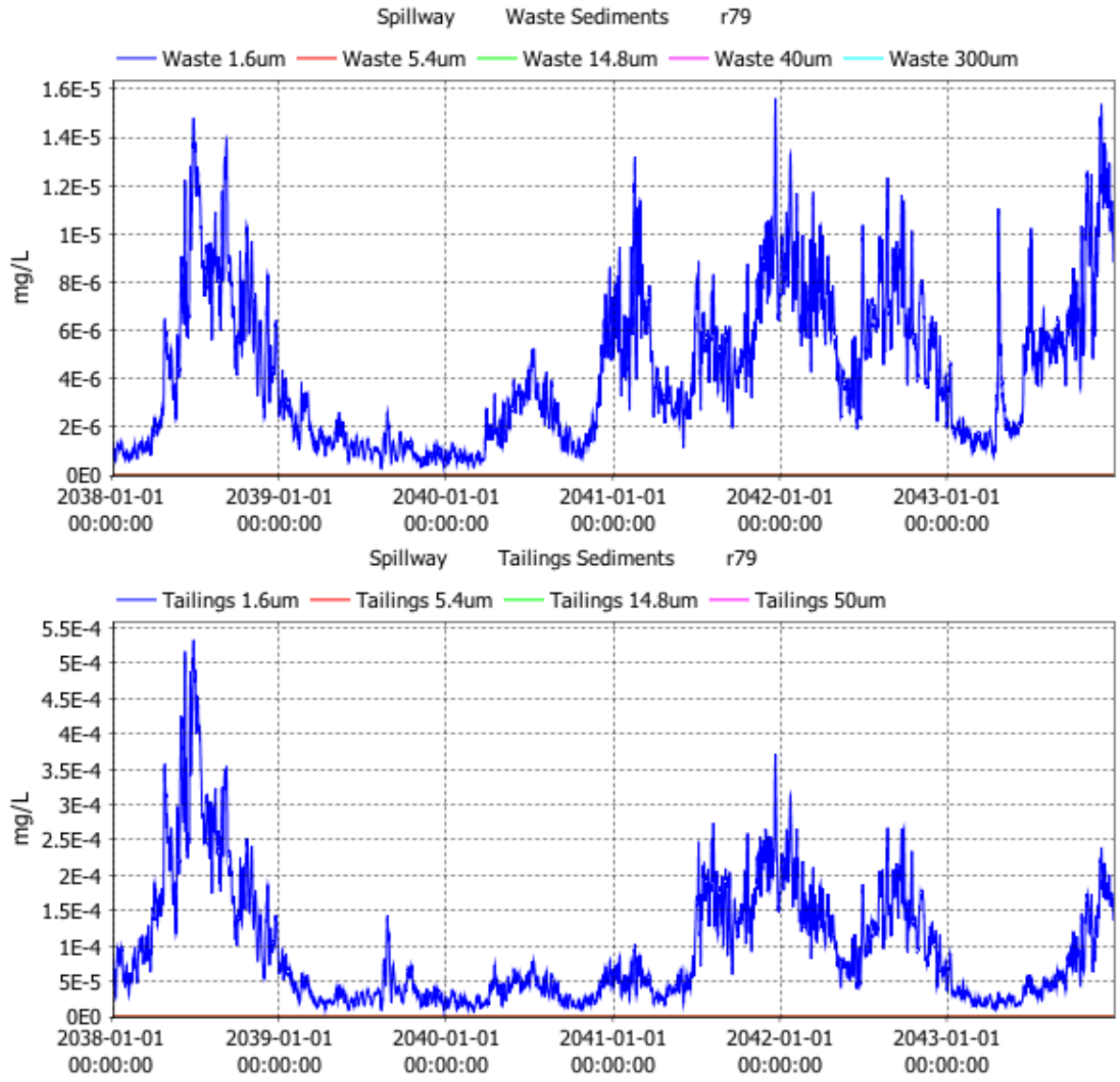

Figure 3.51 Simulated waste rock (top panel) and tailings (bottom panel) concentrations in water running over the spillway during the extended HEP closure simulation with derived mobility.

3.3.5 Downstream Release

Tables of the simulated properties of the downstream release waters for the filling simulation from the deep tunnel (Table 3.8), low level HEP intake (Table 3.9), operational level HEP intake (Table 3.10), spillway (Table 3.11) and combined volume-weighed combination of operation HEP intake water and spillway release water (Table 3.12) are provided below. Summaries of the operation level HEP intake, spillway and volume-weighted combination have been provided for the equal mobility operational simulation (Table 3.13 to Table 3.15) and derived mobility operational simulation (Table 3.16 to Table 3.18). Summaries of spillway releases after HEP closure for the equal mobility and derived mobility case are provided in Table 3.19 and Table 3.20, respectively. Illustrations of the time series of downstream release water are provided in the Appendix. Note that the contribution to downstream release from barging of waste rock is considered separately in Section 3.3.6 below.

A summary table of sediment concentrations in the downstream release water is provided in Table 3.7. The results show that during the filling simulation less than 7% of the incoming catchment sediments (which includes sediment contribution from mine related activities

upstream of the reservoir, see Section 3.2.4 for details) are released from the embankment. Average concentrations are highest at approximately 50 mg L-1 during operation of the deep tunnel, reducing to an average release concentration of approximately 16 mg L-1 (combined HEP and spillway) when the high level HEP is operating. A large majority of the released sediment is the finest 2-micron size fraction.

In the second simulation when the reservoir is full and the HEP is operating, despite a small increase in the percentage of catchment TSS exiting the reservoir (up to 7.25%) there is less inflow TSS so the average concentrations released downstream reduces to approximately 12 mg L-1 and is mostly fine catchment sediment. There is only a very small increase in the TSS release concentrations between the equal mobility and derived mobility case, which is because of increased resuspension of the catchment sediments that settle in the reservoir and an increased contribution from waste rock and tailings sediments (see Table 3.16 to Table 3.18) when the particulates are more mobile under the derived mobility case.

Undertaking a budget of the store of waste rock and tailings on the reservoir bed over the duration of the simulations suggests that in the equal mobility simulation when the HEP and spillway are operating there is approximately 146 t/yr of tailings (and no waste rock) that is resuspended. Of this resuspended tailings an average of only 1.84 t/yr exits the reservoir. For the derived mobility simulation there is an estimated 340,000 t/yr of tailings that are resuspended and 160 t/yr that is released downstream. For the derived mobility case there is also an additional 146,000 t/yr of waste rock that is resuspended and 164 t/yr that is released downstream. The results also show that released waste rock and tailings consist almost entirely of 1.6-micron particles. The residual waste rock and tailings that are resuspended but not released make up the suspended concentration that eventually re-deposit in the reservoir when quiescent conditions prevail.

Over time the deposition of catchment sediments in the reservoir and redistribution (but limited loss) of stored waste rock and tailings alters the bed elevation. Figure 3.52 illustrates that for the equal mobility case there is mean deposition of catchment sediment near the headwaters in the upper reaches for the reservoir that leads to bed elevation increases of up to 0.16 m/yr. The increase in elevation reduces further into to the reservoir as the particles settle out of suspension as the inflows move through the reservoir. For the derived mobility case there is a similar pattern of deposition near the headwaters that leads to increases in bed elevation in these areas; however, there is far more complex re-distribution of the catchment sediments and waste rock and tailings, owing to their higher mobility, that leads to a combination of erosion and deposition zones. The results suggest that in this simulation the deposition of resuspended sediments in the deep water near the embankment leads to an average increase in elevation of less than 0.05 m/yr. A faster deposition rate would be expected when the HEP is closed because there is less inflowing and resuspended sediment released downstream from the spillway.

Table 3.7 Summary table of sediment attributed in downstream release water.

Simulation	Percentage of incoming catchment sediments released downstream		Average Concentrations (mg L^{-1})	
	% TSS	% Catchment 2-micron	TSS	2-micron catchment
Filling Simulation				
Deep Tunnel	5.5%	16.5%	49.4 mg L^{-1}	40.0 mg L^{-1}
Low level HEP	4.6%	15.3%	17.4 mg L^{-1}	16.7 mg L^{-1}
Op. HEP	6.2%	19.9%	22.1 mg L^{-1}	21.3 mg L^{-1}
Spillway	0.7%	2.2%	4.1 mg L^{-1}	4.0 mg L^{-1}
Op. HEP + Spill.	6.9%	22.1%	16.4 mg L^{-1}	15.8 mg L^{-1}
Operation Simulation – Equal Mobility, HEP open.				
Op. HEP	7.0%	23.0%	12.8 mg L^{-1}	12.0 mg L^{-1}
Spillway	0.2%	0.6%	2.5 mg L^{-1}	2.4 mg L^{-1}
Op. HEP + Spill.	7.2%	23.6%	12.0 mg L^{-1}	11.2 mg L^{-1}
Operation Simulation – Derived Mobility, HEP open.				
Op. HEP	7.1%	23.1%	12.9 mg L^{-1}	12.1 mg L^{-1}
Spillway	0.2%	0.6%	2.5 mg L^{-1}	2.5 mg L^{-1}
Op. HEP + Spill.	7.3%	23.7%	12.0 mg L^{-1}	11.3 mg L^{-1}
HEP Closure Simulation – Equal Mobility				
Spillway	4.7%	15.3%	7.0 mg L^{-1}	6.6 mg L^{-1}
HEP Closure Simulation – Derived Mobility				
Spillway	4.7%	15.3%	6.9 mg L^{-1}	6.6 mg L^{-1}

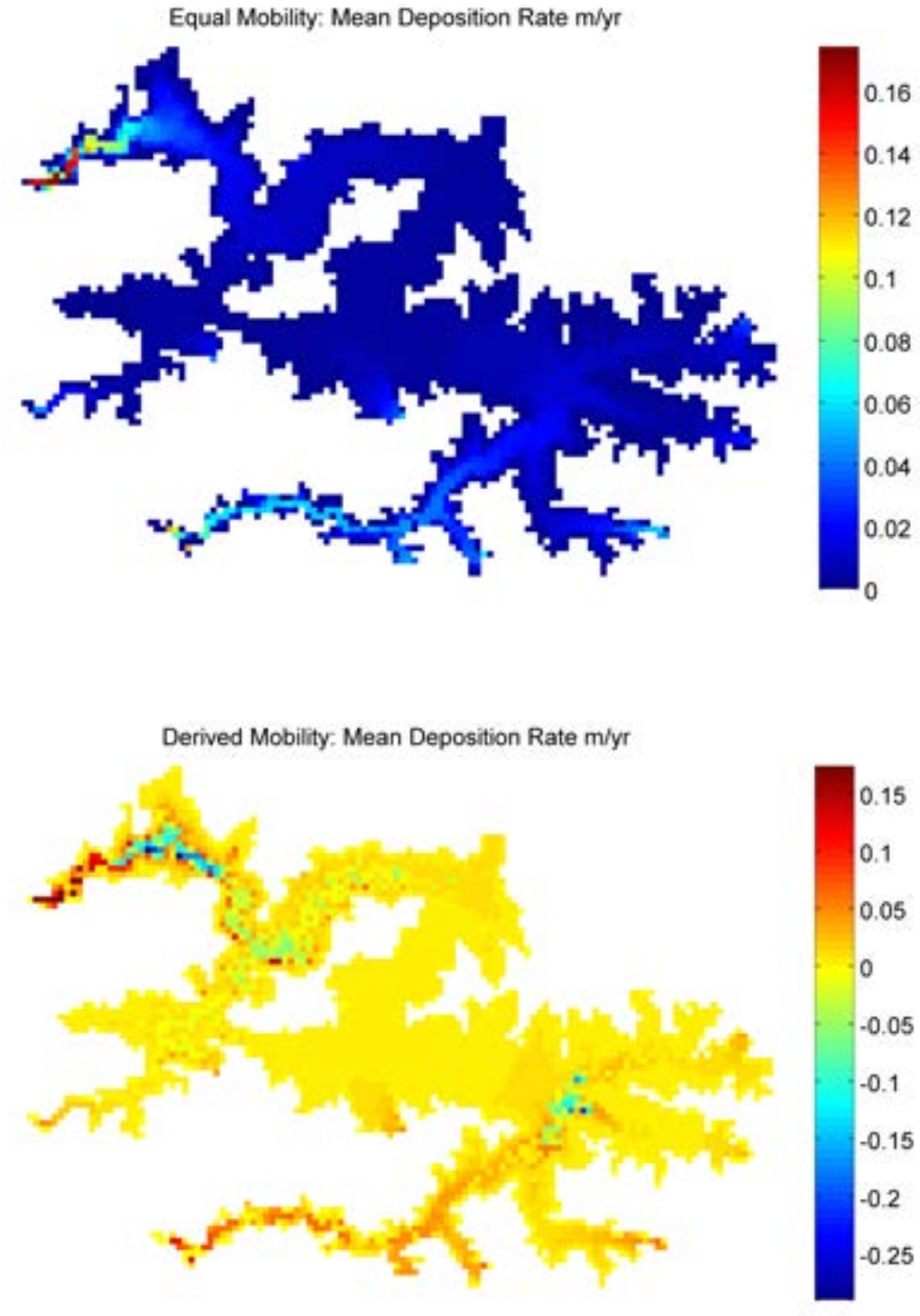

Figure 3.52 Average change in bed height per year for the operational simulation with HEP operating for the equal mobility case (top panel) and derived mobility case (bottom panel).

Table 3.8 Simulated properties of water extracted from the deep tunnel during filling simulation (with equal mobility of sediments).

Constituent	**Average**	**Minimum**	**5th Percentile**	**95th Percentile**	**Maximum**
HEP Deep Tunnel Intake Water					
TSS (mg L^{-1})	49.3	0.0	30.7	67.1	374.8
Temperature (°C)	21.9	21.1	21.3	22.4	25.0
Water Age (days)	67.1	0.0	6.5	135.9	145.3
Henumai Tracer	0.2	0.0	7.8E-2	0.3	0.3
Niar Tracer	0.1	0.0	5.9E-2	0.2	0.2
Aribai Tracer	6.2E-2	0.0	2.9E-2	8.9E-2	0.1
Dama Tracer	5.7E-2	0.0	2.7E-2	8.3E-2	9.8E-2
Isai Tracer	3.2E-2	0.0	2.0E-2	5.9E-2	7.7E-2
Nena Tracer	0.3	0.0	0.2	0.5	0.6
Loc2 Tracer	4.1E-2	0.0	1.5E-2	0.1	0.1
Ok Binai Tracer	1.5E-2	0.0	4.0E-3	4.5E-2	9.5E-2
Loc6 Tracer	2.0E-2	0.0	8.3E-3	3.9E-2	0.2
Loc8 Tracer	1.8E-2	0.0	7.5E-3	5.0E-2	7.5E-2
Catchment 2 micron (mg L^{-1})	39.9	0.0	29.1	46.2	220.5
Catchment 4 micron (mg L^{-1})	8.8	0.0	1.1	22.9	143.6
Catchment 8 micron (mg L^{-1})	0.6	0.0	4.0E-5	2.5	33.1
Catchment 16 micron (mg L^{-1})	4.9E-3	0.0	0.0	8.4E-4	1.3

Table 3.9 Simulated properties of water extracted from the low level HEP intake during filling simulation (with equal mobility of sediments).

Constituent	**Average**	**Minimum**	**5th Percentile**	**95th Percentile**	**Maximum**
HEP Low Level Intake Water					
TSS (mg L^{-1})	17.4	3.7	10.2	27.3	45.4
Temperature (°C)	23.8	23.0	23.1	24.4	24.6
Water Age (days)	275.8	113.7	148.6	542.9	561.1
Henumai Tracer	0.2	1.2E-2	0.1	0.3	0.3
Niar Tracer	0.1	9.1E-3	7.5E-2	0.2	0.2
Aribai Tracer	5.3E-2	4.5E-3	3.4E-2	7.5E-2	9.0E-2
Dama Tracer	5.0E-2	5.5E-3	3.2E-2	6.7E-2	7.7E-2
Isai Tracer	4.6E-2	1.1E-2	3.3E-2	5.7E-2	7.7E-2
Nena Tracer	0.2	6.2E-2	0.1	0.4	0.5
Loc2 Tracer	5.0E-2	1.4E-2	2.6E-2	8.8E-2	0.2
Ok Binai Tracer	1.5E-2	4.8E-3	8.4E-3	2.3E-2	6.9E-2
Loc6 Tracer	3.0E-2	1.0E-2	1.7E-2	4.5E-2	0.1
Loc8 Tracer	2.7E-2	9.4E-3	1.5E-2	3.9E-2	0.1
Catchment 2 micron (mg L^{-1})	16.7	3.7	9.7	26.5	44.4
Catchment 4 micron (mg L^{-1})	0.7	1.3E-3	0.2	1.3	2.5
Catchment 8 micron (mg L^{-1})	3.4E-4	0.0	0.0	1.8E-3	9.7E-3
Catchment 16 micron (mg L^{-1})	0.0	0.0	0.0	0.0	0.0

Table 3.10 Simulated properties of water extracted from the operational level HEP intake during filling simulation (with equal mobility of sediments).

Constituent	**Average**	**Minimum**	**5th Percentile**	**95th Percentile**	**Maximum**
HEP High Level Intake Water					
TSS (mg L^{-1})	22.1	4.4	12.0	37.5	62.0
Temperature (°C)	24.6	23.7	23.9	25.7	26.2
Water Age (days)	475.4	302.8	349.7	619.8	785.9
Henumai Tracer	0.2	2.8E-2	0.1	0.3	0.3
Niar Tracer	0.1	2.3E-2	7.5E-2	0.2	0.2
Aribai Tracer	4.9E-2	2.1E-2	3.4E-2	6.3E-2	7.3E-2
Dama Tracer	4.8E-2	1.8E-2	3.1E-2	6.9E-2	9.9E-2
Isai Tracer	3.0E-2	1.5E-2	2.1E-2	4.9E-2	7.8E-2
Nena Tracer	0.2	3.6E-2	0.1	0.3	0.5
Loc2 Tracer	4.4E-2	7.9E-3	2.2E-2	7.1E-2	9.2E-2
Ok Binai Tracer	1.3E-2	2.3E-3	6.8E-3	2.1E-2	3.1E-2
Loc6 Tracer	2.7E-2	4.5E-3	1.4E-2	4.5E-2	7.0E-2
Loc8 Tracer	1.8E-2	3.0E-3	7.8E-3	3.4E-2	7.9E-2
Catchment 2 micron (mg L^{-1})	21.3	4.4	11.4	36.5	60.6
Catchment 4 micron (mg L^{-1})	0.8	8.0E-5	0.3	1.7	3.3
Catchment 8 micron (mg L^{-1})	2.5E-3	0.0	0.0	1.2E-2	0.2
Catchment 16 micron (mg L^{-1})	0.0	0.0	0.0	0.0	0.0

Table 3.11 Simulated properties of water released from spillway during filling simulation (with equal mobility of sediments).

Constituent	**Average**	**Minimum**	**5th Percentile**	**95th Percentile**	**Maximum**
Spillway Release Water					
TSS (mg L^{-1})	4.1	1.0	1.6	7.4	11.7
Temperature (°C)	27.3	25.5	26.1	28.5	29.1
Water Age (days)	388.7	287.2	304.6	466.6	525.0
Henumai Tracer	4.4E-2	1.2E-2	2.8E-2	6.5E-2	7.8E-2
Niar Tracer	3.4E-2	1.1E-2	2.1E-2	4.9E-2	6.1E-2
Aribai Tracer	6.4E-2	1.6E-2	4.0E-2	9.5E-2	0.1
Dama Tracer	6.6E-2	1.8E-2	3.5E-2	0.1	0.1
Isai Tracer	0.1	4.5E-2	7.0E-2	0.1	0.2
Nena Tracer	0.2	5.2E-2	9.5E-2	0.3	0.3
Loc2 Tracer	4.6E-2	1.3E-2	2.3E-2	7.0E-2	8.5E-2
Ok Binai Tracer	2.4E-2	7.7E-3	1.3E-2	3.5E-2	4.1E-2
Loc6 Tracer	5.2E-2	1.5E-2	2.6E-2	7.9E-2	9.4E-2
Loc8 Tracer	4.9E-2	1.2E-2	2.6E-2	6.7E-2	0.1
Catchment 2 micron (mg L^{-1})	4.0	1.0	1.6	7.2	9.9
Catchment 4 micron (mg L^{-1})	7.0E-2	0.0	3.4E-4	0.3	2.5
Catchment 8 micron (mg L^{-1})	3.0E-5	0.0	0.0	1.0E-5	2.1E-2
Catchment 16 micron (mg L^{-1})	0.0	0.0	0.0	0.0	0.0

Table 3.12 Volume weighted simulated properties of water extracted from the combined operational HEP intake and released from the spillway during filling simulation (with equal mobility of sediments).

Constituent	**Average**	**Minimum**	**5th Percentile**	**95th Percentile**	**Maximum**
Combined Release (volume-weighted)					
TSS (mg L^{-1})	16.4	4.4	9.2	26.8	43.1
Temperature (°C)	25.4	24.1	24.6	26.6	27.4
Water Age (days)	445.5	313.3	355.8	545.7	616.7
Henumai Tracer	0.1	2.7E-2	8.3E-2	0.2	0.3
Niar Tracer	0.1	2.2E-2	5.9E-2	0.2	0.2
Aribai Tracer	5.5E-2	2.4E-2	4.2E-2	6.8E-2	8.4E-2
Dama Tracer	5.5E-2	2.5E-2	4.0E-2	7.2E-2	9.2E-2
Isai Tracer	5.4E-2	2.0E-2	3.0E-2	8.0E-2	0.1
Nena Tracer	0.2	7.2E-2	0.1	0.3	0.4
Loc2 Tracer	4.3E-2	1.4E-2	2.8E-2	6.3E-2	9.1E-2
Ok Binai Tracer	1.6E-2	4.7E-3	1.0E-2	2.3E-2	3.1E-2
Loc6 Tracer	3.4E-2	1.1E-2	2.1E-2	5.1E-2	7.0E-2
Loc8 Tracer	2.7E-2	5.2E-3	1.5E-2	4.2E-2	7.9E-2
Catchment 2 micron (mg L^{-1})	15.8	4.4	8.8	26.2	41.9
Catchment 4 micron (mg L^{-1})	0.6	8.0E-5	0.2	1.1	2.0
Catchment 8 micron (mg L^{-1})	1.4E-3	0.0	0.0	7.1E-3	7.8E-2
Catchment 16 micron (mg L^{-1})	0.0	0.0	0.0	0.0	0.0

Table 3.13 Simulated properties of water extracted from the operational HEP intake during operational simulation with waste rock and tailings storage and equal mobility of catchment sediments and waste rock and tailings.

Constituent	**Average**	**Minimum**	**5th Percentile**	**95th Percentile**	**Maximum**
HEP Intake Water					
TSS (mg L^{-1})	12.8	0.0	8.1	18.5	26.8
Temperature (°C)	24.7	24.0	24.2	25.1	25.3
Water Age (days)	374.8	0.0	136.4	539.5	676.9
Henumai Tracer	0.2	0.0	6.3E-2	0.2	0.3
Niar Tracer	0.1	0.0	4.1E-2	0.2	0.2
Aribai Tracer	4.5E-2	0.0	9.3E-3	6.6E-2	8.7E-2
Dama Tracer	4.6E-2	0.0	5.7E-3	7.5E-2	0.1
Isai Tracer	3.4E-2	0.0	2.6E-3	4.7E-2	6.0E-2
Nena Tracer	0.2	0.0	6.6E-2	0.3	0.4
Loc2 Tracer	3.8E-2	0.0	1.3E-2	5.9E-2	8.1E-2
Ok Binai Tracer	1.2E-2	0.0	1.6E-4	2.0E-2	3.2E-2
Loc6 Tracer	2.5E-2	0.0	2.1E-3	3.8E-2	5.2E-2
Loc8 Tracer	1.9E-2	0.0	2.7E-3	2.9E-2	4.3E-2
Catchment 2 micron (mg L^{-1})	12.0	0.0	7.6	17.3	24.7
Catchment 4 micron (mg L^{-1})	0.8	0.0	0.3	1.9	4.3
Catchment 8 micron (mg L^{-1})	2.1E-3	0.0	0.0	9.0E-3	0.2
Catchment 16 micron (mg L^{-1})	0.0	0.0	0.0	0.0	0.0
Tailings 1.6 micron (mg L^{-1})	2.7E-4	0.0	0.0	1.7E-3	9.9E-3
Tailings 5.4 micron (mg L^{-1})	0.0	0.0	0.0	0.0	1.0E-5
Tailings 14.8 micron (mg L^{-1})	0.0	0.0	0.0	0.0	0.0
Tailings 50 micron (mg L^{-1})	0.0	0.0	0.0	0.0	0.0
Waste rock 1.6 micron (mg L^{-1})	0.0	0.0	0.0	0.0	0.0
Waste rock 5.4 micron (mg L^{-1})	0.0	0.0	0.0	0.0	0.0

Waste rock 14.8 micron (mg L^{-1})	0.0	0.0	0.0	0.0	0.0

Table 3.14 Simulated properties of water released from the spillway during operational simulation (when HEP is operating) with waste rock and tailings storage and equal mobility of catchment sediments and waste rock and tailings.

Constituent	**Average**	**Minimum**	**5th Percentile**	**95th Percentile**	**Maximum**
Spillway Release Water					
TSS (mg L^{-1})	2.5	0.0	0.6	5.2	8.4
Temperature (°C)	27.6	25.9	26.6	28.9	29.4
Water Age (days)	370.9	20.1	284.8	459.9	539.9
Henumai Tracer	2.9E-2	0.0	1.2E-2	4.7E-2	7.1E-2
Niar Tracer	2.2E-2	0.0	8.8E-3	3.5E-2	5.2E-2
Aribai Tracer	6.7E-2	0.0	2.5E-2	9.9E-2	0.1
Dama Tracer	5.9E-2	0.0	2.1E-2	8.5E-2	0.1
Isai Tracer	0.1	0.0	7.4E-2	0.2	0.2
Nena Tracer	0.1	0.0	5.2E-2	0.2	0.3
Loc2 Tracer	4.0E-2	0.0	1.6E-2	6.8E-2	8.0E-2
Ok Binai Tracer	2.4E-2	0.0	9.5E-3	3.8E-2	4.6E-2
Loc6 Tracer	5.2E-2	0.0	2.3E-2	8.2E-2	9.5E-2
Loc8 Tracer	5.4E-2	0.0	2.6E-2	8.0E-2	0.1
Catchment 2 micron (mg L^{-1})	2.4	0.0	0.6	4.9	7.8
Catchment 4 micron (mg L^{-1})	5.6E-2	0.0	0.0	0.3	1.3
Catchment 8 micron (mg L^{-1})	2.0E-5	0.0	0.0	1.0E-5	5.0E-3
Catchment 16 micron (mg L^{-1})	0.0	0.0	0.0	0.0	0.0
Tailings 1.6 micron (mg L^{-1})	0.0	0.0	0.0	0.0	0.0
Tailings 5.4 micron (mg L^{-1})	0.0	0.0	0.0	0.0	0.0
Tailings 14.8 micron (mg L^{-1})	0.0	0.0	0.0	0.0	0.0
Tailings 50 micron (mg L^{-1})	0.0	0.0	0.0	0.0	0.0
Waste rock 1.6 micron (mg L^{-}	0.0	0.0	0.0	0.0	0.0

^{1})					
Waste rock 5.4 micron (mg L^{-1})	0.0	0.0	0.0	0.0	0.0
Waste rock 14.8 micron (mg L^{-1})	0.0	0.0	0.0	0.0	0.0

Table 3.15 Simulated volume-weighted average of properties of water extracted from the operational HEP intake and release from the spillway during operational simulations with waste rock and tailings storage and equal mobility of catchment sediments and waste rock and tailings.

Constituent	**Average**	**Minimum**	**5th Percentile**	**95th Percentile**	**Maximum**
Combined Release (volume-weighted)					
TSS (mg L^{-1})	12.0	0.0	7.9	16.8	21.7
Temperature (°C)	24.9	24.1	24.3	25.6	27.0
Water Age (days)	371.2	4.2E-2	136.4	524.2	676.9
Henumai Tracer	0.1	0.0	6.3E-2	0.2	0.3
Niar Tracer	9.9E-2	0.0	4.1E-2	0.1	0.2
Aribai Tracer	4.7E-2	0.0	9.3E-3	6.6E-2	8.7E-2
Dama Tracer	4.7E-2	0.0	5.7E-3	7.5E-2	0.1
Isai Tracer	4.1E-2	0.0	4.6E-3	7.0E-2	0.1
Nena Tracer	0.2	0.0	6.7E-2	0.3	0.4
Loc2 Tracer	3.7E-2	0.0	1.3E-2	5.7E-2	7.7E-2
Ok Binai Tracer	1.2E-2	0.0	1.6E-4	2.1E-2	3.2E-2
Loc6 Tracer	2.7E-2	0.0	2.1E-3	4.1E-2	5.6E-2
Loc8 Tracer	2.1E-2	0.0	3.6E-3	3.5E-2	4.9E-2
Catchment 2 micron (mg L^{-1})	11.2	0.0	7.4	15.8	19.5
Catchment 4 micron (mg L^{-1})	0.7	0.0	0.3	1.5	3.5
Catchment 8 micron (mg L^{-1})	1.6E-3	0.0	0.0	6.7E-3	0.1
Catchment 16 micron (mg L^{-1})	0.0	0.0	0.0	0.0	0.0
Tailings 1.6 micron (mg L^{-1})	2.5E-4	0.0	0.0	1.7E-3	8.3E-3
Tailings 5.4 micron (mg L^{-1})	0.0	0.0	0.0	0.0	0.0

Tailings 14.8 micron (mg L^{-1})	0.0	0.0	0.0	0.0	0.0
Tailings 50 micron (mg L^{-1})	0.0	0.0	0.0	0.0	0.0
Waste rock 1.6 micron (mg L^{-1})	0.0	0.0	0.0	0.0	0.0
Waste rock 5.4 micron (mg L^{-1})	0.0	0.0	0.0	0.0	0.0
Waste rock 14.8 micron (mg L^{-1})	0.0	0.0	0.0	0.0	0.0

Table 3.16 Simulated properties of water extracted from the operational HEP intake during operational simulation with waste rock and tailings storage and derived mobility of catchment sediments and waste rock and tailings.

Constituent	**Average**	**Minimum**	**5th Percentile**	**95th Percentile**	**Maximum**
HEP Intake Water					
TSS (mg L^{-1})	12.9	0.0	8.1	18.8	27.7
Temperature (°C)	24.7	23.9	24.2	25.1	25.4
Water Age (days)	376.2	4.2E-2	136.4	538.7	727.1
Henumai Tracer	0.2	0.0	6.3E-2	0.2	0.3
Niar Tracer	0.1	0.0	4.1E-2	0.2	0.2
Aribai Tracer	4.5E-2	0.0	9.4E-3	6.6E-2	8.7E-2
Dama Tracer	4.6E-2	0.0	5.8E-3	7.5E-2	0.1
Isai Tracer	3.4E-2	0.0	2.6E-3	4.8E-2	6.2E-2
Nena Tracer	0.2	0.0	6.4E-2	0.3	0.4
Loc2 Tracer	3.7E-2	0.0	1.3E-2	5.9E-2	8.3E-2
Ok Binai Tracer	1.2E-2	0.0	1.6E-4	1.9E-2	3.1E-2
Loc6 Tracer	2.5E-2	0.0	2.1E-3	3.8E-2	5.2E-2
Loc8 Tracer	1.8E-2	0.0	2.7E-3	2.9E-2	4.3E-2
Catchment 2 micron (mg L^{-1})	12.1	0.0	7.6	17.4	25.3
Catchment 4 micron (mg L^{-1})	0.8	0.0	0.3	1.9	4.3
Catchment 8 micron (mg L^{-1})	2.2E-3	0.0	0.0	9.0E-3	0.2
Catchment 16 micron (mg L^{-1})	0.0	0.0	0.0	0.0	0.0

Tailings 1.6 micron (mg L^{-1})	2.4E-2	0.0	1.5E-3	0.1	0.4
Tailings 5.4 micron (mg L^{-1})	0.0	0.0	0.0	0.0	1.0E-5
Tailings 14.8 micron (mg L^{-1})	0.0	0.0	0.0	0.0	0.0
Tailings 50 micron (mg L^{-1})	0.0	0.0	0.0	0.0	0.0
Waste rock 1.6 micron (mg L^{-1})	2.4E-2	0.0	1.5E-3	7.2E-2	0.4
Waste rock 5.4 micron (mg L^{-1})	0.0	0.0	0.0	0.0	6.1E-4
Waste rock 14.8 micron (mg L^{-1})	0.0	0.0	0.0	0.0	0.0

Table 3.17 Simulated properties of water released from the spillway during operational simulation (when HEP is operating) with waste rock and tailings storage and derived mobility of catchment sediments and waste rock and tailings.

Constituent	**Average**	**Minimum**	**5th Percentile**	**95th Percentile**	**Maximum**
Spillway Release Water					
TSS (mg L^{-1})	2.5	0.0	0.6	5.2	8.4
Temperature (°C)	27.6	25.9	26.6	28.9	29.4
Water Age (days)	370.7	20.1	284.5	460.2	538.8
Henumai Tracer	2.9E-2	0.0	1.2E-2	4.8E-2	7.1E-2
Niar Tracer	2.2E-2	0.0	8.9E-3	3.6E-2	5.1E-2
Aribai Tracer	6.7E-2	0.0	2.5E-2	9.8E-2	0.1
Dama Tracer	5.8E-2	0.0	2.1E-2	8.5E-2	0.1
Isai Tracer	0.1	0.0	7.4E-2	0.2	0.2
Nena Tracer	0.1	0.0	5.2E-2	0.2	0.3
Loc2 Tracer	4.1E-2	0.0	1.6E-2	6.8E-2	8.0E-2
Ok Binai Tracer	2.4E-2	0.0	9.4E-3	3.9E-2	4.6E-2
Loc6 Tracer	5.2E-2	0.0	2.2E-2	8.2E-2	9.5E-2
Loc8 Tracer	5.4E-2	0.0	2.6E-2	8.0E-2	0.1
Catchment 2 micron (mg L^{-1})	2.5	0.0	0.6	4.9	7.9
Catchment 4 micron (mg L^{-1})	5.5E-2	0.0	0.0	0.3	1.3

Catchment 8 micron (mg L^{-1})	2.0E-5	0.0	0.0	1.0E-5	5.2E-3
Catchment 16 micron (mg L^{-1})	0.0	0.0	0.0	0.0	0.0
Tailings 1.6 micron (mg L^{-1})	0.0	0.0	0.0	0.0	0.0
Tailings 5.4 micron (mg L^{-1})	0.0	0.0	0.0	0.0	0.0
Tailings 14.8 micron (mg L^{-1})	0.0	0.0	0.0	0.0	0.0
Tailings 50 micron (mg L^{-1})	0.0	0.0	0.0	0.0	0.0
Waste rock 1.6 micron (mg L^{-1})	0.0	0.0	0.0	0.0	0.0
Waste rock 5.4 micron (mg L^{-1})	0.0	0.0	0.0	0.0	0.0
Waste rock 14.8 micron (mg L^{-1})	0.0	0.0	0.0	0.0	0.0

Table 3.18 Simulated volume-weighted average of properties of water extracted from the operational HEP intake and release from the spillways during operational simulations with waste rock and tailings storage and derived mobility of catchment sediments and waste rock and tailings.

Constituent	**Average**	**Minimum**	**5th Percentile**	**95th Percentile**	**Maximum**
Combined Release (volume-weighted)					
TSS (mg L^{-1})	12.1	0.0	7.9	17.1	21.9
Temperature (°C)	24.9	23.9	24.3	25.6	27.0
Water Age (days)	372.1	4.2E-2	136.4	522.9	727.1
Henumai Tracer	0.1	0.0	6.2E-2	0.2	0.3
Niar Tracer	1.0E-1	0.0	4.1E-2	0.1	0.2
Aribai Tracer	4.7E-2	0.0	9.4E-3	6.6E-2	8.7E-2
Dama Tracer	4.7E-2	0.0	5.8E-3	7.5E-2	0.1
Isai Tracer	4.1E-2	0.0	4.6E-3	6.9E-2	0.1
Nena Tracer	0.2	0.0	6.6E-2	0.3	0.4
Loc2 Tracer	3.7E-2	0.0	1.3E-2	5.7E-2	7.7E-2
Ok Binai Tracer	1.2E-2	0.0	1.6E-4	2.1E-2	3.1E-2
Loc6 Tracer	2.6E-2	0.0	2.1E-3	4.1E-2	5.7E-2

Loc8 Tracer	2.1E-2	0.0	3.7E-3	3.5E-2	4.9E-2
Catchment 2 micron (mg L^{-1})	11.3	0.0	7.5	16.0	19.4
Catchment 4 micron (mg L^{-1})	0.7	0.0	0.3	1.5	3.5
Catchment 8 micron (mg L^{-1})	1.6E-3	0.0	0.0	7.0E-3	0.1
Catchment 16 micron (mg L^{-1})	0.0	0.0	0.0	0.0	0.0
Tailings 1.6 micron (mg L^{-1})	2.0E-2	0.0	1.4E-3	8.5E-2	0.4
Tailings 5.4 micron (mg L^{-1})	0.0	0.0	0.0	0.0	0.0
Tailings 14.8 micron (mg L^{-1})	0.0	0.0	0.0	0.0	0.0
Tailings 50 micron (mg L^{-1})	0.0	0.0	0.0	0.0	0.0
Waste rock 1.6 micron (mg L^{-1})	2.2E-2	0.0	1.5E-3	6.7E-2	0.3
Waste rock 5.4 micron (mg L^{-1})	0.0	0.0	0.0	0.0	3.7E-4
Waste rock 14.8 micron (mg L^{-1})	0.0	0.0	0.0	0.0	0.0

Table 3.19 Simulated properties of water released from the spillway after HEP closure with waste rock and tailings storage and equal mobility of catchment sediments and waste rock and tailings.

Constituent	**Average**	**Minimum**	**5th Percentile**	**95th Percentile**	**Maximum**
Spillway Release Water					
TSS (mg L^{-1})	7.0	2.7	4.3	9.9	14.2
Temperature (°C)	25.9	24.6	25.0	26.9	27.2
Water Age (days)	453.9	325.9	360.0	552.1	618.4
Henumai Tracer	0.2	7.8E-2	0.1	0.2	0.2
Niar Tracer	0.1	5.8E-2	8.3E-2	0.1	0.1
Aribai Tracer	5.6E-2	3.2E-2	4.5E-2	6.8E-2	8.1E-2
Dama Tracer	5.4E-2	3.1E-2	4.4E-2	6.6E-2	8.3E-2
Isai Tracer	5.0E-2	3.1E-2	3.8E-2	6.5E-2	8.9E-2
Nena Tracer	0.2	8.5E-2	0.1	0.3	0.3
Loc2 Tracer	4.2E-2	1.8E-2	3.0E-2	5.5E-2	7.1E-2

Ok Binai Tracer	1.6E-2	7.5E-3	1.2E-2	2.0E-2	3.0E-2
Loc6 Tracer	3.2E-2	1.6E-2	2.3E-2	4.2E-2	6.1E-2
Loc8 Tracer	2.5E-2	9.8E-3	1.7E-2	3.6E-2	5.6E-2
Catchment 2 micron (mg L^{-1})	6.6	2.7	4.2	9.2	12.4
Catchment 4 micron (mg L^{-1})	0.4	1.4E-2	6.5E-2	0.8	1.8
Catchment 8 micron (mg L^{-1})	7.2E-4	0.0	0.0	3.4E-3	2.0E-2
Catchment 16 micron (mg L^{-1})	0.0	0.0	0.0	0.0	0.0
Tailings 1.6 micron (mg L^{-1})	0.0	0.0	0.0	0.0	0.0
Tailings 5.4 micron (mg L^{-1})	0.0	0.0	0.0	0.0	0.0
Tailings 14.8 micron (mg L^{-1})	0.0	0.0	0.0	0.0	0.0
Tailings 50 micron (mg L^{-1})	0.0	0.0	0.0	0.0	0.0
Waste rock 1.6 micron (mg L^{-1})	0.0	0.0	0.0	0.0	0.0
Waste rock 5.4 micron (mg L^{-1})	0.0	0.0	0.0	0.0	0.0
Waste rock 14.8 micron (mg L^{-1})	0.0	0.0	0.0	0.0	0.0

Table 3.20 Simulated properties of water released from the spillway after HEP closure with waste rock and tailings storage and derived mobility of catchment sediments and waste rock and tailings.

Constituent	**Average**	**Minimum**	**5th Percentile**	**95th Percentile**	**Maximum**
Spillway Release Water					
TSS (mg L^{-1})	6.9	2.8	4.4	9.9	14.1
Temperature (°C)	25.9	24.6	25.0	26.9	27.2
Water Age (days)	456.4	323.7	357.1	547.6	606.5
Henumai Tracer	0.2	8.1E-2	0.1	0.2	0.2
Niar Tracer	0.1	5.9E-2	8.4E-2	0.1	0.1
Aribai Tracer	5.6E-2	3.3E-2	4.5E-2	6.7E-2	8.0E-2
Dama Tracer	5.4E-2	3.2E-2	4.4E-2	6.6E-2	8.0E-2
Isai Tracer	5.0E-2	3.1E-2	3.8E-2	6.5E-2	8.7E-2

Nena Tracer	0.2	0.1	0.1	0.3	0.3
Loc2 Tracer	4.2E-2	2.0E-2	3.0E-2	5.5E-2	7.1E-2
Ok Binai Tracer	1.6E-2	7.6E-3	1.2E-2	2.0E-2	2.9E-2
Loc6 Tracer	3.2E-2	1.6E-2	2.4E-2	4.1E-2	6.1E-2
Loc8 Tracer	2.5E-2	9.9E-3	1.7E-2	3.6E-2	5.5E-2
Catchment 2 micron (mg L^{-1})	6.6	2.7	4.2	9.3	12.5
Catchment 4 micron (mg L^{-1})	0.4	1.4E-2	6.4E-2	0.8	1.8
Catchment 8 micron (mg L^{-1})	7.1E-4	0.0	0.0	3.4E-3	1.9E-2
Catchment 16 micron (mg L^{-1})	0.0	0.0	0.0	0.0	0.0
Tailings 1.6 micron (mg L^{-1})	9.0E-5	1.0E-5	2.0E-5	2.6E-4	5.3E-4
Tailings 5.4 micron (mg L^{-1})	0.0	0.0	0.0	0.0	0.0
Tailings 14.8 micron (mg L^{-1})	0.0	0.0	0.0	0.0	0.0
Tailings 50 micron (mg L^{-1})	0.0	0.0	0.0	0.0	0.0
Waste rock 1.6 micron (mg L^{-1})	0.0	0.0	0.0	1.0E-5	2.0E-5
Waste rock 5.4 micron (mg L^{-1})	0.0	0.0	0.0	0.0	0.0
Waste rock 14.8 micron (mg L^{-1})	0.0	0.0	0.0	0.0	0.0

3.3.6 Barge Deposition

The impacts of barge disposition of mine waste rock was assessed by applying a continuous deposition of 18 5000-ton barges per day at sites 1 km, 2 km and 4 km upstream for the embankment in in the Nena arm. The results (see Figure 3.53) show a clear reduction in waste rock contribution to total TSS in the HEP intake waters as the barge deposition location moves upstream of the embankment. There is also a shift in the size distribution of waste rock material particle size that is reaching the embankment. When barge deposition occurs at 1 km from the embankment the contributions to TSS from barged waste rock material in the HEP intake water is dominated by the large contribution of 14.6-micron particles; in this case the TSS in the HEP intake reaches up to 300 mg L^{-1}. When barging takes place at distances further from the embankment the overall TSS and the waste rock material contribution is increasingly dominated by the finer fractions that settle more slowly. For barge dispositions at 4 km upstream, the results indicate that the catchment contributions and not the contributions from waste rock material dominate TSS concentrations in the HEP intake.

The results also show that for each scenario, and aside from diurnal fluctuations (in response to the 6-hour hydrograph), there is a relatively steady-state contribution from waste rock sediment to the HEP intake TSS when the deposition rate and location is constant. Whilst there

is period of increase in TSS in the HEP intake water at the beginning of the simulation and some lower-frequency changes (in response to the hydrodynamics) thereafter, the model does not suggest an upward trend in waste rock contribution to the TSS in the HEP intake water over the duration of the simulation. It is therefore likely that the TSS contribution from waste rock material in the HEP intake waters will adjust to the proposed barge deposition schedule to reach a steady state that is depended on the location and rate. At the end of the barge deposition period, which was set in the model at 11 November 2005, there is a rapid return to background conditions.

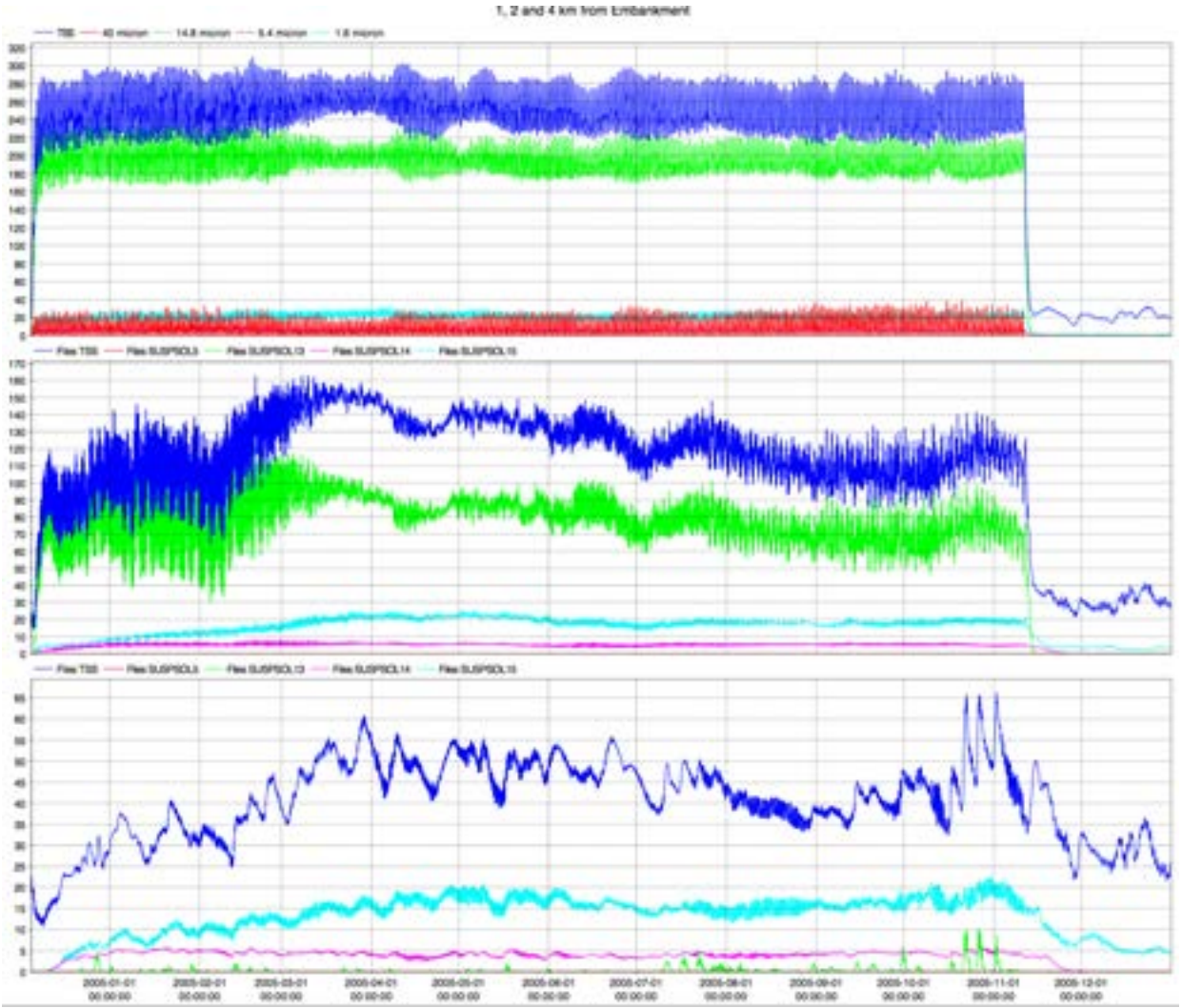

Figure 3.53 Simulated concentrations of fine waste rock sediments and TSS in the HEP intake water during continuous barge disposition (18 barges per day) at 1 km (top panel), 2 km (middle) and 4 km up the Nena arm (bottom) from the embankment.

4 Water Quality

4.1 Overview

In this section the modelled hydrodynamic and sediment characteristics in the FRHEP reservoir have been coupled with available data and information taken from relevant literature to develop an assessment of likely water quality in the FRHEP reservoir and exiting the reservoir through the HEP intake and spillway. The analysis has been confined to oxygen, nutrient, organic matter and primary production and discusses how these relate to other water quality variables such as alkalinity and hardness. Although raised in the discussion below, this assessment does not provide an analysis of the chemistry of metals, sulphate, alkalinity or hardness.

Where appropriate, the assessment addresses water quality in terms of three layers in the vertical stratification – the epilimnion, metalimnion and hypolimnion – that are defined in Section 3.3. In addition, the discussion has been separated into a sequence of stages from an initial filling stage, an intermediate stabilisation phase after filling, to long-term changes.

Water quality data collected at monitoring sites within the Frieda River catchment and nearby region were provided as raw data and statistical summaries by SRK (2017d) and used to develop the water quality discussion.

4.2 Initial Response to Filling

Modelling results indicate that, once constructed, the reservoir will fill rapidly (within 3 years). This will result in the inundation of a large area of vegetation and soils. Thus, water quality in the filled reservoir will initially be dominated by microbiological decomposition of labile organic matter and later influenced by the continued steady decomposition of more refractory organic components. During the first (approximately) 2 years significant fluctuations in dissolved oxygen (DO) will be evident in the epilimnion of the water body with periods of very low oxygen or even occasional anoxia. Rapid metabolically-driven depletion of DO in the surface waters of tropical lakes is described by Townsend (1996). The intensity of this surface DO depletion in the FRHEP reservoir will be largely governed by metabolic processes and partial mixing episodes but will be also compensated by comparatively high DO concentrations present in perennial inflows from inflowing streams. Given the stratification and mixing dynamics evident in the modelling, periods of DO depletion in the surface layers are likely to occur under low wind conditions where mixing of atmospheric oxygen into the epilimnion is reduced. Some oxygen from inflows will be mixed into the epilimnion, but much of this is predicted to typically intrude below the epilimnion.

Early decomposition of vegetation will initially also impart significant true colour to the reservoir water. ‘True’ colour in water is measured after filtration to remove particulate material and is comprised of organic molecules of high molecular weight (mainly humates and fulvates) that impart a yellow/brown appearance to water. This will have little effect on the HEP aspects of the reservoir but may be relevant to the downstream Frieda and Sepik rivers during early overflow periods. It is likely however, that based on available total organic carbon (TOC) and dissolved organic carbon (DOC) data, background true colour concentrations in the downstream portions of the river system, notably the Sepik River, are moderately high although there is no true colour data available to confirm this.

Early fluctuations in DO concentrations will be accompanied by significant pH shifts associated with the generation of organic acids (humates, fulvates and tannins) from decomposition of organic material. The extent of these pH fluctuations will in turn, be governed by the alkalinity of the water. Alkalinity may be described as a measure of the buffering capacity of water and relates to the relative dominance of inorganic carbon species in water. These are carbon

dioxide (or carbonic acid), bicarbonate and carbonate. Elevated alkalinity (buffering capacity) is not simply related to the ratios of these carbon species but is largely related to the dominance and absolute concentration of the bicarbonate (HCO_3^-) ion (Stumm and Morgan, 1996). Thus, it is the concentration of this ion (as well as its relative dominance) that provides the 'buffering capacity' required to neutralize acidity (H^+ ions or protons) in water. Background total alkalinity data for the streams that will feed the FRHEP reservoir vary from <<20 mg L^{-1} to around 50 mg L^{-1} (as $CaCO_3$). Flow corrected calculations (from all stream sources) of the likely final alkalinity in the reservoir will need to be determined to provide a reasonably accurate estimate of likely fluctuations in pH due to organic acid generation during the early, post-filling phase of the reservoir's evolution. Issues related to alkalinity at later post-filling periods are further discussed below.

Limited information is available on nutrient and phytoplankton dynamics of newly constructed reservoirs in tropical regions. In the context of the proposed FRHEP reservoir, the most relevant historical studies available are from the 1950's and 1960's by Talling et al. The most relevant of these is a study conducted on a cyclically recharged riverine lake located on the White Nile (Prowse and Talling, 1958; rep. 2003). In reference to this and using information from Boland (2008) and Lamche et al. (2012), who reported on water quality changes in a recently modified reservoir (increased spillway height) located in Australia's far northern tropical, monsoonal region (12°S) that underwent rapid recharge, likely sequences of initial nutrient and phytoplankton can be described.

Immediately after filling the nutrient dynamics in the reservoir will likely be dominated by elevated concentrations of ammonium substantially higher in the hypolimnion but nonetheless still elevated in the epilimnion compared to the ANZECC (2000) guideline for Australian tropical lakes and reservoirs of 10 µg/L (expressed as NH_4^+-N). For circumneutral pH, similar ammonia-nitrogen (NH_3-N) concentrations can be expected, but are likely to remain well below the maximum permitted concentrations of NH_3-N for protection of freshwater aquatic life (3.6 mg L^{-1} NH_3-N at pH of 7 and a temperature of 25^{o}C as stipulated in the PNG Environment (Water Quality Criteria) Regulation, 2002). Ammonium concentrations will be associated with the rapid decomposition of labile organic matter and interstitial soil components following inundation. This initial ammonification will likely be accompanied by increases in available silica in the reservoir. This will also occur due to the rapid inundation of soils in the bed of the reservoir and result in a substantial increase in diatom population in the euphotic epilimnion. Diatoms are a group of algae that are enclosed in a silica frustule (shell) and frequently dominate in the early stages of rapid recharge in reservoirs. Prowse and Talling (2003) reported rapid increases in the diatom *Melosira granulata* (also known as *Aulacoseira granulata*) in their study cited above.

Data available from inflowing streams indicate that biologically available concentrations of phosphorus (P) are generally low although total P concentrations are quite high but likely bound to clays (John Chapman, pers. comms.) and therefore biologically relatively unavailable. Nonetheless, a considerable amount of bioavailable P will be released from the inundated soils and will likely exceed 10 µg L^{-1} in the epilimnion of the reservoir. This P concentration is generally considered the concentration above which lakes and reservoirs progress from an oligotrophic state to a mesotrophic state (Vollenweider, 1968).

The initial colonization by diatoms of the reservoir's photic epilimnion will likely continue for 6 to 12 months after filling, during which period this group will be the dominant primary producers. Following this there will be a succession toward dominance by Cyanobacteria. This will occur due to the microbiological denitrification of oxidized nitrogen species to nitrogen gas and its subsequent release to the atmosphere. Denitrification can occur in littoral areas where soils are anaerobic especially after rapid inundation when littoral regions are dominated by decomposing vegetation. In many tropical reservoirs this is a regular feature of seasonal recharge when exposed littoral areas are seasonally inundated. This process demonstrates that nitrogen is a 'non-conservative' component of a reservoir's nutrient budget. That is, it can

deplete through internal processes that occur within the reservoir. This compares with the conservative phosphorus component that can only be depleted by primarily advective processes. As this denitrification continues the ratio of nitrogen to phosphorus concentrations will decrease toward what is known as the 'Redfield ratio', an N:P ratio of 16. Values above this ratio may be considered as indicative of waters with a low potential for significant algal growth compared to the 'high risk' ratio of equal to or less than 16:1, a value Redfield (1958) gives as a threshold, below which Cyanobacteria dominance becomes more likely, even inevitable.

The predicted period of cyanobacterial dominance will likely extend for a further 6 months or so but steadily diminish as the reservoir's nitrogen cycle stabilizes leading to establishment of a more diverse phytoplankton community likely to be dominated by the 'green algae' (Chlorophyta). Certainly, there will be continuing seasonal changes in the relative dominance of phytoplankton groups, most likely influenced by seasonal successions of diatoms, dinoflagellates etc. but the general trend will be toward a species diversity indicative of an oligotrophic water body. This will also coincide with the development of stable, submerged and emergent macrophyte beds in the shallow (<7 metres deep) littoral regions fringing the deeper regions of the reservoir.

The littoral zone between 210 and 220 m RL covers approximately 8% of the reservoir area. Whilst exchange between the littoral and pelagic zones of the reservoir will be considerably faster than the rates of vertical exchange, model results indicate (see Figure 4.1) lateral heterogeneity is likely to develop over the expanse of the reservoir. Littoral areas that are isolated from the flow paths of rivers will exchange less frequently into the main body of the reservoir and are therefore likely to develop with differences in water chemistry and biology that relate to differences in the rates of exchange. These areas may develop macrophyte growth more quickly, which in turn amplifies diurnal heating and cooling of the shallows that may then increase lateral exchange.

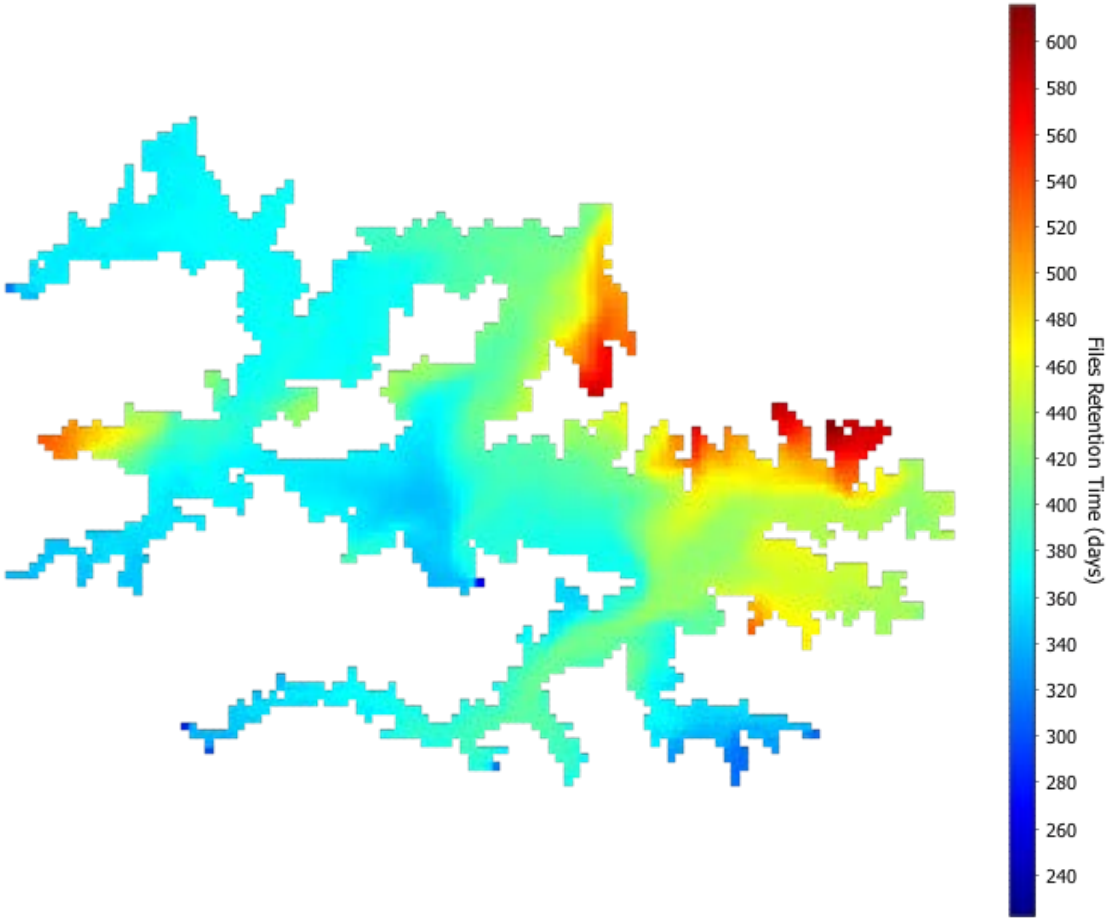

Figure 4.1 Water retention time at the surface 18 months after filling of the FRHEP.

4.3 Stabilisation

After the initial responses described above, significant macrophyte growth will begin in the littoral regions of the reservoir. The success and rate of development of these plant communities will be dependent on inoculation rates by seeds and spores many of which will accompany inflows to the reservoir but most importantly be governed by the clarity of the epilimnion that will determine the rate at which macrophyte photosynthesis can proceed. It is reasonable to assume that the littoral, fringing sediments will provide sufficient nutrients to sustain substantial plant growth. To a less important extent the success of macrophyte establishment will initially be dependent on water height fluctuations. As the communities establish however, their response to water height fluctuations will favour those groups that can rapidly adapt to these changes resulting in dominance of species with such capacity. Given sufficient surface water clarity, macrophytes will typically establish at depths to approximately 7 m deep.

The photic depth can be estimated as the depth to which 1% for incident light at the surface penetrates; following Beer-Lambert law, this yields $4.61/K_d$, where K_d is the Photosynthetically Active Radiation (PAR) light extinction coefficient estimated by the model (see Figure 4.2). The K_d values simulated by the model are dependent on the TSS, whereby each sediment size adds a specific attenuation of PAR of 0.1 $m^2 g^{-1}$ (approximated from observations of James et

al. 2002; Gallegos et al. 2006). The results indicate that because of the high TSS near the major rivers inflowing into the FRHEP reservoir the total light attenuation is high and therefore the photic depth is restricted. The mean simulated K_d in the remainder of the littoral zone away from the rivers is typically less than 0.5 m^{-1}, which indicates that the photic depth in these regions will be at approximately 9 m.

Once a sufficiently adaptive macrophyte community is established it, along with the established phytoplankton, will provide a significant contribution to the reservoir water total alkalinity. Macrophytes will also stabilize littoral shoreline sediments not only mitigating sediment resuspension but also providing a degree of shoreline 'filtration' particularly for sheet flows that might enter the reservoir under high runoff periods.

Suspended clay concentrations and turbidity will be critical to the actual photic depth available for macrophyte growth. Should clay suspension in the surface layer be a factor inhibiting macrophyte growth in the new reservoir, it can be complexed by hardness (divalent cations, particularly Ca and Mg) sourced from lime and/or dolomite to improve the clarity of surface epilimnetic water. As discussed above, the modelling results suggest that water clarity in the surface is adequate to support macrophyte growth to 9 m. However, the model considers only TSS input from the catchments (and resuspension of stored waste rock and tailings) and resuspension via flow currents. Intermittent drawn-down will expose bare littoral banks so that that resuspension of fine sediments may occur due to run-off, surface waves during windy weather, and potentially barge wake. The fate of suspended material once it reaches a receiving water body is complex with binding of the original particles occurring over several distinct stages of aggregation (Krone, 1972) to form what Johnson (1974) and Chase (1979) call organic-mineral aggregates. Flocculation requires that the particles first collide and then cohere (Terwindt, 1976). The former precondition would be more readily met in water bodies with significant concentrations of soluble electrolytes (Stumm and Morgan, 1970). Should insufficient divalent cations be present to assist such clarification, consideration should be given to the addition of lime and/or dolomite to incoming stream beds to enhance this process.

It should be noted that the presence of significant biomass of littoral macrophytes will, along with algae in the open reservoir regions, increase the photosynthetic activity (in daylight hours) and assist the generation of increased concentrations of bicarbonate in the reservoir and hence its capacity to buffer any acidity that might enter the epilimnion during partial mixing events. While this macrophyte-sourced bicarbonate is produced in the littoral regions of the reservoir diurnal patterns of warming and cooling in these macrophyte beds will generate near-surface currents that will transport it into the open regions of the reservoir (Boland, 1993). This will assist in providing additional buffering capacity to the reservoir if inflow buffering from the source catchments is low.

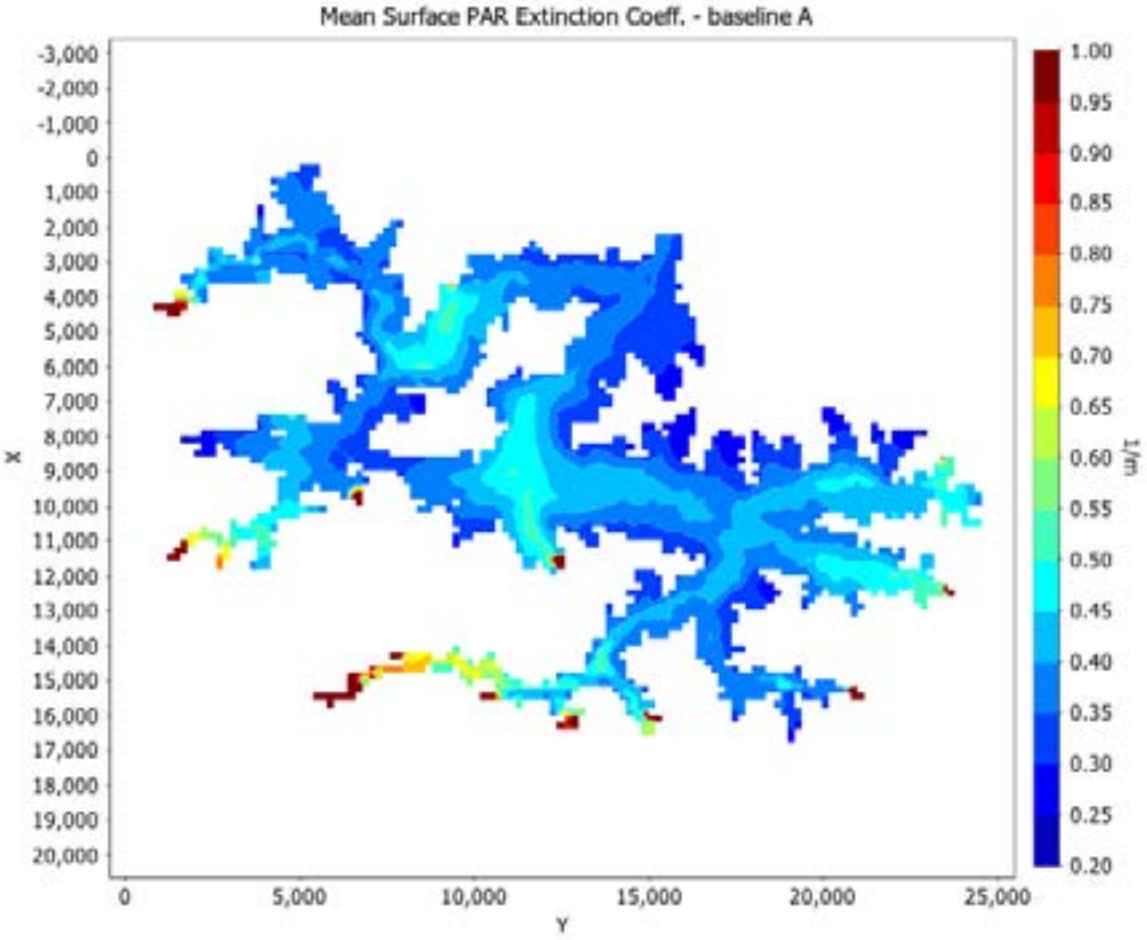

Figure 4.2 Mean light extinction coefficient at the surface during baseline simulation (a).

4.4 Long-term Change

The depth of the FRHEP outlet may influence long-term water quality in the reservoir. As opposed to most water supply reservoirs the offtake will be at a fixed relative level. The adaption of the reservoir to the outflow will be dependent on its recharge rate, which will be considerably greater than most water supply reservoirs, and resultant water quality changes will be more dependent on variations in recharge than outflow rates. Given that the recharge of the proposed reservoir is likely to be rapid compared to the proposed FRHEP extractions draw down of the reservoir will pose little risk to the water quality in the broader reservoir.

As noted above inflow concentrations of clay-bound phosphorus are quite high (based on data supplied) but will, in the presence of sufficient concentrations of divalent cations tend to settle toward the bed of the reservoir. Initially, the deposition of waste rock material onto these sediments will tend to render them isolated from the epilimnion with very little risk of resuspension or vertical migration. Indeed, the modelled mixing characteristics of the reservoir already described will tend to confine these phosphorus complexes to the stable regions of the hypolimnion even if not ‘protected’ by a layer of waste rock material.

Significant partial mixing events in the reservoir may mobilize acidity associated with the waste rock and tailings deposits in the deeper, hypolimnion regions of the reservoir, or waste rock and tailings that has been mobilised to other, potentially shallower regions in the reservoir. The effect of such acidity entering the epilimnion will be critically dependant on the concentrations

of alkalinity in this upper region of the water body (i.e. its 'buffering capacity'). The USEPA, in a study of the effects of acid rain on lakes, used data provided by Godfrey et al. (1996) to classify the susceptibility of lakes to rapid pH change due to acid addition and arrived at a lake alkalinity concentration of 20 mg/L (as $CaCO_3$) as being 'non-sensitive' to pH change. As stated, this study was related to acid rain and not the upward, vertical migration of protons originating from waste rock and tailings material. Thus, it is likely that a prudent, 'safe' alkalinity concentration for the FRHEP reservoir be higher than the 20 mg/L cited.

Modelling of the mobility of mine waste rock and tailings storage (Section 3.3.3) and the fate of waste rock and tailings leachate (see Appendix) indicate that there is: (a) likely to be some mobility of the finer fraction of the stored material, including migration into the upper reaches of the Niar arm, where exposure to DO is more likely due to the high DO concentrations of inflow waters; and (b) partial mixing events that entrain waste rock and tailings leachate into the waters above – in the same exchange these events will bring higher DO water into contact with the stored material. Whilst DO was not explicitly modelled the results of tailings deposition, retention time and tracers for the major inflows (Figure 4.3) indicate potential overlap between concentrated new inflow waters (likely to have high DO concentrations) and deposited waste rock and tailings. This is most evident in the upper Nena arm of the reservoir. In the upper Niar arm the waters that come into contact with the tailings at the bottom are considerably older (average of approximately 100 days), over which time oxygen depletion would be expected in the absence of renewal from surface processes.

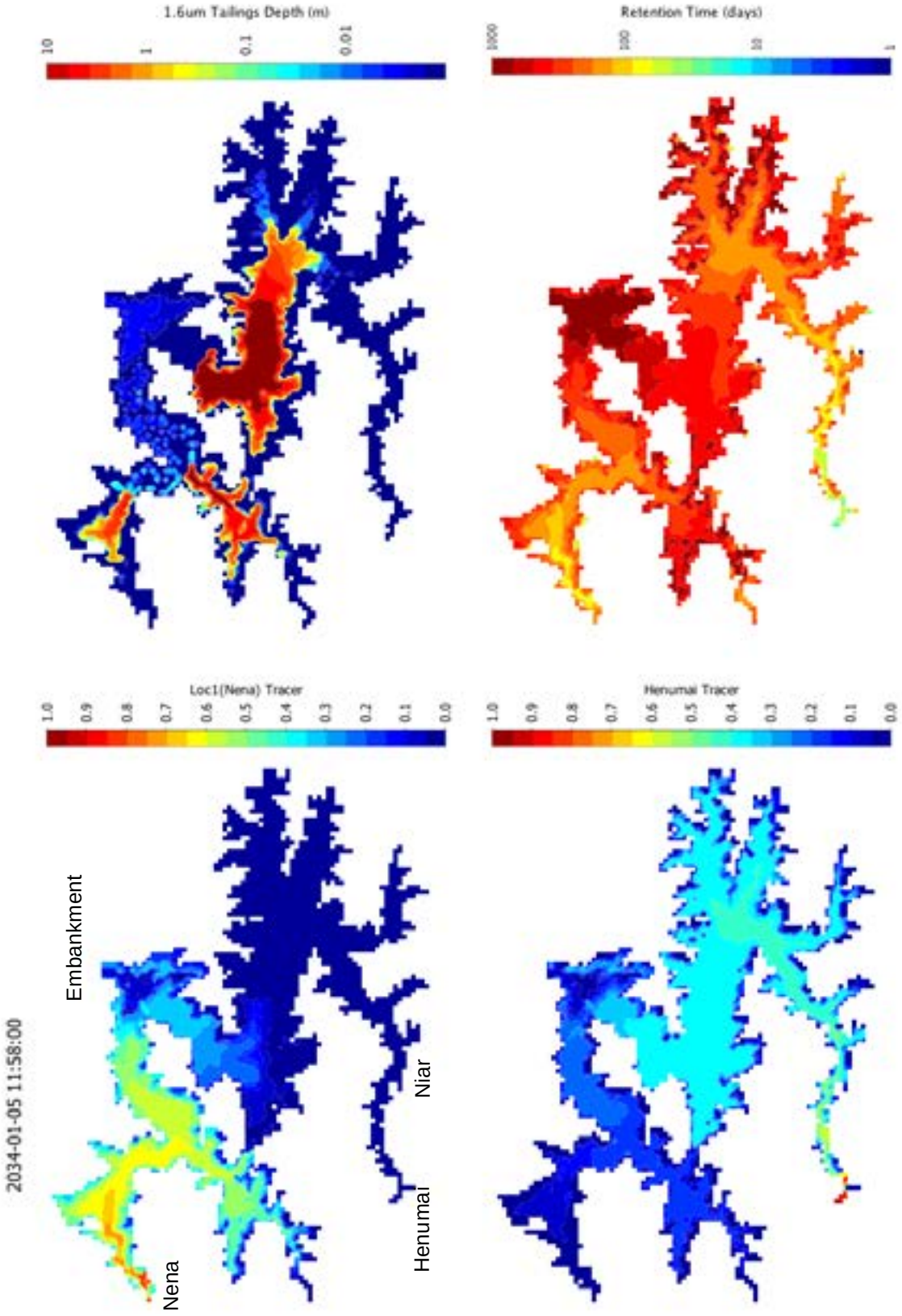

Figure 4.3 After 7 years of simulation: bottom sediment depth of 1.6 micron tailings (median for 2034), bottom water age (minimum for 2034), and Henumai and Nena inflow tracer concentration (maximum for 2034).

4.5 Downstream Release

Potential implications for downstream release water in response to the limnology of the FRHEP reservoir are summarised in Table 4.1. The table shows values from the Frieda River Airstrip monitoring site (W23, see Figure 4.4) and values that have been derived from the FRHEP model directly (for temperature and TSS) or estimated using statistical water quality values that have been applied to the simulated HEP discharge waters. Estimates were derived from the weighted average of the mean tracer concentrations in the modelled HEP release water and the 10^{th} and 90^{th} percentile values of the constituents recorded at sites upstream of the embankment. Water quality values from site W18 have been applied to tracers from Nena, Loc2 and Loc8 (see Figure 3.3); W22 to Henumai, Niar, Ariba and Dama flows; W41 to Isai flows; and W43 to Ok Binai and Loc6. A 15% volume contribution has been assigned to rainwater (no contribution to concentrations) and the residue flow, most of which comes from the Niar arm, has been assumed to have values consistent with site W22. The values from ANZECC (2000) for tropical waters have been included in the table as a reference for trigger values for physical and chemical stressors in tropical Australian water bodies with slightly disturbed ecosystems. A brief description of potential implications for downstream release due to internal processes in the reservoir is provided in the table.

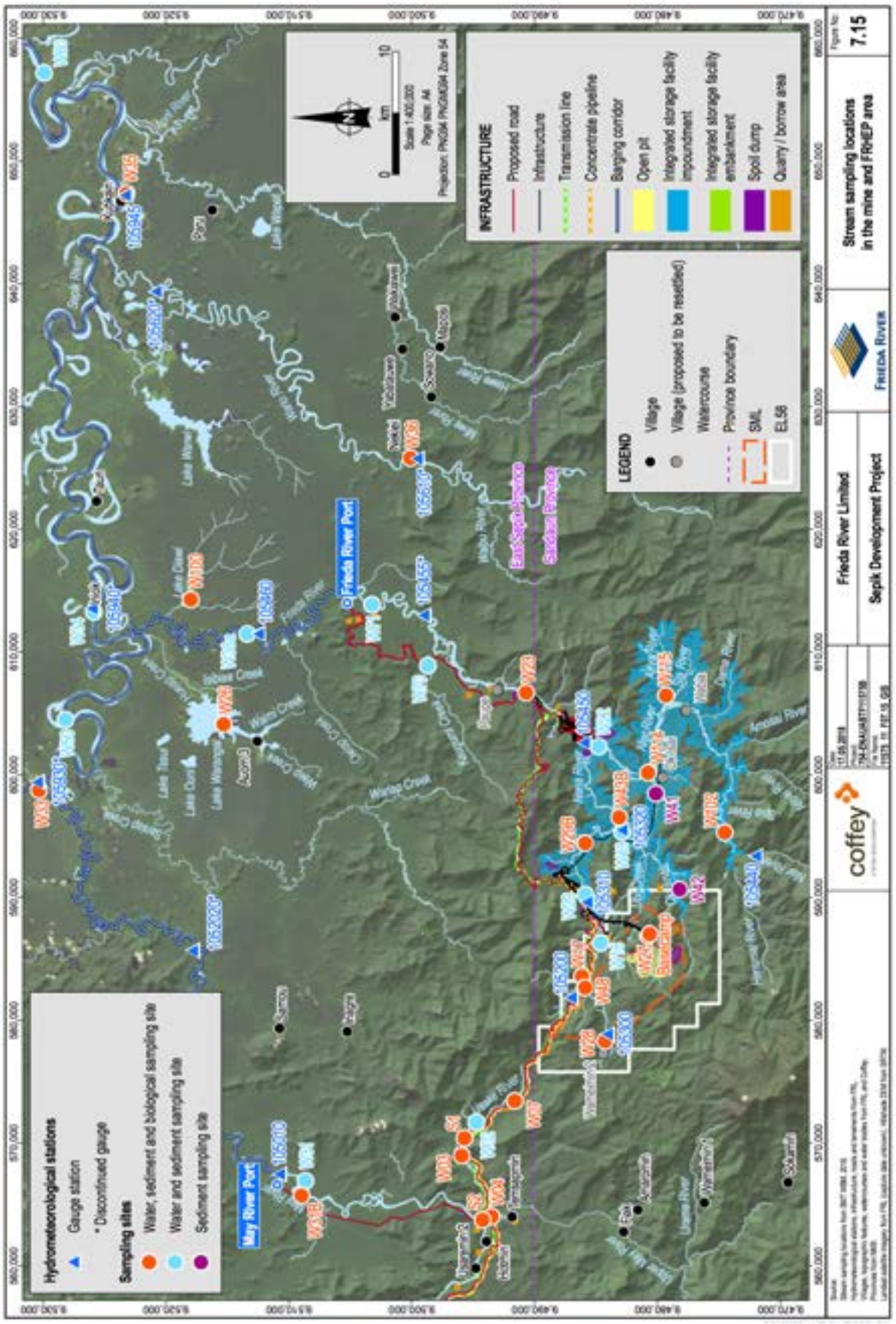

Figure 4.4 Water quality monitoring stations (provided by Coffey, 2018).

Table 4.1 Summary of potential implications for downstream release from the FRHEP reservoir. Model predictions shown are for operational HEP intake during the filling simulation.

Parameter	Percentile	FR Airstrip W23	Modelled/Calculated [b,c]	ANZECC Range [a] Upland River	Lowland River	Freshwater lakes & reservoirs
Temp. (Deg C)	10th	23.14	23.97			
	90th	28.31	25.58			
	Modelled temperature range similar to FR (Frieda River station W23) but slightly cooler, possibly due to depth of HEP extraction or sampling, they may be bias towards warmer daytime temperatues. Modelled spillway release temperatures are higher with 90th percentile of over 28 degrees C.					
TSS (mg/L)	10th	*17.36*	13.51			
	90th	*272.11*	33.32			
	Large reduction from high inputs concentraions compared to river system due to settling of sediments in the resevoir. Note that there is potential increases due to waste and tailings deposition (see revelant report sections for a discussion).					
Turb (NTU) [b]	10th	15.66	*10.38*	2 to 15	2 to 15	2 to 200
	90th	364.66	*37.52*			
	Significant reduction in TSS will reduce turbidity. Whilst there is the potential for contributions from primary production, this is unlikely to compensate for reduction in TSS and will be confined mostly to spillway release due to the depth of the HEP intake being below the euphotic depth. Releases are likely to be over the ANZECC value for river flow, however, the river data shows far higher naturally dervied values prior to FRHEP construction.					
DO (% Sat.)	10th	96.33	99.28	90 to 120	85 to 120	90 to 120
	90th	97.10	103.96			
	Prior to stabilsation widespread DO depletion may occur, with in-situ and release values below ANZECC guidelines and possibly anoxic. Deoxygenated release water is likely to be quickly re-oxygenated during the release process.					

Parameter	Percentile	FR Airstrip W23	Calculated [b,c]	ANZECC Range [a]	Upland River	Lowland River	Freshwater lakes & reservoirs
TN (mg/L)	10th	0.10	0.13		0.15	0.2 to 0.3	0.350
	90th	0.28	0.44				
	Potentially higher concentrations than ANZECC range early prior to stabilsation due to contributions from river inputs and from decomposition of inundated vegetation. This is likely to reduce during denitrification later in the pre-stablisation phase. When a stable biota forms TN likely be within ANZECC guidelines range.						
NH4 as N (mg/L)	10th	0.01	0.02		0.006	0.010	0.010
	90th	0.12	0.29				
	Potential increase (above ANZECC range) in early stages due to ammonification from decaying organic matter. Subsequent stabilisation over time to values less than upstream river concentrations as incoming NH4 is utilised within the reservoir, moreso than the reduction observed between river stations. May remain elevated in the de-oxygenated hypolimion waters. Partial mixing may entain these waters into the HEP release water, however oxidation will reduce NH4, but increase NO3 in the release water.						
NOx as N (mg/L)	10th	0.01	0.02		0.003	0.010	0.010
	90th	0.04	0.05				
	Potential increase in early stages in response to increase in nitrogen release from decomposition. Dominated by NO3 due to oxidising conditions near the surface and in the release waters.						
TP (mg/L)	10th	0.01	0.02		0.01	0.010	0.010
	90th	0.19	0.07				
	Significant reduction in clay-bound contribution to total phosporous due to sedimentation in the reservoir, which is opposite to riverine data showing an increase in TP between sites. Up to 75% of fine clay will be settled in the resevoir which suggests a similar reduction in clay-bound total phosphus may result so levels are likely to be below ANZECC guidelines.						
FRP (mg/L) [c]	10th	0.01	0.01		0.005	0.004	0.005
	90th	0.01	0.01				
	Detection limit of 10 ug/L is very high to assess likely state. The fate of the P will be related to the ionic strength of the inflows in particular the concentrations of multivalent cations.						

Parameter	Percentile	FR Airstrip W23	Calculated [b,c]	ANZECC Range [a] Upland River	Lowland River	Freshwater lakes & reservoirs
TOC (mg/L)	10th	1.00	0.85			
	90th	3.00	2.00			
	Likely to be elevated above river concentrations early after construction but subject to rapid degradation by UV light and will decrease after early stages accompanied by the adaption of phytoplanktion and macrophytes to the reservoir dynamics.					
DOC (mg/L)	10th	1.00	0.85			
	90th	2.00	1.96			
	As per TOC, depletion with exposure to UV light is likely.					
Notes	[a] Default trigger values for physical and chemical stressors for tropical Australia for slightly disturbed ecosystems. Table 3.3.4 - 3.3.5, Chapter 3 — Aquatic ecosystems, NATIONAL WATER QUALITY MANAGEMENT STRATEGY PAPER No. 4, Australian and New Zealand Guidelines for Fresh and Marine Water Quality (October 2000). [b] Values in italics are derived from relationship between NTU and TSS for data at Frieda Airstrip W23 data. NTU = 1.3712xTSS - 8.1344, R^2 = 0.97047. [c] Detection limit of 0.01 mg/L inhibits analysis.					

5 Greenhouse Gas Emissions

5.1 Overview

Hydroelectric reservoirs are known to produce greenhouse gas (GHG) emissions, primarily through the decomposition of organic material and the bubbling of gas from reservoir sediments. The three main GHGs emitted by reservoirs are methane (CH_4), carbon dioxide (CO_2) and nitrous oxide (N_2O) and the net greenhouse gas effect of reservoirs has been a point of research since the mid-1990s, given the potential impact of these releases on climate change. A recent global synthesis of GHG emissions from hydroelectric reservoirs (Deemer et al. 2016) found that hydroelectric reservoirs produce 500 to 1200 Pg CO_2-equivalent per annum from an estimated combined surface area of 3.1 x 10^4 km^2.

This chapter aims to estimate the emissions of methane, carbon dioxide and nitrous oxide from the FRHEP reservoir based in the findings of previous research on GHG emissions from reservoirs. This chapter also discusses the variability in GHG emissions from hydroelectric reservoirs and how this may affect the presented results.

5.2 Background

The potential for hydroelectric reservoirs to emit GHGs is thought to be caused by microbial breakdown of vegetation following reservoir flooding. Research in this area was motivated by attempts of the International Panel for Climate Change (IPCC) to compare net emissions of power generation methods (Rosa and Schaeffer 1995). Rudd et al. (1993) identified methane (CH_4) and carbon dioxide (CO_2) as the primary GHG emissions released by hydroelectric reservoirs; however, nitrous oxide (N_2O) is now also measured (Deemer et al. 2016).

The global warming potential (GWP) of CH_4 is another main point of research, as this influences the overall estimations of GHG emissions from a reservoir. GWP is defined by Rosa and Schaeffer (1995, pp. 149) as 'ratio of the instantaneous radiative forcing of a particular GHG and that of an equal and simultaneous emission of a reference gas', which is typically CO_2. GWP allows GHG emissions to be converted into a single CO_2-equivalent emission. Currently, the GWP of CH_4 used by the IPCC is 34 (that is, one unit emission of CH_4 is equivalent to 34 unit emissions of CO_2) (Fearnside 2015). However, Fearnside (2015) argues that this estimate relies heavily on assumptions that are not universal.

There are numerous methods for investigating GHG emissions in hydroelectric reservoirs, as well as multiple emissions pathways. The three main pathways of emissions are; diffusion of gases across the reservoir surface, bubbling emissions of methane from anaerobic digestion in the sediments, and downstream emissions, where gases are released at the turbines or further downstream from the reservoir (Hertwich 2013). There is a significant amount of spatial and temporal variability in these emissions, which may introduce uncertainty into the measurement results and into any attempts to determine emissions levels.

Despite the uncertainty, research indicates that hydroelectric reservoirs are likely to be CH_4 sources and have the potential to be either CO_2 sources or sinks.

5.3 Emissions Estimates

5.3.1 Estimation Methods

Two simple methods for GHG emissions estimates have been identified in the literature and applied to FRHEP. Barros et al. (2011) found a strong negative correlation between fluxes of CH_4 and CO_2 and reservoir age and latitude. There is a declining exponential regression for each input variable and GHG flux, as shown in Figure 5.1. Deemer et al. (2016) performed a

statistical analysis between three greenhouse gases with a range of reservoir characteristics and water quality variables to determine the best predictor variable: CH_4 was best correlated with chlorophyll-a concentration; CO_2 was best correlated with mean annual rainfall; and N_2O was correlated with nitrate concentration (Figure 5.2). Despite the scatter, the relationships offer the capability to make an approximate estimate of the potential emissions from FRHEP. Deemer et al. (2016) also notes that latitude has been more recently identified as being poorly correlated with emissions.

Importantly, these emissions estimates do not include a carbon budget or account for sequestration processes. For example, photosynthetic organisms either living in the reservoir or that colonise littoral zones during changes in reservoir levels may sequester carbon dioxide, therefore offsetting potential emissions.

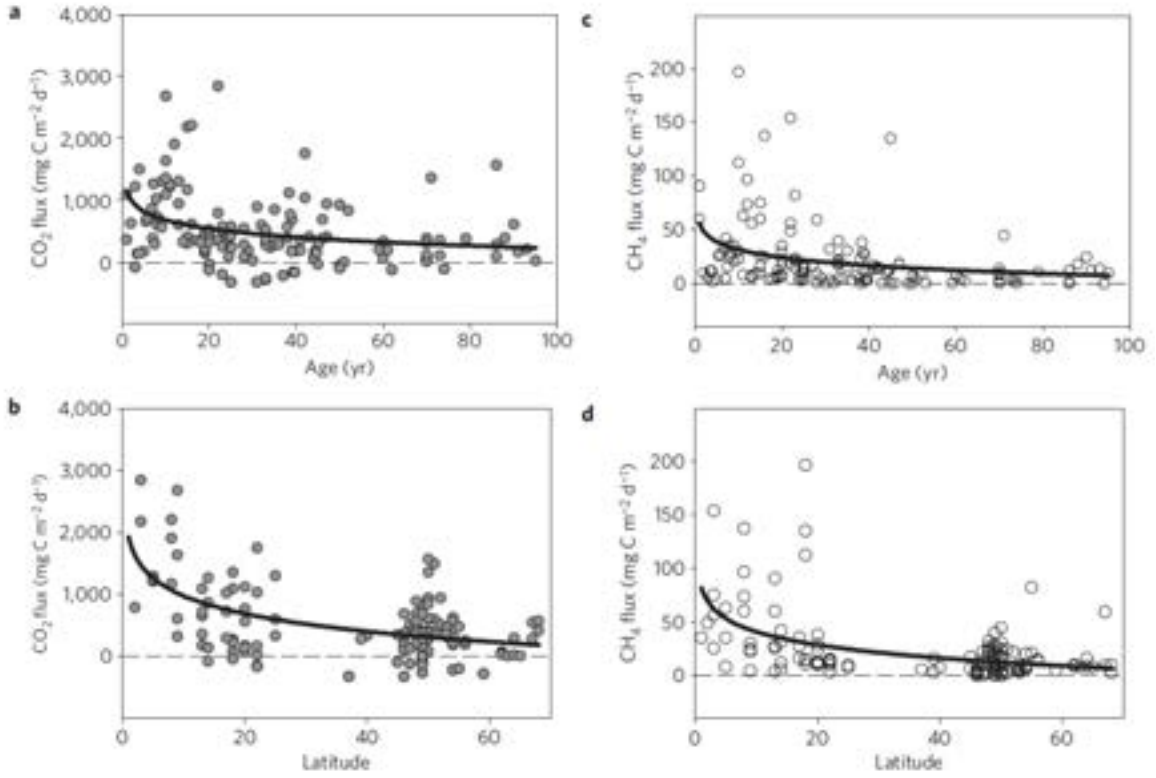

Figure 5.1 Negative exponential correlation between reservoir age and latitude with CO_2 and CH_4 (adapted from Barros et al. 2011)

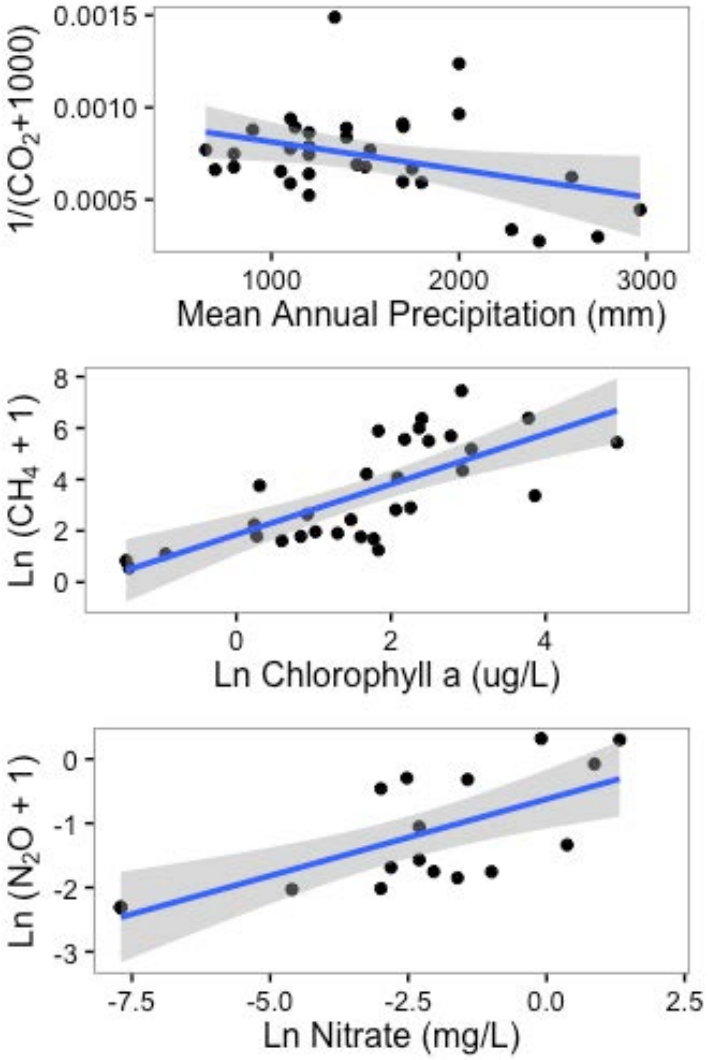

Figure 5.2 Best identified predictors of GHG flux from Deemer et al. (2016).

5.3.2 Estimate for FRHEP

By applying the latitude of FRHEP, an annual precipitation of 7,700 mm, Chlorophyll-a concentrations of 20 µg L^{-1} (Hydronumerics, 2011) and nitrate concentration of 0.02 mg L^{-1} (from water quality data) GHG emission estimates were determined for the two methods (see Table 5.1). Note that the estimates were not extrapolated beyond the ranges that were shown in the documented figures for the annual rainfall. CO_2-equivalent emissions were calculated following Deemer et al. (2016) using:

$$CO_2\text{-equivalent } \left(\frac{mg}{m^2 d}\right) = \mathrm{CH_4}\ \left(\frac{mg}{m^2 d}\right) \times 34 + \mathrm{CO_2}\ \left(\frac{mg}{m^2 d}\right) + \mathrm{NO_2}\ \left(\frac{mg}{m^2 d}\right) \times 298.$$

Estimation using methods from Barros et al. (2011) correlates reasonably well with Deemer et al. (2016). The estimation for N_2O from Deemer et al. (2016) indicates no emissions, so this estimate was not included in the CO_2-equivalent calculation. Moreover, no tropical reservoirs in the data set used to derive the relationships contained both in-water nitrate concentration (input) and nitrous oxide (output) data. The two estimates show a potential emissions range from approximately 3200 to 5100 mg CO_2-equivalent m^{-2} d^{-1}.

The estimates above were calculated using relationships that have been derived from data collected in reservoirs subjected to a range of climates, including temperate and boreal. However, tropical reservoirs are known to emit higher levels of GHGs than reservoirs in other

climates (Fearnside 2015, Li and Zhang 2014). Re-casting the relationships of Deemer et al. (2016), with regressions that were re-fitted using only data from tropical reservoirs (and omitting those above 1000 m ASL) (see Figure 5.3) increased the estimated emissions to approximately 6040 mg CO_2-equivalent m^{-2} d^{-1} (see Table 5.1). This equates to approximately 273,000 t/yr of CO_2-equivalent GHG emissions from the FRHEP water body. Total GHG emissions for PNG in 2000 was estimated by the United Nations Framework Convention on Climate Change (UNFCCC) to have been 14,251,300 t CO_2-equivalent (UNFCCC, 2014). This suggests that FRHEP may contribute 1 to 2% of GHG emissions in PNG (based on total emissions estimates from 2000). Note that FRHEP is one component of the FRCGP and a separate GHG assessment for the whole of project is being completed by others (SLR).

The potential spatial and temporal variability of GHG emissions is examined in the following section. We note for example that reservoir age is not considered in Table 5.1, and emissions could change over the life of a reservoir or due to large significant changes in reservoir operations.

Table 5.1 Estimated mean daily areal flux of methane (CH_4), carbon dioxide (CO_2), nitrous oxide and CO_2-equivalent

Method	**CH_4 (mg m^{-2} d^{-1})**	**CO_2 (mg m^{-2} d^{-1})**	**N_2O (mg m^{-2} d^{-1})**	**CO_2-equivalent (mg m^{-2} d^{-1})**
Barros et al. (2011)	55	1300	-	3170
Deemer et al. (2016)	120.5	1000	-0.79	5097
Deemer et al. (2016) – Tropical Lakes	133.6	1500		6042

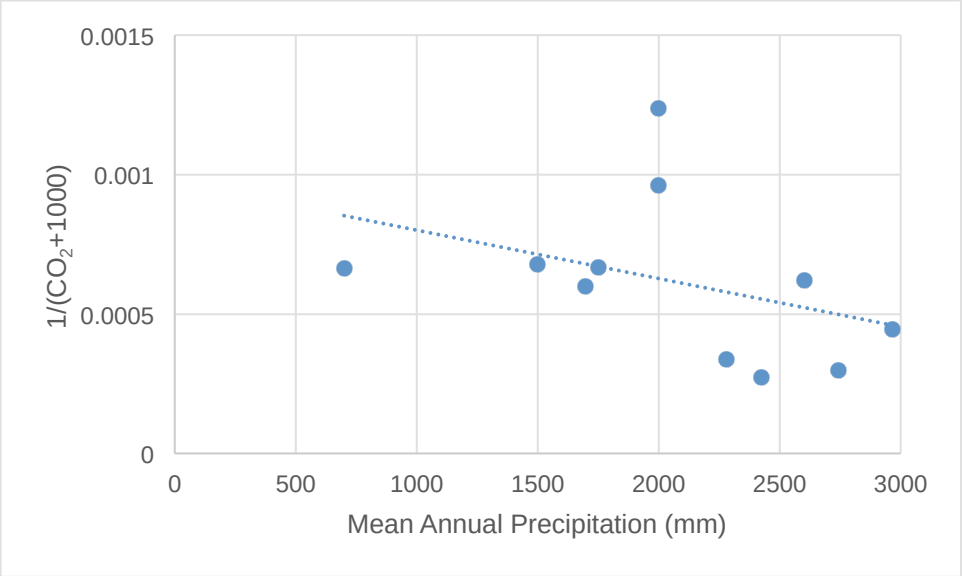

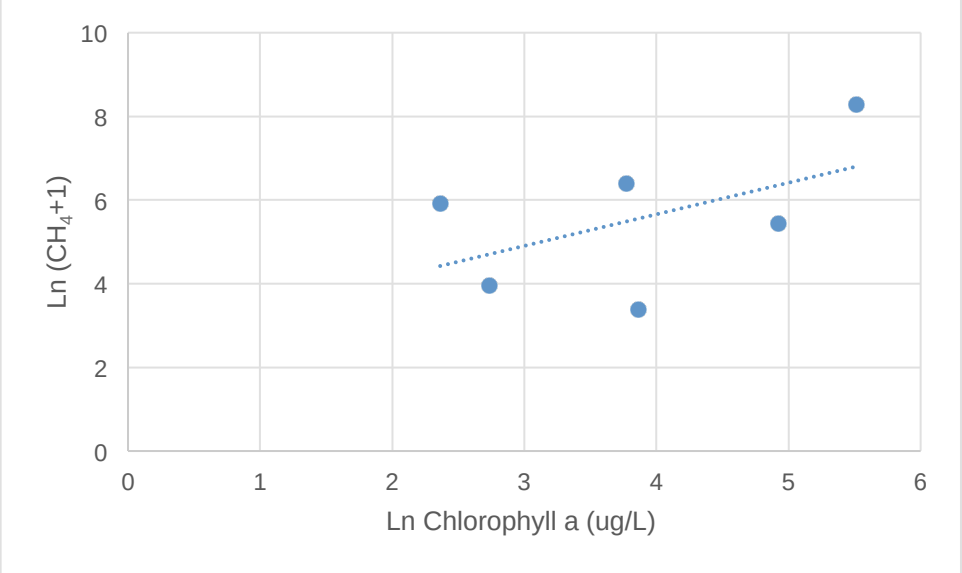

Figure 5.3 Regressions from Deemer et al. (2016) applied using only tropical reservoir data (excluding reservoirs above 1000 m in elevation).

5.3.3 Analogous Reservoirs

Figure 5.4 shows a comparison of this estimate for FRHEP with other non-eutrophic tropical reservoirs below 1000 m ASL. Three reservoirs were in a similar total emissions range as FRHEP: Petit Saut in French Guinea, and Samuel and Tucurui reservoirs in Brazil, all of which are HEP reservoirs constructed in dense tropical forests (Rosa et al. 2003). The characteristics of these reservoirs have has been summarised in Table 5.2.

Of these three reservoirs, Petit Saut emits the highest amount of methane. Lima et al. (2005) suggest that methane oxidation is less efficient in shallower reservoirs, resulting in higher bubbling methane emissions. However, Petit Saut has a higher average depth than Samuel, and twice the magnitude of methane emissions (Deemer et al. 2016). The elevated methane release was linked by Guerin et al. (2006) to a weir installed downstream of Petit Saut reservoir, which increases aeration and degassing, at times accounting for 70% of all CH_4 emissions from Petit Saut (Abril et al. 2005). Samuel Reservoir has the lowest methane

emissions despite being the shallowest reservoir (Deemer et al. 2016). This is likely due to high variability in methane emissions, which are not captured in a single emissions figure. Decomposition of flooded vegetation in Petit Saut was found to be the primary source of carbon emissions for ten years following construction (Abril et al. 2005). This illustrates the high level of emissions expected during the early stages of a reservoir's lifespan.

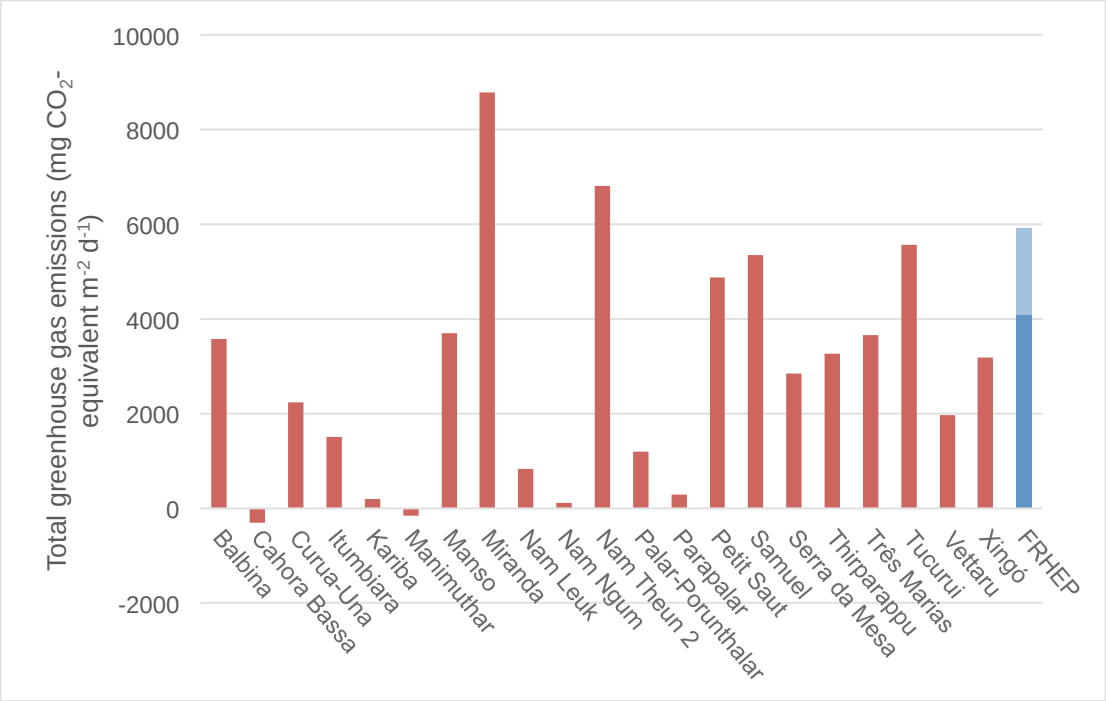

Figure 5.4 Gross emissions from tropical hydroelectric plants with estimate for FRHEP (mg CO_2-equivalent m^{-2} d^{-1}). Light blue indicates estimated range for FRHEP

Table 5.2 Characteristics and Gross CO_2-equivalent emissions of Tucurui, Petit Saut, Samuel and FRHEP reservoirs.

Reservoir	**Mean Depth (m)**	**Surface Area (km^2)**	**Capacity (km^3)**	**Gross CO_2-equivalent emissions (mg/m^2d)**
FRHEP	75	124 (at MOL)	9	6040
Tucurui	18.9	2430	46	5573
Petit Saut	9.6	365	3.5	4877
Samuel	8.6	558	5	5355

5.4 Spatial and Temporal Variability

Variability within reservoirs increases the complexity of measuring and aggregating GHG emissions making reliable measurement and estimation difficult. Emissions also vary considerably in time, often beginning with an initial peak as the decomposition of inundated vegetation slows over time, as shown in Demarty et al. (2011) (Figure 5.5). Decommissioning of a reservoir and the potential release of gases when sediments are exposed at lower water

levels (Pacca 2007) may lead to a second emissions spike, increasing the lifetime emissions of a reservoir.

For the FRHEP the planned deposition of waste rock and tailings into the reservoir may accelerate the reduction in emissions over time because of the burial of flooded vegetation. One pathway for emissions is ebullition, which is the bubbling of methane to the reservoir surface from sediments. Ebullition has a high level of spatial variability (and for this reason is often omitted from measurements - Delsontro et al. 2010, Deemer et al. 2016), however an estimated 60 % of all emissions of CH_4 are caused by ebullition (Deemer et al. 2016; Deshmukh et al. 2014; Li and Zhang 2014). This high share of emissions via ebullition may mean that the addition of waste rock and tailings into FRHEP could have a strong dampening effect on emissions.

However, there are large areas above the level of the waste rock and tailings in which decomposition of the initial flooded vegetation would still take place. In addition, Rosa et al. (2004) and Barros et al. (2011) also note that variability in emissions may occur when reservoir is drawn down, allowing land-based plants to colonise. These plants then decompose when reservoir levels increase so an increase in drawdown frequency is likely to increase overall emissions.

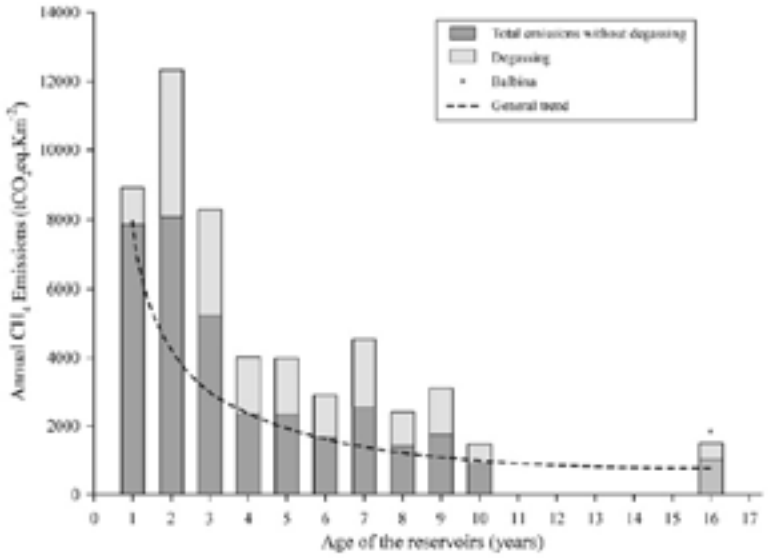

Figure 5.5 Annual emissions (tonnes CO_2-equivalent km^{-2}) from Petit Saut and Balbina Reservoirs, Brazil, from Demarty (2011)

6 Summary and Recommendations

There are a number of key findings regarding the FRHEP reservoir that have been discussed in this report. A broad summary of these findings is provided below. These findings are based on the current project description as presented in the report, and the results of the modelling that has been undertaken.

- The reservoir is likely to be persistently stratified with no regular periods of complete mixing. The addition of waste rock and tailings below the epilimnion of the reservoir is unlikely to alter the top-down stratification structure;
- Inflows from the major rivers form intrusions through the reservoir in the metalimnion at a depth of neutral buoyancy following an initial plunge near the headwaters;
- The HEP intake flow rate and depth play an important role in shaping the stratification and assisting with the short-circuiting of inflow waters through the reservoir. Simulations of HEP closure (and release only via the spillway) indicate that there is significant change in the stratification but no break-down of the stratification;
- The water quality in the reservoir will go through a period of early adjustment to filling that is dominated by decomposition of inundated vegetation. The establishment of macrophyte growth will then stabilise the water quality over time. A summary table of the implications for downstream release is provided Section 4.5;
- There is significant uncertainty associated with the assessment of mobility of waste rock and tailings due to unknown critical shear stress and erosion rate of the stored waste rock and tailings particle mixtures;
- For the likely range of critical shear stress and under base case flow conditions (realisation 88) the simulations suggest that some resuspension of the waste rock and tailings should be expected (the extent will depend on the critical shear stress and erosion rate – see bullet point above). The scenario considered with low required critical bed stress for resuspension (i.e. the derived mobility case) is likely to represent the upper range for waste rock and tailings mobility under base case flow conditions;
- Despite the potential for resuspension, the modelling undertaken in this study suggests that the plumes formed by resuspended waste rock and tailings are likely to be largely confined to the waters beneath the HEP intake or spillway (after closure of the HEP). Resuspended material that does entrain higher into the water column and is subsequently released downstream undergoes significant dilution though mixing and settling before extraction so that the contribution to the TSS release downstream is small;
- For tailings stored in the mid-Niar branch large flow events and storms may induce sufficient bed stress to mobilise (followed by transport to the embankment) the fine fraction of the tailings deposits if there is no sheltering or cohesion offered by the tailings particle size mix to increase the resistance to bed stress. Up-valley migration of deposited material and/or intentional storage of the tailings higher up in the Frieda arm will increase the likelihood of resuspension;
- For tailings stored in the upper Nena branch there is likely to be mobilisation due to higher bed stress that is followed by transport to the embankment of the fine fraction of the tailings. If there is no sheltering or cohesion offered by the tailings particle size mix to increase the resistance to bed stress the resuspension events are likely to be frequent;

- For waste rock stored in the Nena branch the finer portion is likely to resuspend with the frequency and extent of resuspension dependent on the mobility of the fine fractions within the waste rock particle mix;
- Deposition of waste rock by barge near to the embankment (for the 1km and 2 km upstream model tests undertaken) is likely to lead to significant release of the finer fraction of the waste rock through the HEP intake;
- Leachate from the waste rock and tailings is likely to be largely confined to below 180 m RL but will also be released via the HEP intake after considerable dilution (up to 30 times lower concentration than reached above the sediments). However, dilution is likely to periodically reduce (modelling suggest down to 4 times dilution) during partial mixing events. Partial mixing events leading to a dilution of less than 10 times occurred on 8 occasions over the duration of the 10 year simulation; and
- GHG emissions from the FRHEP reservoir are estimated to be up to approximately 6000 mg CO_2-equivalent m^{-2} d^{-1} in the initial stages after filling. A slow down of decomposition of inundated vegetation and burial of that vegetation under stored waste rock and tailings will likely lead to a decline in emissions over time.

Based on the findings presented in this report and the uncertainty associated with the assumptions that have been required, some recommendations for further work are:

- Investigate (by laboratory studies) the potential mobility of the stored waste rock and tailings, specifically the critical shear stress for resuspension and the erosion rates when resuspension occurs;
- Further simulations and sensitivity assessments should be considered using improved knowledge regarding waste rock and tailings mobility. There are key uncertainties associated with the mobility of the waste rock and tailings that are stored in the reservoir and addressing these uncertainties will require additional information about the potential mobility of the waste rock and tailings particles (from laboratory analysis) and re-simulation of their mobility in the FRHEP using the additional information and a range of environmental conditions.
- Additional modelling sensitivity analysis in forward works should include broadening the study of wind related limnological processes, further testing of a finer resolution model to determine the effects of grid resolution on modelling outcomes, and investigating extreme conditions (such as high flows and storms) to provide information about worst-case scenarios.
- Following from the above the changes to suspended solids concentrations and PSD that occur during high flow events should be determined to improve catchment inputs in any further simulations for the FRHEP;
- Decreased detection limits for water quality sampling (most critically for FRP) should be considered to better understand the likely water quality response;
- Additional modelling scenarios to assess the potential in-reservoir and downstream impact of a failure of the tailings pipes. The extent of the impact will depend on the size of failure, the location of the failure in the reservoir (most critically the distance from the embankment) and the depth of the failure; and
- Assessing long-term (e.g. up to 100 years) changes in the limnological behaviour that occur in response to changes in flow and meteorology have not been considered in this report, but should be given consideration in future investigations.

Despite these uncertainties, some key recommendations that arise from this scoping phase study and relate to the project parameters are:

- Careful consideration should be given to storage of waste rock and tailings in the upper reaches of the Nena branch of the FRHEP (as indicated in the current project description) due to the exposure of these areas to higher bed stress that is likely to be sufficient to trigger resuspension of the stored material and transport of the fine fractions of this material throughout the reservoir and downstream of the reservoir; and
- Consideration should to given to the operational rules of the FRHEP reservoir to avoid large and frequent fluctuations in water level that put strain on littoral habitats and potentially reduce the likelihood of establishing a reservoir with good water quality;

7 References

Abril, G., Guerin, F., Richard, S., Delmas, R., Galy-Lacaux, C., Gosse, P., Tremblay, A. Varfalvy, L., dos Santos, M. A., Matvienko, B. 2005. Carbon dioxide and methane emissions and the carbon budget of a 10-year old tropical reservoir (Petit Saut, French Guiana). Global Biogeochemical Cycles, vol. 19

Amorocho, J. and Devries, J.J. 1980. A new evaluation of the wind stress coefficient over water surfaces. J. Geophys. Res. 85, pp. 433–442.

Anohin, V., Imberger J,, Romero, J. and Ivey, G.N. 2006. Effect of Long Internal Waves on the Quality of Water Withdrawn from a Stratified Reservoir. *Journal of Hydraulic Engineering.* Vol 132 (11).

ANZECC & ARMCANZ Australian and New Zealand Environment and Conservation Council & Agriculture and Resource Management Council of Australia and New Zealand (2000): Australian and New Zealand Guidelines for Fresh and Marine Water Quality. National Water Quality Management Strategy No 4; ISBN 0 9578245 0 5; ISSN 1038 7072 (ANZECC Guidelines); p.3.3-12.

ANZECC. 2000. Table 3.3.4 - 3.3.5, Chapter 3 — Aquatic ecosystems, NATIONAL WATER QUALITY MANAGEMENT STRATEGY PAPER No. 4, Australian and New Zealand Guidelines for Fresh and Marine Water Quality (October 2000).

Barbosa, A.R. and Padisak, J. 2002. The forgotten lake stratification pattern:atelomixis, and its ecological importance. Verhandlungen des Internationalen Verein Limnologie, 28:1385-1395.

Barros, N, Cole, J, Tranvik, L, Prairie, Y, Bastviken, D, Huszar, V, Giogeo, P and Roland, F 2011, *Carbon emission from hydroelectric reservoirs linked to reservoir age and latitude,* Nature Geoscience, 4: 593-596

Beadle L. C. 1974. The Inland Waters of Tropical Africa. Longman Group Limited, London.

Boland, K.T. (1993) A Comparison of Two Lakes in Northwest Queensland, Ph.D. thesis, James Cook University of North Queensland, 252 pp

Bengtsson, L., Hellstrom, T., & Rakoczi, L. (1990). Redistribution of sediments in three Swedish lakes. *Hydrobiologia,* 192: 167-181.

BMT WBM. 2018. Frieda River EIS - Water Quality, Sediment Quality and Aquatic Ecology Baseline Report. Report prepared by BMT WBM Pty Ltd.

Boland, K.T. (2008). *Potential Water Quality Impacts associated with raising Darwin River Dam.* Report prepared for HLA Environmental and The Northern Territory Power and Water Authority. Unpublished.

Cao, Z., Pender G. and Meng J. 2006. Explicit formulation of the Shields digram for incipient motion of sediment. Journal of Hydraulic Engineering, 132(10), pp 1097-1099.

Casamitjana X., Serra T., Colomer J., Baserba C. and Pe´rez-Losada, J. 2003. Effects of the water withdrawal in the stratification patterns of a reservoir. *Hydrobiologia* 504: 21–28

Casulli, V. and Cheng, R.T. 1992. Semi-implicit finite difference methods for three-dimensional shallow water flow. *Int. J. Numer. Methods Fluids*. 15, pp. 629–648.

Chase, R.R.P., (1979). Settling Behaviour of Natural Aquatic Particulates. *Limnol. Oceanogr.* 24(3), pp.417-426.

Chung, E.G., Bombardell, F.A., Schladow, S.G. 2009. Sediment resuspension in a shallow lake. Water Res. Research. 45.

Deemer, B, Harrison, J, Li, S, Beaulieu, J, Delsontro, T, Barros et al., N, Bezerra-neto, J, Powers, S, A Dos Santos, M, and Vonk, V 2016, *Greenhouse Gas Emissions from Reservoir Water Surfaces: A New Global Synthesis,* Bioscience, 66: 949 – 964

Demarty, M and Bastien J 2014, *GHG emissions from hydroelectric reservoirs in tropical and equatorial regions,* Energy Policy, 39: 4197 – 4206

Deshmukh, C, Serca, D, Delon, C, Tardif, R, Demarty, M, Jarnot, C, Meyerfeld, Y, Chanudet, V, Guedant, P, Rode, W, Descloux, S, Geurin, F 2014, *Physical controls on CH4 emissions from a newly flooded subtropical freshwater hydroelectric reservoir: Nam Theun 2,* Biogeosciences, 11: 4251-4269

dos Santos, M. A., Rosa, L. P., Sikar, B., Sikar, E., dos Santos, E. O. 2006. Gross greenhouse gas fluxes from hydro-power reservoir compared to thermo-power plants. Energy Policy. 34: 481 – 488

Fearnside, P 2015, *Emissions from tropical hydropower and the IPCC*, Environmental Science and Policy, 50: 225 – 239

Geremew, A.M. and Yanful E.K. 2011. Role of fines on cohesion behaviour of mine tailings inferred from critical shear stress. Can. Geotech J. 48: pp 568-582.

Guerin, F., Abril. G, Richard, S., Burban, B., Reynouard, C., Seyler, P. and Delmas, R. 2005. Methane and carbon dioxide emissions from tropical reservoirs: Significance of downstream rivers. Geophysical Research Letters. Vol. 33

Golder Associates. 2011. Hydraulic and Sediment Impact Analysis Modelling – Task 3, Golder Associates Pty Ltd, report produced for Xstrata Frieda River Limited, August, 2011

Golder Associates. 2018. Sediment Transport Assessment: Frieda River Project – 2017 Study Program Report. Prepared for Frieda River Limited, May 2018.

Hertwich, E 2013, *Addressing Biogenic Greenhouse Gas Emissions from Hydropower in LCA,* American Chemical Society, 47: 9604-9611

Hydronumerics, 2011. Frieda River Project Hydro-power Reservoir Limnology Study. Technical Report prepared for Xstrata Frieda River Ltd.

Hydronumerics, 2017, *Frieda River Hydro Dam Design Study Phase 1: Concept Design and Fatal Flaws*, prepared for SRK Consulting (Australasia) Pty Ltd

Imberger, J. and Patterson, J.C. 1981. A dynamic reservoir simulation model - DYRESM 5. Transport models for inland and coastal waters H. Fischer (ed.). Academic Press., pp. 310– 361

Jacquet, J. 1983. Simulation of the thermal regime of rivers. Mathematical modeling of water quality: Streams, lakes and reservoirs: G.T. Orlob (ed.). Wiley-Interscience.

Johnson, R.G. (1974). Particulate Matter in the Sediment-Water Interface in Coastal Environments*. J. Mar. Res*. 32: pp.313-330.

Krone, R.B. (1976) *Flume Studies in the Transport of Sediment in Esturial Shoaling Processes*. Hydraulics Engineering Laboratory, University of California. Technical Report. No ref. no.

Lamb, M.P., Dietrich, W.E., Venditti, J.G. 2008. Is the critical Shields stress for incipient motion dependent on channel-bed slope?

Lamche, G., Domin, J., Boland, T and Boland, K. (2012). *Limnology and Water Quality in Darwin River Reservoir, Summary 12 months Report, June 2011-May 2012*. Report prepared by Tropical Water Solutions Pty. Ltd. for the Northern Territory Power and Water Authority. Unpublished.

Lewis Jr, W.M. 1995. Tropical lakes: how latitude makes a difference. Tropical limnology, 1:29–44.

Lick, W., 1986. Modelling the transport of fine-grained sedi- ments in aquatic systems. *Sci. Total Environ*. 55, 219–228.

Lima, I. B. T. 2005. Biogeochemical distinction of methane releases fromtwo Amazon hydroreservoirs. Chemosphere. 59: 1697-1702

Mian, M.H., and Yanful, E.K. 2003. Tailings erosion and resuspension in two mine tailings ponds due to wind waves. *Advances in Environmental Research*, 7: 745-765.

Pacca, S 2007, *Impacts from decommissioning of hydroelectric dams: a life cycle perspective,* Climatic Change, 84: 281-294

Parker, G., Garcia, M.H and Fukushima, W.Y. 1997. Experiments on turbidity current over an erodible bed. Journal of Hydraulic Research, (1) 123-147.

Prowse, G.A. and Talling, J.F., (2003), The Seasonal Growth and Succession of Plankton Algae in the White Nile. *Limnology and Oceanography*, 3, doi: 10.4319/lo.1958.3.2.0222.

Redfield A.C. (1958). The biological control of chemical factors in the environment. *American Scientist*, 46:205-221.

Rosa, L and Schaeffer, R 1995, *Global warming potentials: the case of emissions from dams*, Energy Policy, 23: 149-158

Rosa, L, Aurelio, M, Matveinko, B, Oliveira, E and Sikar, E 2004, *Greenhouse Gas emissions from hydroelectric reservoirs in tropical regions*, Climatic Change, 66: 9-21

Rudd, J, Harris, R, Kelly, C and Hecky, R 1993, *Are Hydroelectric Reservoirs Significant Sources of Greenhouse Gases?*, Ambio, 22: 246-248

Sinohydro Bureau, 2017. Hydro Electric Project-Selection Phase Study Site Selection Report (Draft, March 2017).

SKM 2011. Frieda River Project Environmental Impact Statement, Site-Wide Water and Load Balance Report. Document No: FRP03-AAAC-EV-RP-0001. Prepared by SKM, August 2011

SRK Consulting (Canada) Inc. 2016. Frieda River - Hydrology Baseline Report, April 2016. Prepared for PanAust Limited.

SRK 2017a. Frieda River Hydroelectric Power Project Memo PNA007, 9 February 2017, Tailings and Waste rock Capacity Assessment

SRK 2017b. FRHEP – SPS Design Project Memo PNA009, 10 November 2017. Tailings and Mine Waste rock Management.

SRK 2017c. Project Memo PNA009 Frieda River FRHEP - Hydrology for FRHEP design, 17 Feb 2017.

SRK, 2018. Project Memo: PNA009_MEMO_Tailings and Mine Waste rock Management - FRHEP_Rev2.pdf

Stumm W & Morgan JJ. 1996. Aquatic chemistry. 3rd edn, John Wiley & Sons, New York.

Stumm, W. and Morgan, J.J. 1970. *Aquatic Chemistry, An Introduction Emphasizing Chemical Equilibria in Natural Waters.* Wiley-Interscience, New York. p.510.

Talling, J. F. and Lemoalle J. 1998. Ecological Dynamics of Tropical Inland Waters. Cambrige University Press.

Terwindt, J.H.J. (1976). Deposition, Transportation and Erosion of Mud. in; *Interactions Between Sediments and Fresh Water*, ed. H.L. Golterman, Dr. W. Junk, The Hague. pp.19-24.

Townsend SA. 1996. Metalimnetic and hypolimnetic deoxygenation in an Australian tropical reservoir of low trophic status. In: *Perspectives in Tropical Limnology*, F Scheimer and KT Boland (Eds.), SBP Academic Publishing, Amsterdam.

Trolle, D. and Hamilton, D.P. and Hipsey, M.R. and Bolding, K. and Bruggeman, J. and Mooij, W.M. and Janse, J.H. and Nielsen, A. and Jeppesen, E. and Elliott, J.A. and Makler-Pick, V. and Petzoldt, T. and Rinke, K. and Flindt, M.R. and Arhonditsis, G.B. and Gal, G. and Bjerring, R. and Tominaga, K. and Hoen, J. and Downing, A.S. and Marques, D.M. and Fragoso Jr., C.R. and Søndergaard, M. and Hanson, P.C., (2012). *A community-based framework for aquatic ecosystem models*, Hydrobiologia, vol. 683, no. 1, pp. 25-34.

UNFCCC. 2014. Papua New Guinea Second National Communication under the United Nations Framework on Climate Change. A www publication accessed on 13 October 2016 at http://unfccc.int/resource/docs/natc/pngnc2.pdf.

Vyverman, W. 1994. Limnological features of lakes on the Sepik-Ramu floodplain, Papua New Guinea. Australian Journal of Marine and Freshwater Research. 45:1209-1224.

Vollenweider, R. (1968). Scientific Fundamentals of the Eutrophication of Lakes and Flowing Waters, with Particular Reference to Nitrogen and Phosphorus as Factors in Eutrophication. OECD. Paris. DAS/CSI/68.27.

APPENDIX

Frieda River Hydroelectric Project
Limnology Study, Phase 2.

TABLE OF CONTENTS

1 Model Set-up

1.1 Bathymetric Area and Volume

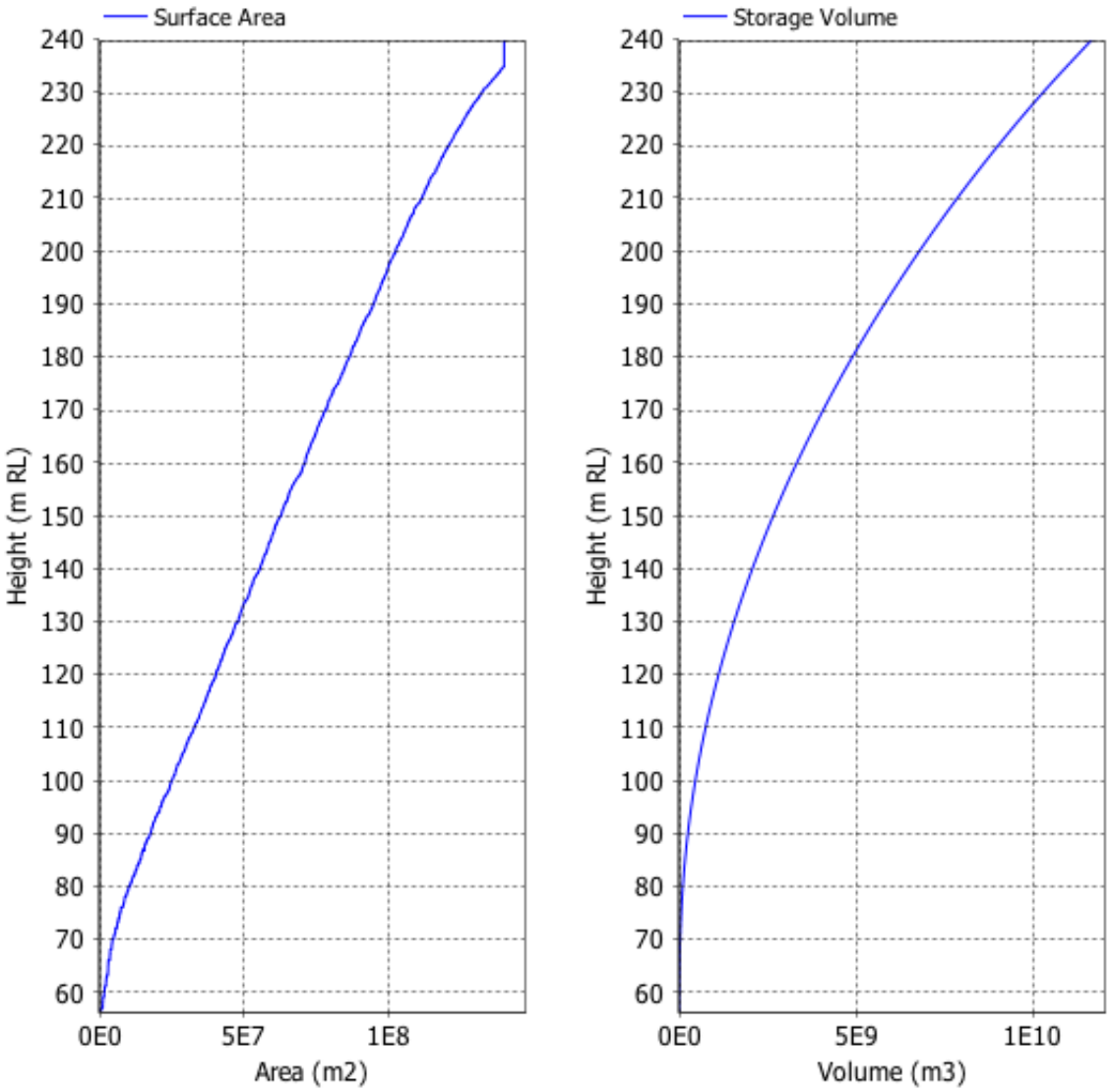

Figure 1.1 Surface area and storage volume curves for model bathymetry.

1.2 Meteorological Inputs

Table 1.1 Basic statistics of meteorological series used to force the model.

Baseline model year		**Mean Daily Max. Air Temp. (°C)**	**5th % Daily Max. Air Temp. (°C)**	**95th % Daily Max. Air Temp. (°C)**	**Mean Daily Min. Air Temp. (°C)**	**5th % Daily Min. Air Temp. (°C)**	**95th % Daily Min. Air Temp. (°C)**	**Mean Daily Max. Solar Rad. (W/m2)**	**5th % Daily Max. Solar Rad. (W/m2)**	**95th % Daily Max. Solar Rad. (W/m2)**
(a)	**(b)**									
2000	2028	27.8	25.1	29.9	19.5	18.4	20.5	4081.5	2278.3	5669.0

2001	2029	28.2	25.2	30.6	19.7	18.8	20.8	3581.7	1925.6	5344.6
2002	2030	27.9	24.3	30.1	19.9	18.7	21.0	4233.8	1881.7	5948.7
2003	2031	27.8	24.8	30.0	19.5	18.5	20.6	4548.1	2605.2	5831.4
2004	2032	27.8	25.1	29.9	19.5	18.4	20.5	4083.3	2278.3	5669.0
2005	2033	27.2	24.1	29.6	19.7	18.7	20.6	3686.4	2047.0	5273.8
2006	2034	27.5	24.6	29.9	19.6	18.6	20.6	3480.4	1817.8	5182.2
2007	2035	27.8	24.8	30.0	19.5	18.5	20.6	4548.1	2605.2	5831.4
2008	2036	27.8	25.1	29.9	19.5	18.4	20.5	4083.3	2278.3	5669.0
2009	2037	27.2	24.1	29.6	19.7	18.7	20.6	3686.4	2047.0	5273.8

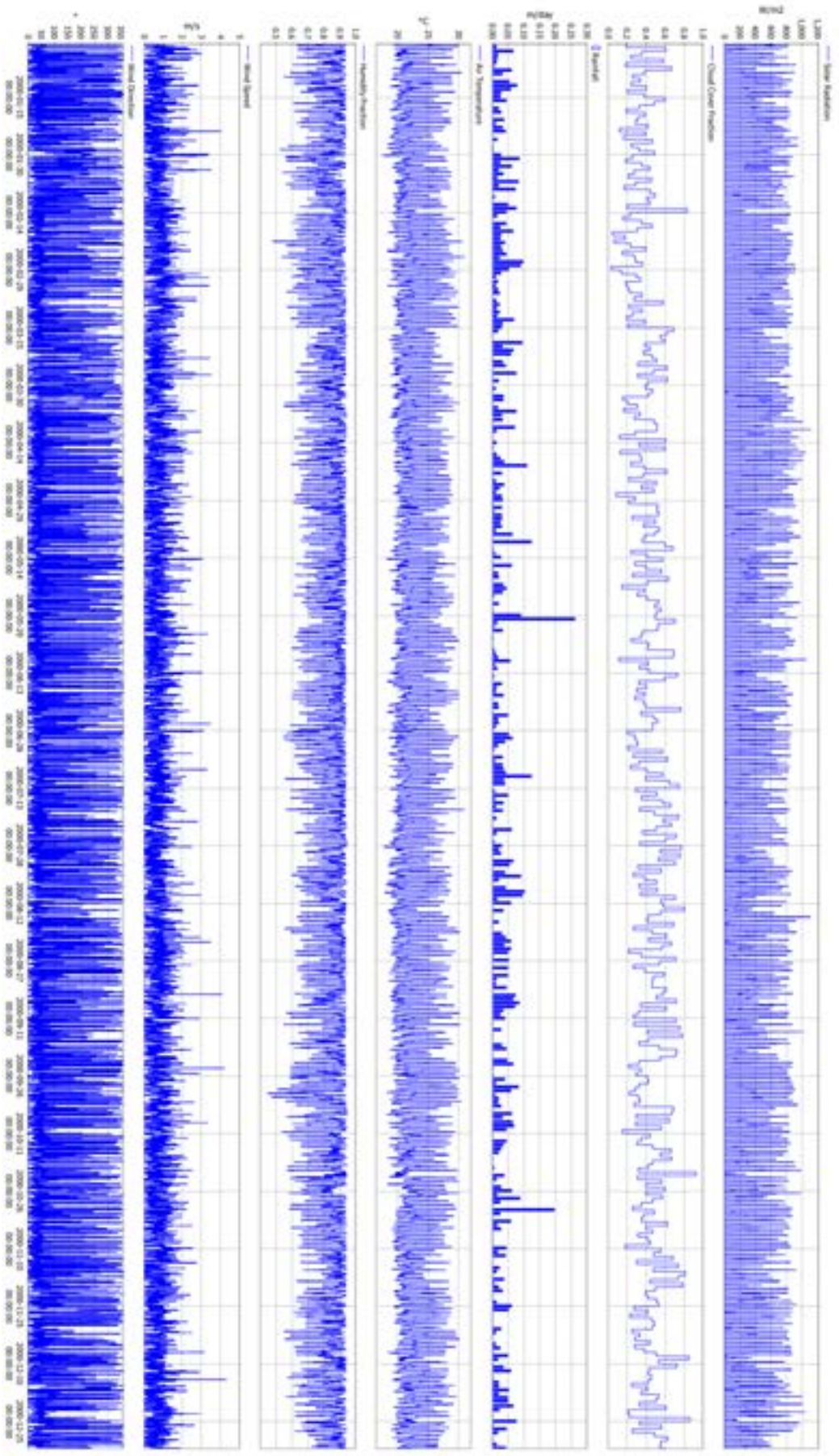

Figure 1.2 Meteorological series used to force the model for 2000, 2028 and 2038.

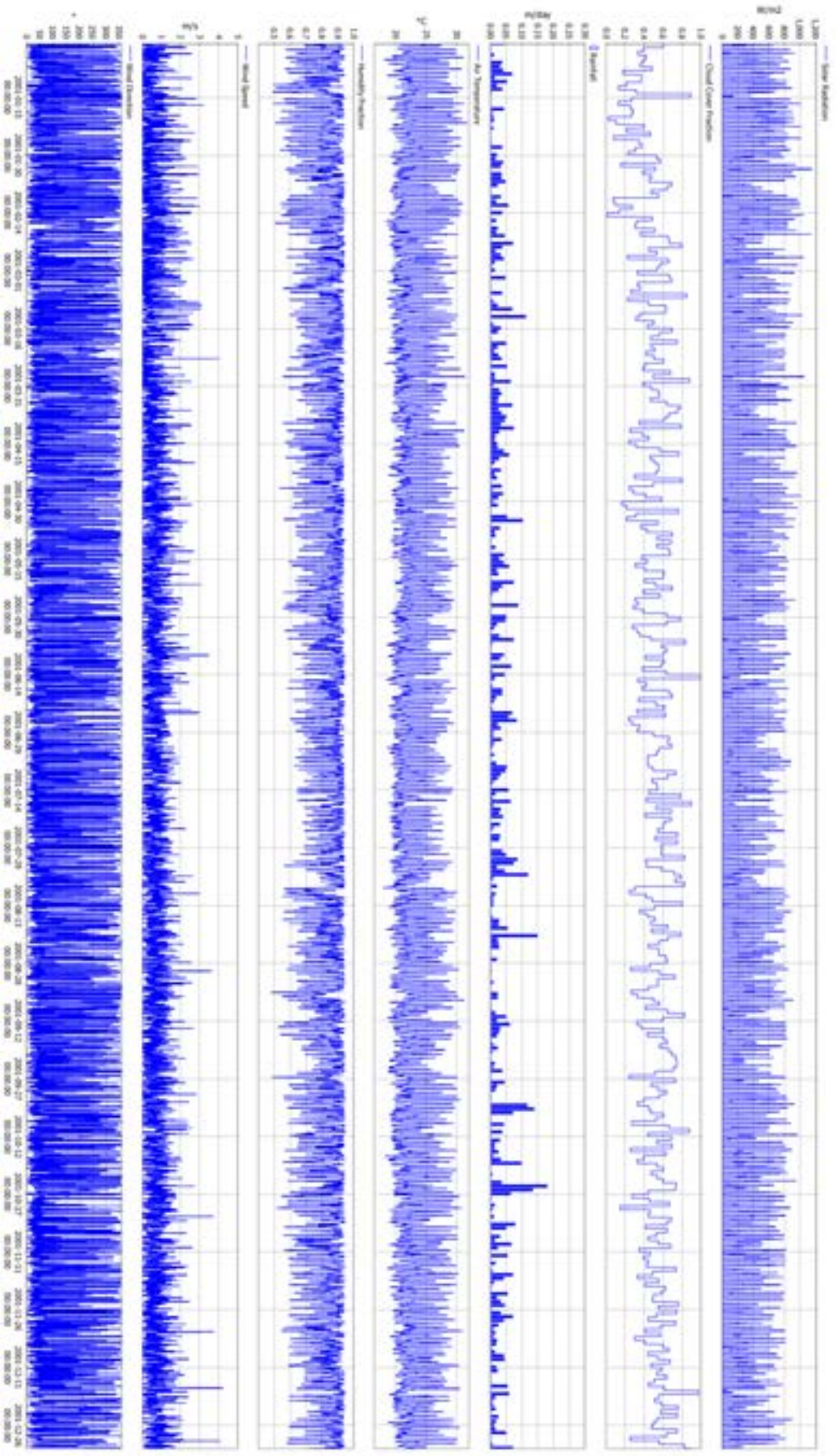

Figure 1.3 Meteorological series used to force the model for 2001, 2029 and 2039.

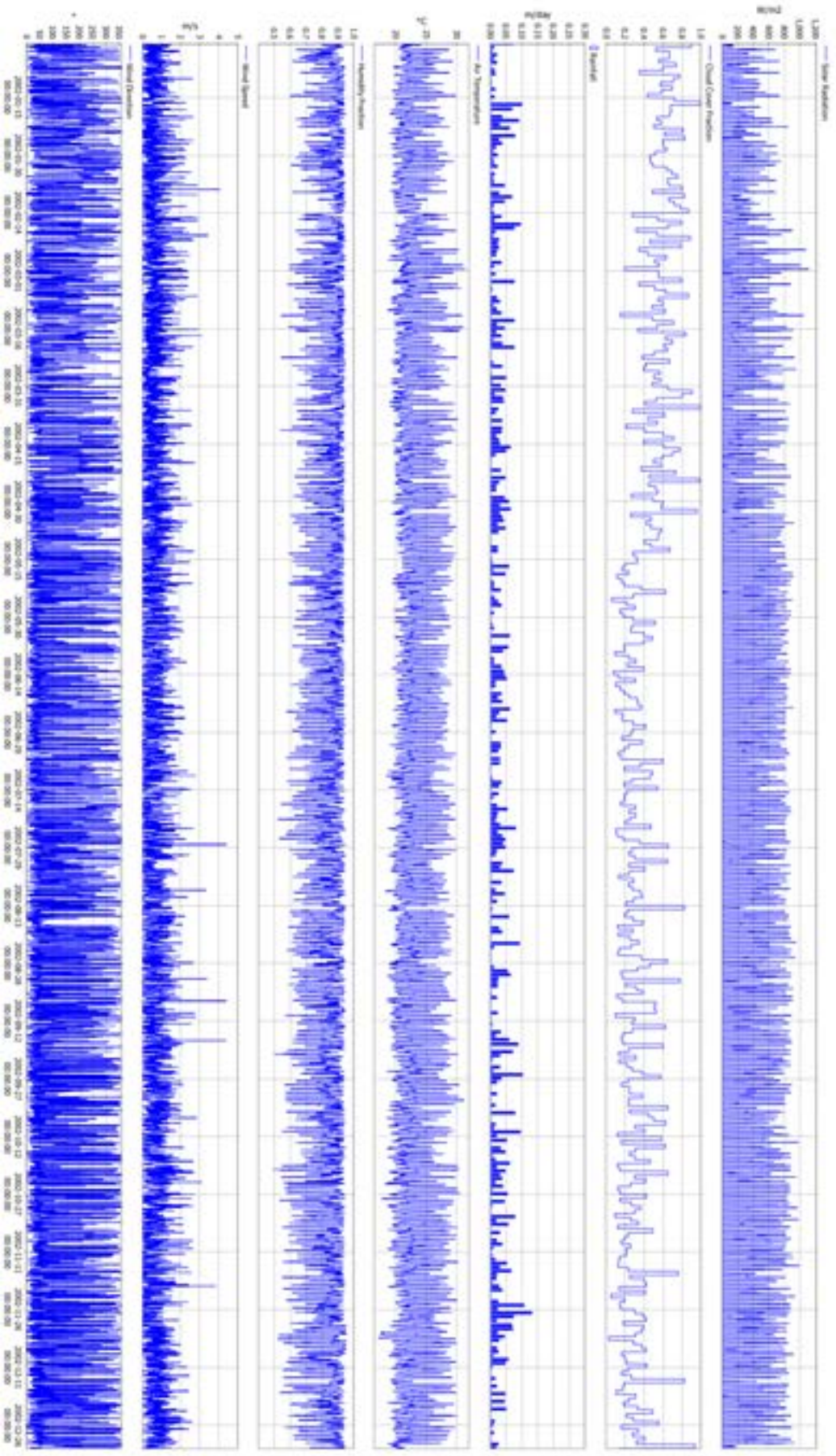

Figure 1.4 Meteorological series used to force the model for 2002, 2030 and 2040.

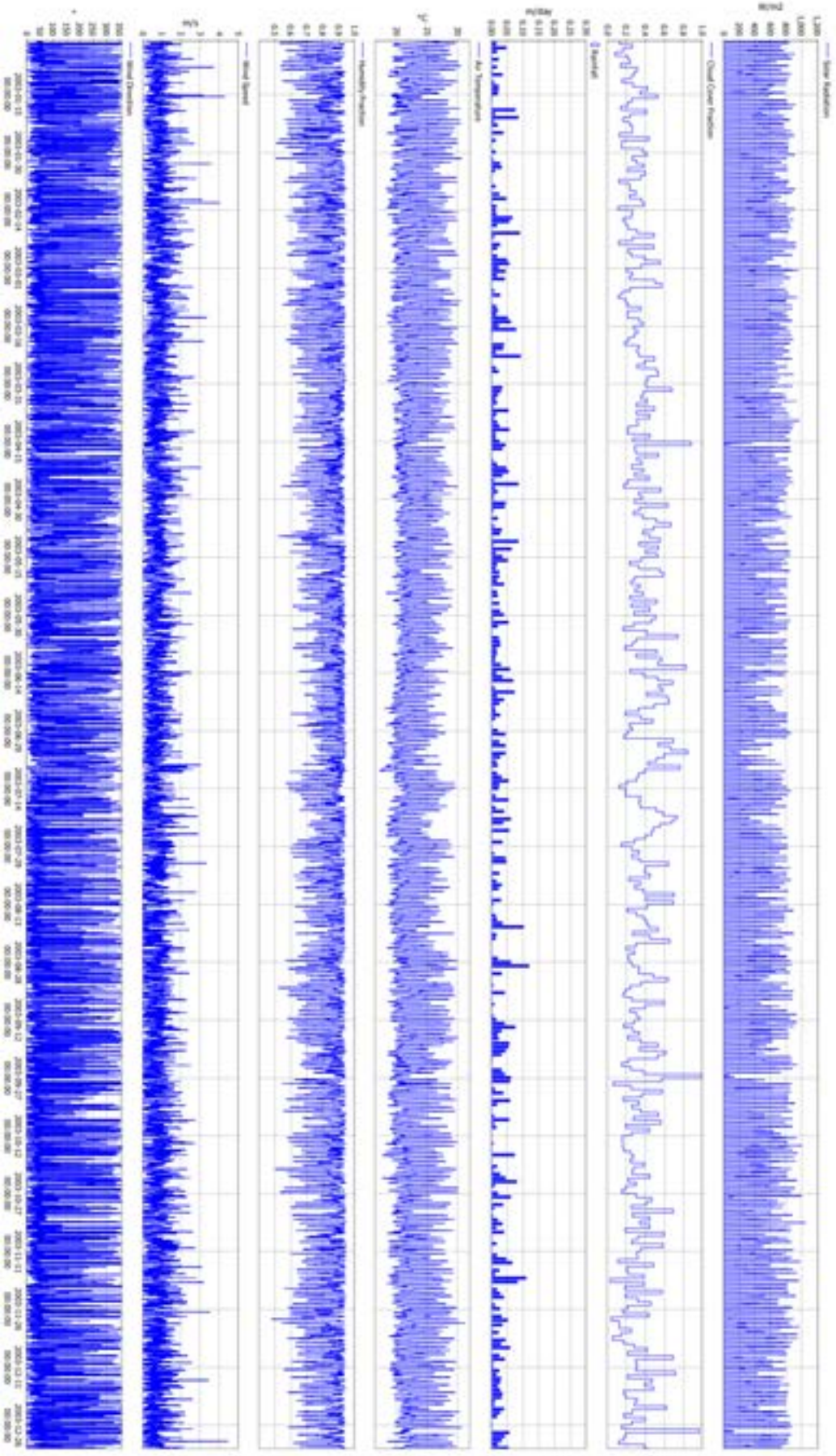

Figure 1.5 Meteorological series used to force the model for 2003, 2031 and 2041.

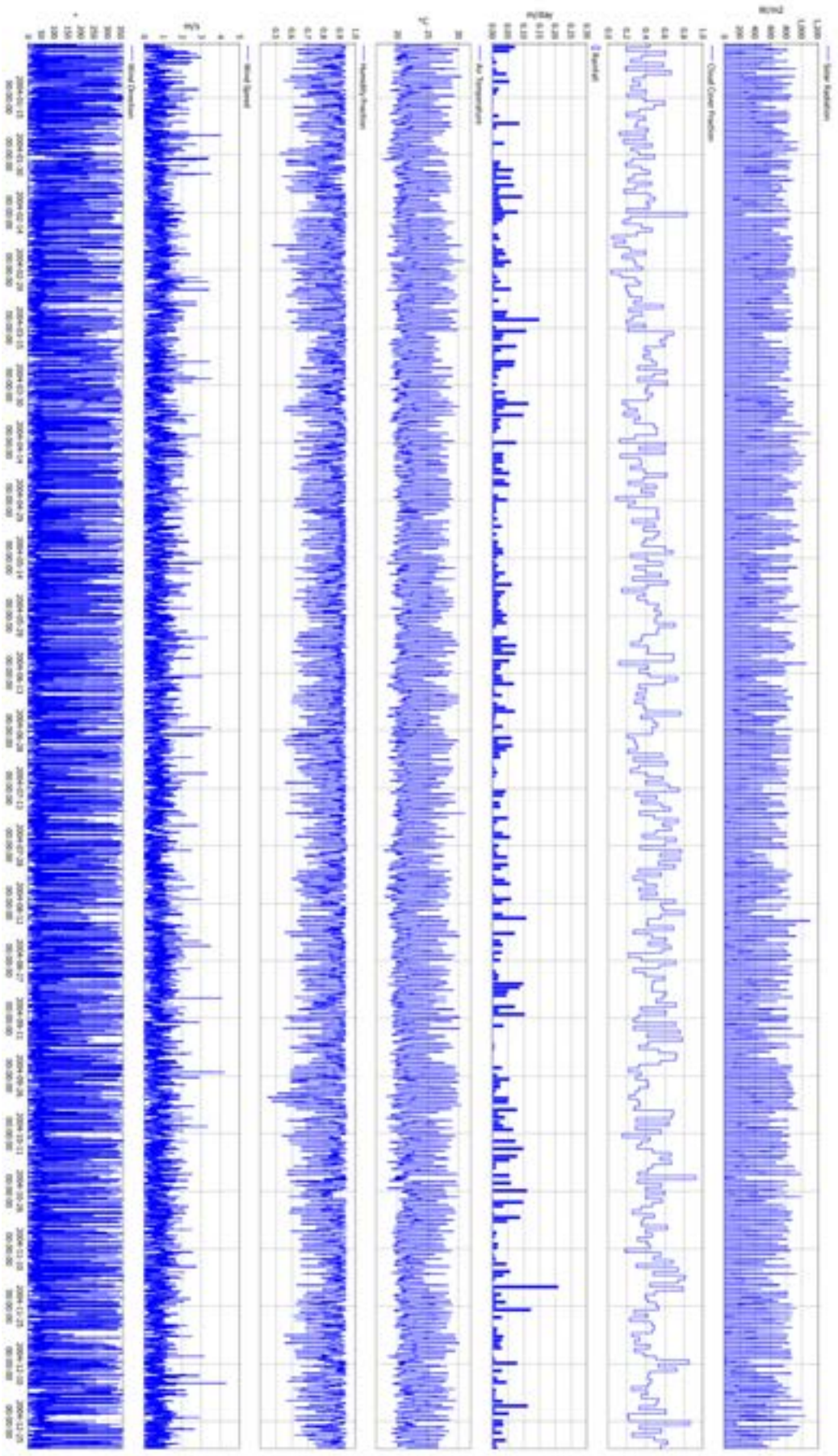

Figure 1.6 Meteorological series used to force the model for 2004, 2032 and 2042.

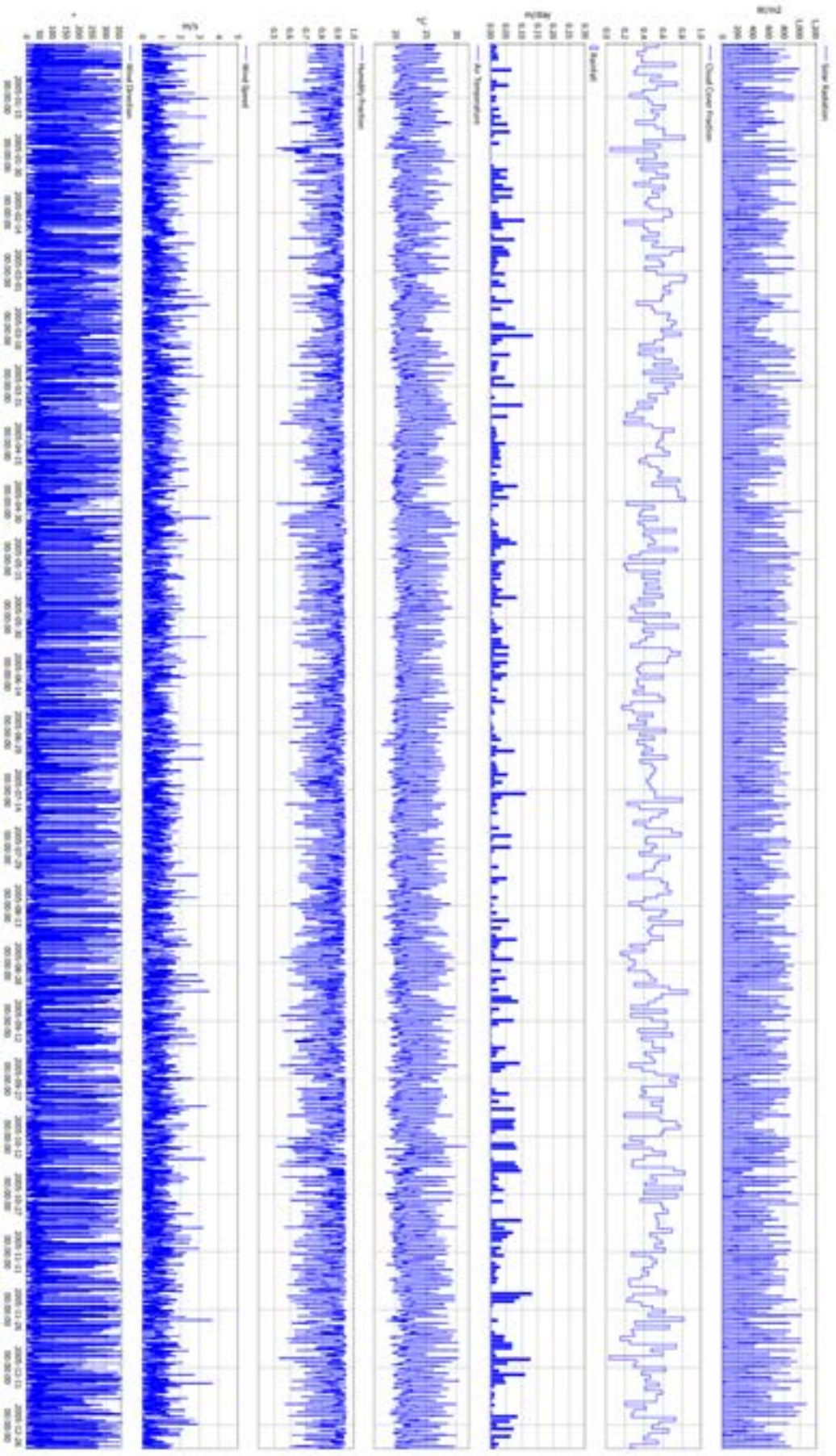

Figure 1.7 Meteorological series used to force the model for 2005, 2033 and 2043.

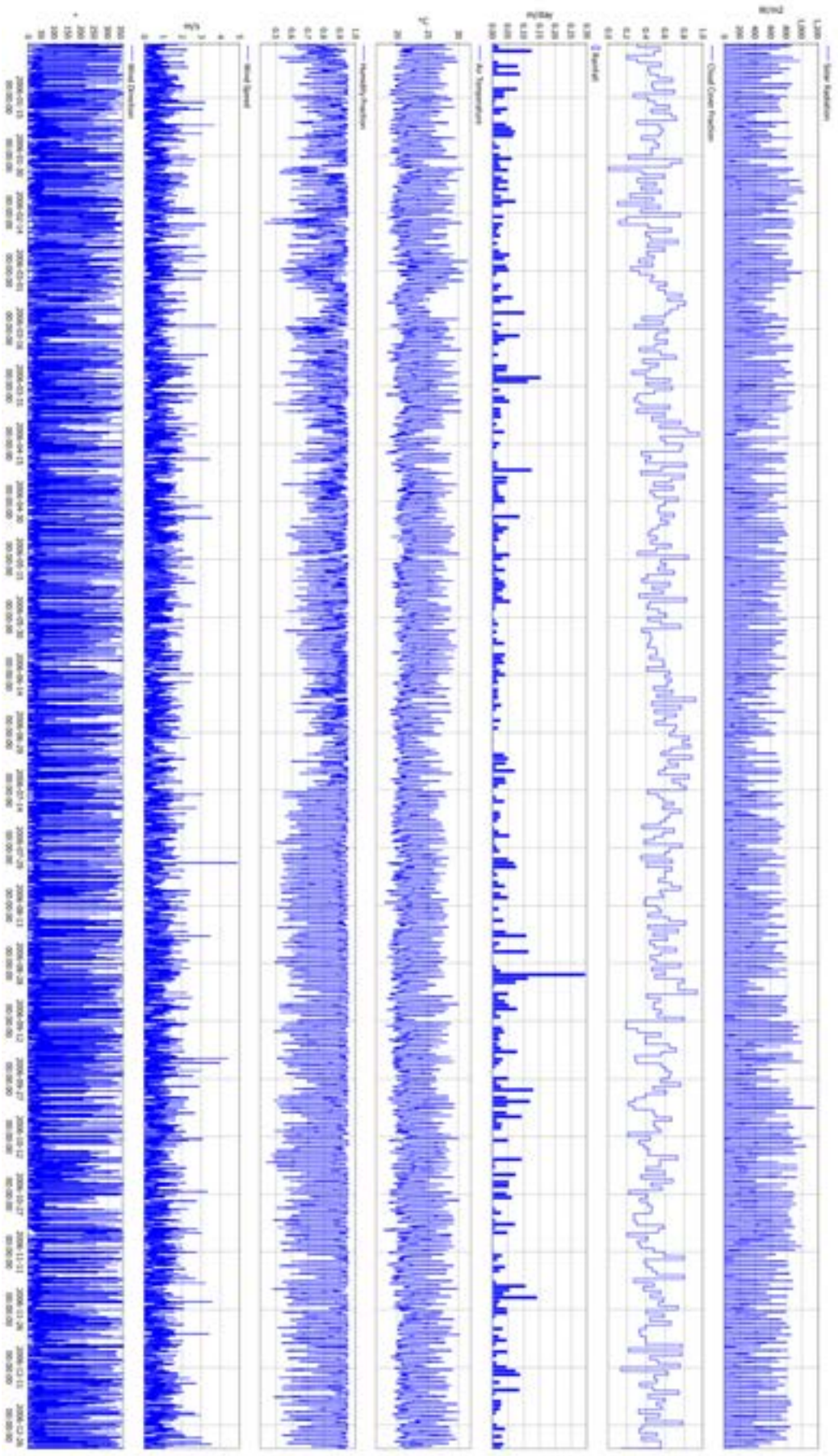

Figure 1.8 Meteorological series used to force the model for 2006, 2034 and 2044.

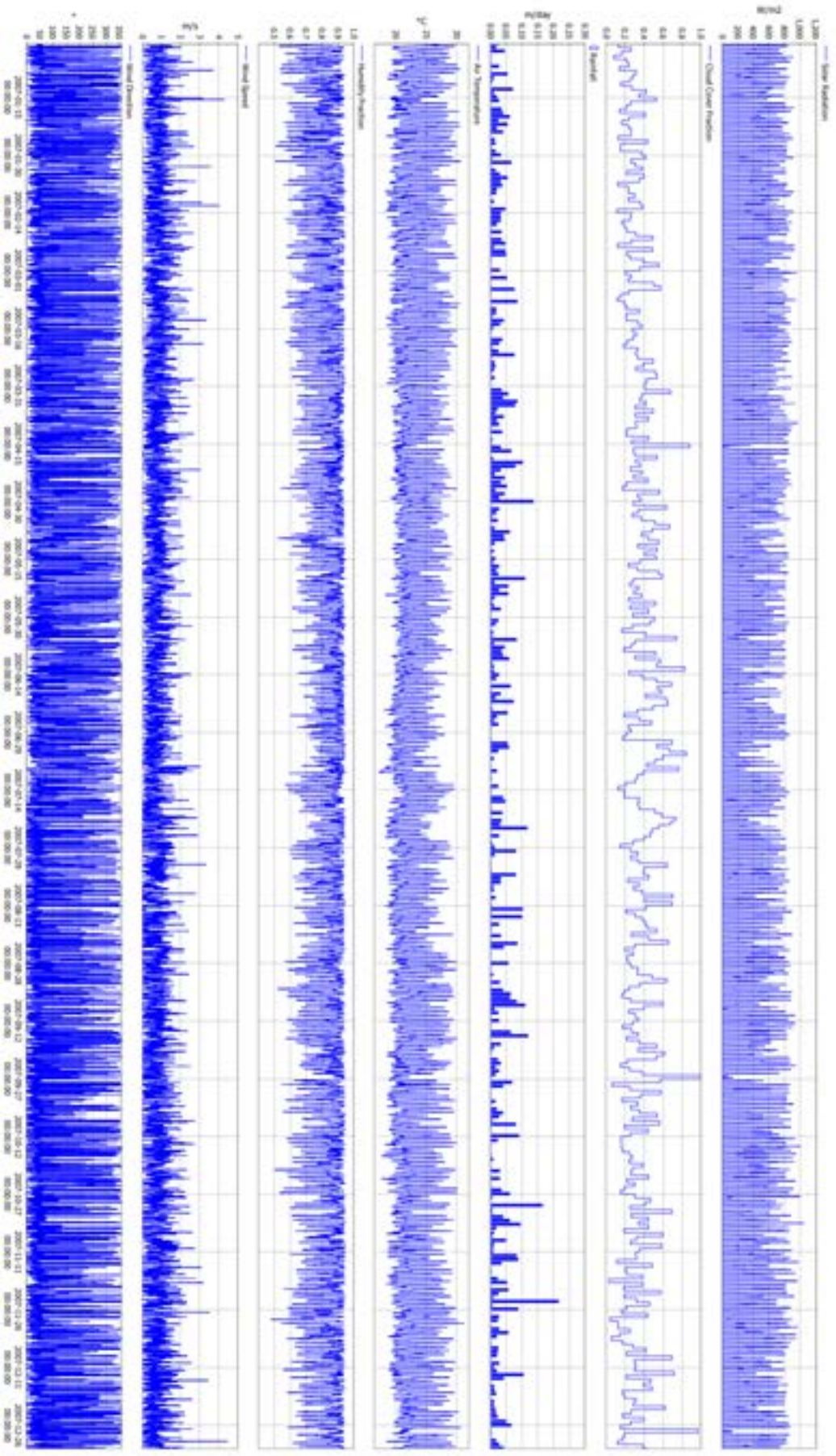

Figure 1.9 Meteorological series used to force the model for 2007 and 2035.

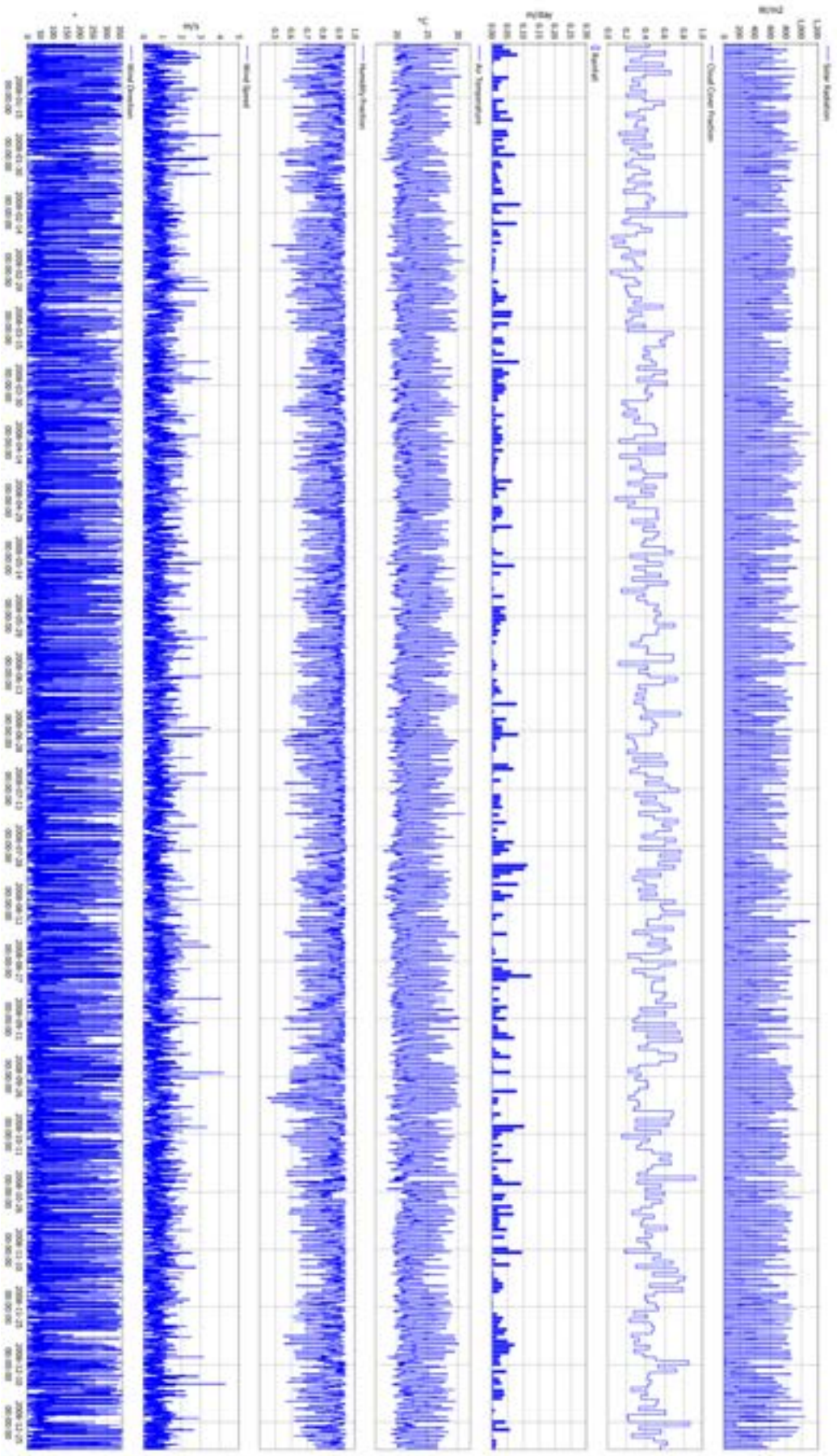

Figure 1.10 Meteorological series used to force the model for 2008 and 2036.

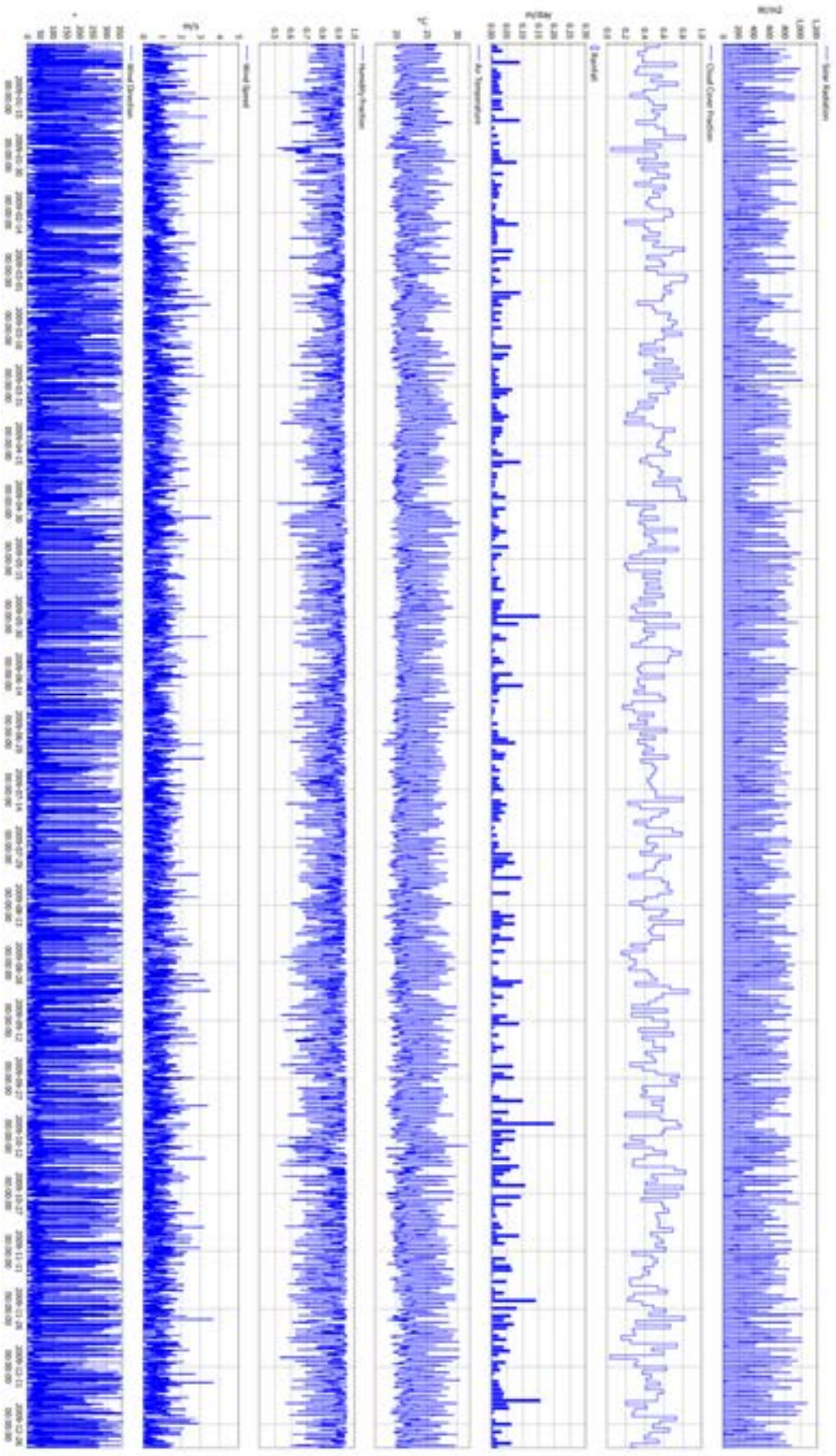

Figure 1.11 Meteorological series used to force the model for 2009 and 2037.

1.3 Inflow Properties

Table 1.2 Inflow and rainfall total volumes from 43 year time series. Rainfall volume based on surface area of 127 km^2.

Inflow	Tracer	TOTAL (GL)	PERCENTAGE
Henumai	1	51566.3	16.1
Niar	2	35564.5	11.1
Apai		3557.1	1.1
Spia		3557.1	1.1
Aribai	3	17782.5	5.6
Amosai		14224.4	4.5
Dama	4	17782.5	5.6
Ariya		5334.2	1.7
Sia		10669.6	3.3
Isai	5	16003.9	5.0
Loc1(Nena)	6	59937.1	18.7
Loc2	7	12618.7	3.9
Loc5(Ok Binai)	8	5041.3	1.6
Loc6	9	9822.5	3.1
Loc7		2045.5	0.6
Loc8	10	7961.3	2.5
Rainfall		46436.6	14.5

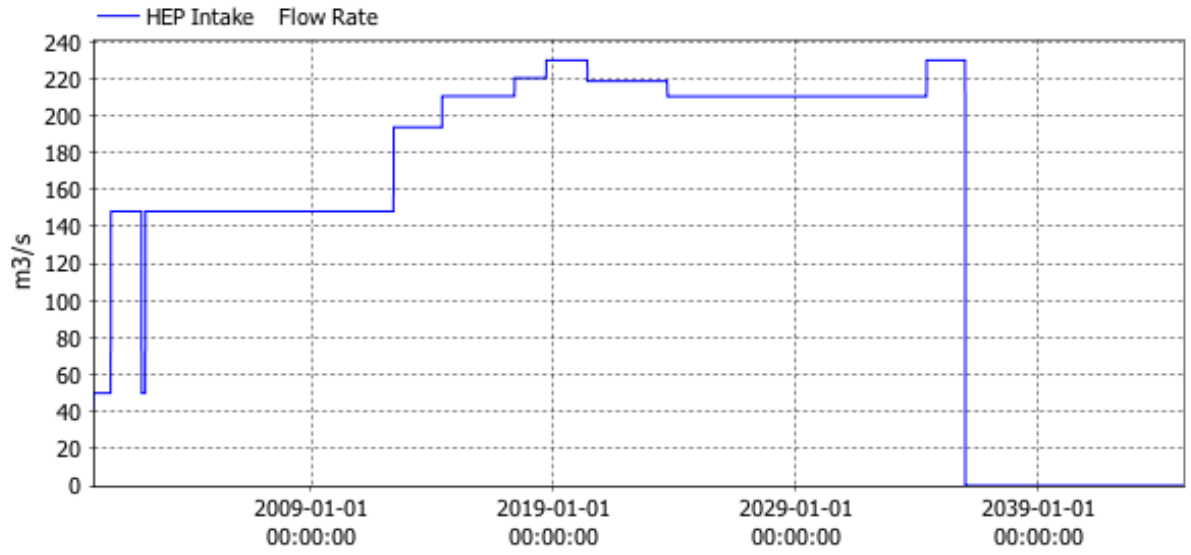

Figure 1.12 Flow rate used in model for HEP intakes for 2000-2044.

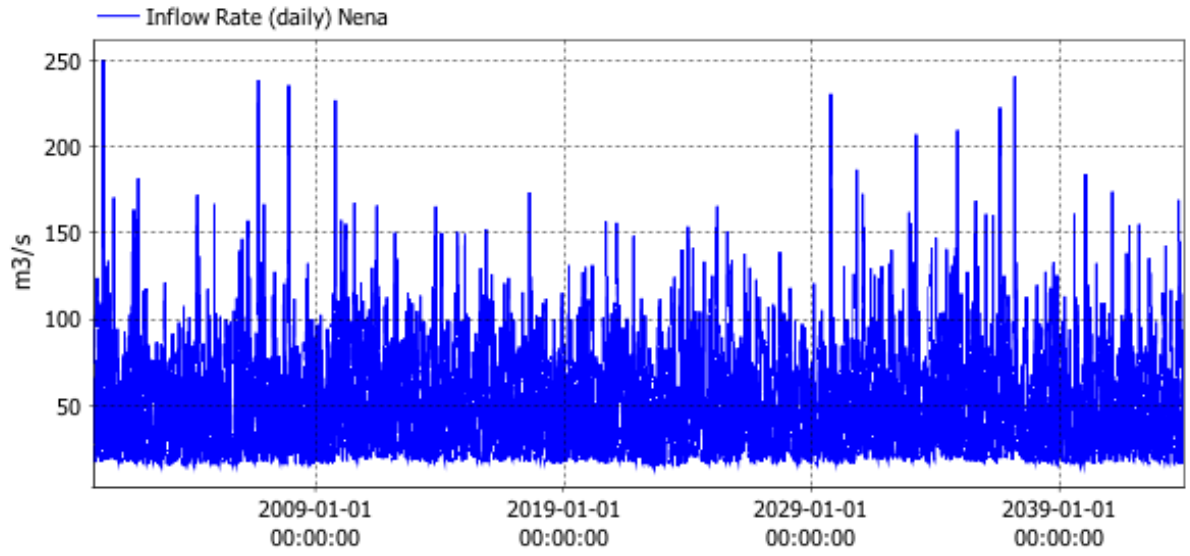

Figure 1.13 Daily flow rate for Nena inflow for 2000-2044.

1.3.1 Inflow Water Temperature

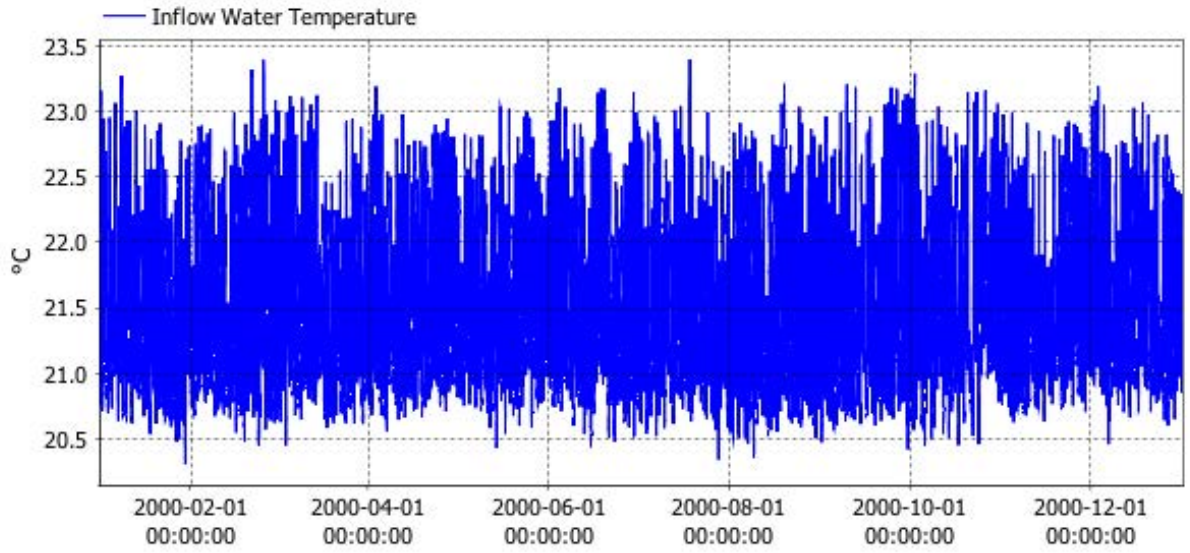

Figure 1.14 Model inflow water temperature for 2000, 2028 and 2038.

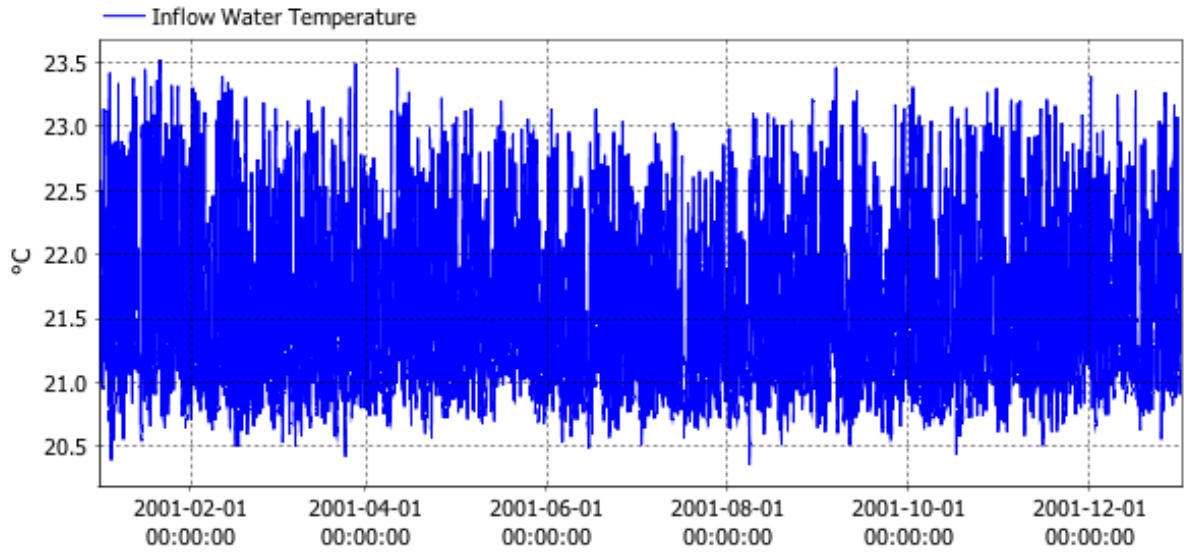

Figure 1.15 Model inflow water temperature for 2001, 2029 and 2039.

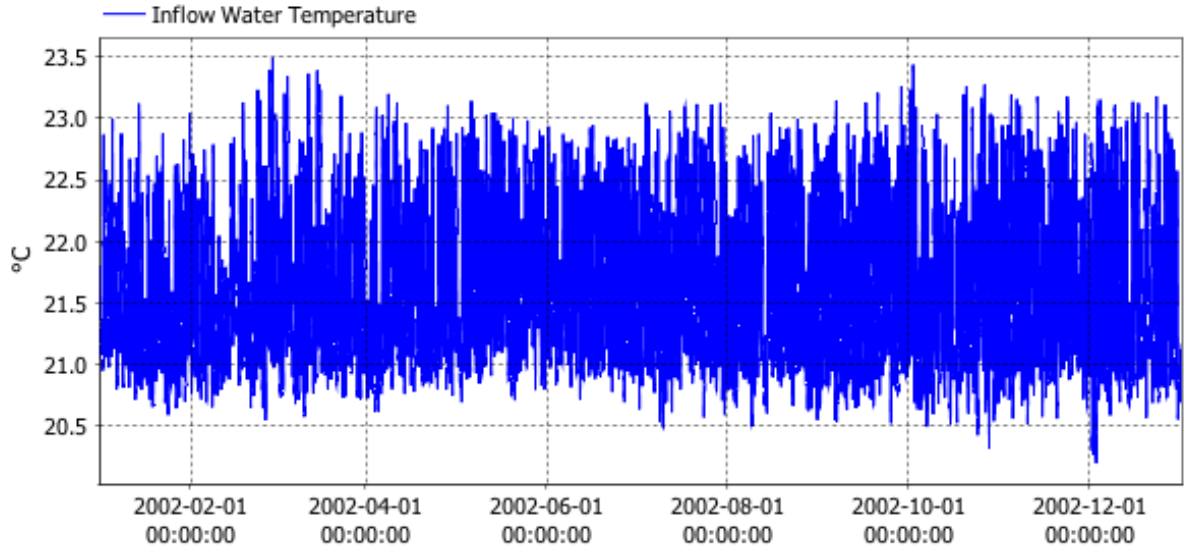

Figure 1.16 Model inflow water temperature for 2002, 2030 and 2040.

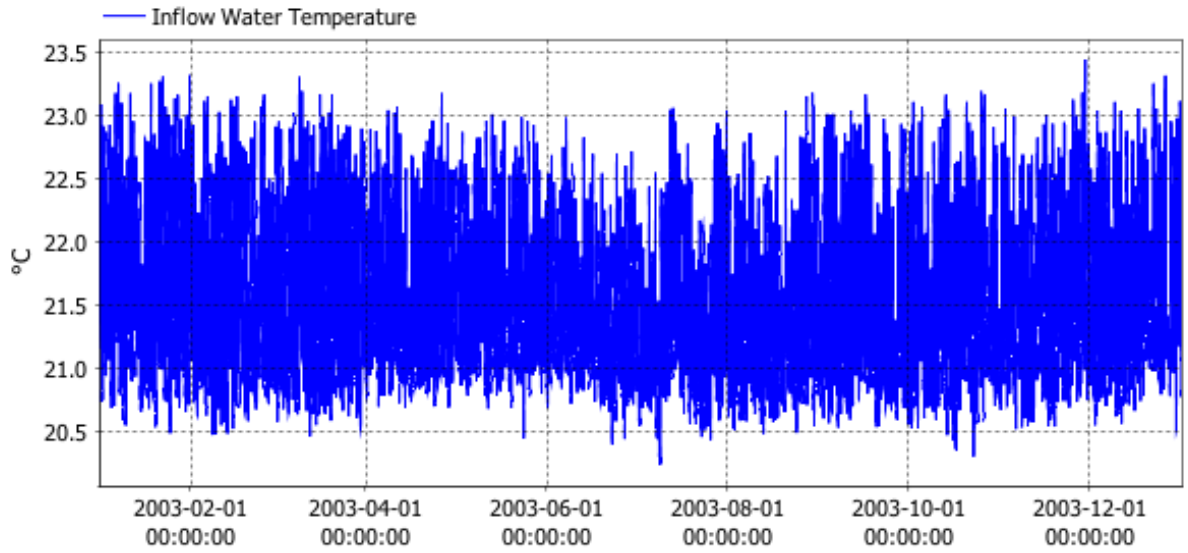

Figure 1.17 Model inflow water temperature for 2003, 2031 and 2041.

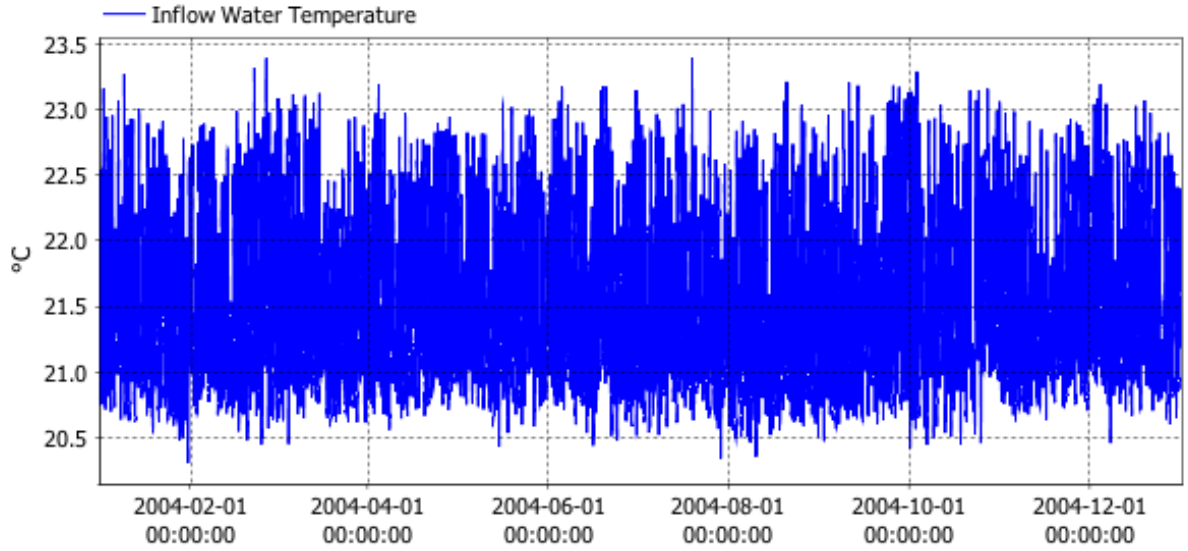

Figure 1.18 Model inflow water temperature for 2004, 2032 and 2042.

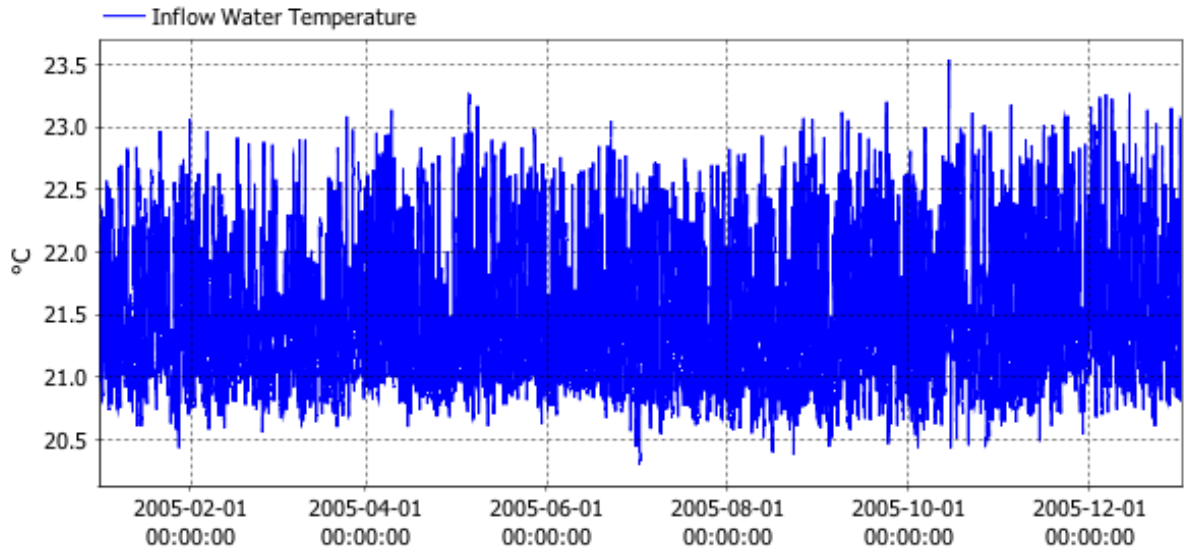

Figure 1.19 Model inflow water temperature for 2005, 2033 and 2043.

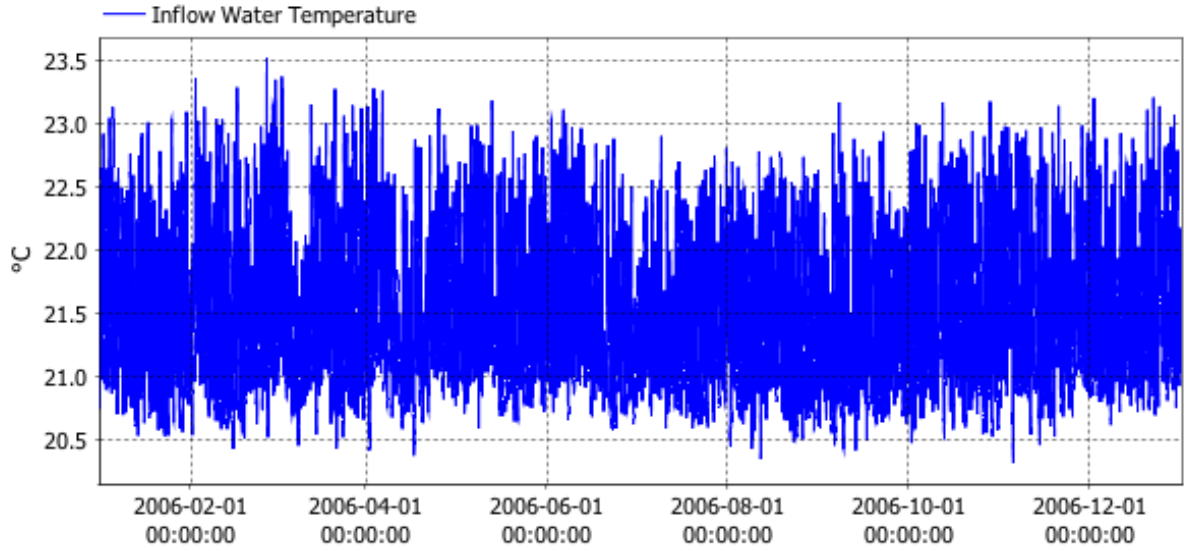

Figure 1.20 Model inflow water temperature for 2006, 2034 and 2044.

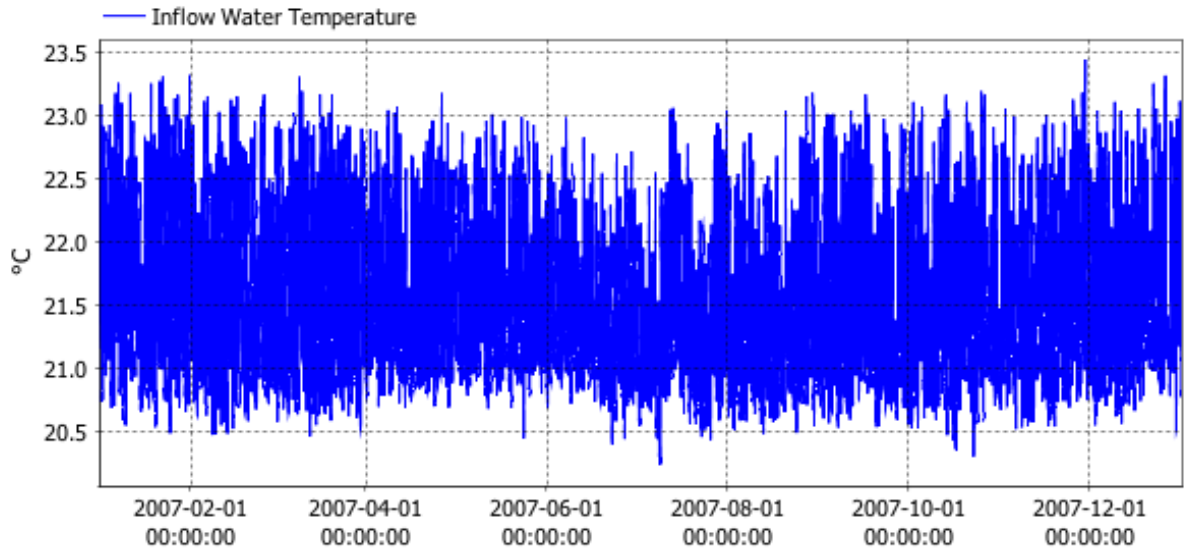

Figure 1.21 Model inflow water temperature for 2007 and 2035.

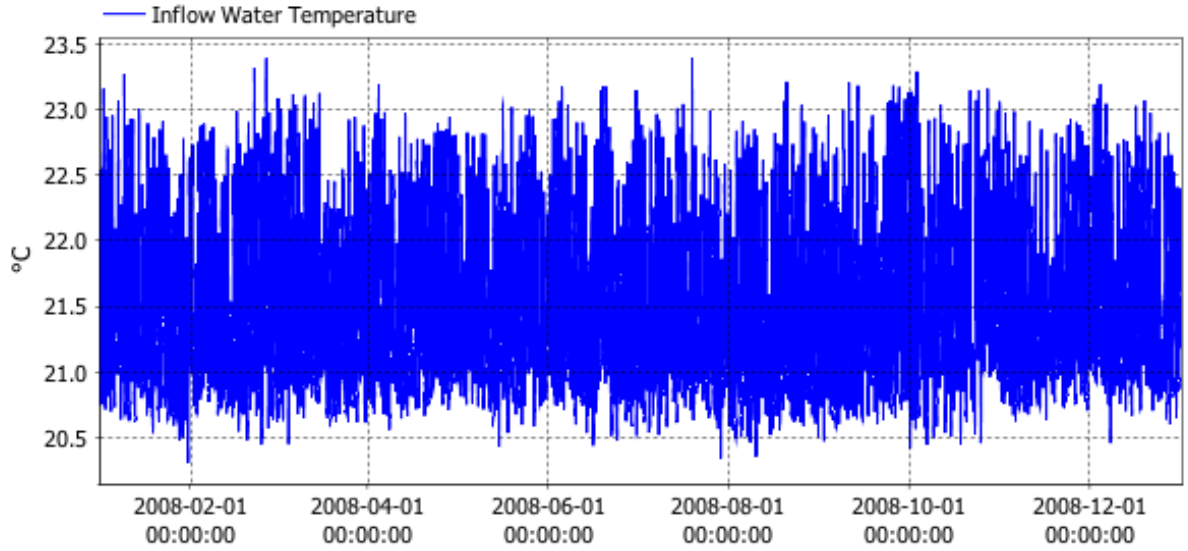

Figure 1.22 Model inflow water temperature for 2008 and 2036.

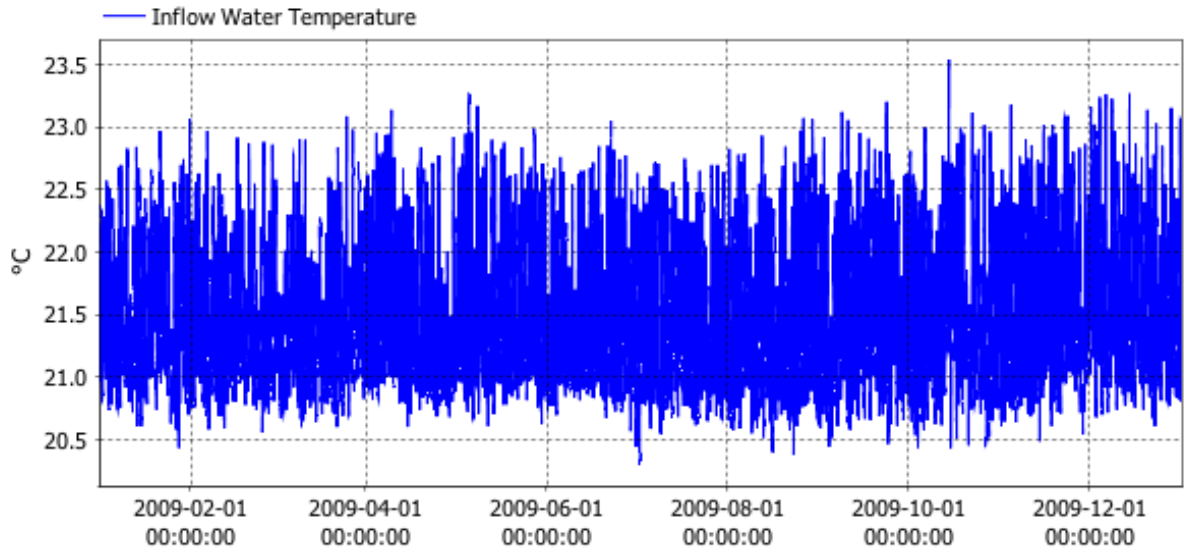

Figure 1.23 Model inflow water temperature for 2009 and 2037.

1.3.2 Inflow Flow Rates

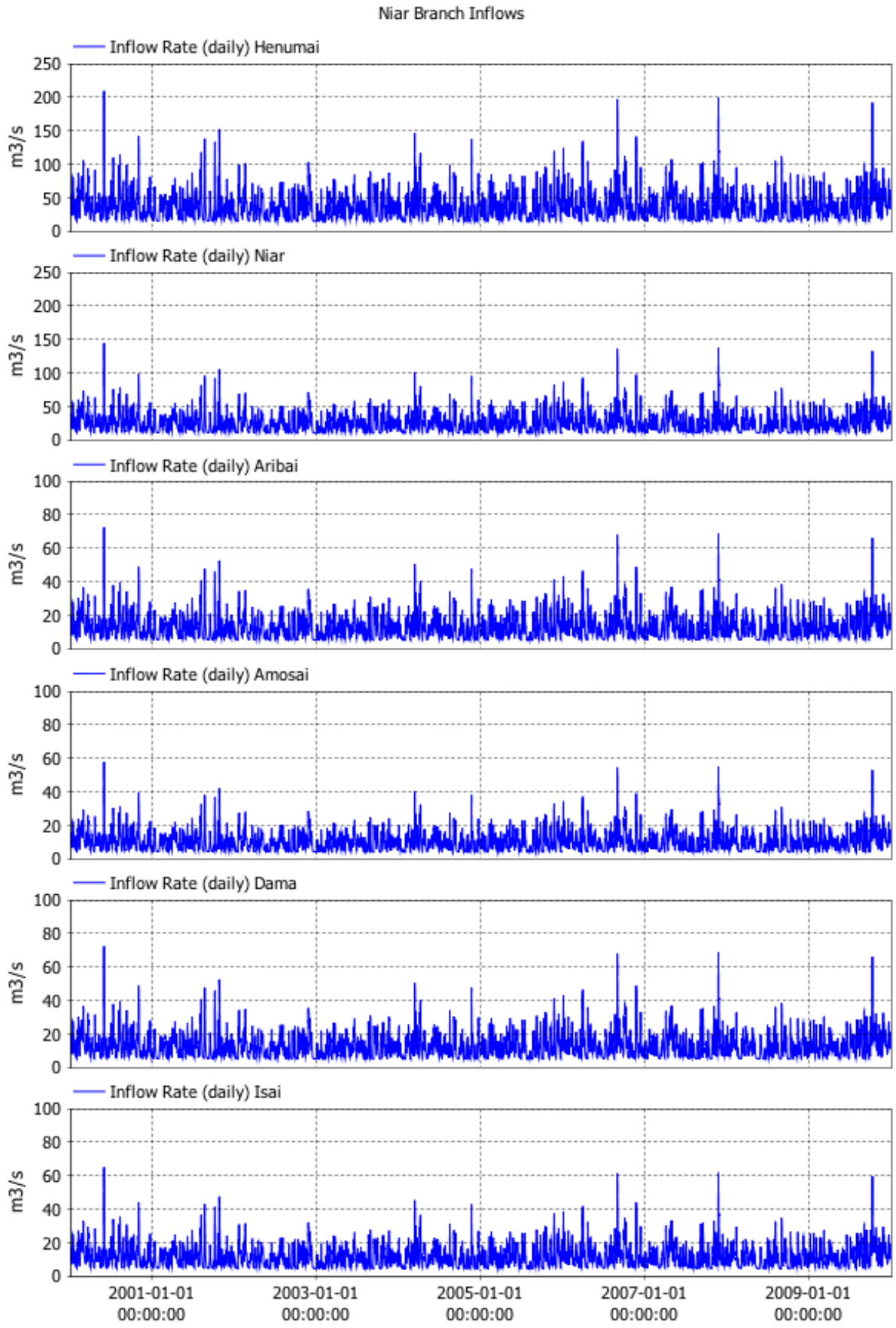

Figure 1.24 Daily inflow rates used in model for large tributaries of the Niar branch for 2000-2009.

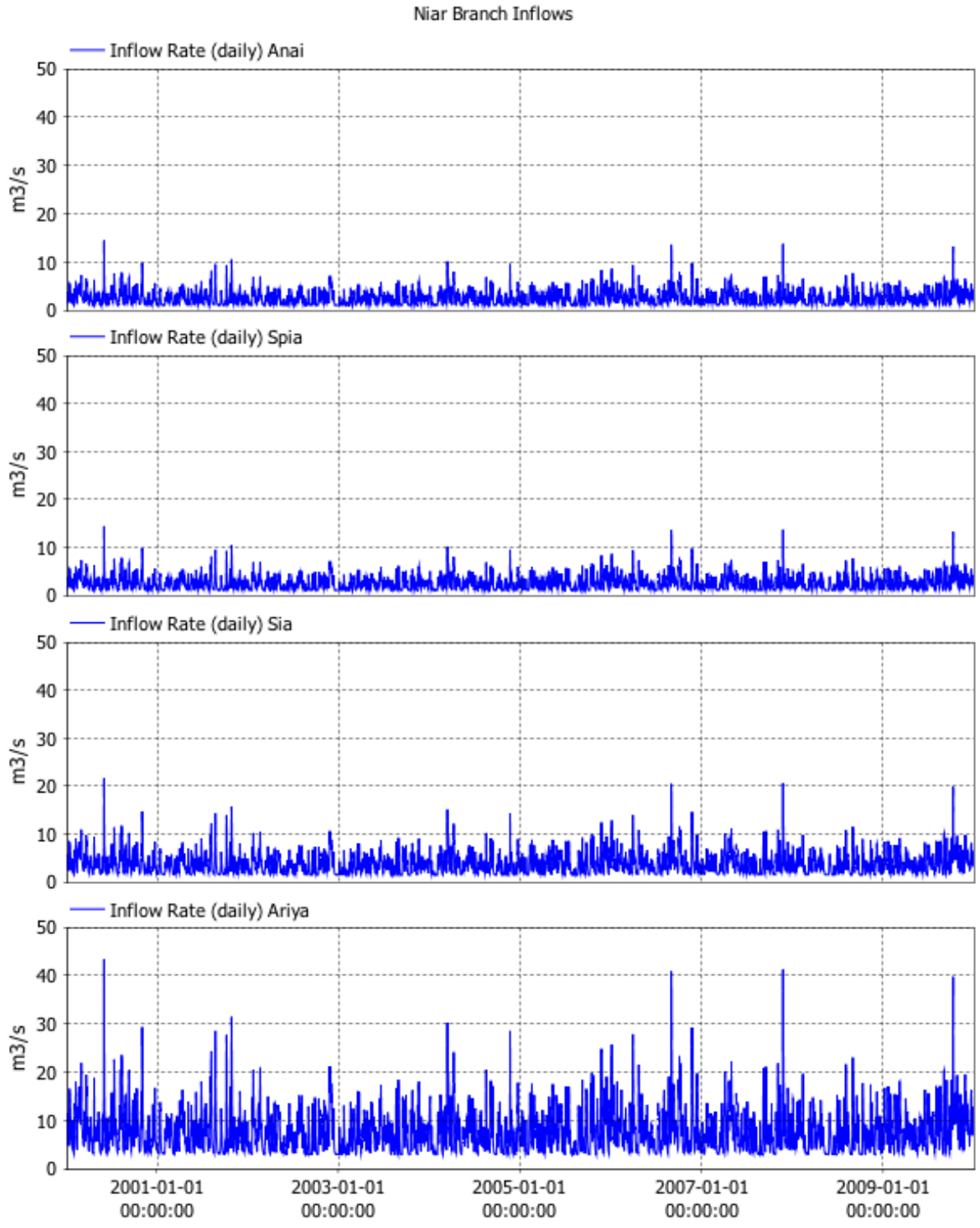

Figure 1.25 Daily inflow rates used in model for small tributaries of the Niar branch for 2000-2009.

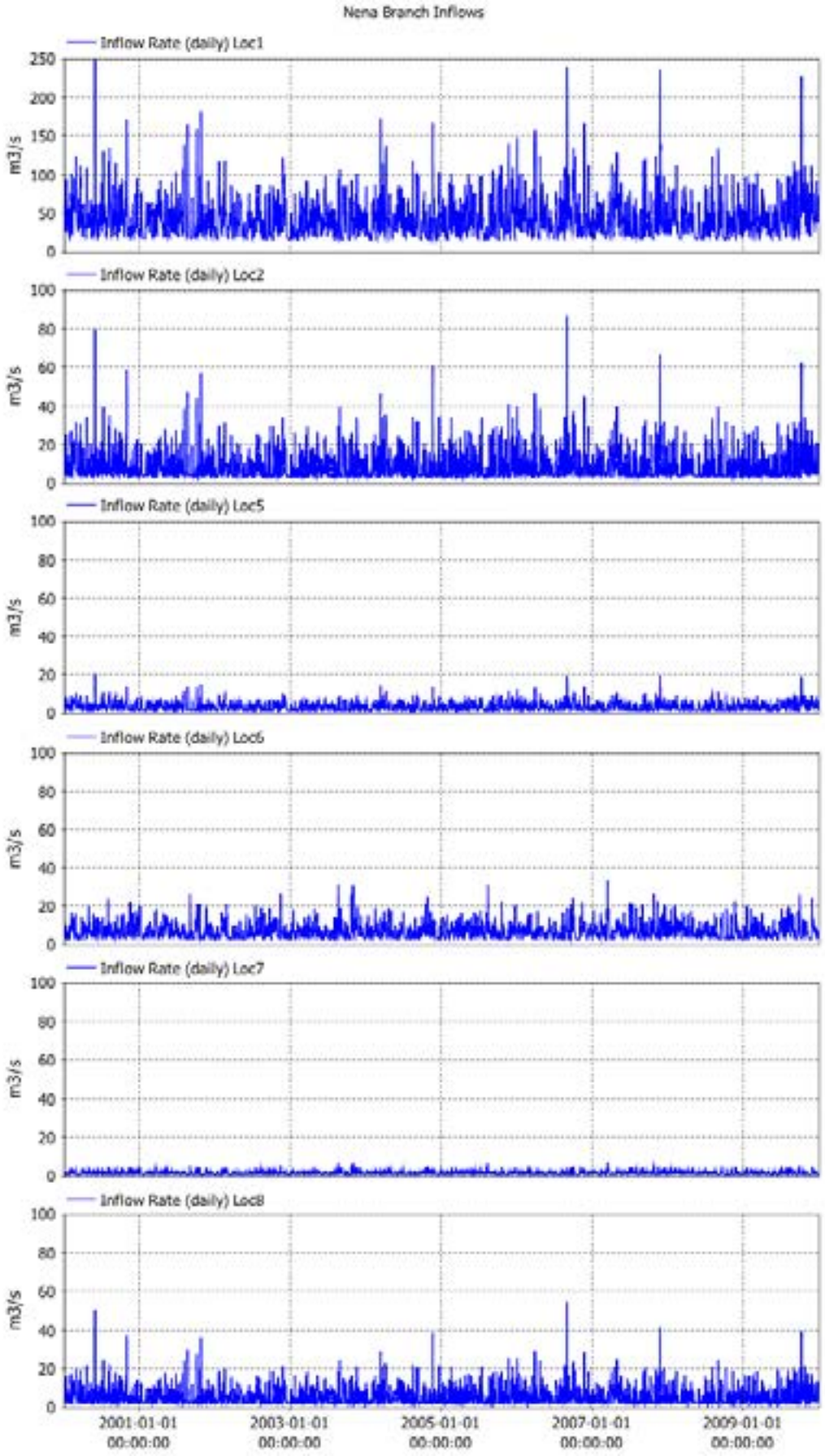

Figure 1.26 Daily inflow rates used in model for tributaries of the Nena branch for 2000-2009.

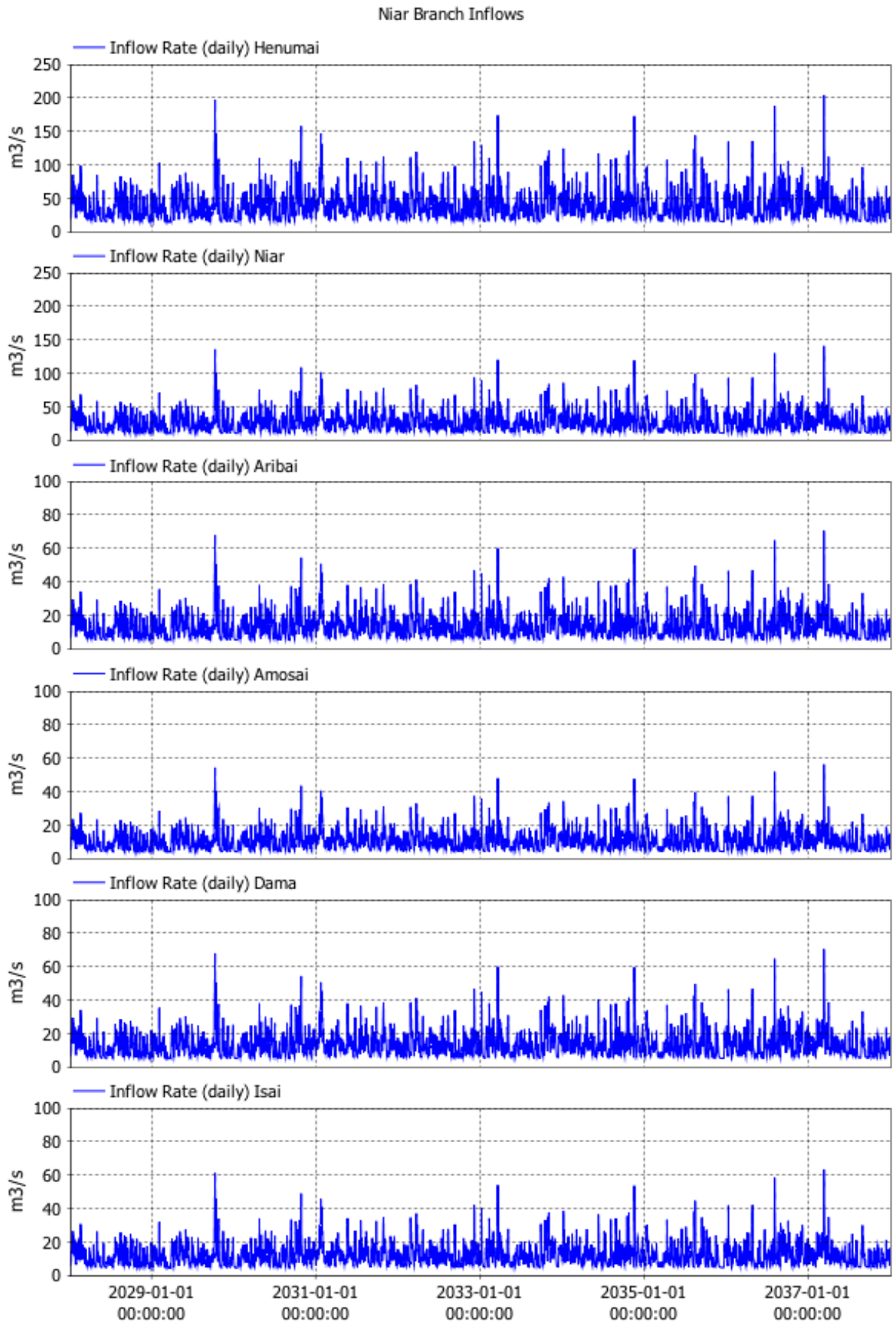

Figure 1.27 Daily inflow rates used in model for large tributaries of the Niar branch for 2028-2037.

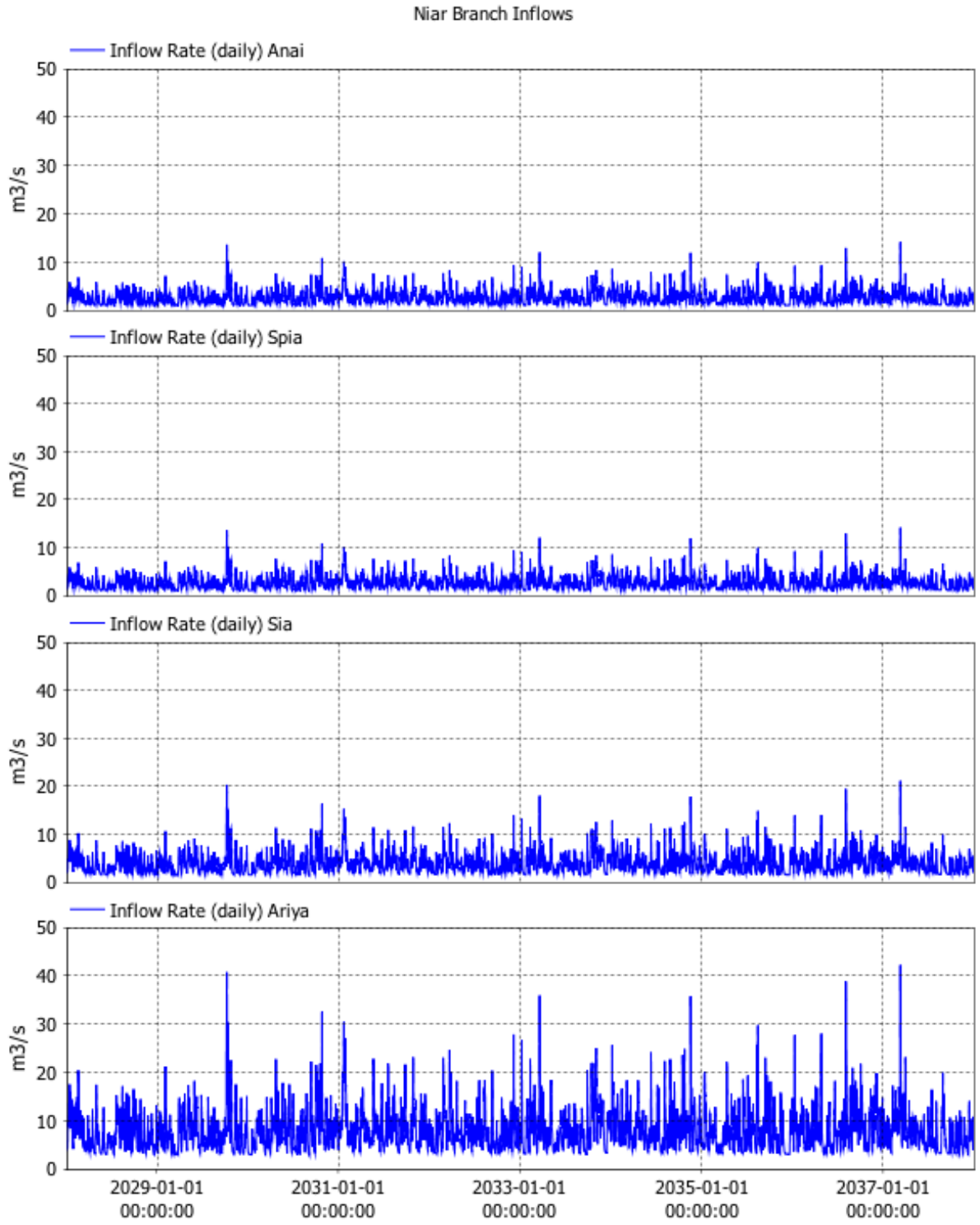

Figure 1.28 Daily inflow rates used in model for small tributaries of the Niar branch for 2028-2037.

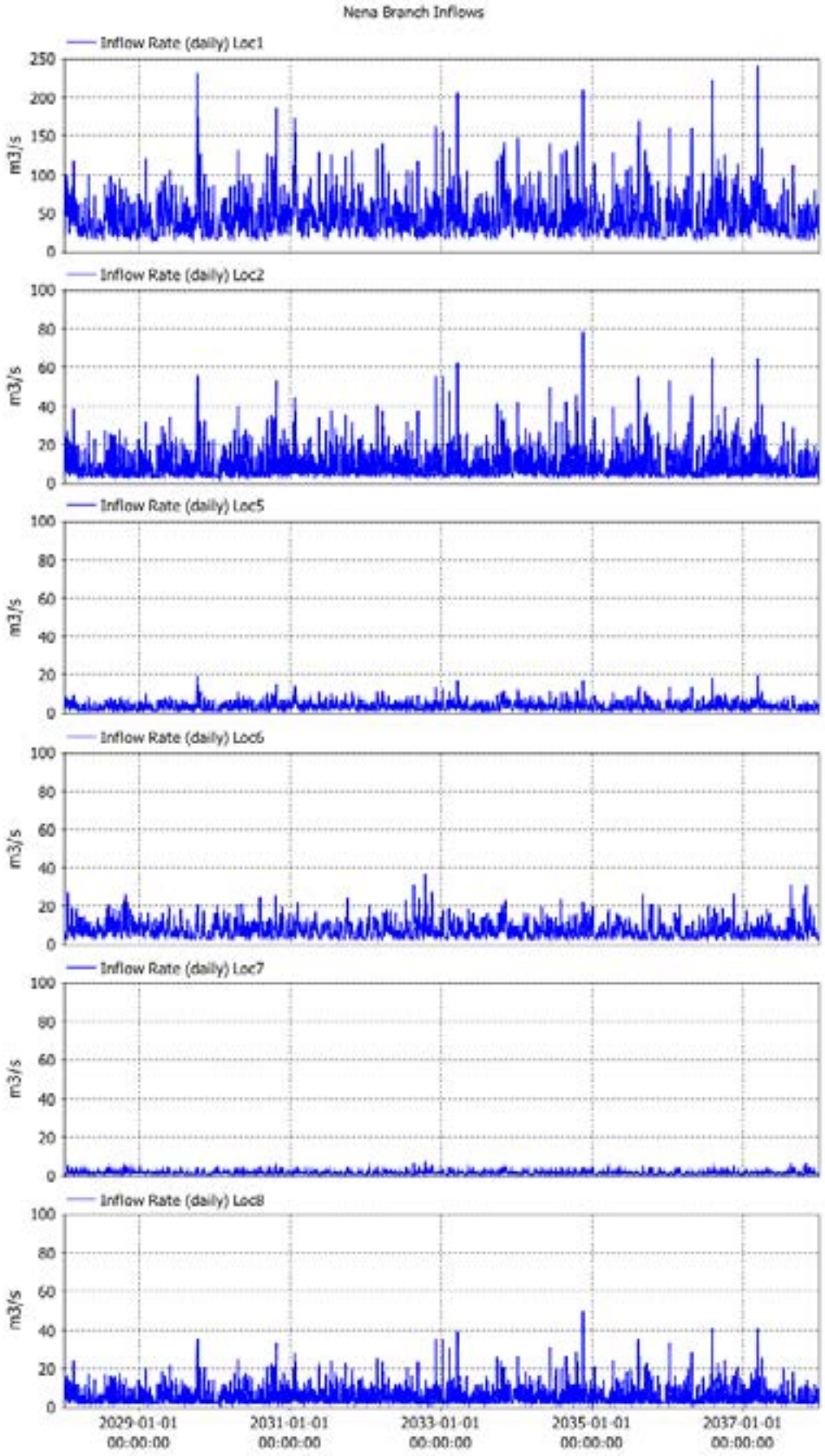

Figure 1.29 Daily inflow rates used in model for tributaries of the Nena branch for 2028-2037.

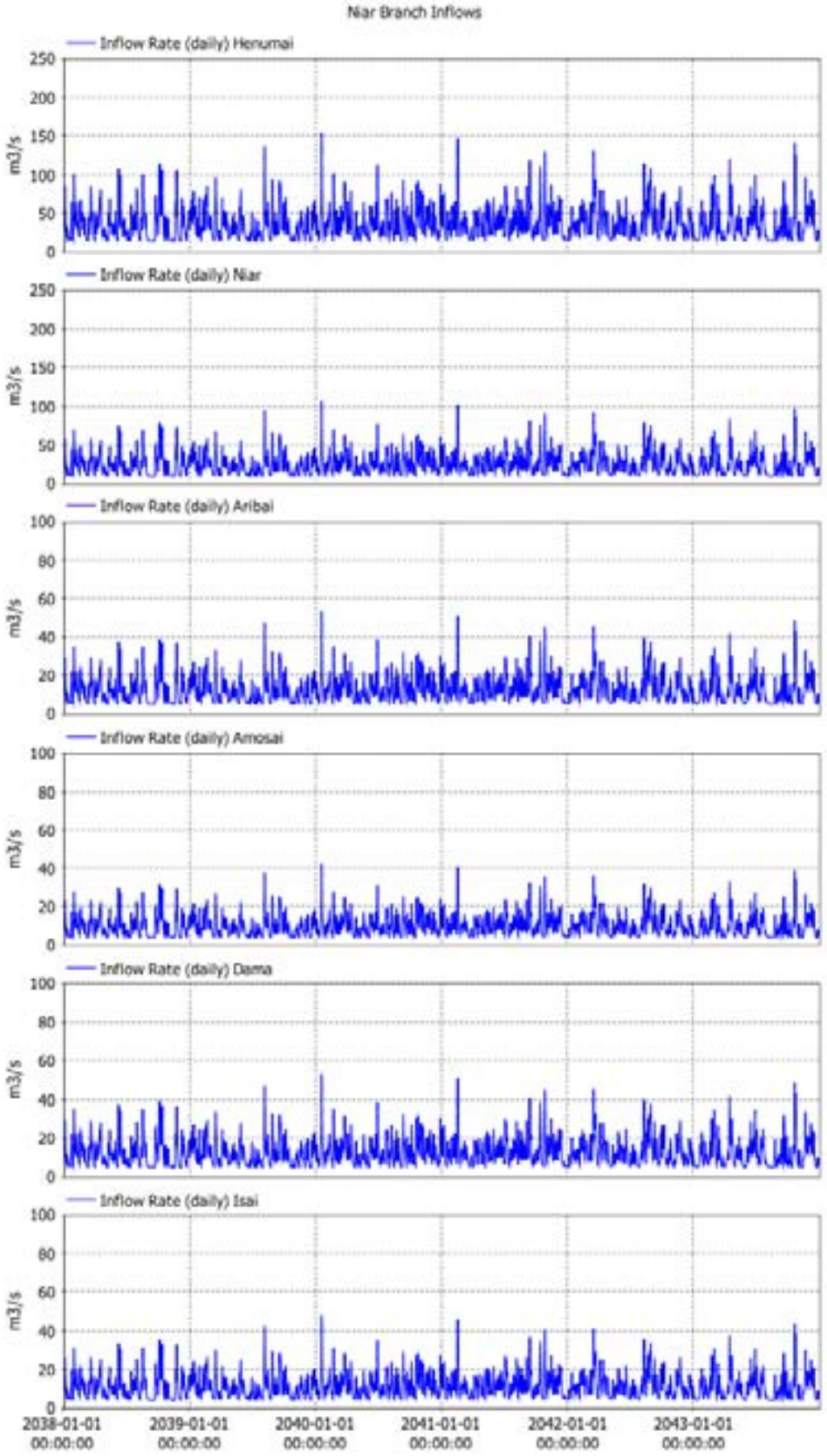

Figure 1.30 Daily inflow rates used in model for large tributaries of the Niar branch for 2038-2044.

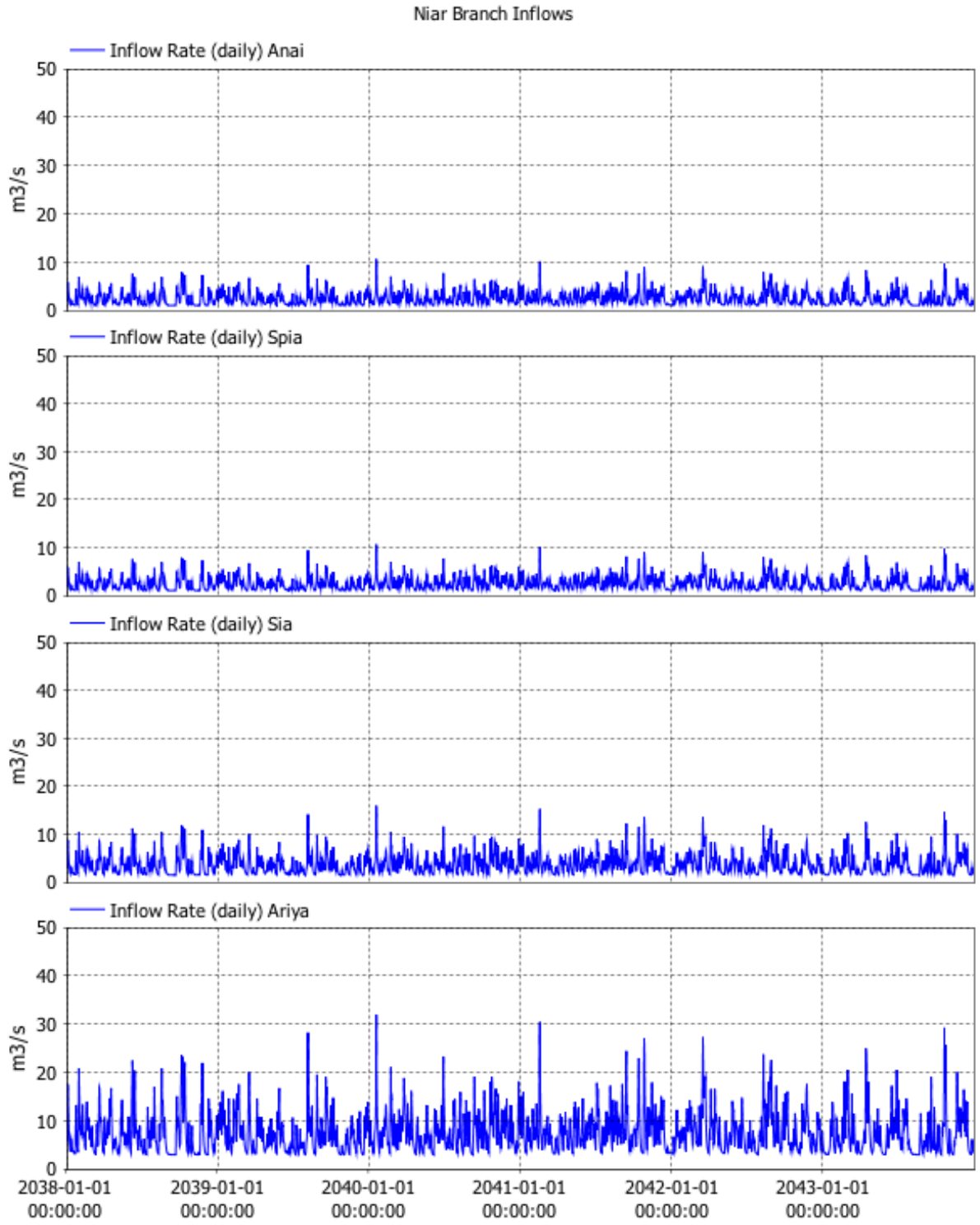

Figure 1.31 Daily inflow rates used in model for small tributaries of the Niar branch for 2038-2044.

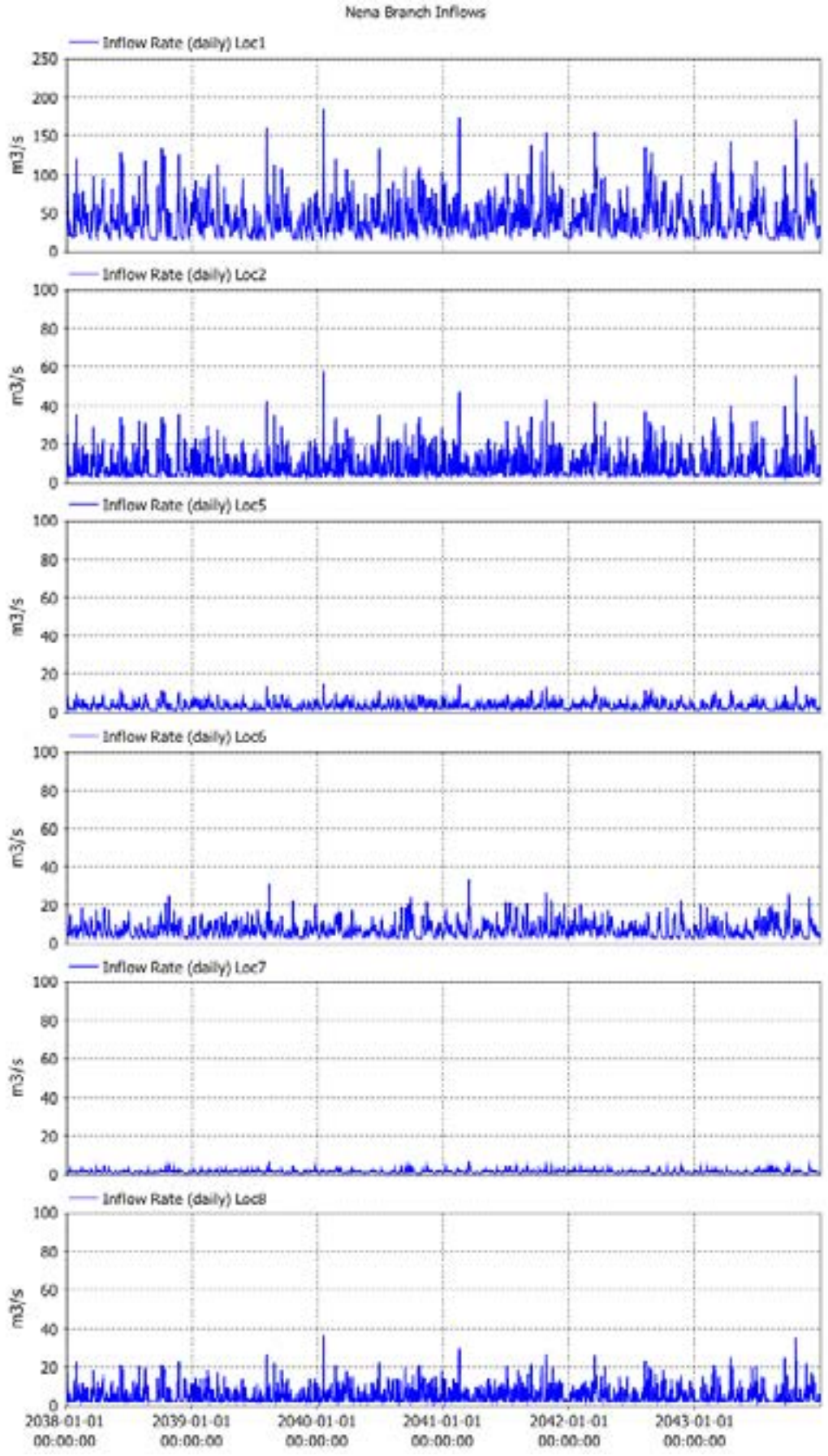

Figure 1.32 Daily inflow rates used in model for tributaries of the Nena branch for 2038-2044.

1.3.3 Inflow Suspended Solids Concentrations

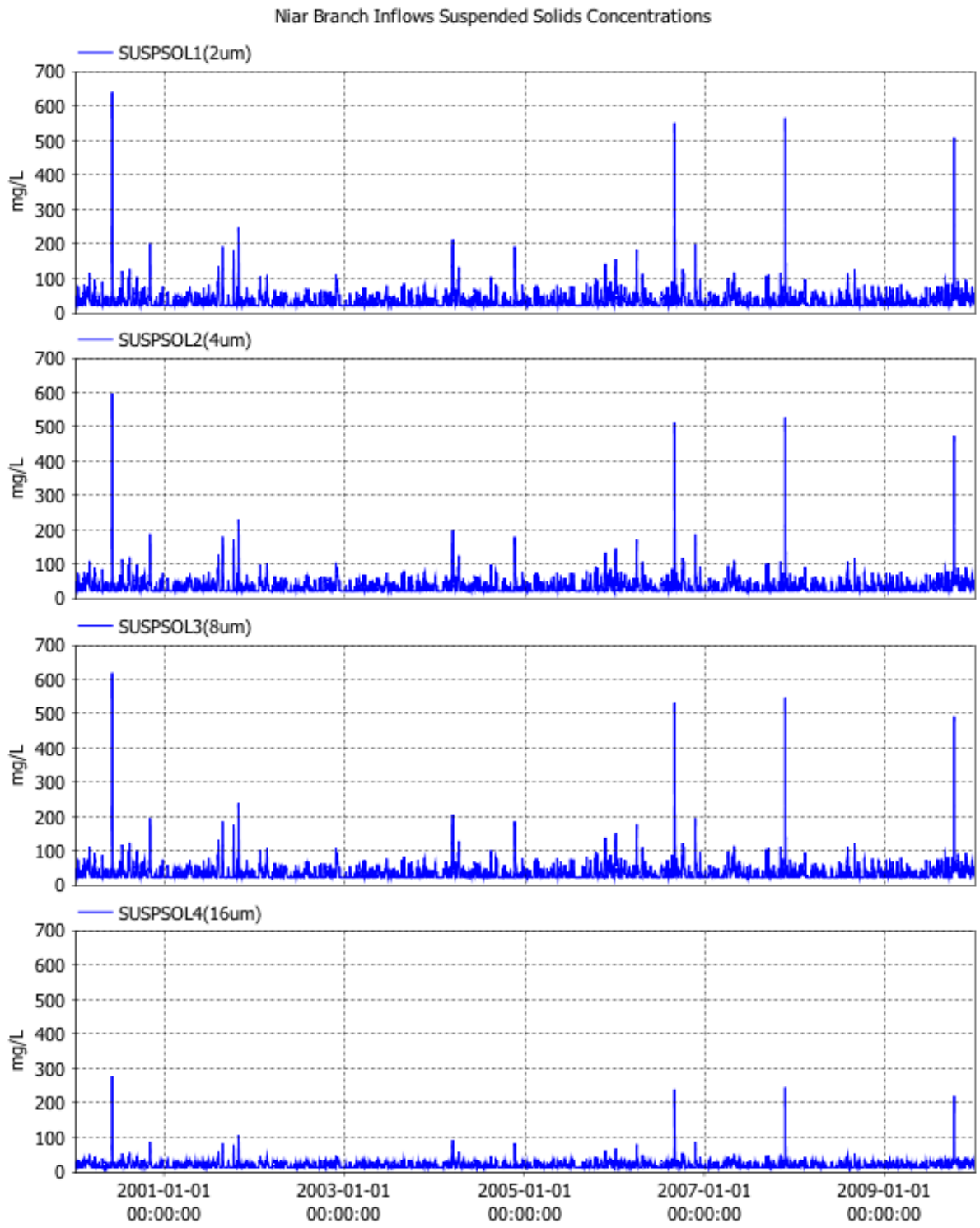

Figure 1.33 Suspended solids concentrations used in model for tributaries of the Niar branch for 2000-2009.

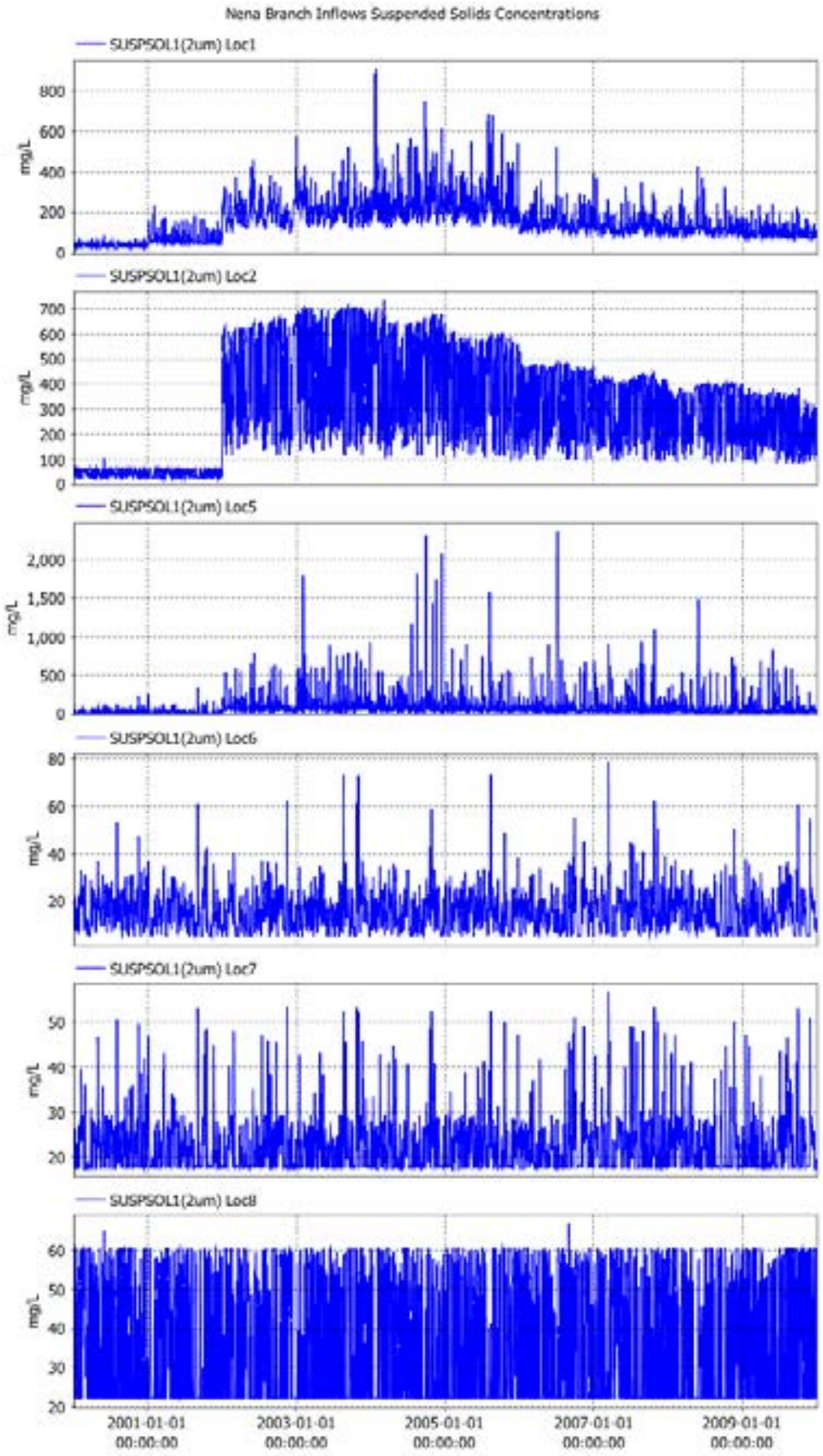

Figure 1.34 Suspended 2um particle concentrations used in model for tributaries of the Nena branch for 2000-2009.

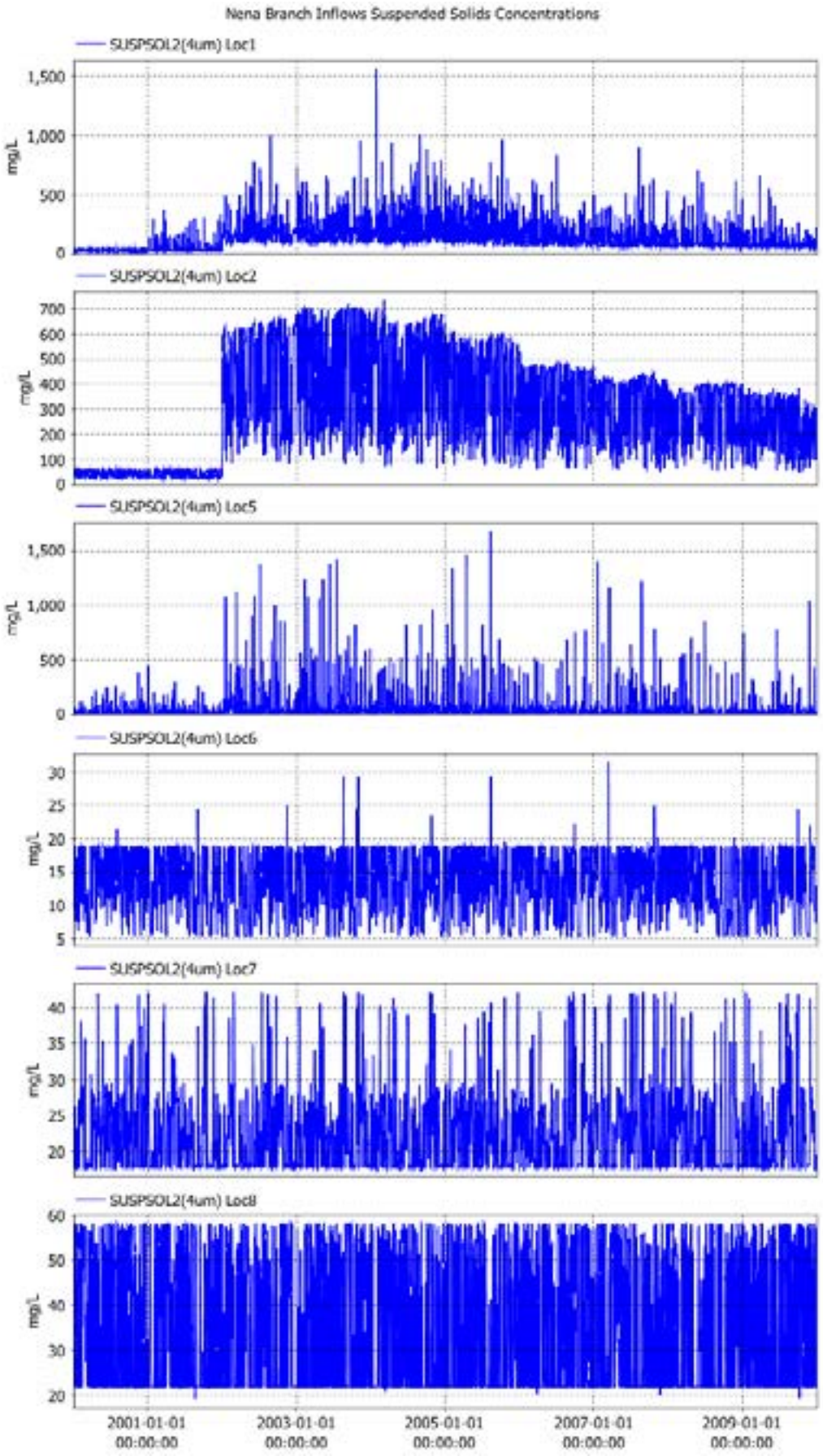

Figure 1.35 Suspended 4um particle concentrations used in model for tributaries of the Nena branch for 2000-2009.

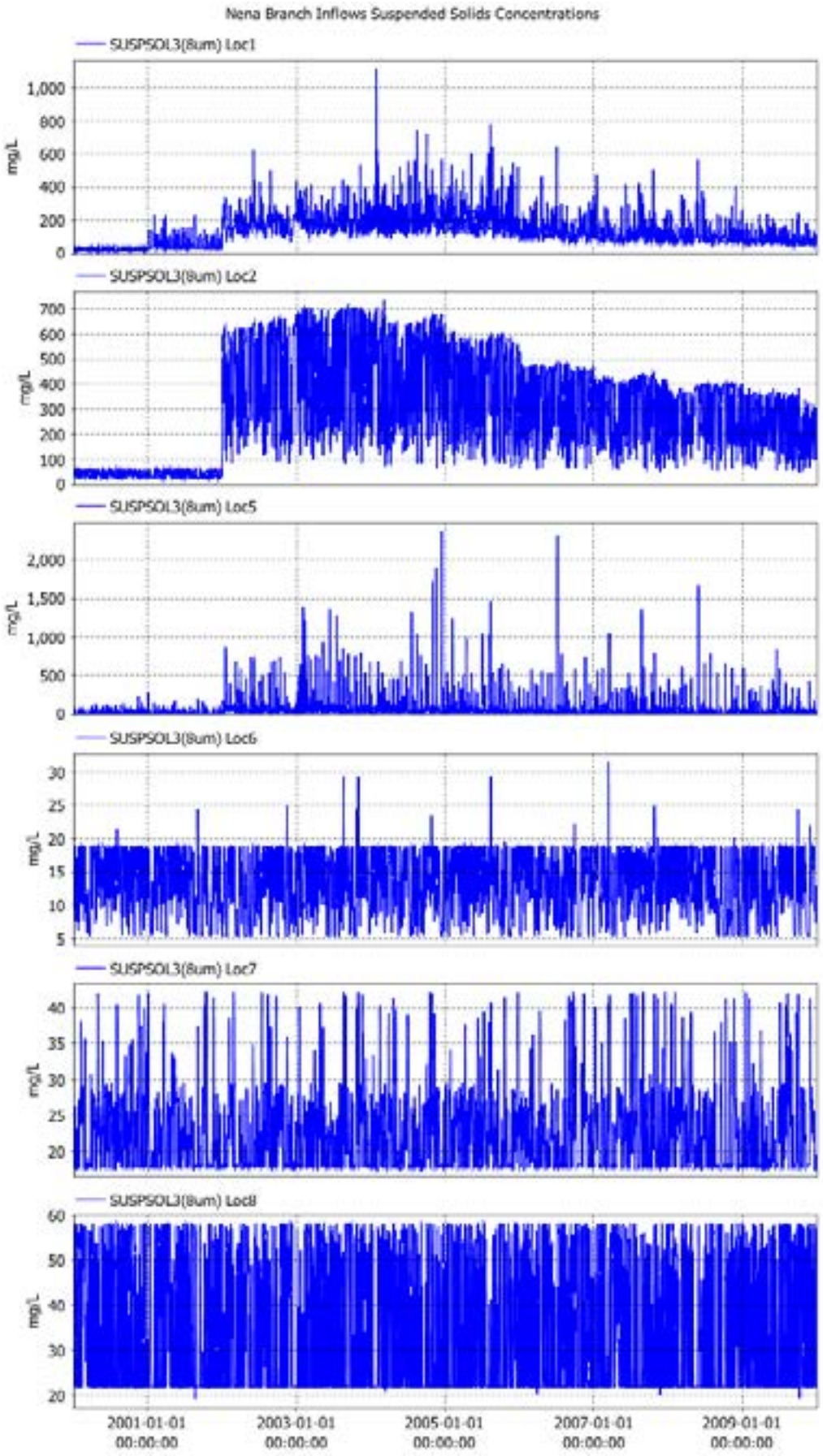

Figure 1.36 Suspended 8um particle concentrations used in model for tributaries of the Nena branch for 2000-2009.

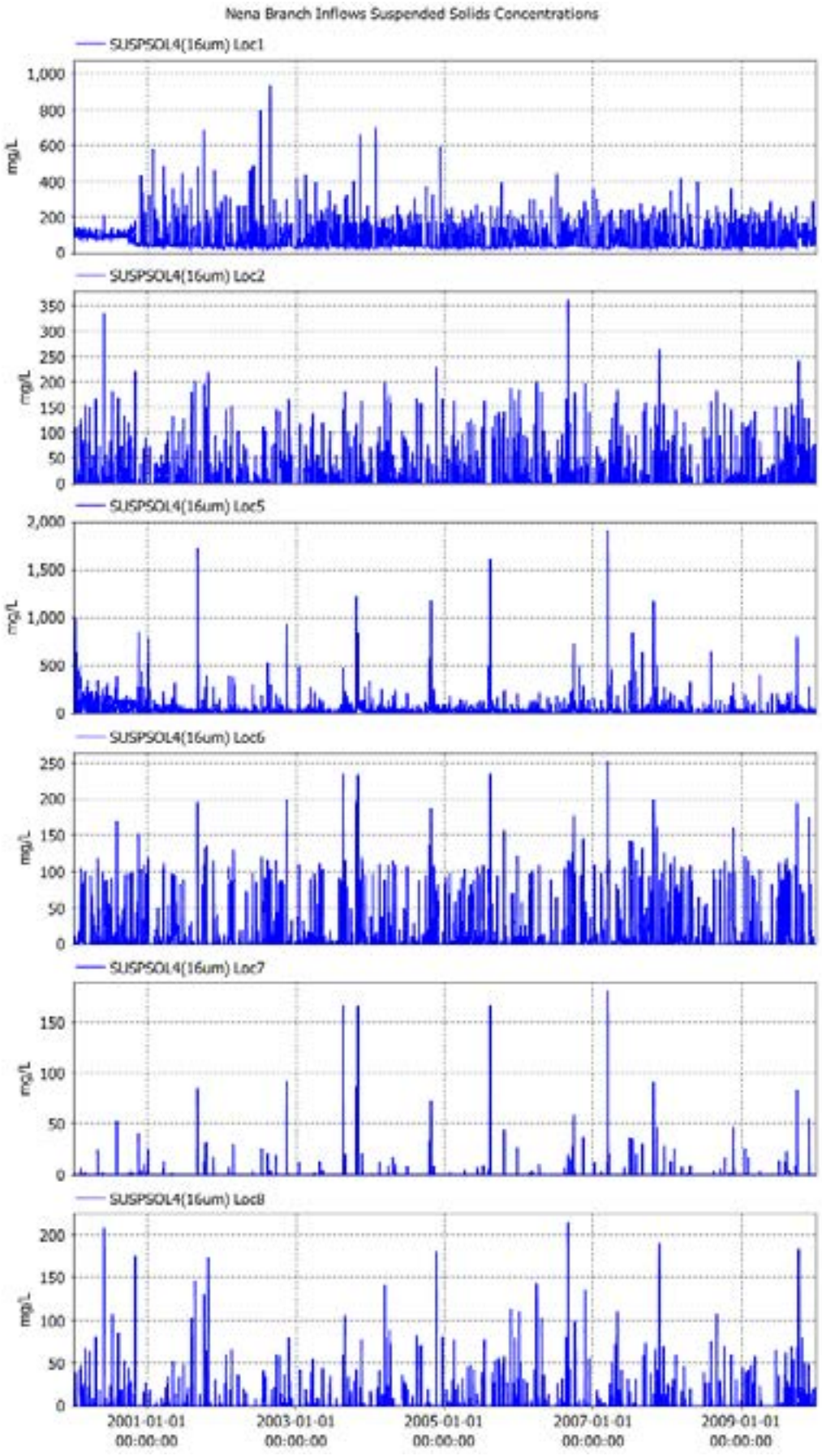

Figure 1.37 Suspended 16um particle concentrations used in model for tributaries of the Nena branch for 2000-2009.

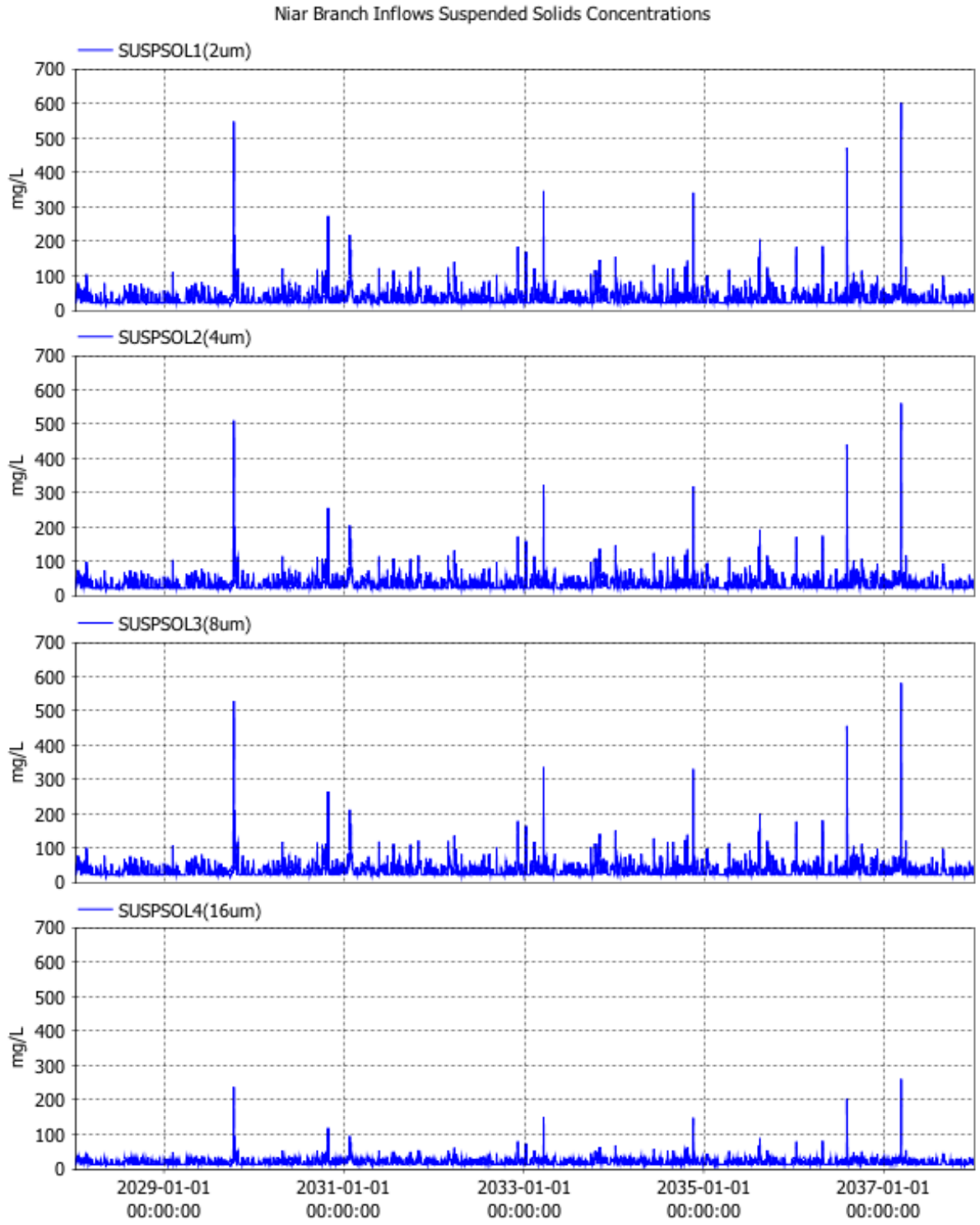

Figure 1.38 Suspended solids concentrations used in model for tributaries of the Niar branch for 2028-2037.

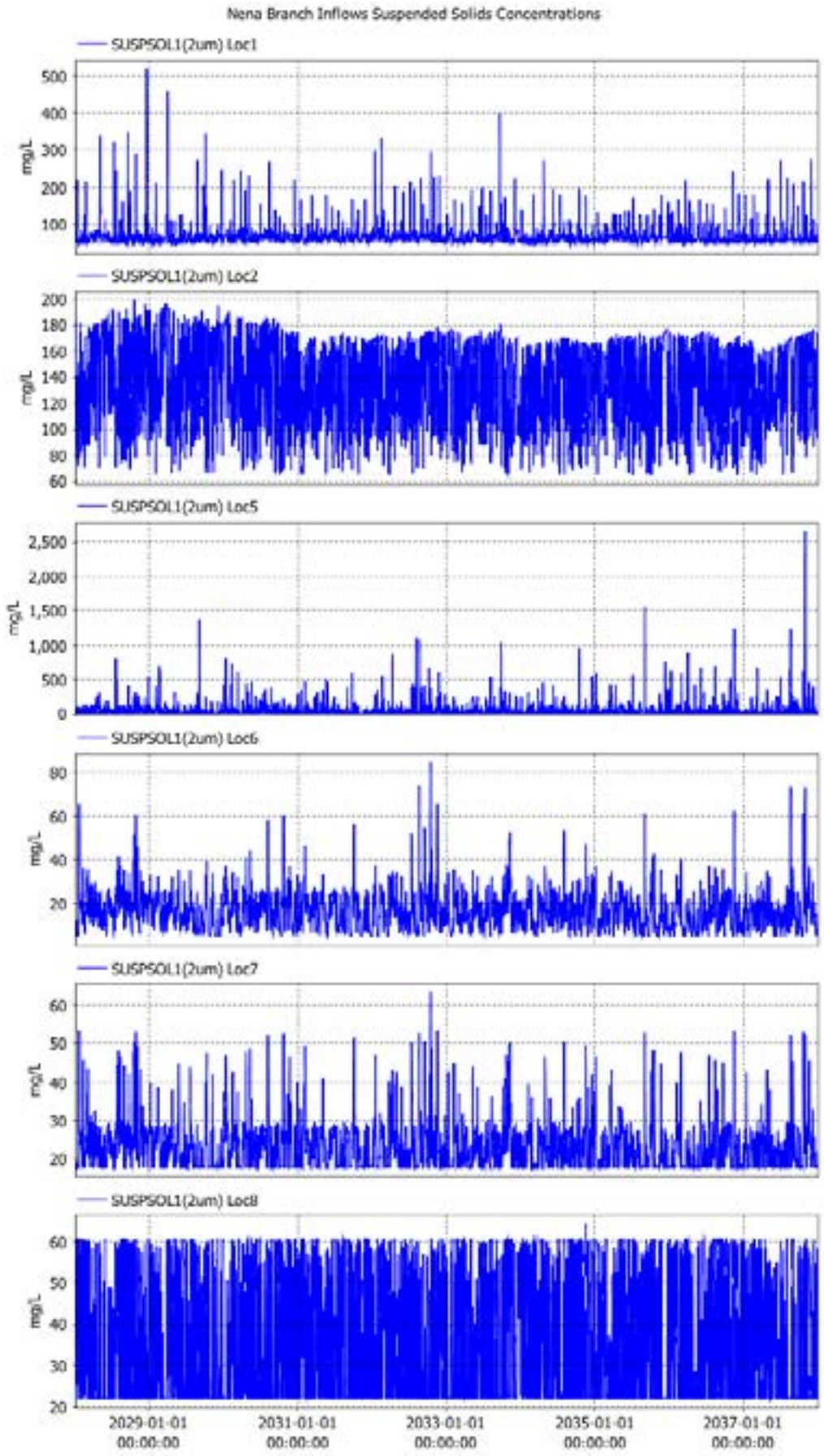

Figure 1.39 Suspended 2um particle concentrations used in model for tributaries of the Nena branch for 2000-2009.

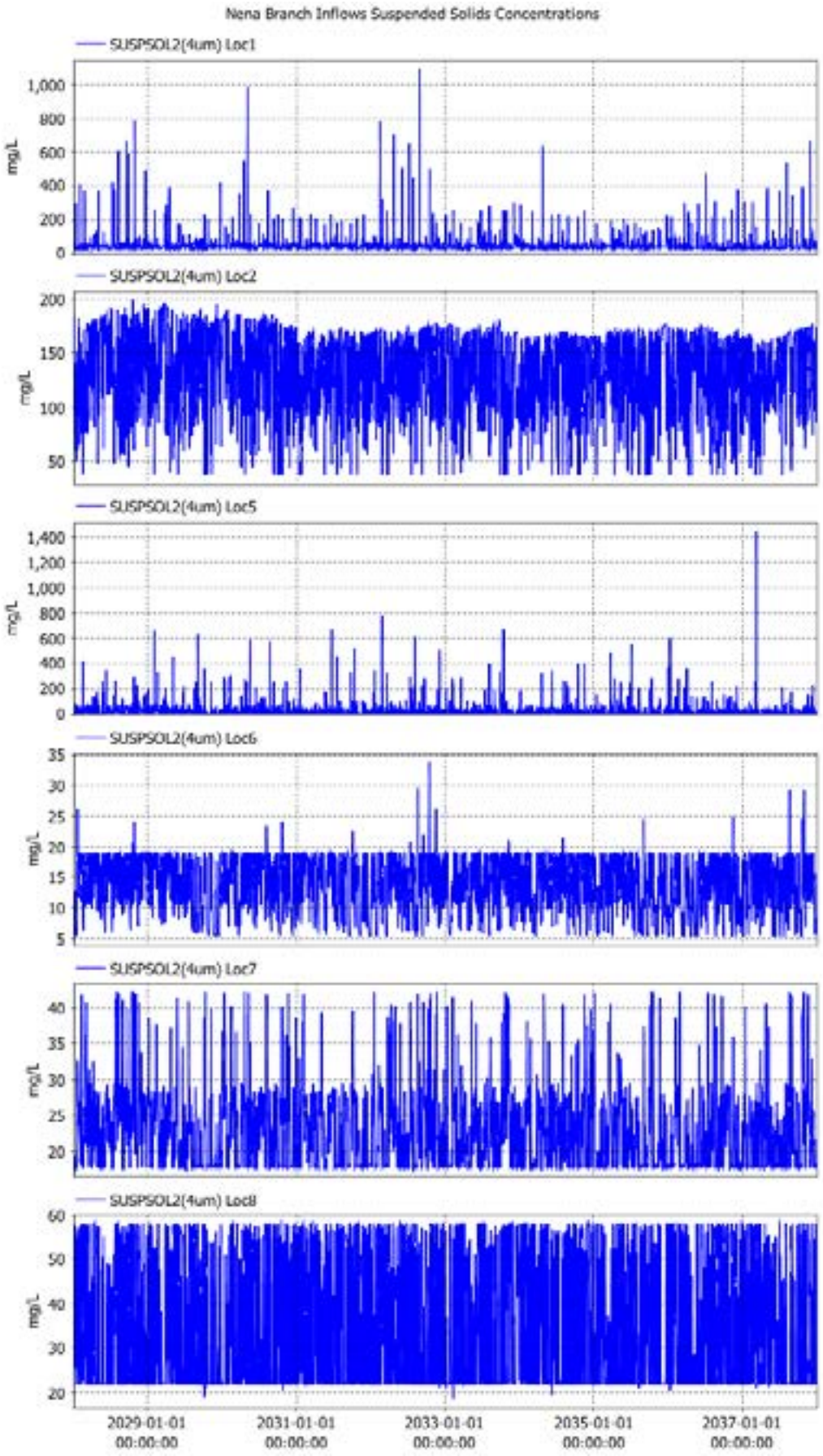

Figure 1.40 Suspended 4um particle concentrations used in model for tributaries of the Nena branch for 2028-2037.

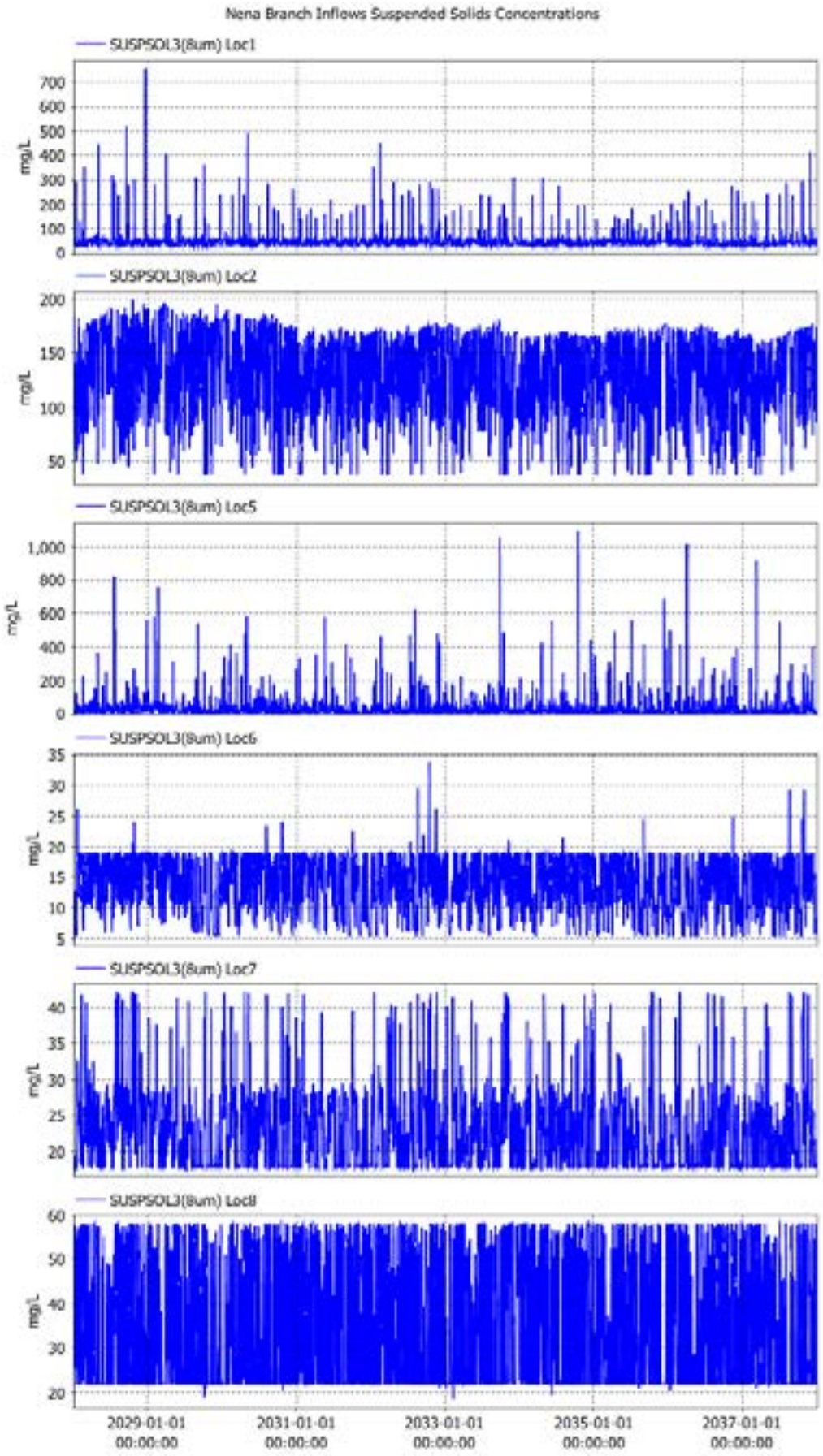

Figure 1.41 Suspended 8um particle concentrations used in model for tributaries of the Nena branch for 2028-2037.

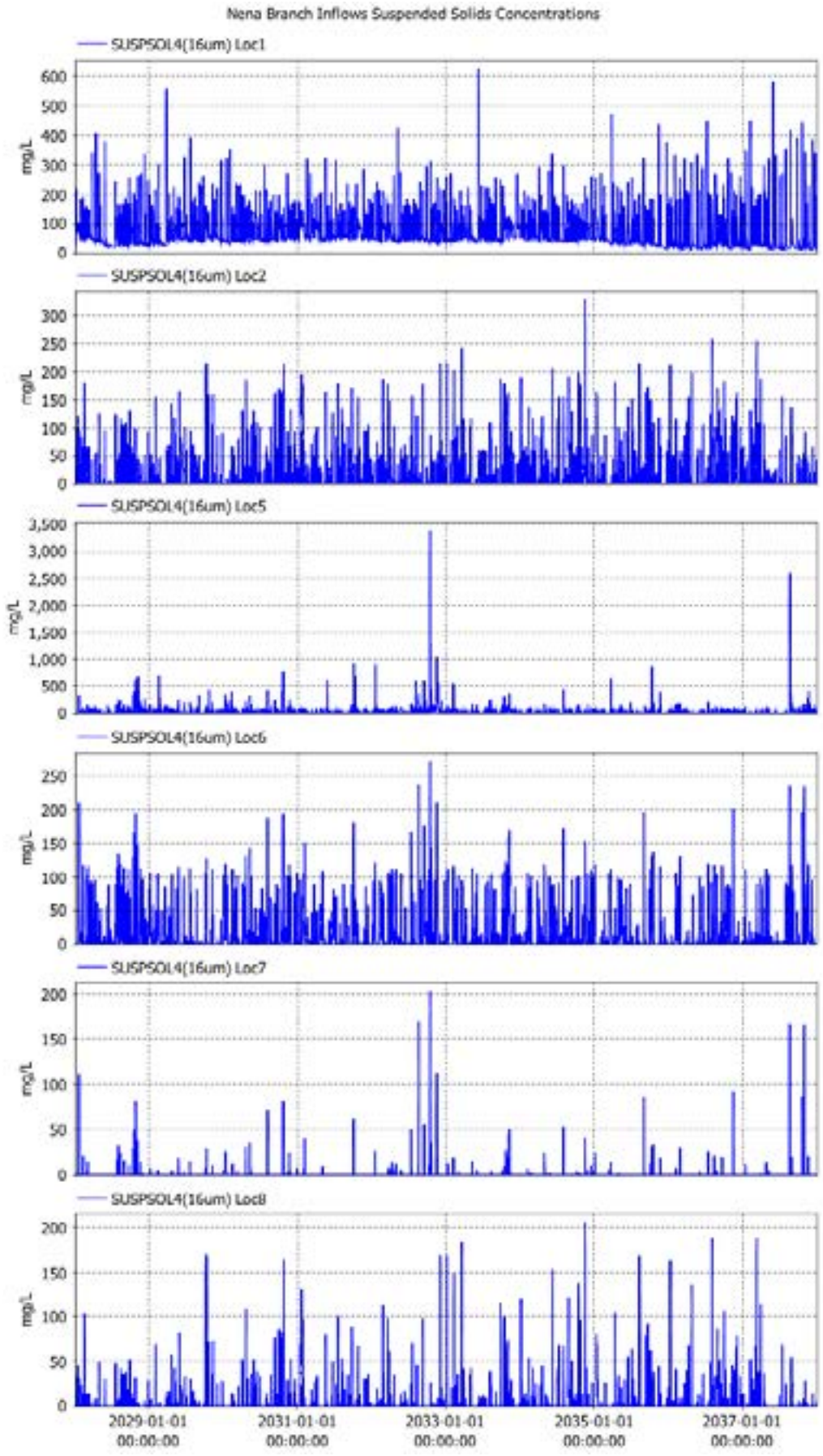

Figure 1.42 Suspended 16um particle concentrations used in model for tributaries of the Nena branch for 2028-2037.

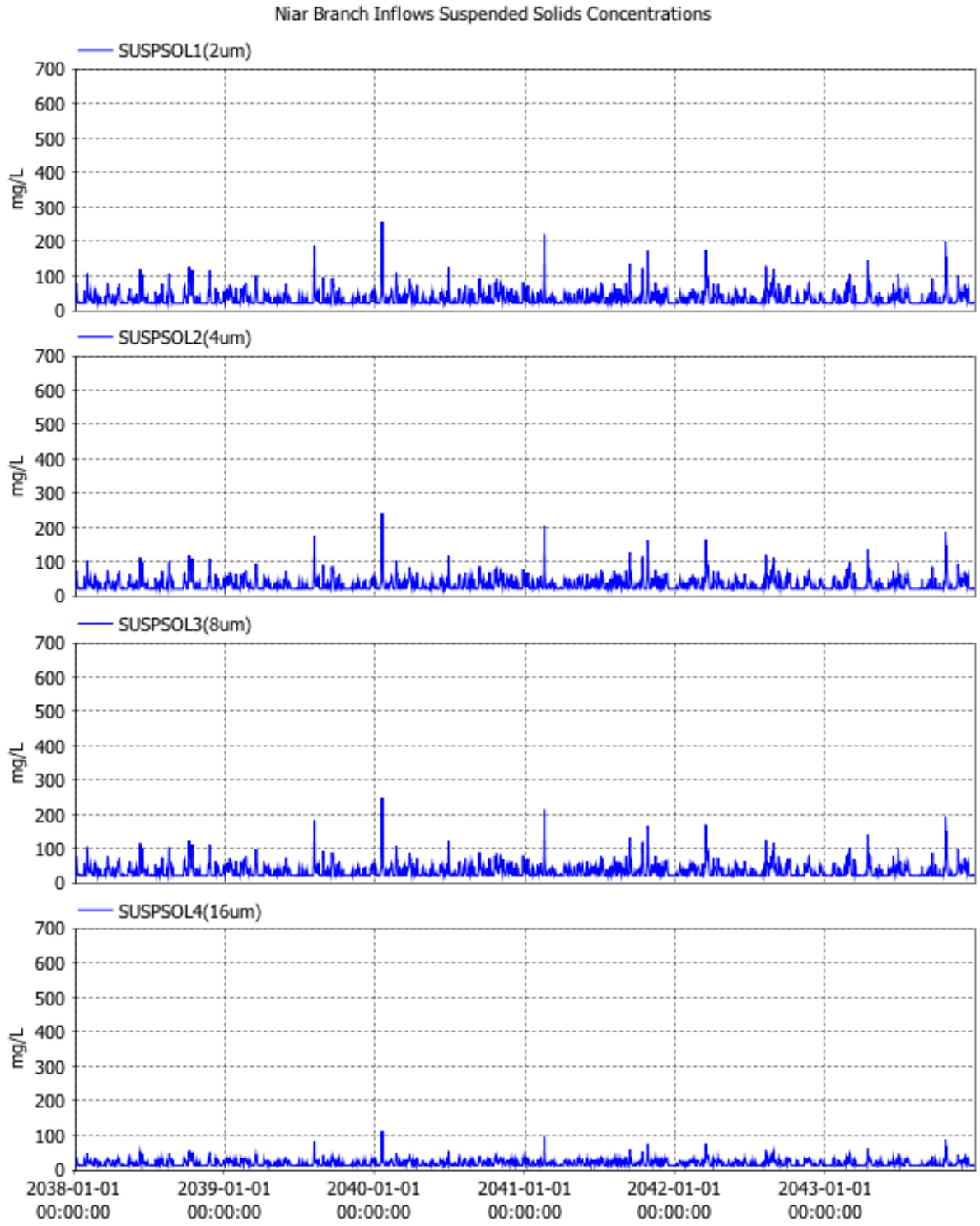

Figure 1.43 Suspended solids concentrations used in model for tributaries of the Niar branch for 2038-2044.

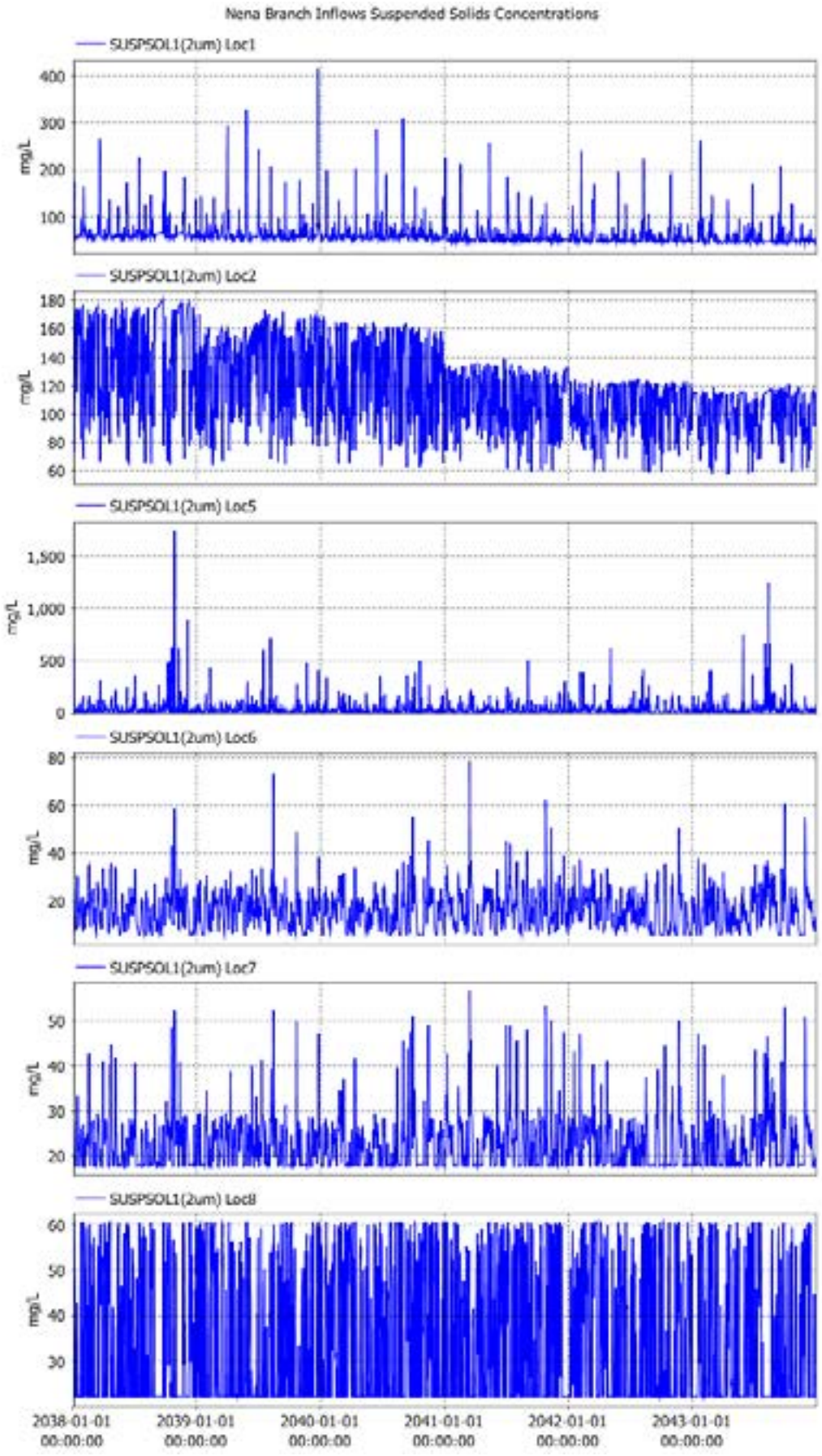

Figure 1.44 Suspended 2um particle concentrations used in model for tributaries of the Nena branch for 2038-2044.

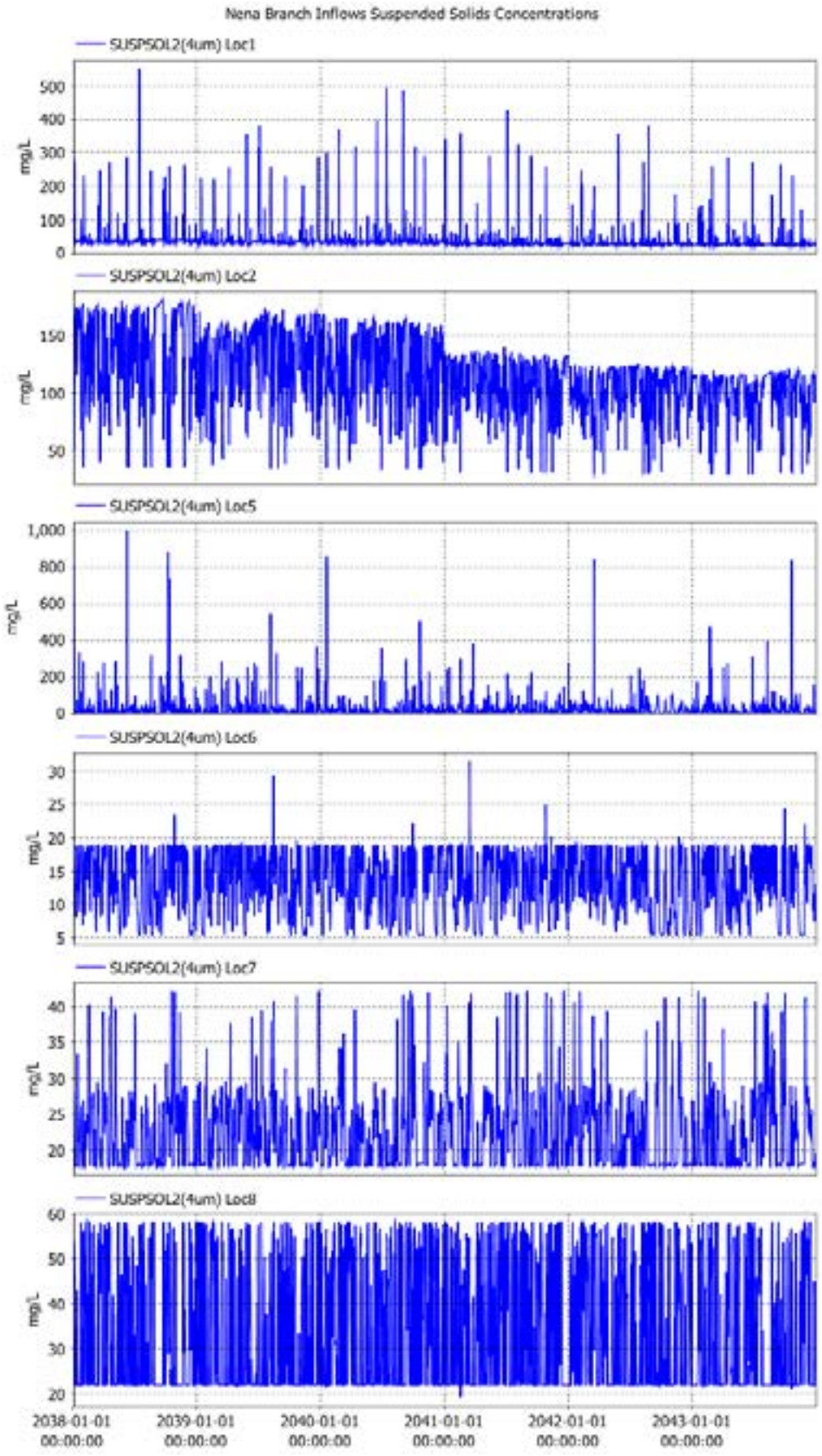

Figure 1.45 Suspended 4um particle concentrations used in model for tributaries of the Nena branch for 2038-2044.

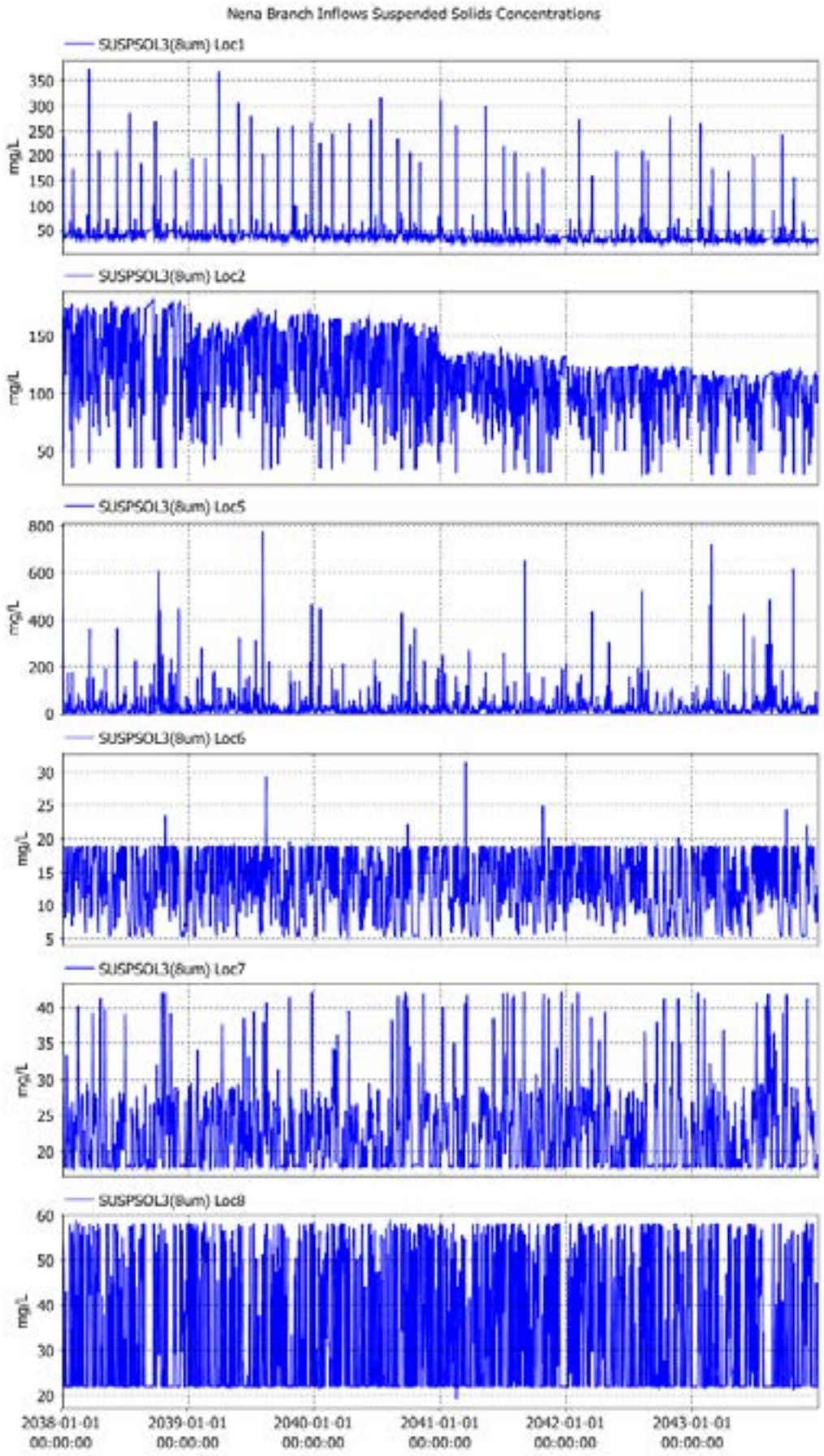

Figure 1.46 Suspended 8um particle concentrations used in model for tributaries of the Nena branch for 2038-2044.

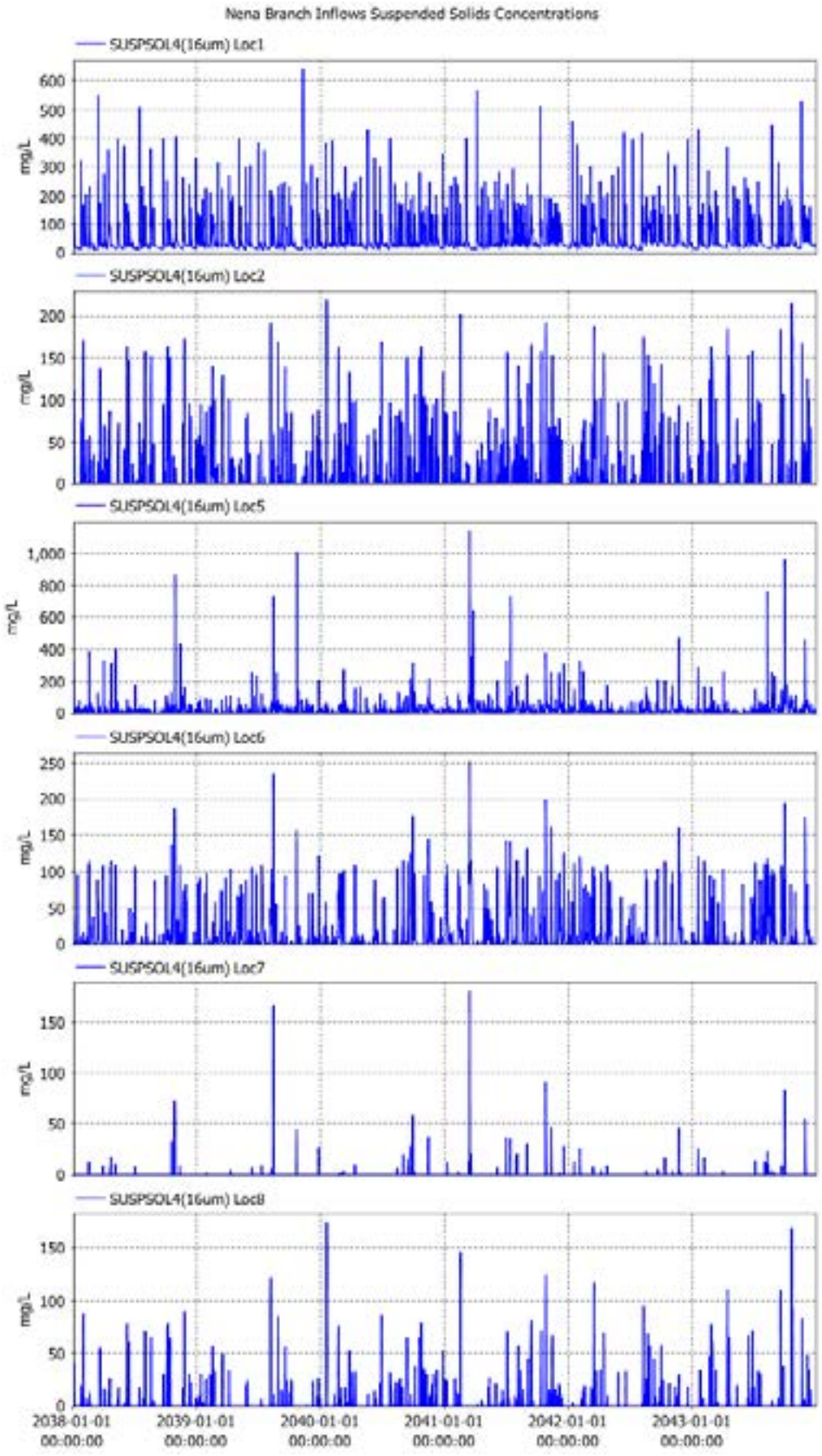

Figure 1.47 Suspended 16um particle concentrations used in model for tributaries of the Nena branch for 2038-2044.

2 Model Results

2.1 Downstream Release

2.1.1 Filling Simulation

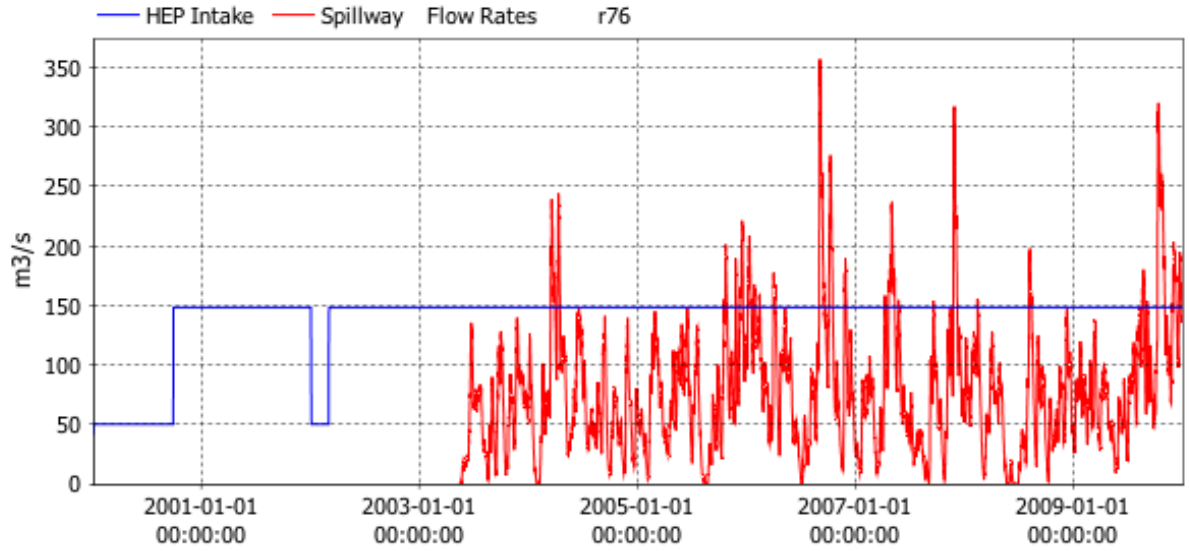

Figure 2.1. Release rate from HEP and spillway during filling simulation.

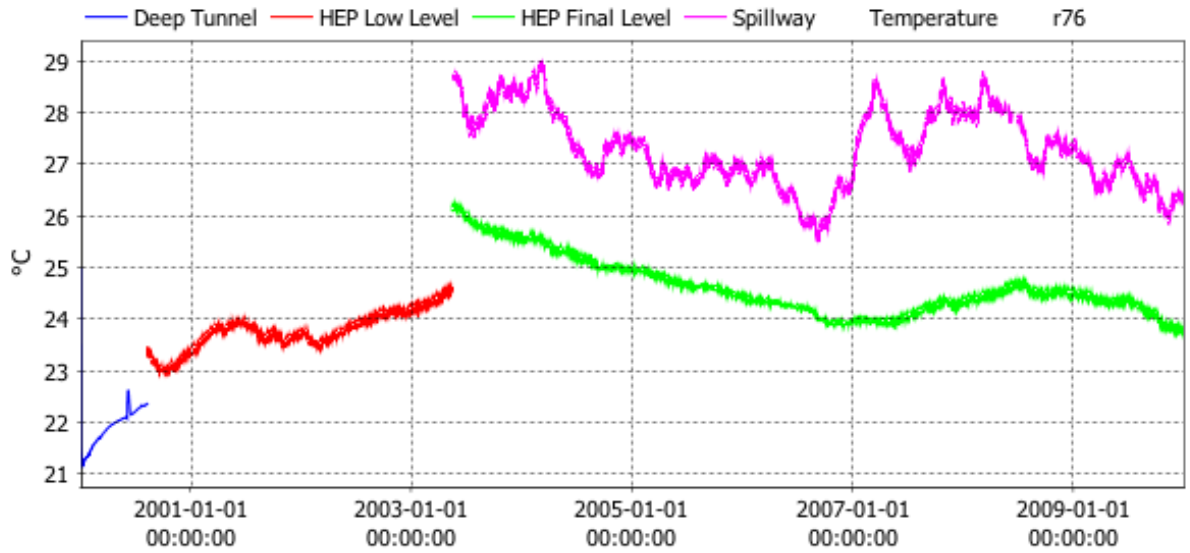

Figure 2.2. Simulated temperature of water extracted from deep diversion tunnel, HEP intakes and spillway during filling simulation.

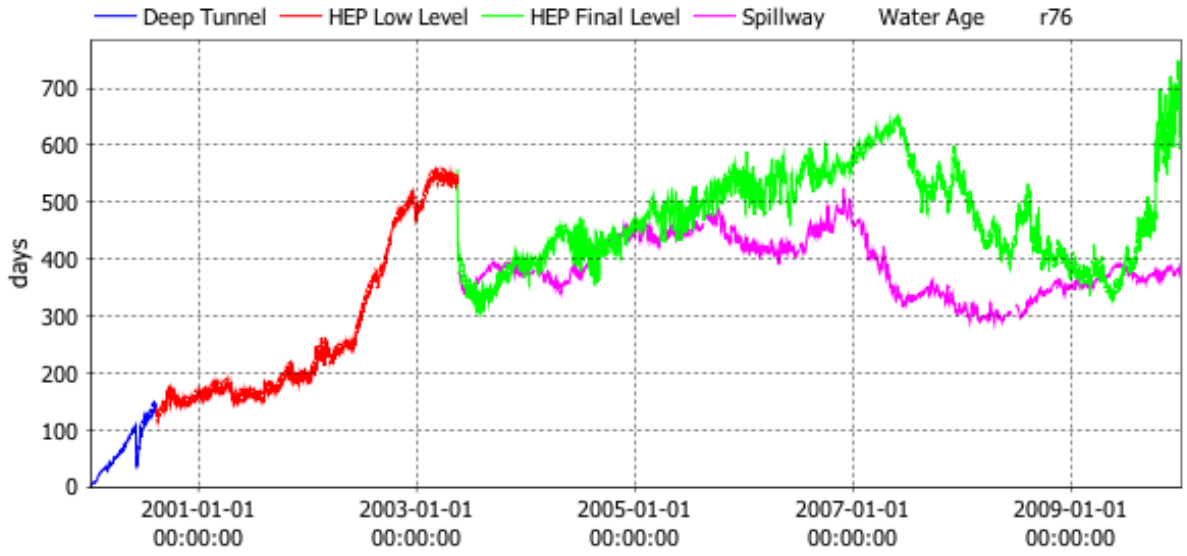

Figure 2.3. Simulated age of water extracted from deep diversion tunnel, HEP intakes and spillway during filling simulation.

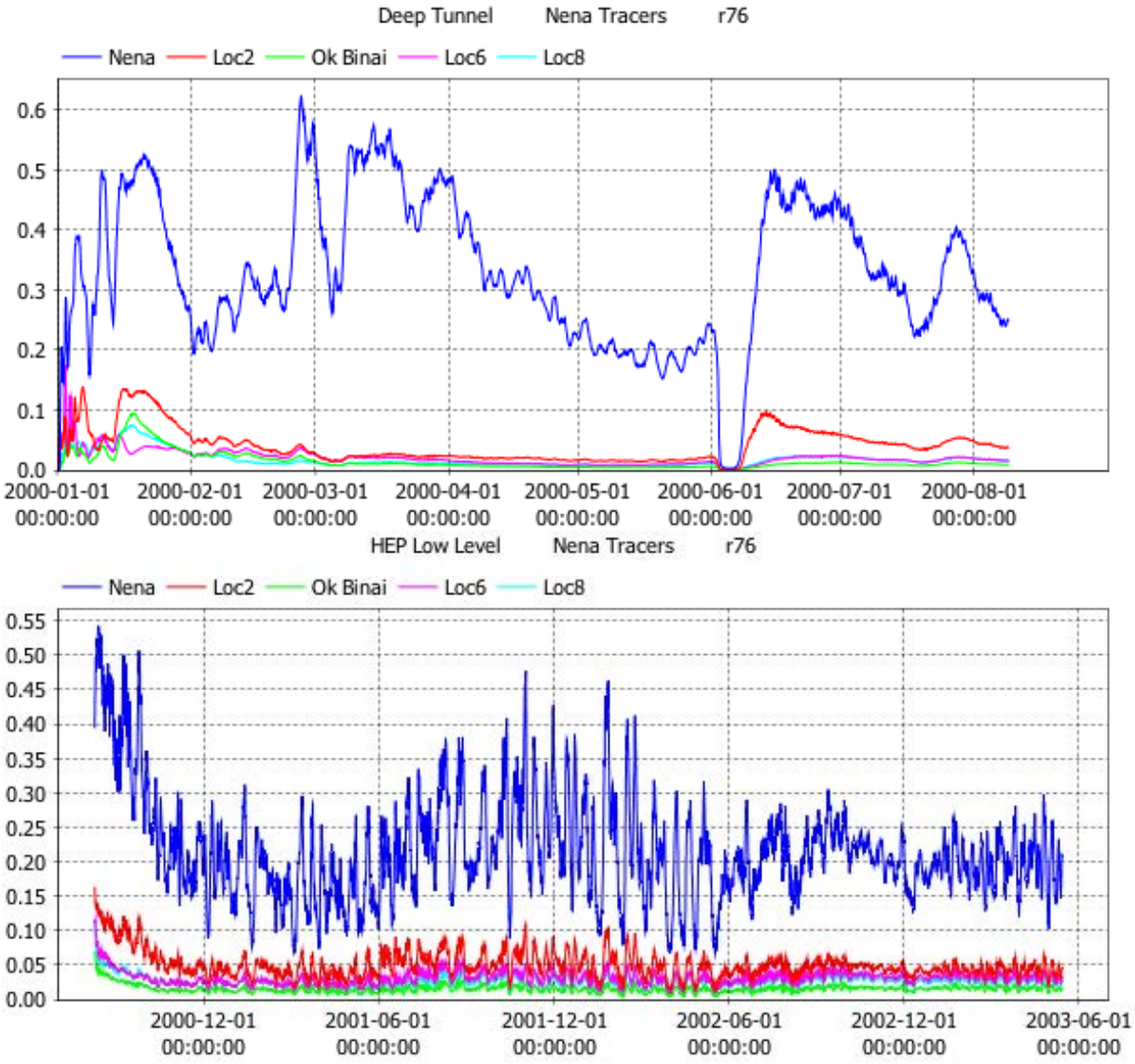

Figure 2.4. Simulated Nena arm tributary tracer concentrations in water extracted from deep diversion tunnel (top panel) and HEP low level intake (bottom panel) during filling simulation.

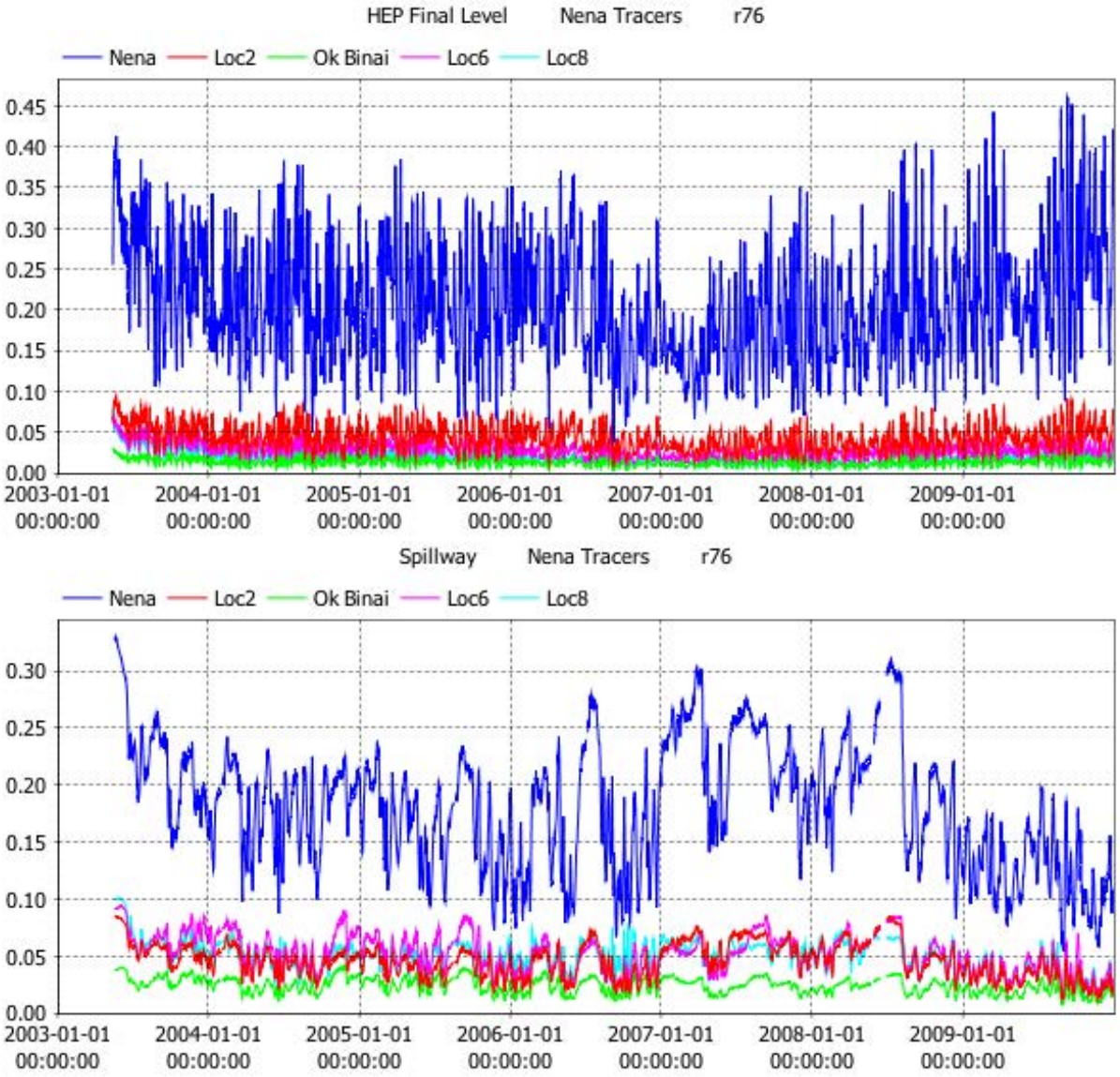

Figure 2.5. Simulated Nena arm tributary tracer concentrations in water extracted from HEP final level intake (top panel) and spillway (bottom panel) during filling simulation.

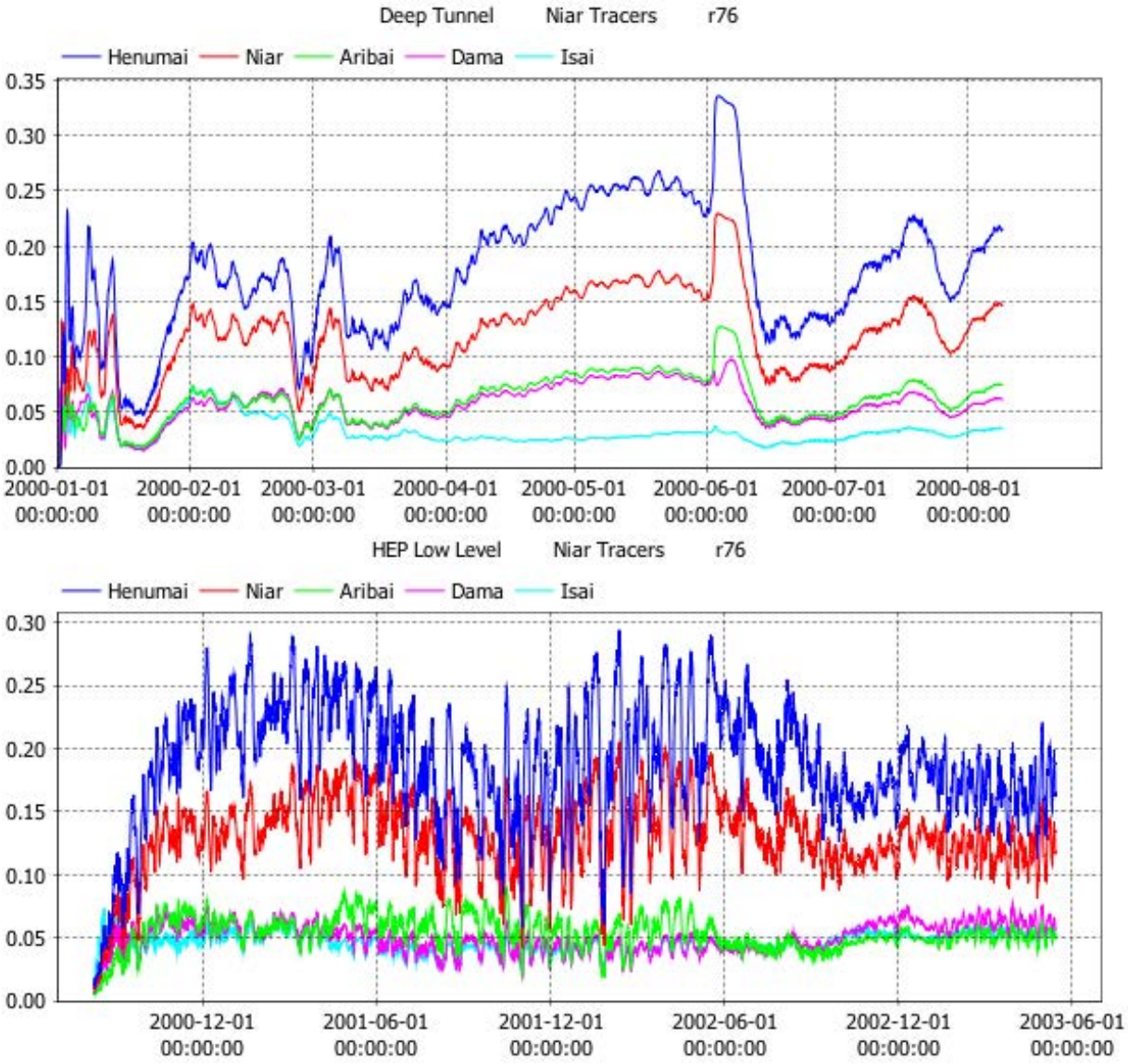

Figure 2.6. Simulated Niar arm tributary tracer concentrations in water extracted from deep diversion tunnel (top panel) and HEP low level intake (bottom panel) during filling simulation.

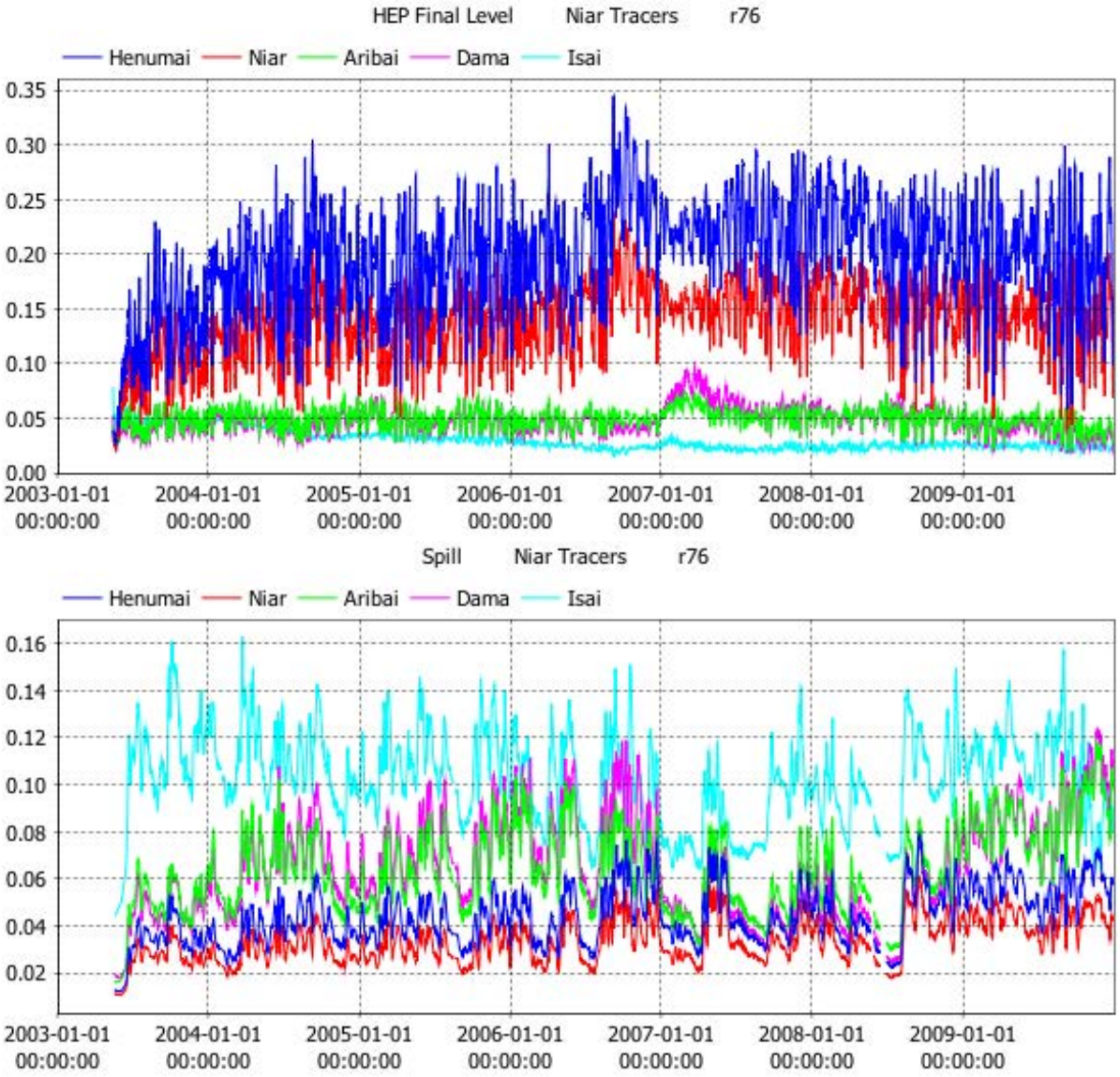

Figure 2.7. Simulated Niar arm tributary tracer concentrations in water extracted from HEP final level intake (top panel) and spillway (bottom panel) during filling simulation.

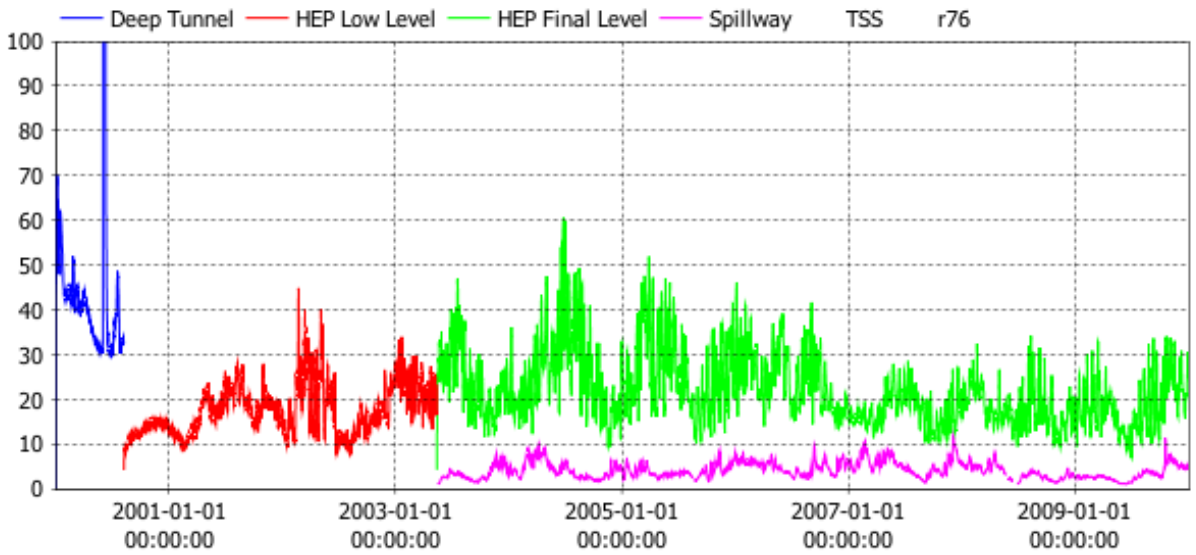

Figure 2.8. Simulated TSS of water extracted from deep diversion tunnel, HEP intakes and spillway during filling simulation.

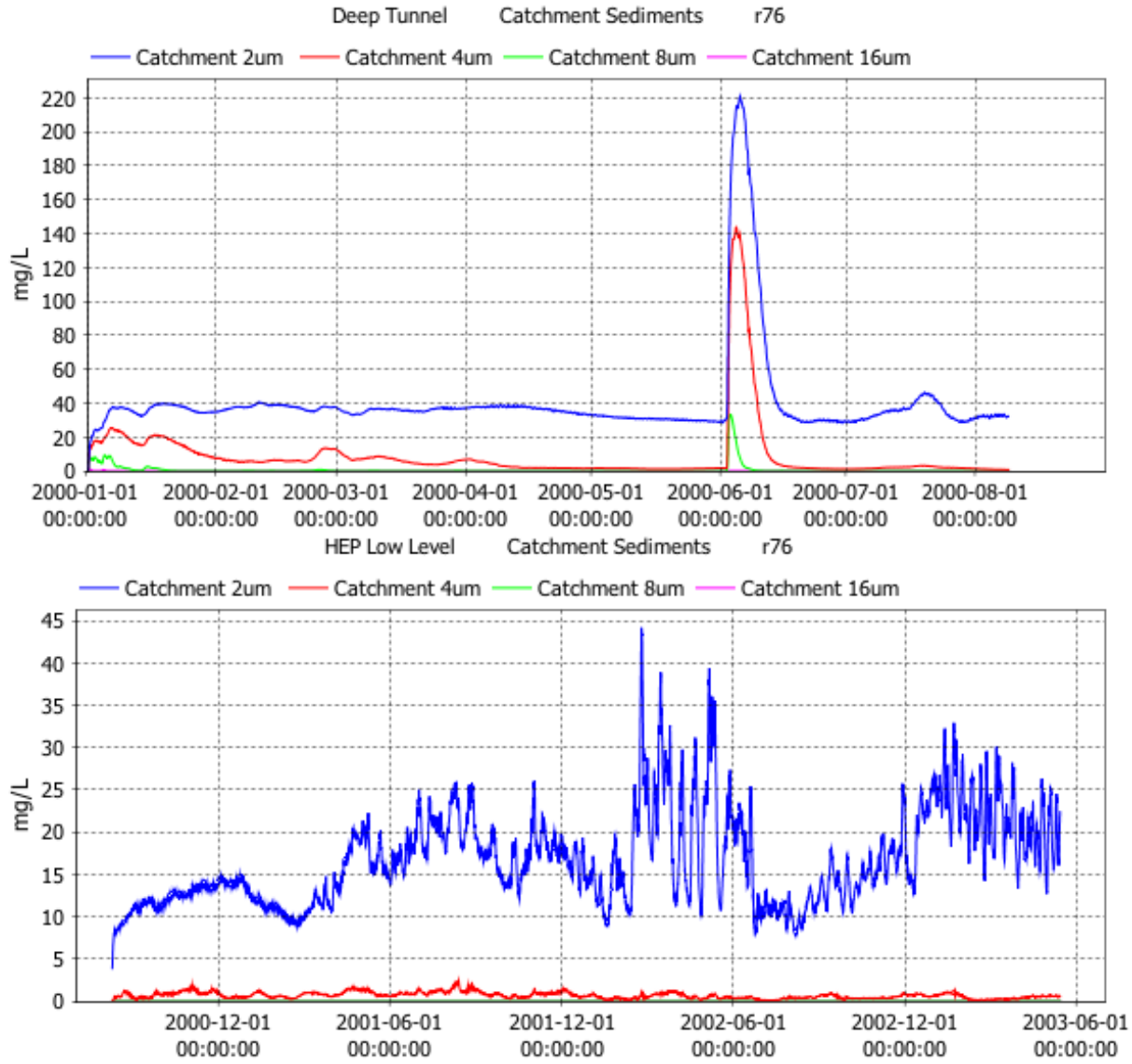

Figure 2.9. Simulated catchment sediment concentrations in water extracted from deep diversion tunnel (top panel) and HEP low level intake (bottom panel) during filling simulation.

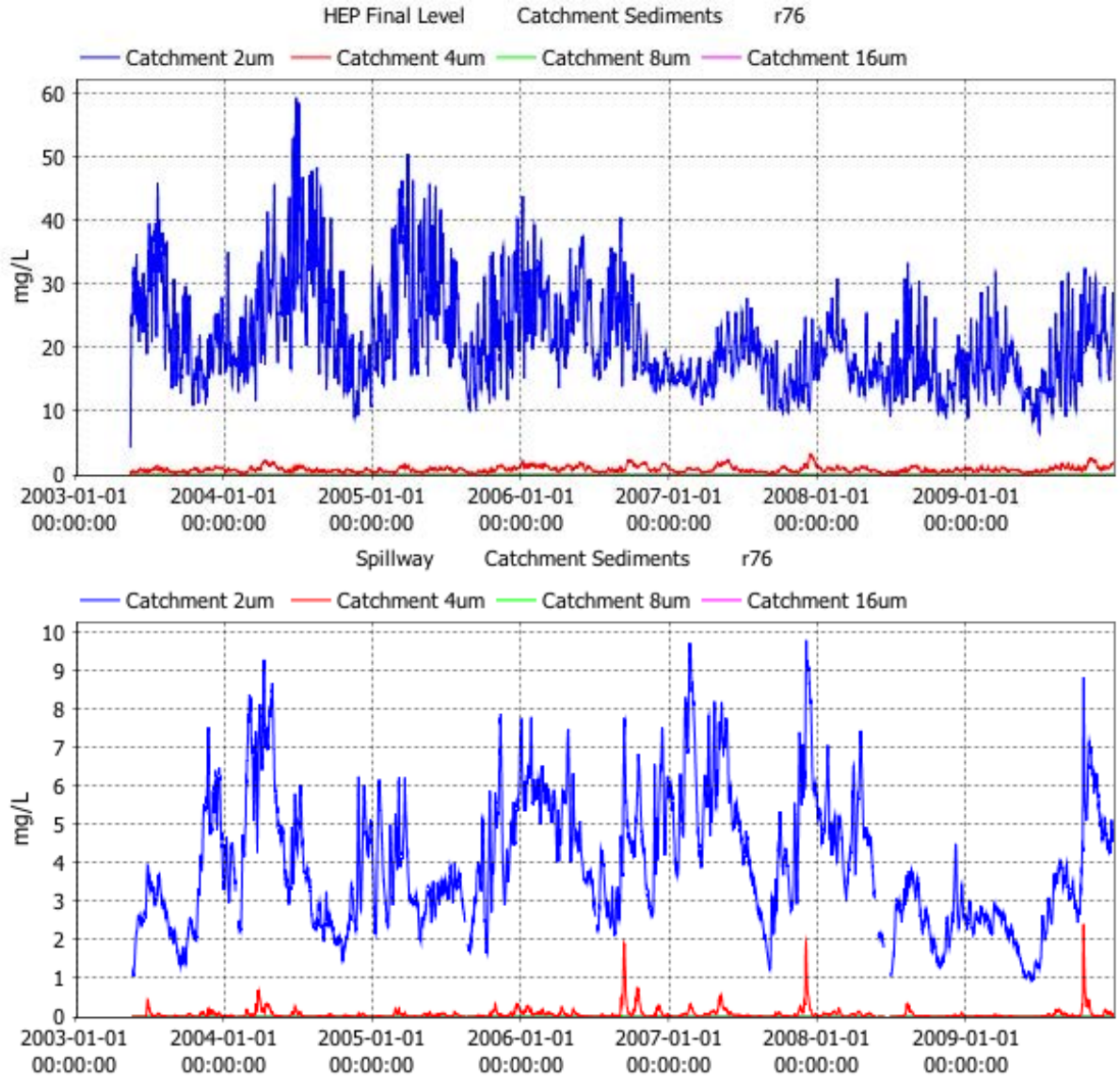

Figure 2.10. Simulated catchment sediment concentrations in water extracted from HEP final level intake (top panel) and spillway (bottom panel) during filling simulation.

2.1.2 Operations Simulation – Equal Mobility

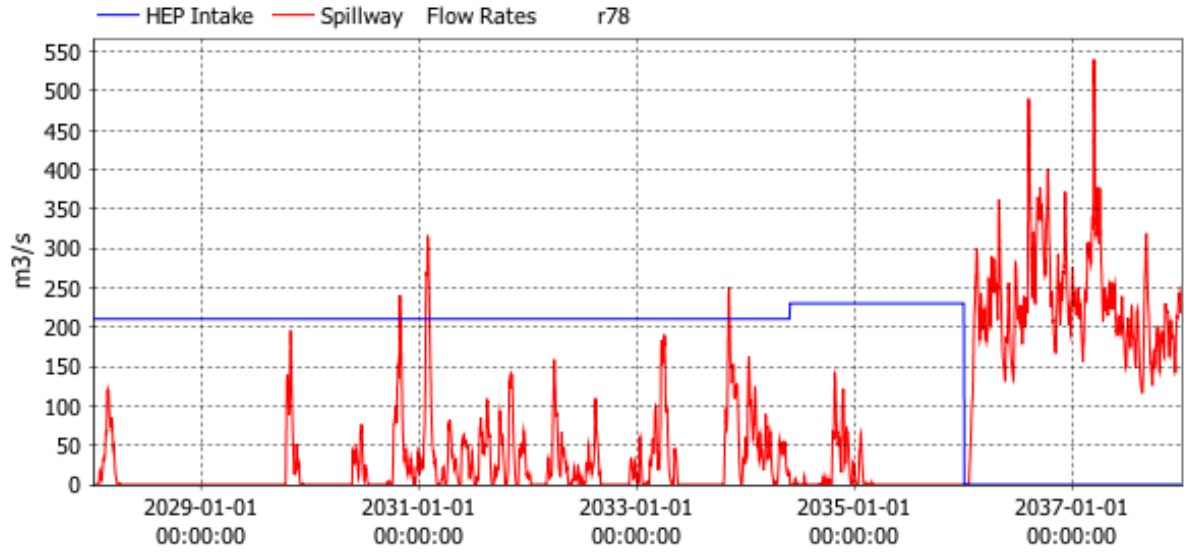

Figure 2.11. Release rate from HEP and spillway during operations simulation with equal mobility.

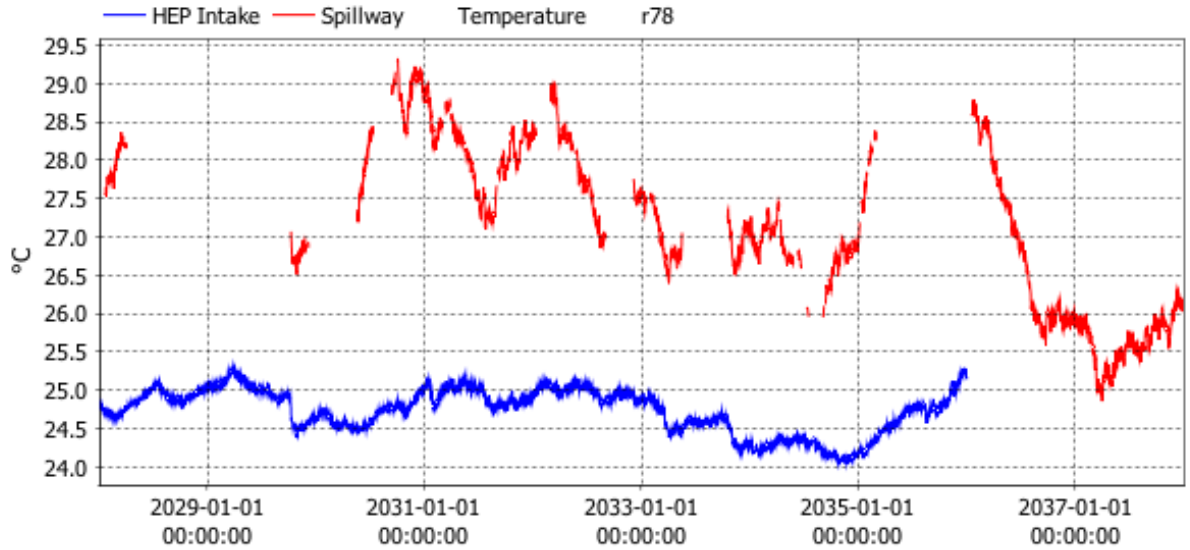

Figure 2.12. Simulated temperature of water extracted from HEP intake and spillway during operations simulation with equal mobility.

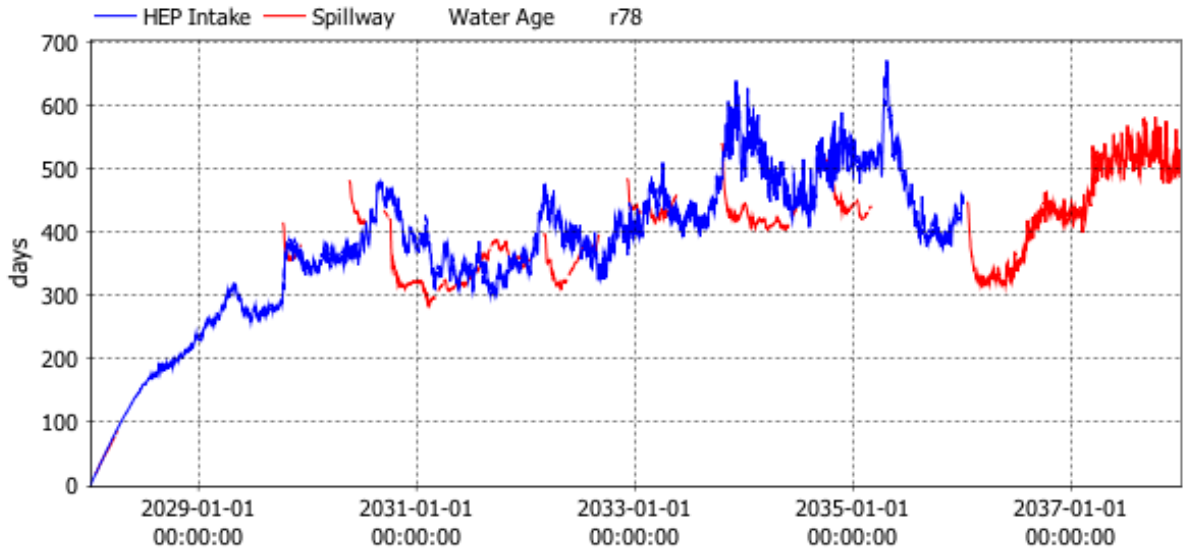

Figure 2.13. Simulated age of water extracted from HEP intake and spillway during operations simulation with equal mobility.

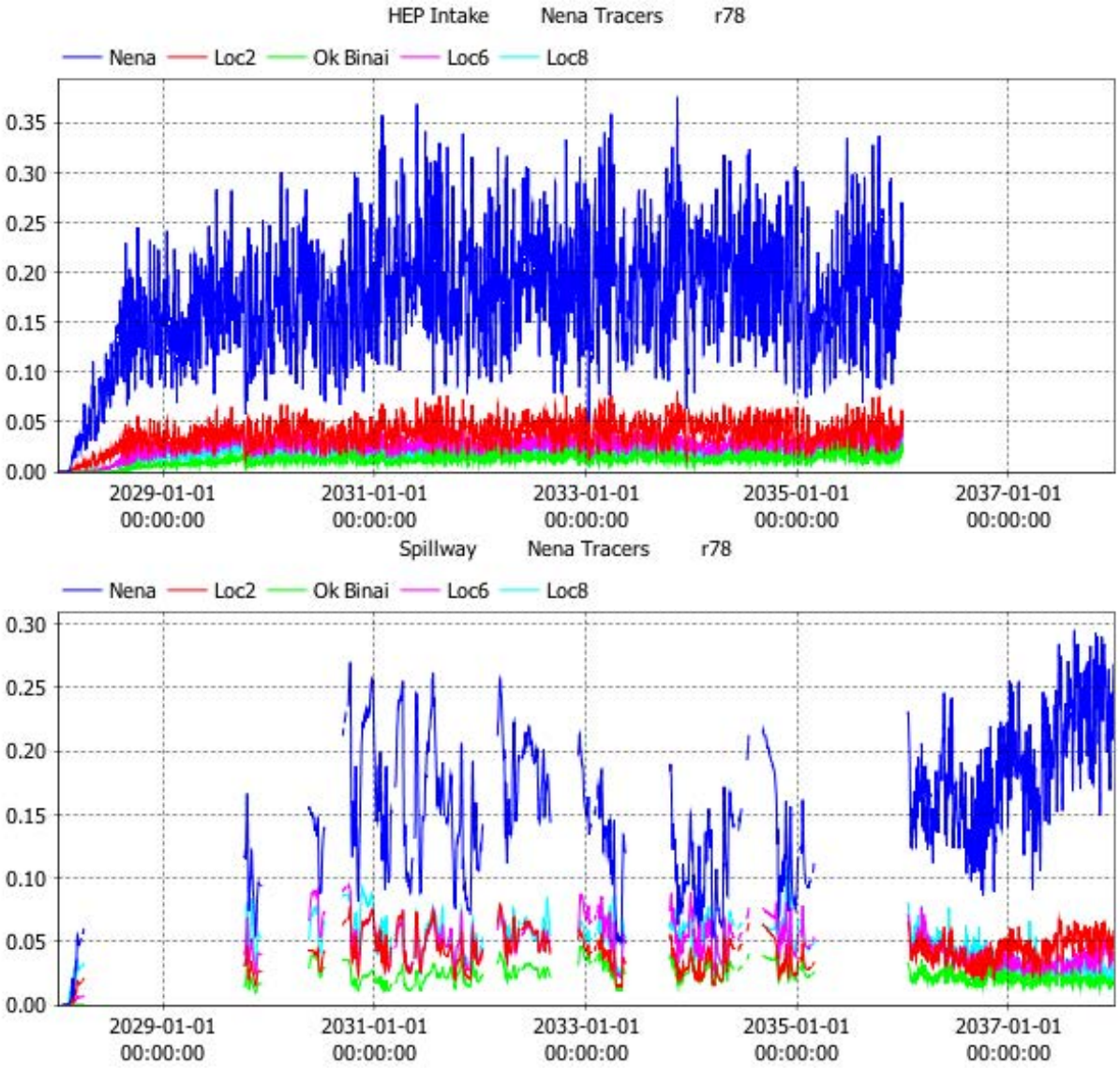

Figure 2.14. Simulated Nena arm tributary tracer concentrations in water extracted from HEP intake (top panel) and spillway (bottom panel) during operations simulation with equal mobility.

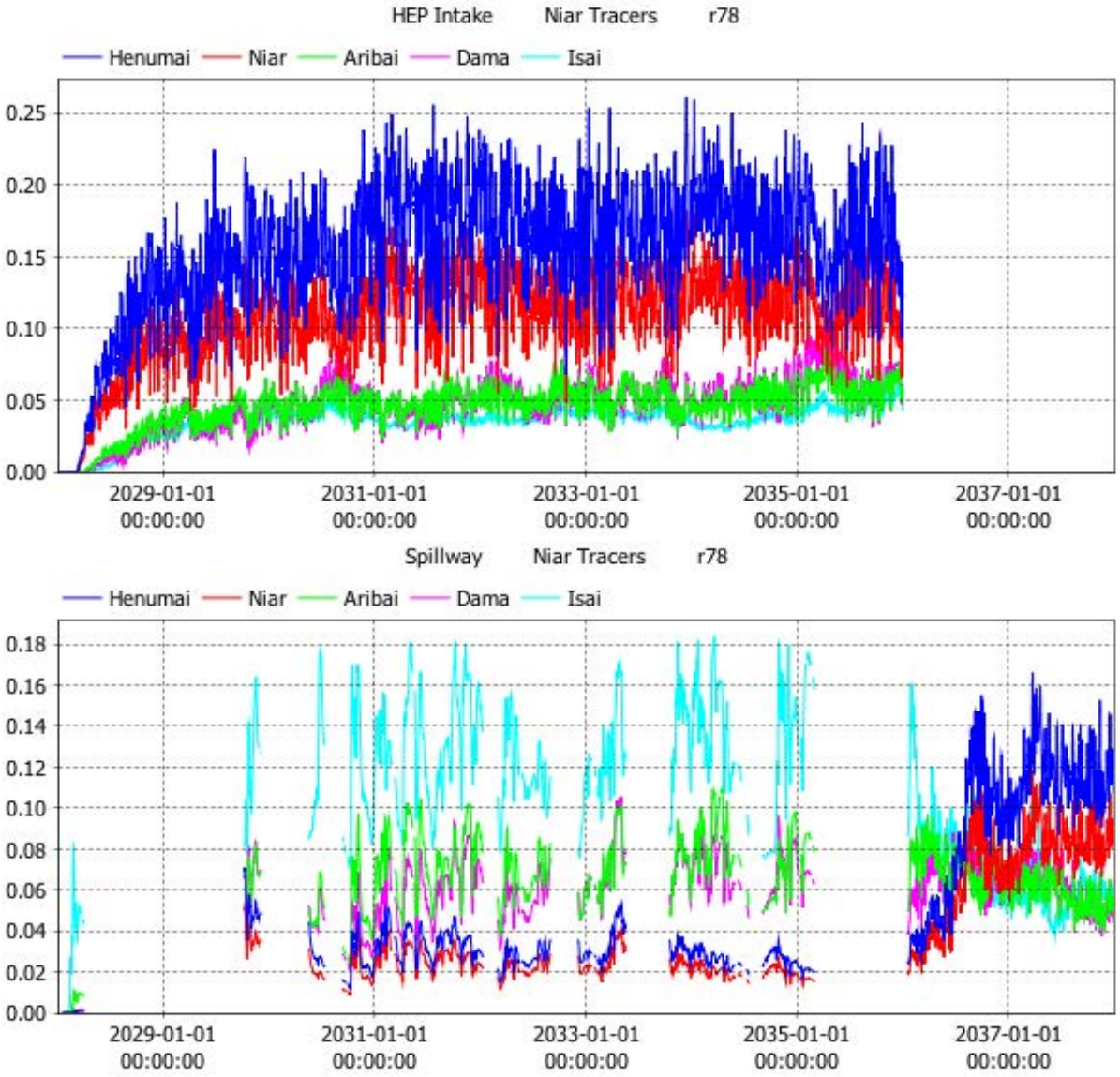

Figure 2.15. Simulated Niar arm tributary tracer concentrations in water extracted from HEP intake (top panel) and spillway (bottom panel) during operations simulation with equal mobility.

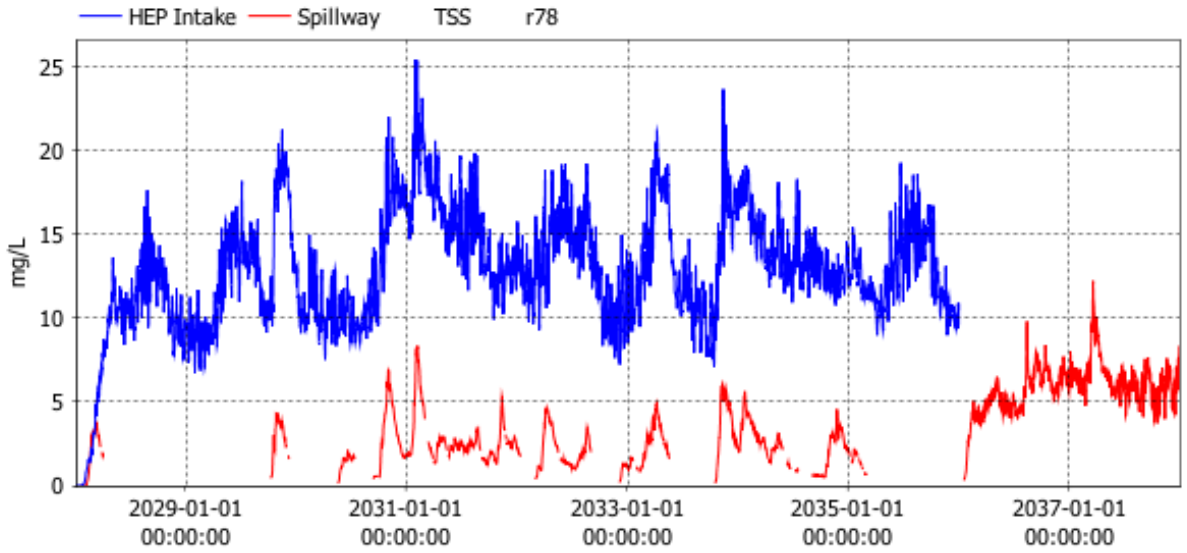

Figure 2.16 Simulated TSS of water extracted from HEP intake and spillway during operations simulation with equal mobility.

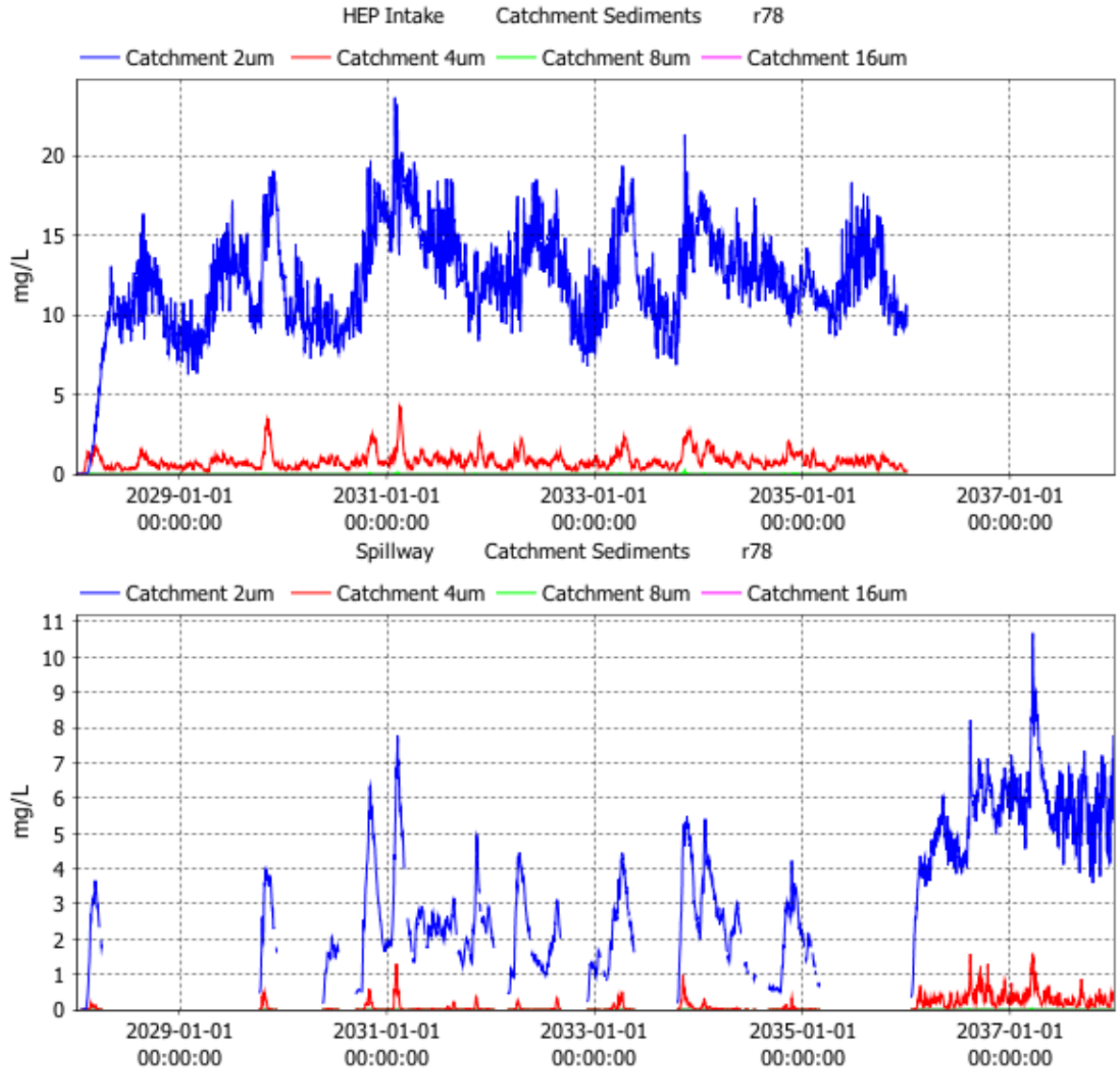

Figure 2.17. Simulated catchment sediment concentrations in water extracted from HEP intake (top panel) and spillway (bottom panel) during operations simulation with equal mobility.

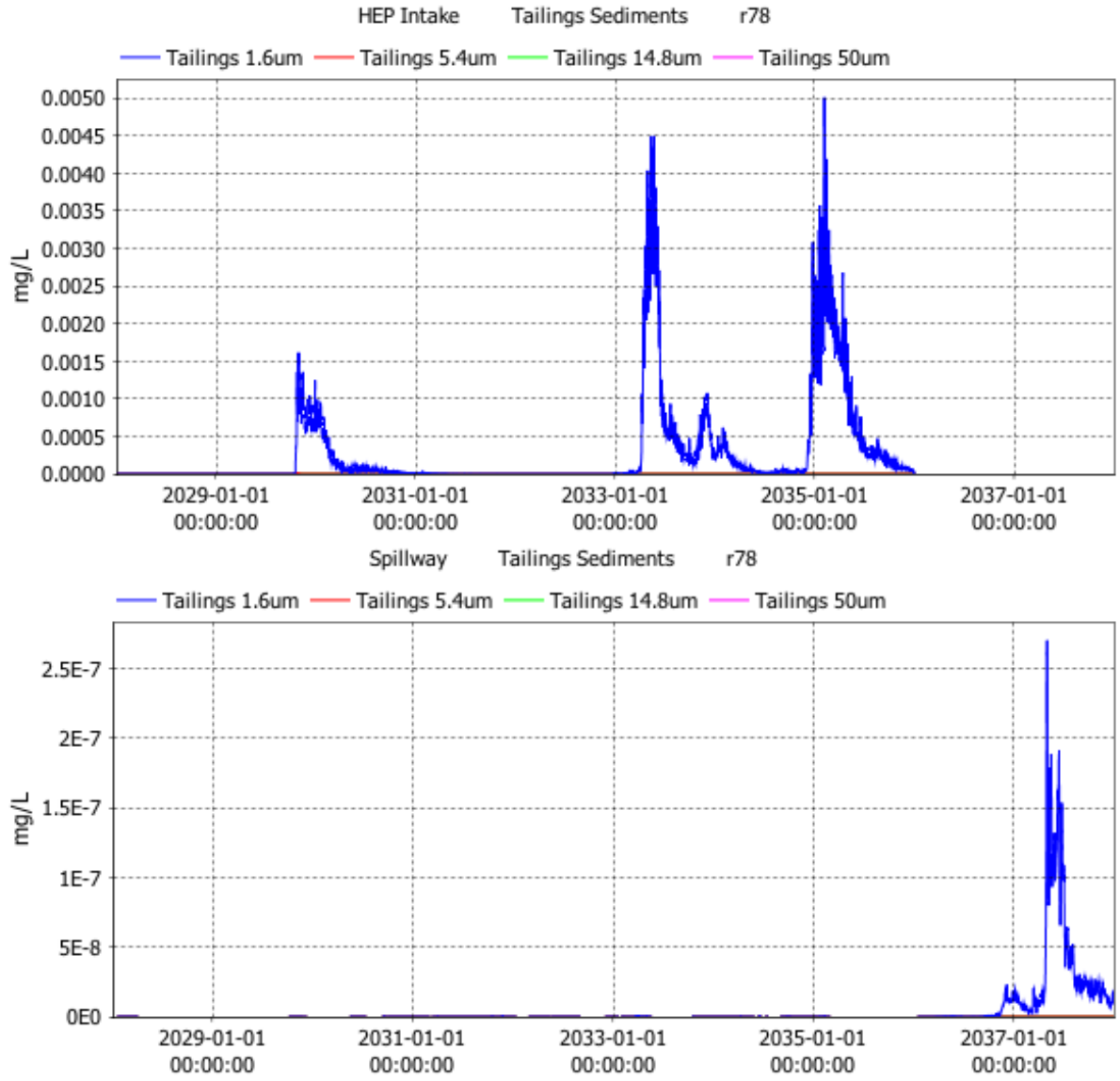

Figure 2.18. Simulated tailings concentrations in water extracted from HEP intake (top panel) and spillway (bottom panel) during operations simulation with equal mobility.

2.1.3 Operations Simulation – Derived Mobility

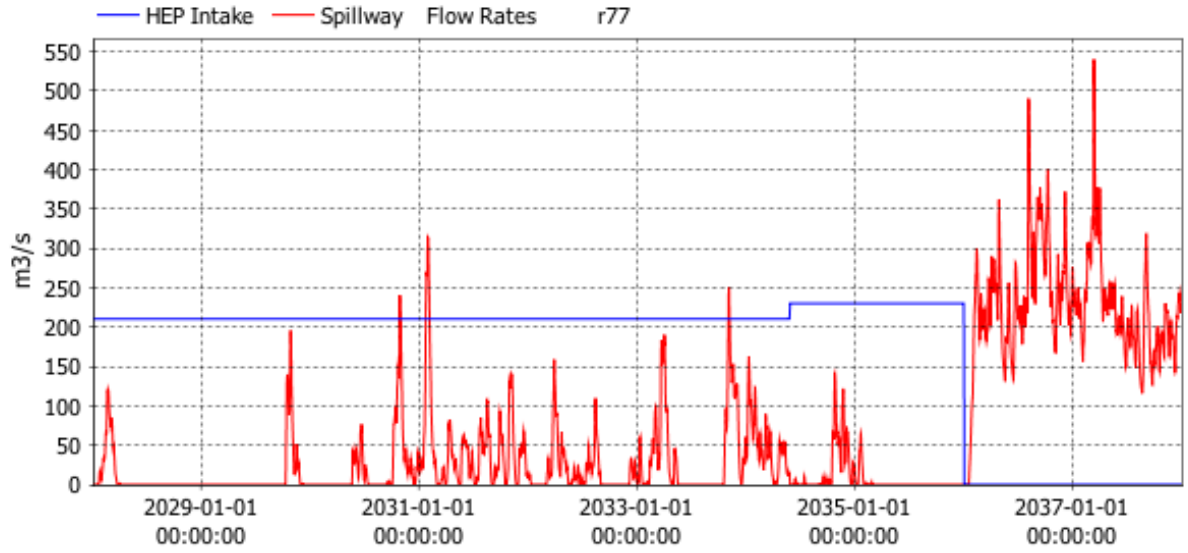

Figure 2.19. Release rate from HEP and spillway during operations simulation with derived mobility.

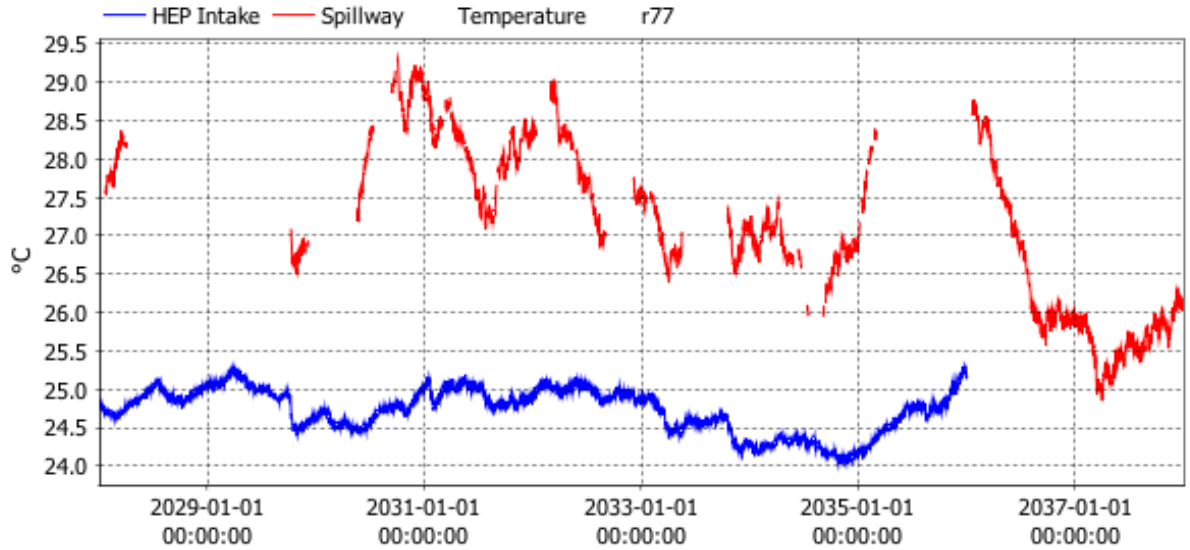

Figure 2.20. Simulated temperature of water extracted from HEP intake and spillway during operations simulation with derived mobility.

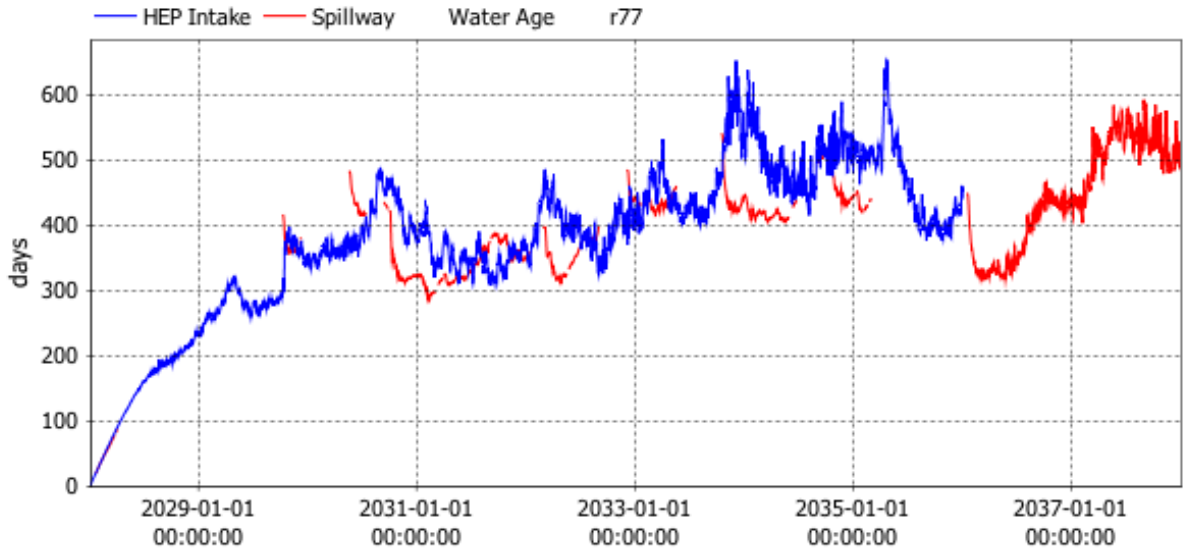

Figure 2.21. Simulated age of water extracted from HEP intake and spillway during operations simulation with derived mobility.

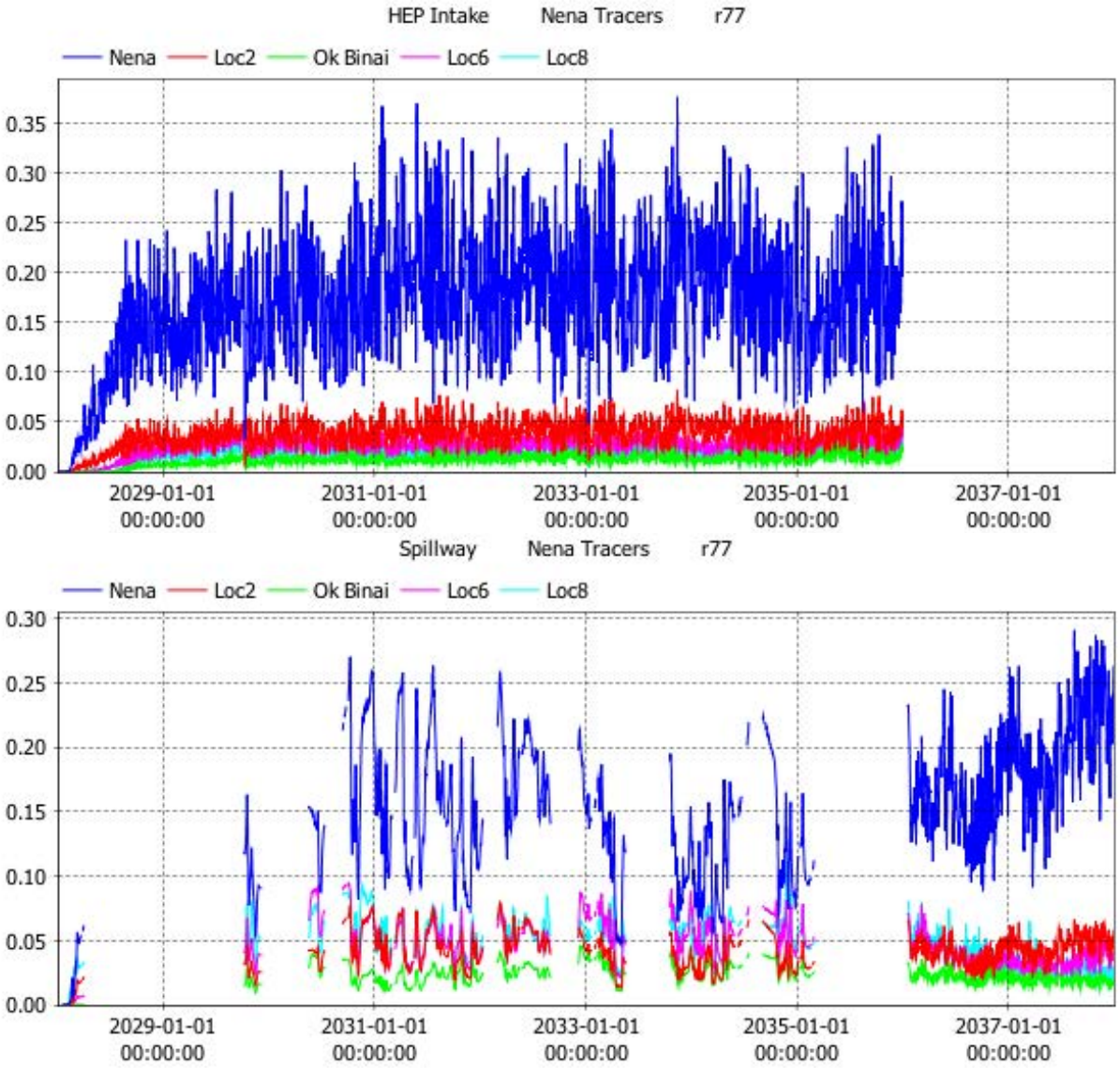

Figure 2.22. Simulated Nena arm tributary tracer concentrations in water extracted from HEP intake (top panel) and spillway (bottom panel) during operations simulation with derived mobility.

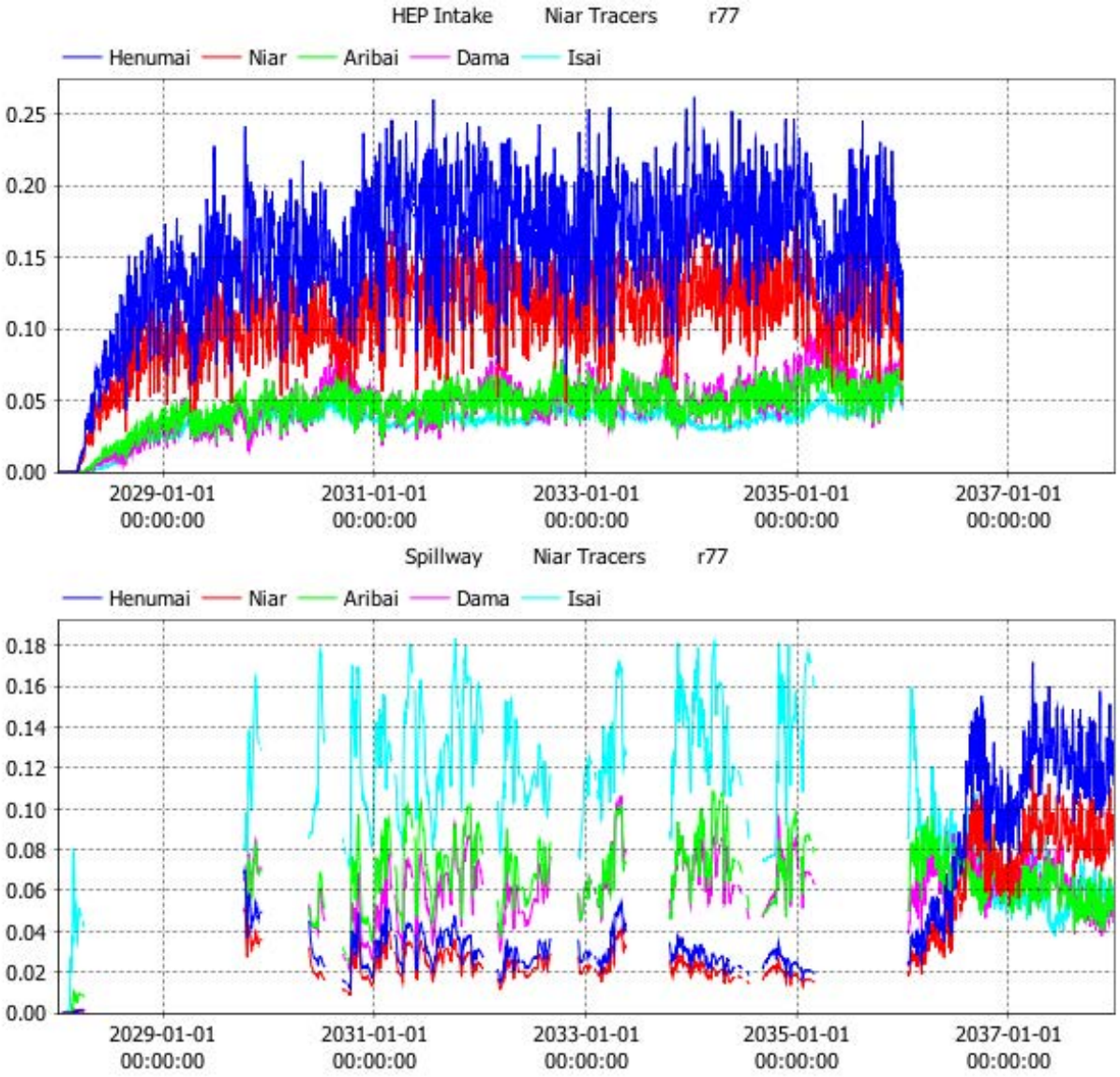

Figure 2.23. Simulated Niar arm tributary tracer concentrations in water extracted from HEP intake (top panel) and spillway (bottom panel) during operations simulation with derived mobility.

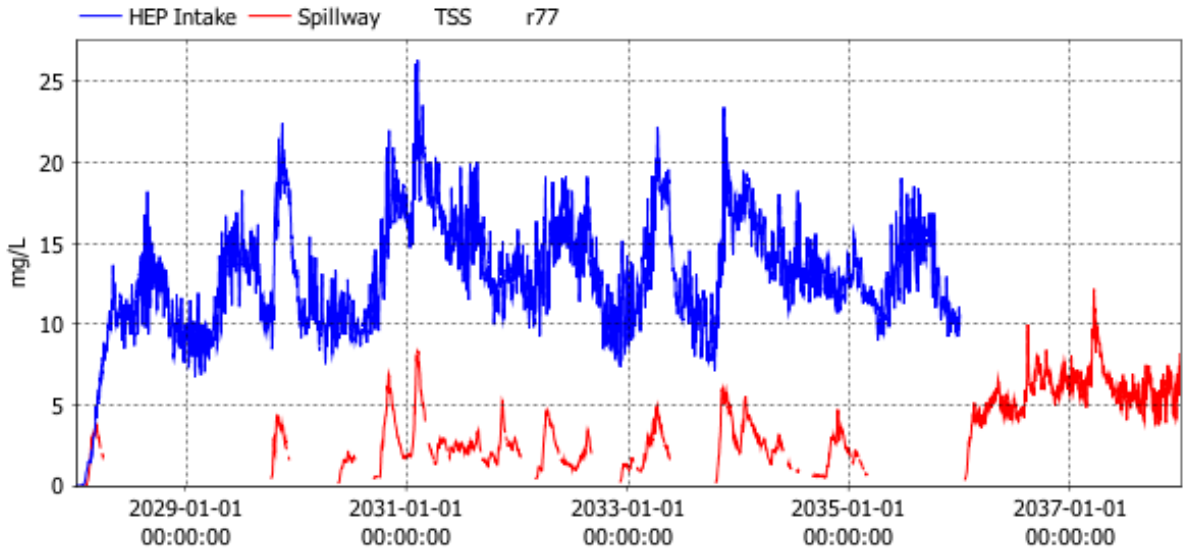

Figure 2.24. Simulated TSS of water extracted from HEP intake and spillway during operations simulation with derived mobility.

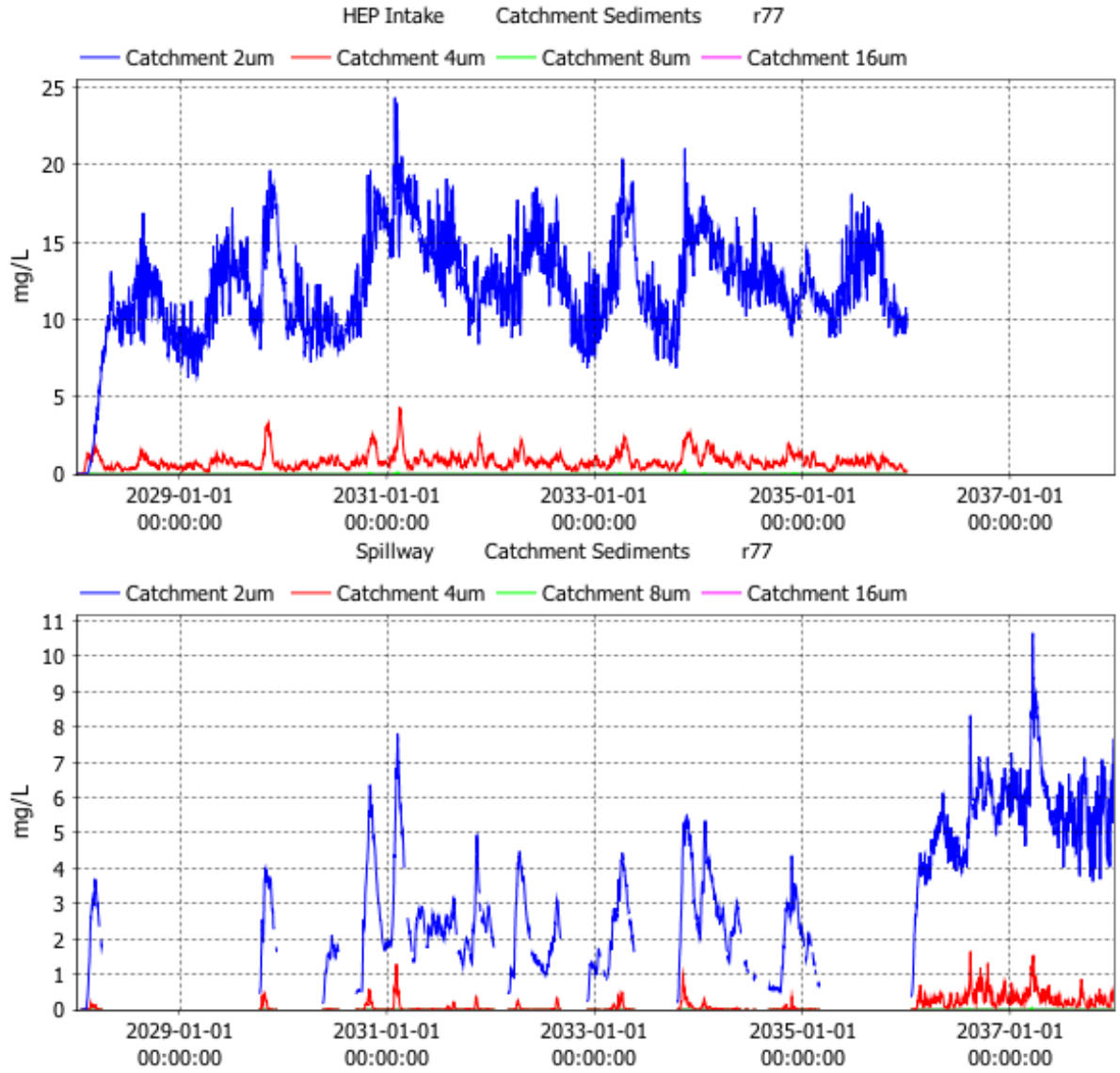

Figure 2.25. Simulated catchment sediment concentrations in water extracted from HEP intake (top panel) and spillway (bottom panel) during operations simulation with derived mobility.

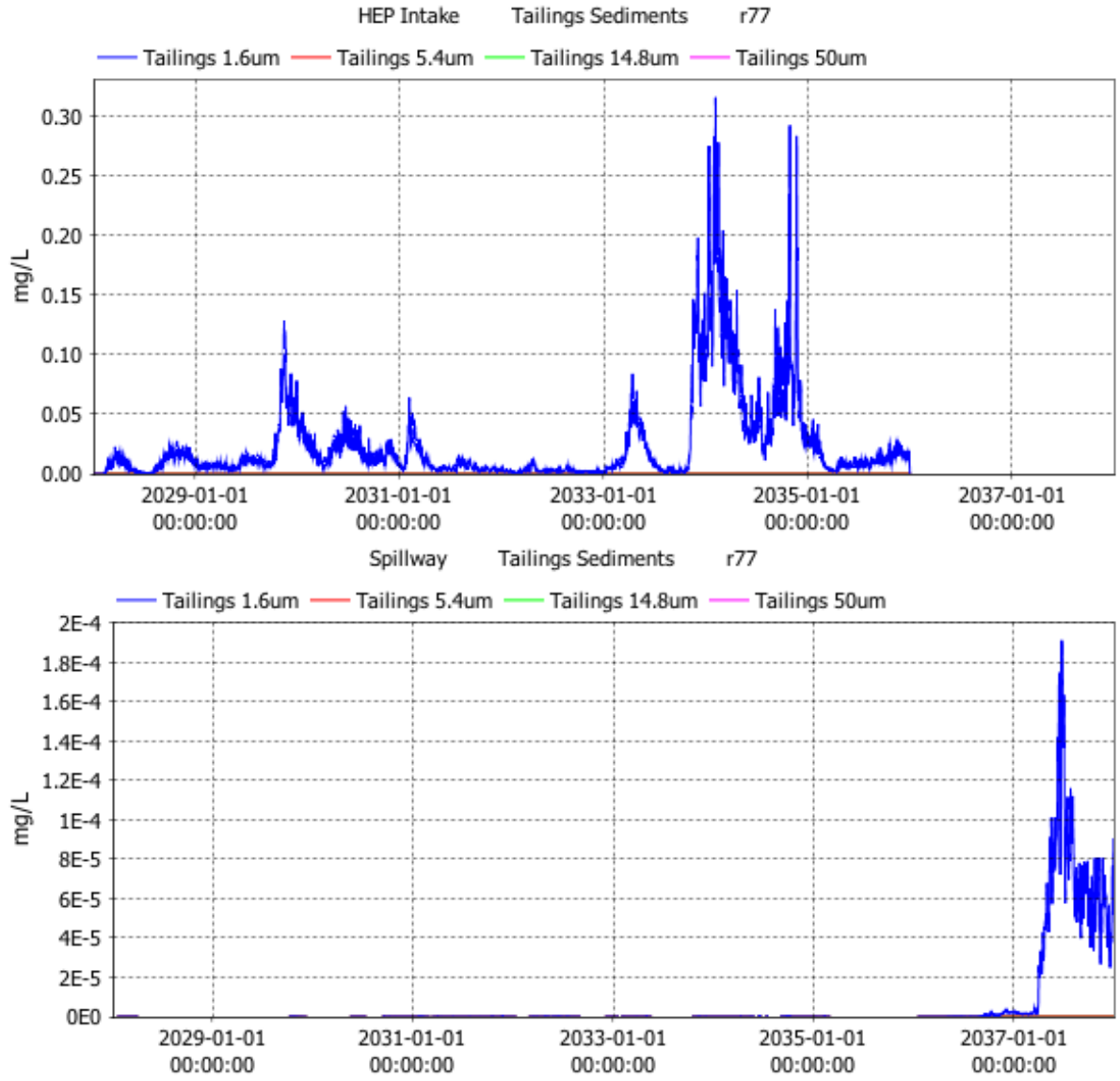

Figure 2.26. Simulated tailings concentrations in water extracted from HEP intake (top panel) and spillway (bottom panel) during operations simulation with derived mobility.

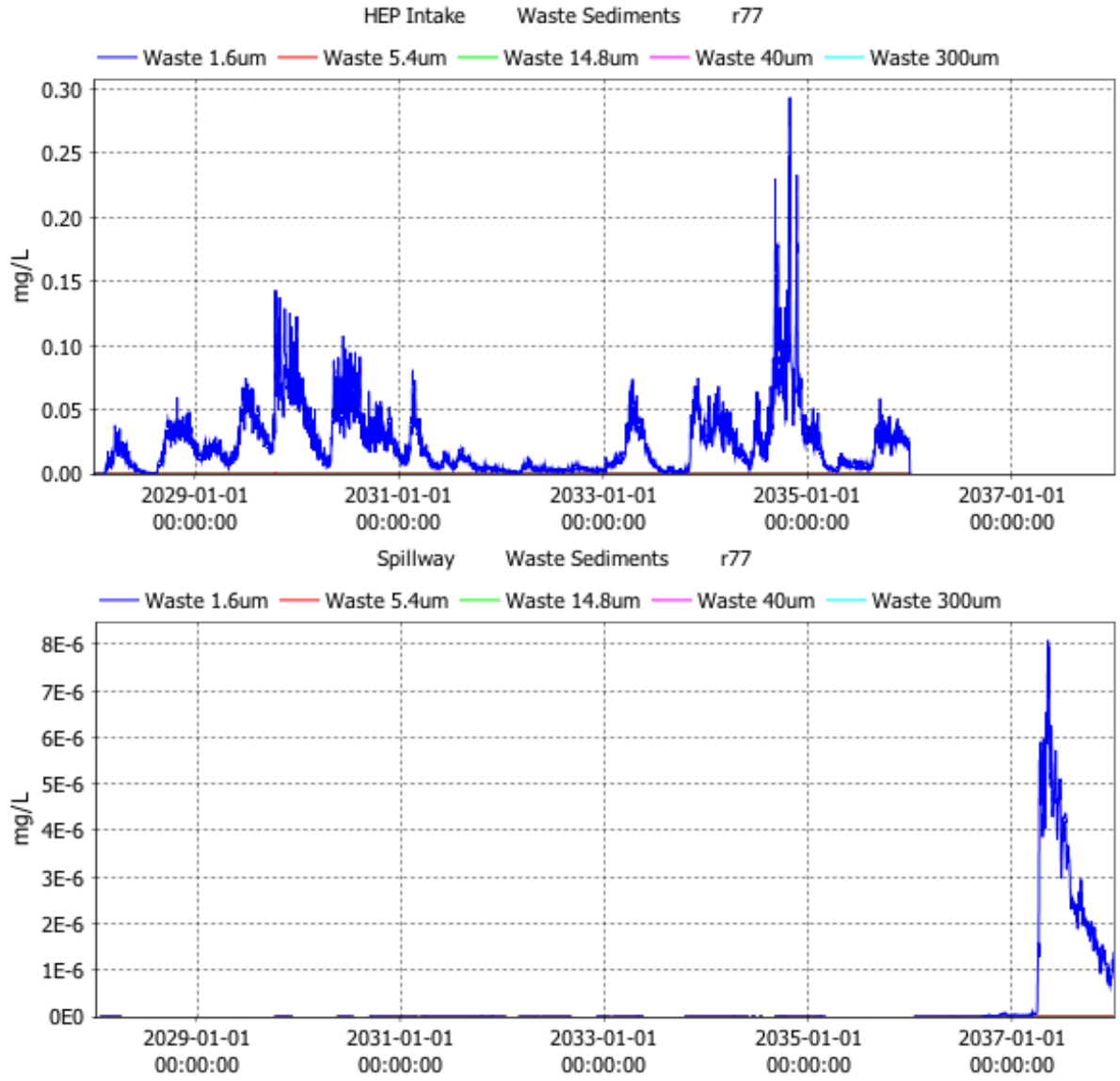

Figure 2.27. Simulated waste rock concentrations in water extracted from HEP intake (top panel) and spillway (bottom panel) during operations simulation with derived mobility.

2.1.4 HEP Closure Simulation – Equal Mobility

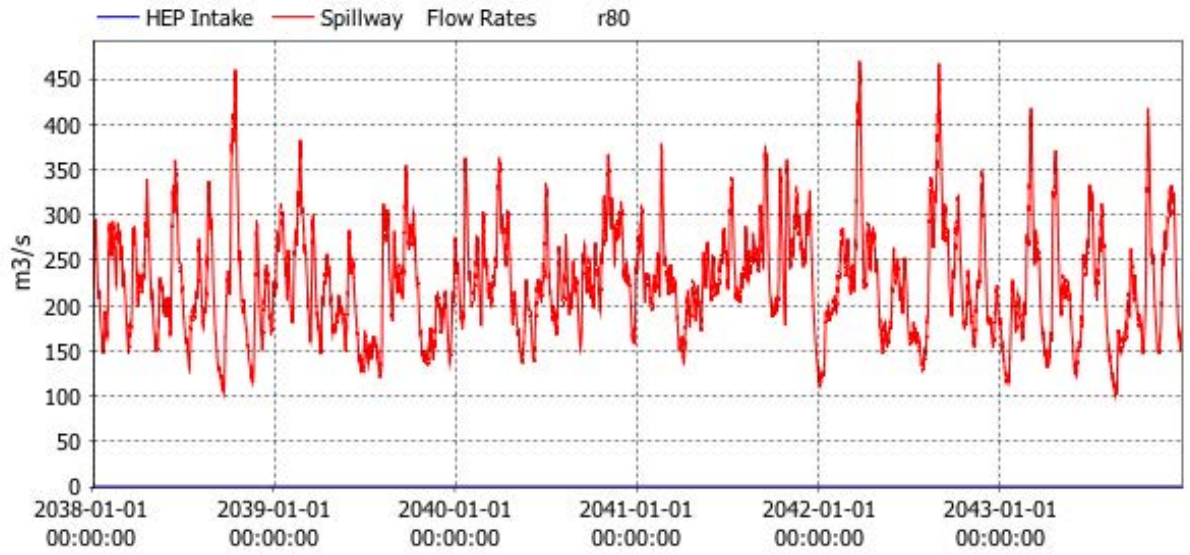

Figure 2.28. Release rate from HEP and spillway during HEP closure simulation with equal mobility.

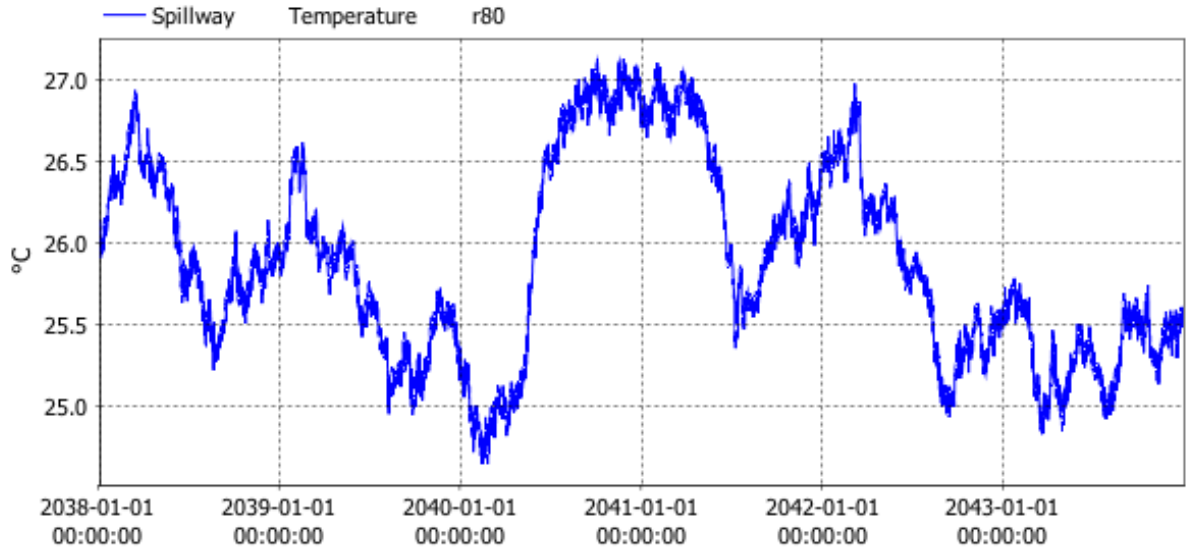

Figure 2.29. Simulated temperature of water extracted from spillway during HEP closure simulation with equal mobility.

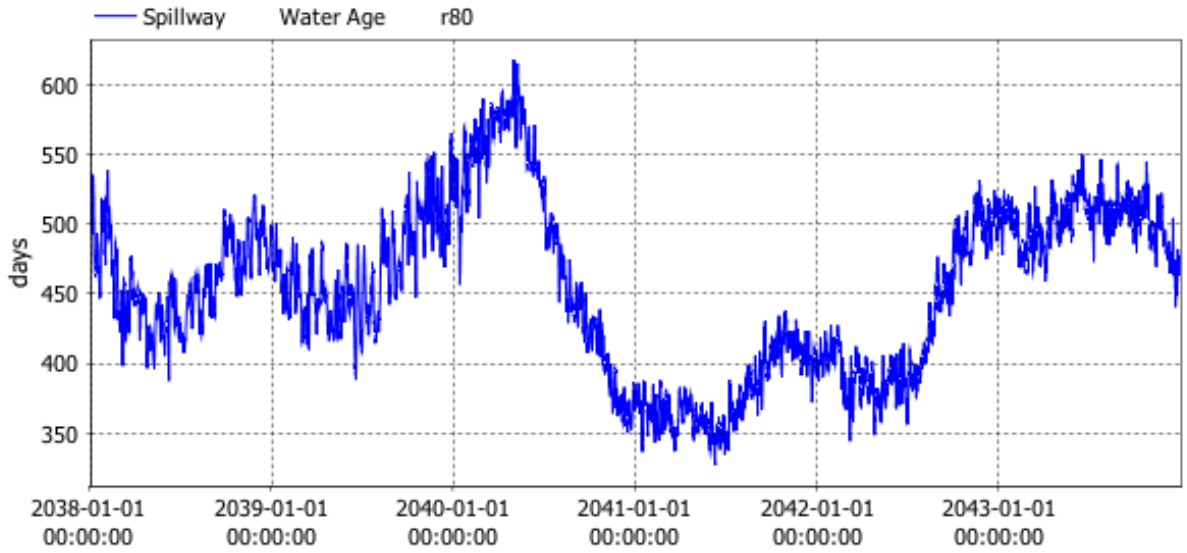

Figure 2.30. Simulated age of water extracted from spillway during HEP closure simulation with equal mobility.

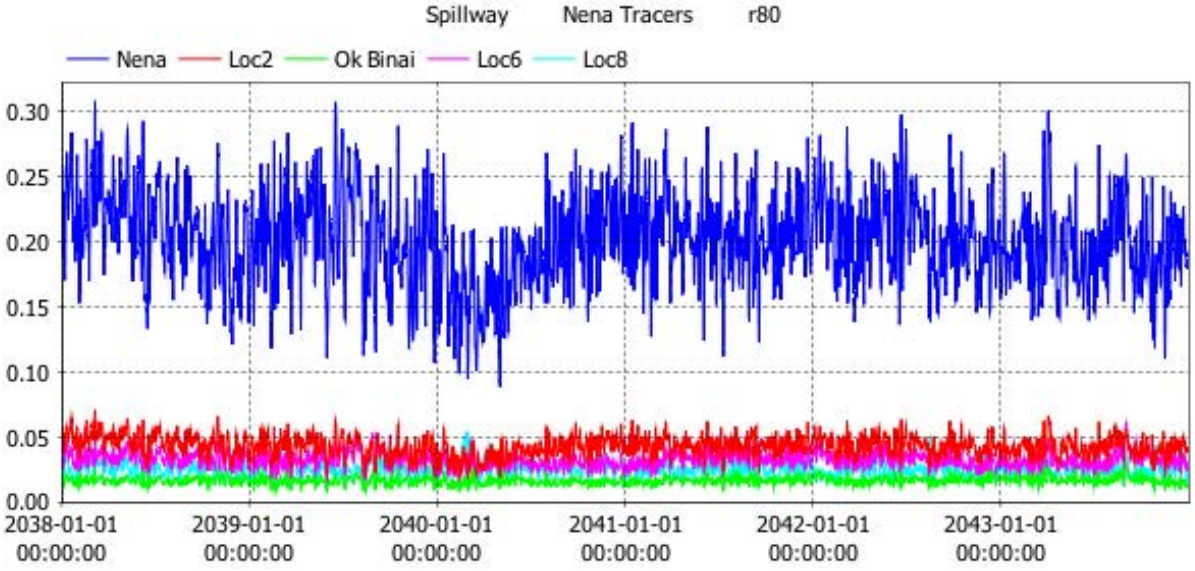

Figure 2.31. Simulated Nena arm tributary tracer concentrations in water extracted from spillway during HEP closure simulation with equal mobility.

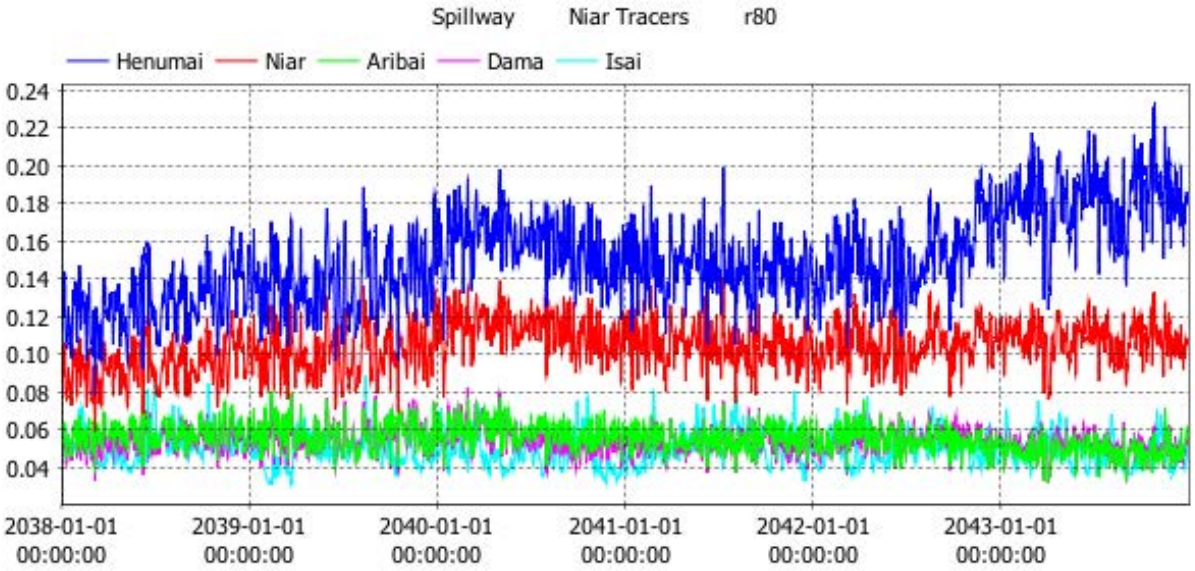

Figure 2.32. Simulated Niar arm tributary tracer concentrations in water extracted from spillway during HEP closure simulation with equal mobility.

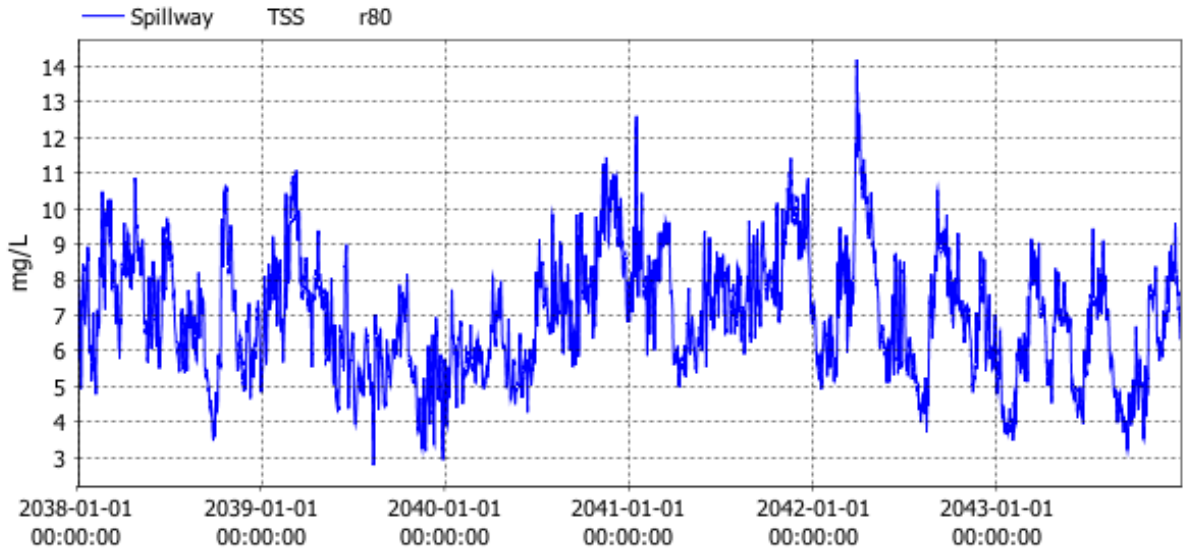

Figure 2.33. Simulated TSS of water extracted from spillway during HEP closure simulation with equal mobility.

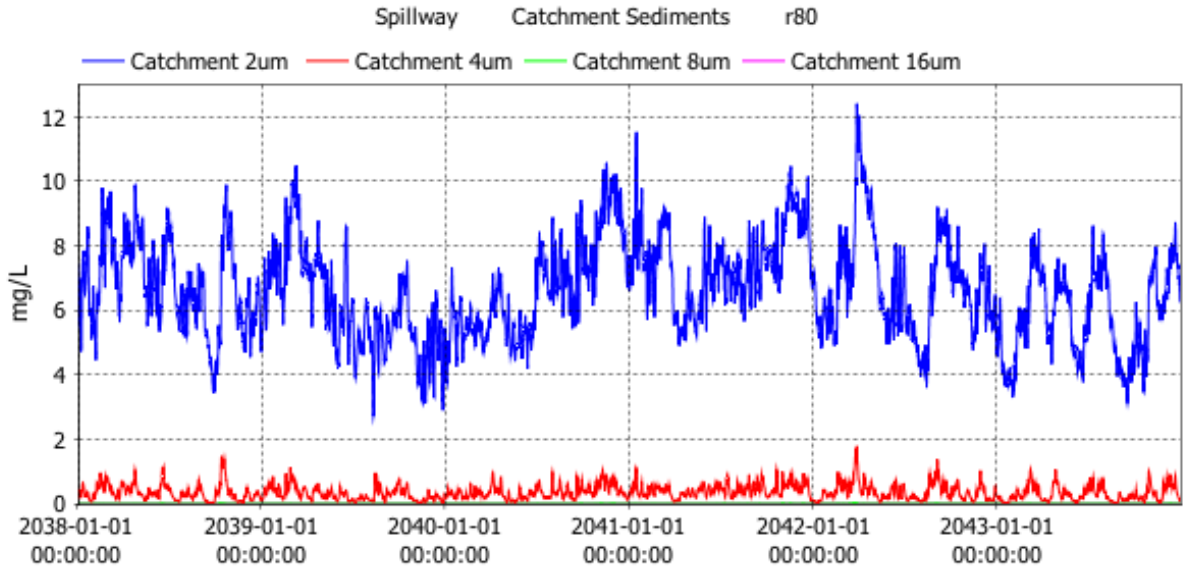

Figure 2.34. Simulated catchment sediment concentrations in water extracted from spillway during HEP closure simulation with equal mobility.

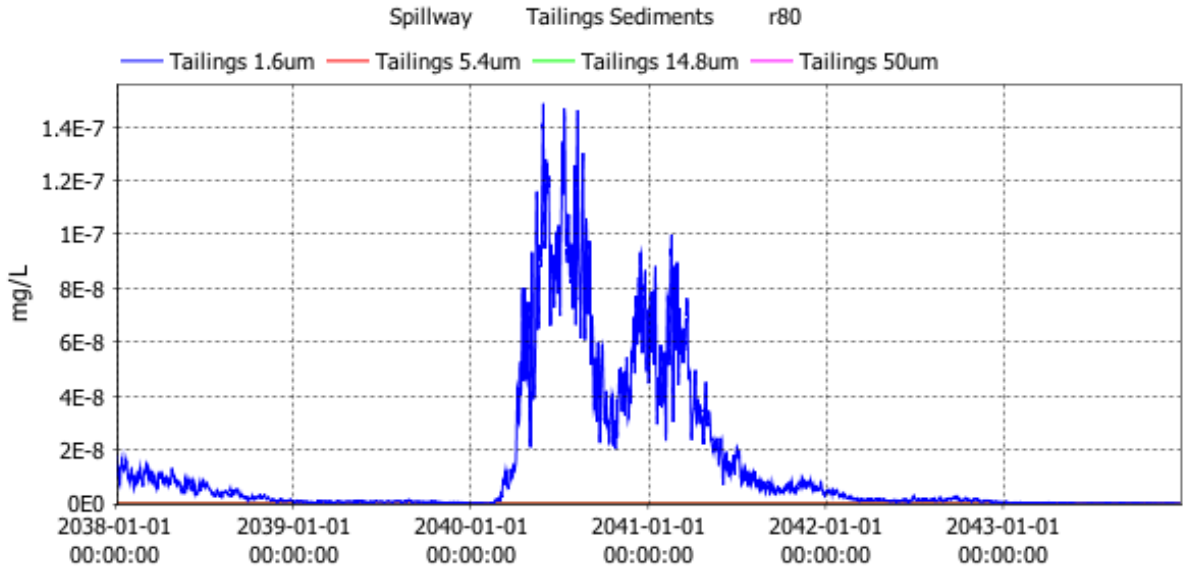

Figure 2.35. Simulated tailings concentrations in water extracted from spillway during HEP closure simulation with equal mobility.

2.1.5 HEP Closure Simulation – Derived Mobility

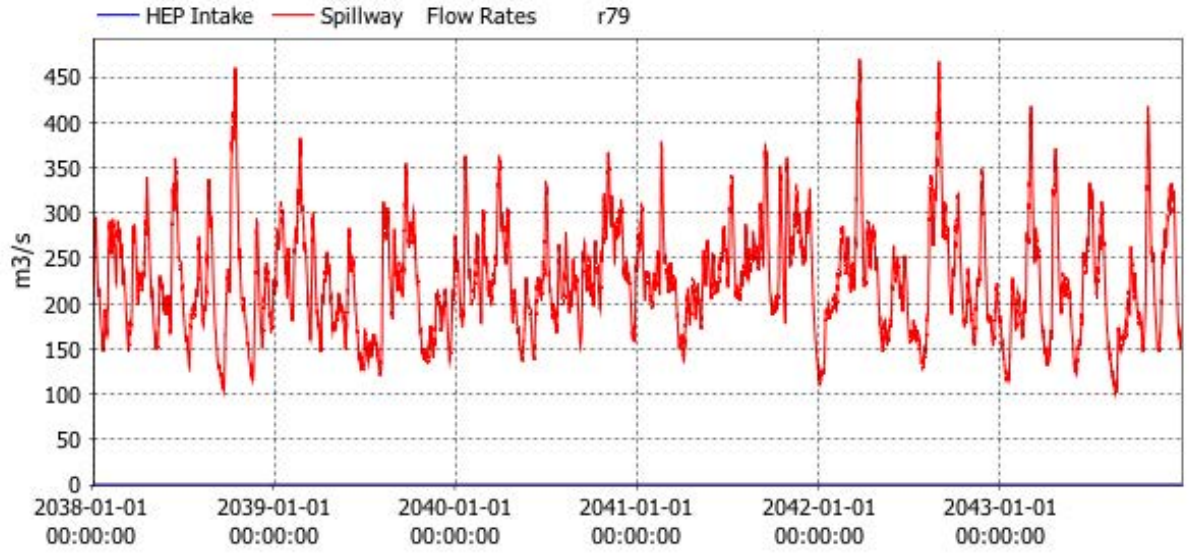

Figure 2.36. Release rate from HEP and spillway during HEP closure simulation with derived mobility.

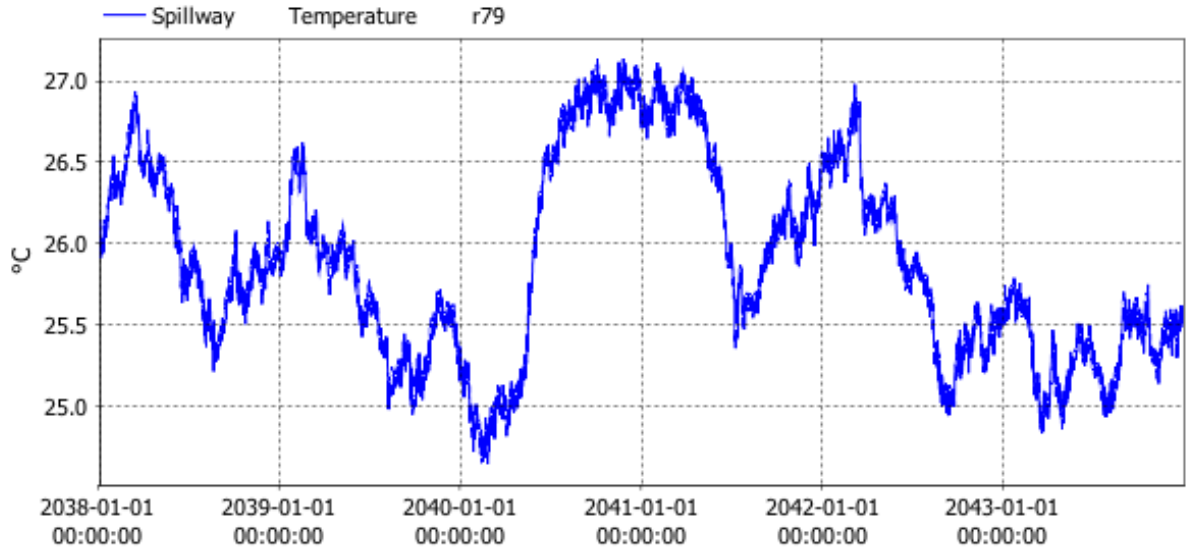

Figure 2.37. Simulated temperature of water extracted from spillway during HEP closure simulation with derived mobility.

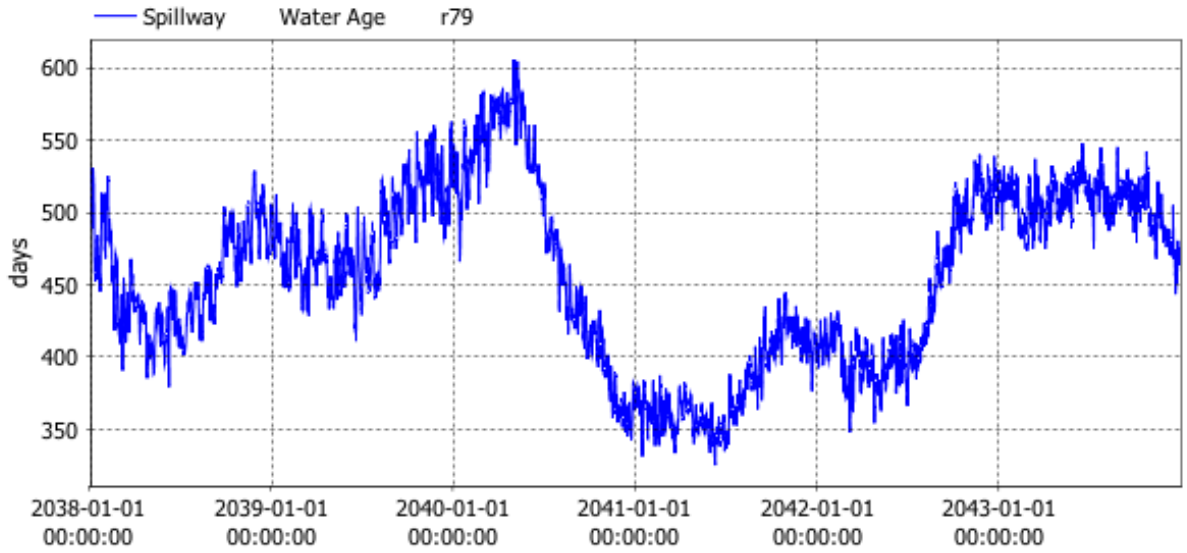

Figure 2.38. Simulated age of water extracted from spillway during HEP closure simulation with derived mobility.

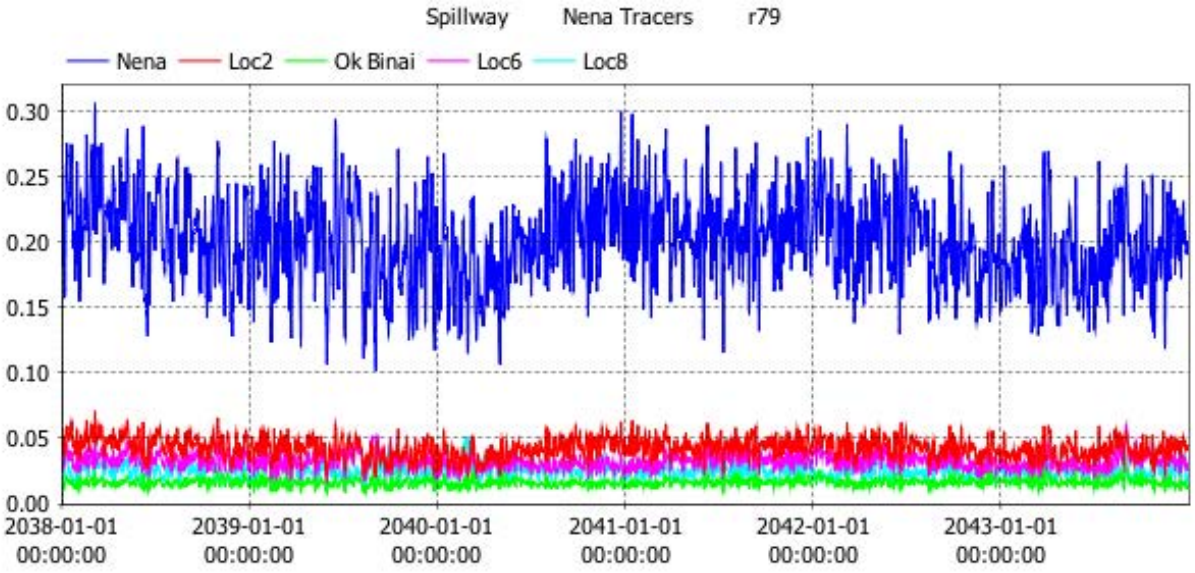

Figure 2.39. Simulated Nena arm tributary tracer concentrations in water extracted from spillway during HEP closure simulation with derived mobility.

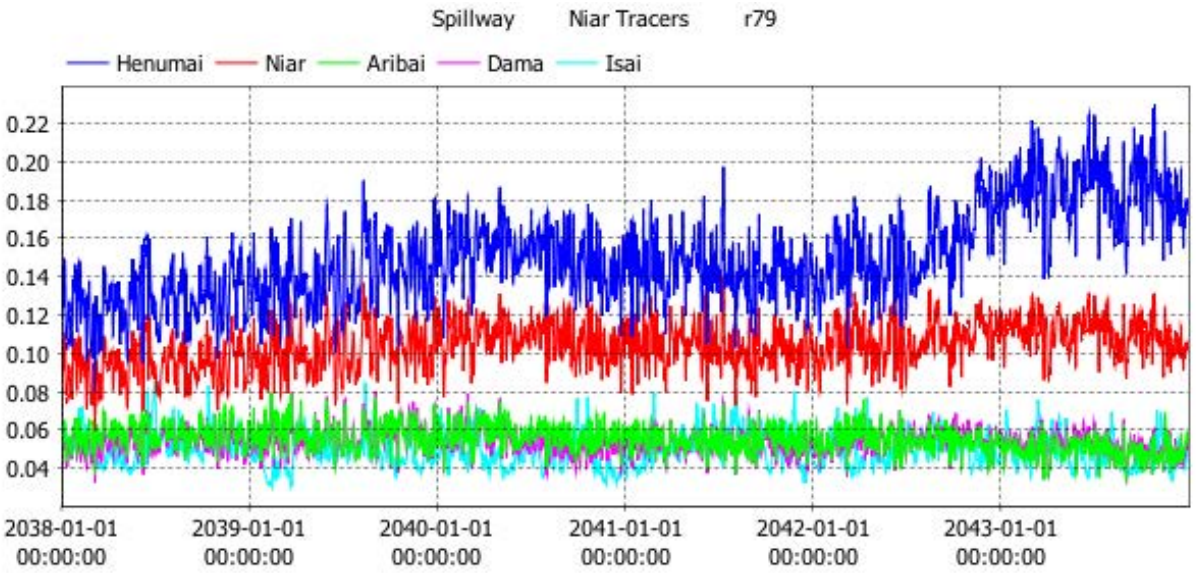

Figure 2.40. Simulated Niar arm tributary tracer concentrations in water extracted from spillway during HEP closure simulation with derived mobility.

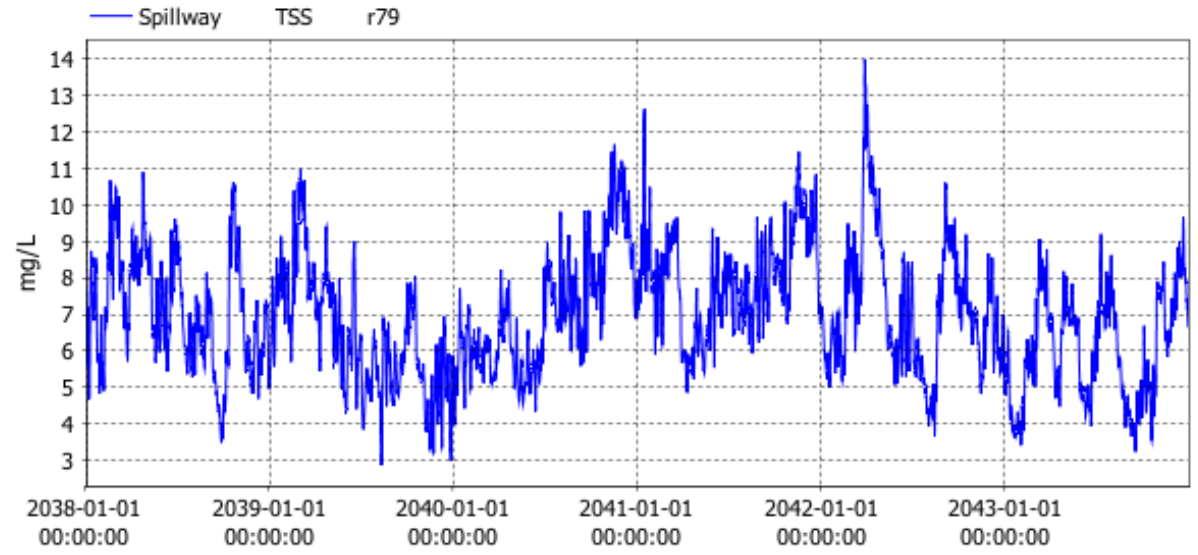

Figure 2.41. Simulated TSS of water extracted from spillway during HEP closure simulation with derived mobility.

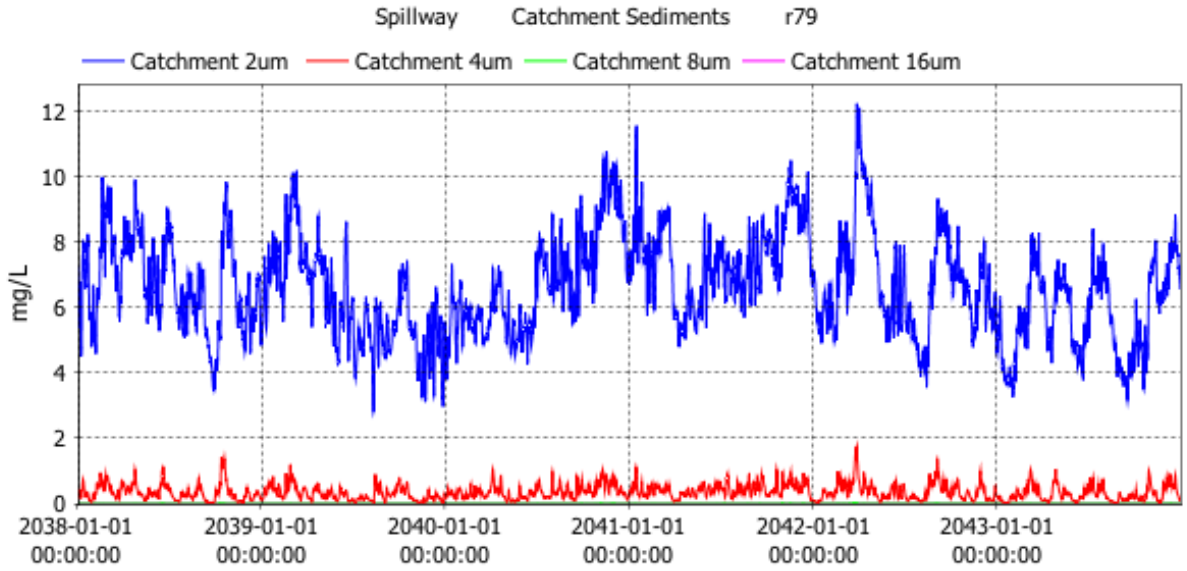

Figure 2.42. Simulated catchment sediment concentrations in water extracted from spillway during HEP closure simulation with derived mobility.

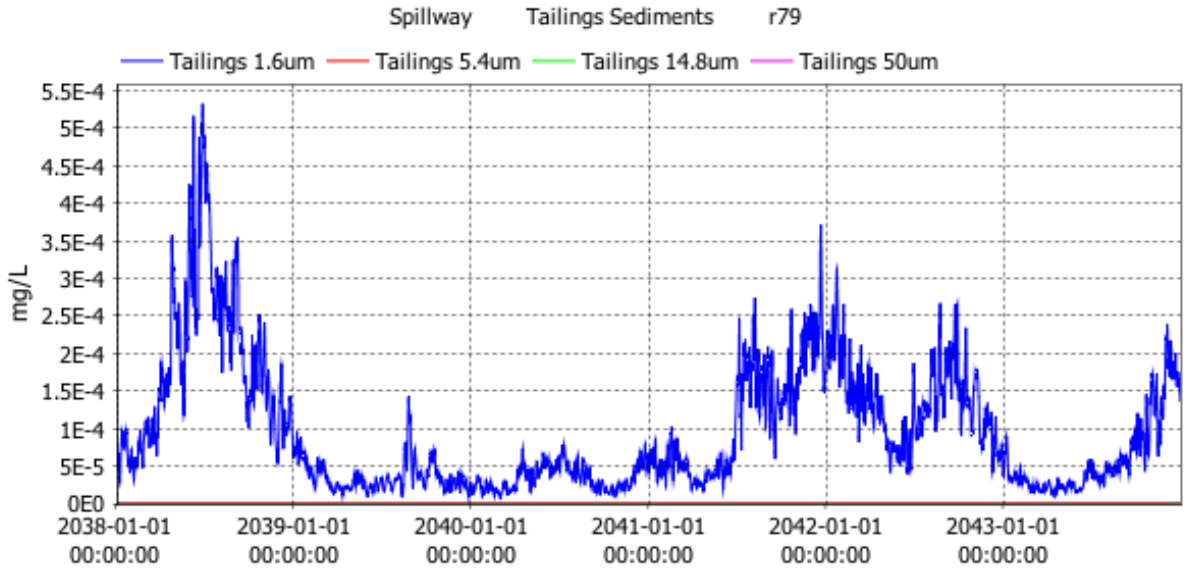

Figure 2.43. Simulated tailings concentrations in water extracted from spillway during HEP closure simulation with derived mobility.

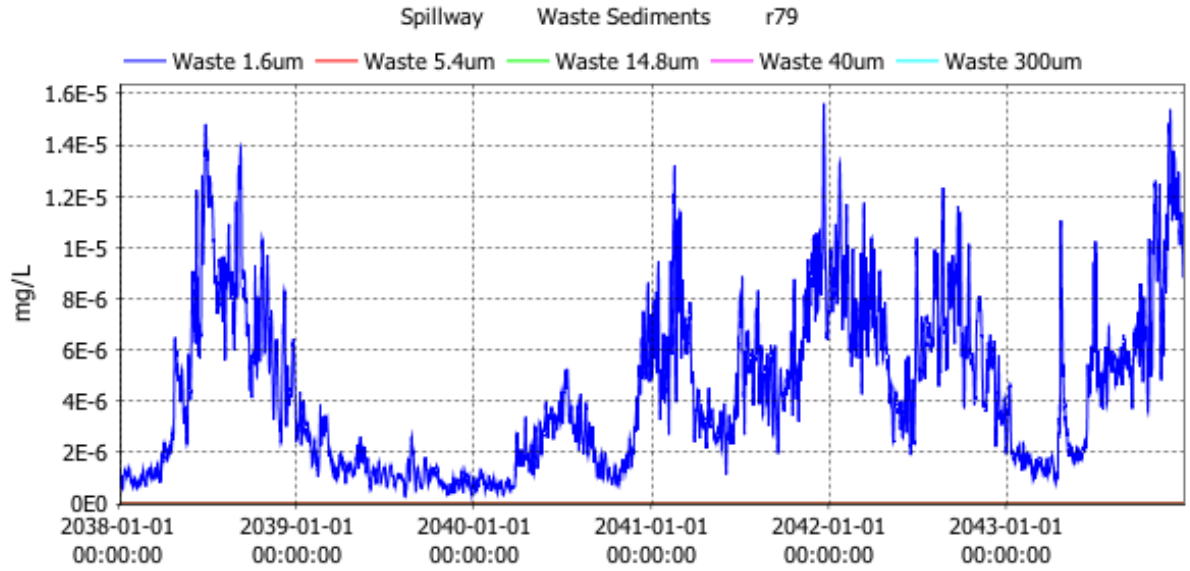

Figure 2.44. Simulated waste rock concentrations in water extracted from spillway during HEP closure simulation with derived mobility.

3 Sensitivity Tests

3.1.1 Overview

A series of sensitivity simulations were undertaken using a preliminary model that was applied on an earlier description of the project and prior to selection of the preferred project description. The difference between the model results using the earlier and updated project description and the results of the sensitivity tests are described below.

The sensitivity tests include changes to the hydrograph period, inflow temperature, meteorological data and HEP operations. Each test was performed over a sub-period of the operational simulation with the HEP operating. Whilst the sensitivity simulations were not repeated for the updated project description (due to project timeframes), the findings from the analyses that were performed with the preliminary model still provide an important indication of the model inputs and parameters that are likely to have the largest impact on the model results

Although the tests demonstrate changes to the results they also suggest that, with the exception of modifications to the HEP operation, the changes to the results are small. This indicates that the simulated persistent thermal stratification is resilient when challenged with systematic changes in model forcing and only subject to significant change in the event of large environmental and operational changes.

A series of scenario simulations were also undertaken using the preliminary model and are reported below. The scenarios were designed to assess the changes to the limnology that may occur under different environmental and operational conditions. These include flow events, storm conditions, low water level and leachate release from the stored waste rock and tailings.

3.1.2 Preliminary Model

At the time of undertaking the sensitivity simulations the model set-up was based on an earlier FRHEP project description (hereafter referred to as the preliminary project description and preliminary model) that included an earlier embankment design and waste rock and tailings storage plan (see Figure 3.1). The embankment design was different to the final design in the following ways:

- No deep tunnel or low-level intake. Environmental flow 50 m^3s^{-1} was extracted over the height of the embankment until reservoir filled to minimum operational level of 202.5 m RL;
- HEP intake level was 5.4 m higher at 191 m RL; and
- Spillway height was 8.1 m lower at 218 m RL.

Waste rock was to be deposited up to 162.5 m RL in the inundated Nena and Ok Binai valleys. Tailings will be deposited to 162.5 m RL from the junction of Nena and Niar Rivers up to the mid-Niar. The preliminary project description included waste rock to be deposited by barge and tailings deposited at the bottom of the FRHEP through a tremie pipe system.

The most significant changes between the preliminary and final simulations were: firstly, introducing a low-level HEP intake during filling in the updated model, which draws down the temperature stratification and modifies the way in which the major inflows form intrusions in the reservoir; and, secondly, the updated project description included the storage of tailings in the upper Nena arm of the reservoir, which has implications for increased mobility due to exposure to higher bed shear near the headwaters of the Nena River.

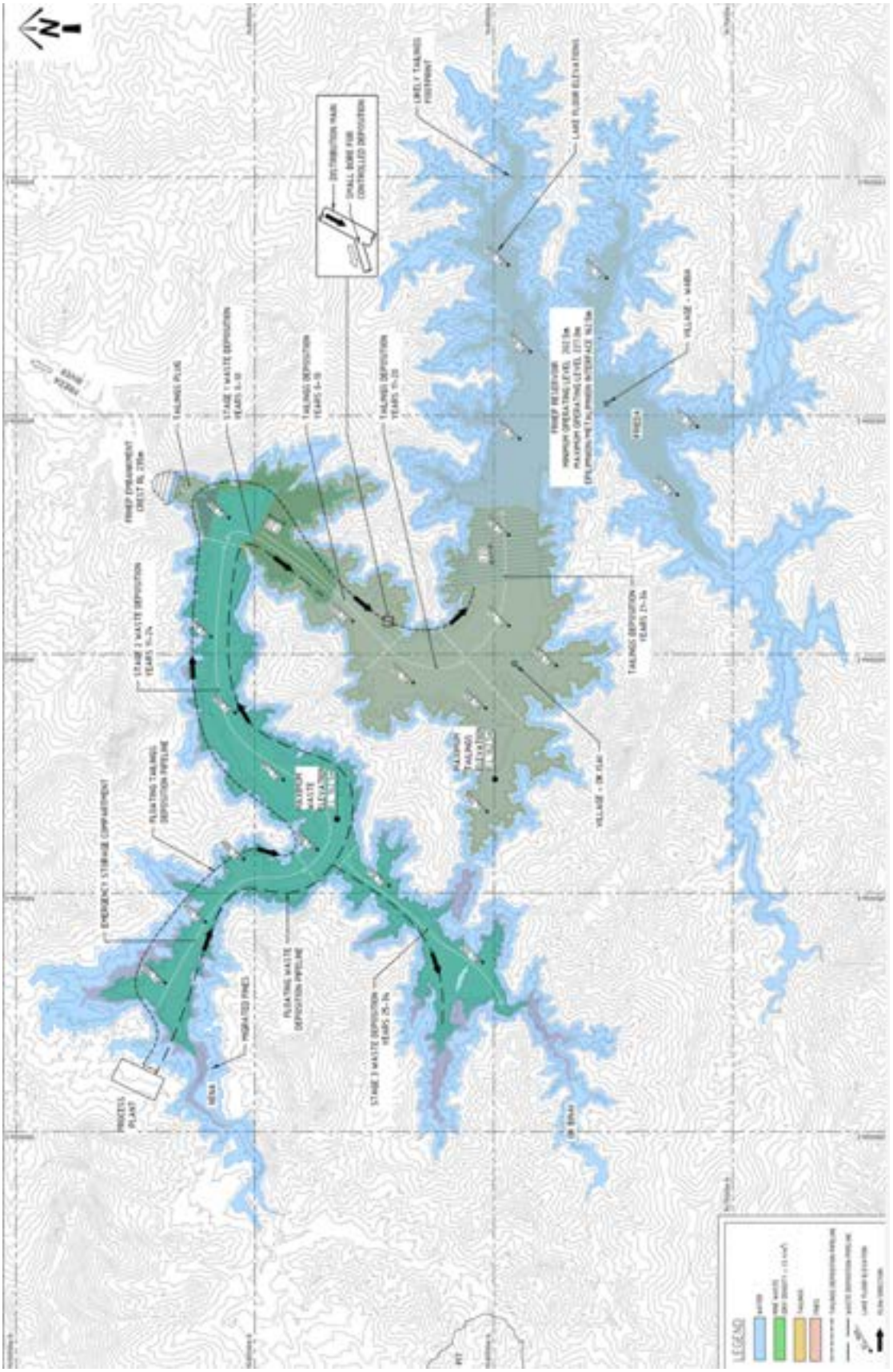

Figure 3.1 Footprint of FRHEP reservoir waste rock and tailings storage areas (SRK, 2017b)

3.1.3 Grid Test

A short simulation using a finer 100 m x 100 m grid was undertaken to assess the effects of the grid size on the model outputs. Because of the complex set-up and long simulation times required for the finer grid simulation only the four largest rivers were included in the sensitivity test; the same simple set-up was repeated for the 200 m x 200 m grid and the outputs from the two models were compared. The simulations started on 1 January 2028 and ran for one year with a starting water level at 225 m RL. The model time-step was 60 seconds for finer grid model and 120 seconds for coarser grid model.

Comparisons between the outputs of the two models with different grid sizes are illustrated in Figure 3.2 to Figure 3.4. The results suggest that the models are generally consistent for key limnological measures of temperature stratification, water age and the dilution of inflows prior to intake through the HEP. The finer grid model is likely to provide more accurate results because it is able to better resolve the hydrodynamics and reduce numerical diffusion; these effects are evident in Figure 3.4, which shows that peaks in the Nena river inflow concentration in the HEP intake are larger and show greater variation for the finer grid model. However, in this scoping phase study use of the finer grid was not feasible given the long run-times and the number of simulations that have been undertaken.

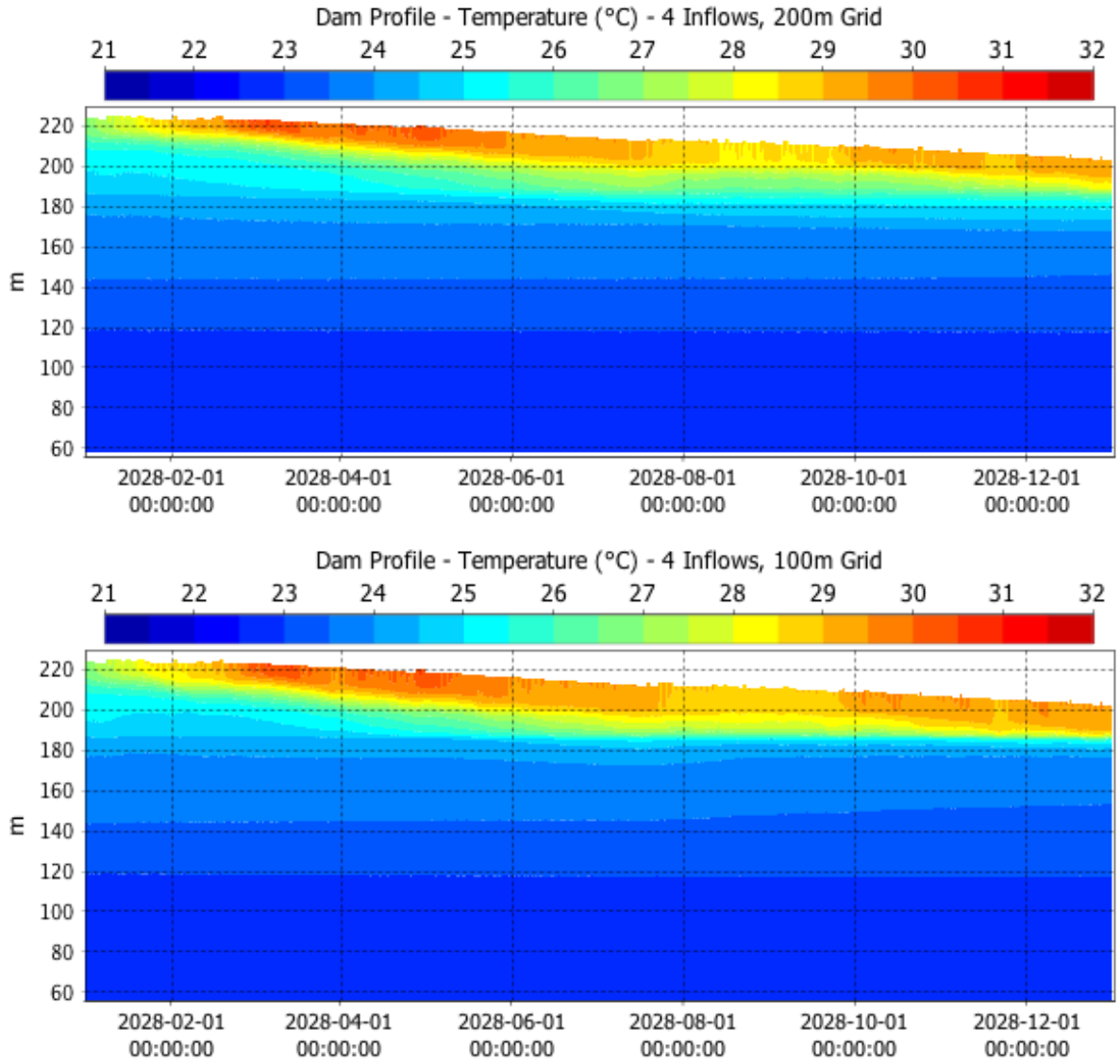

Figure 3.2 Simulated temperature profiles from the 200 m x 200 m grid model (top panel) compared to the 100 x 100 m grid model (bottom panel).

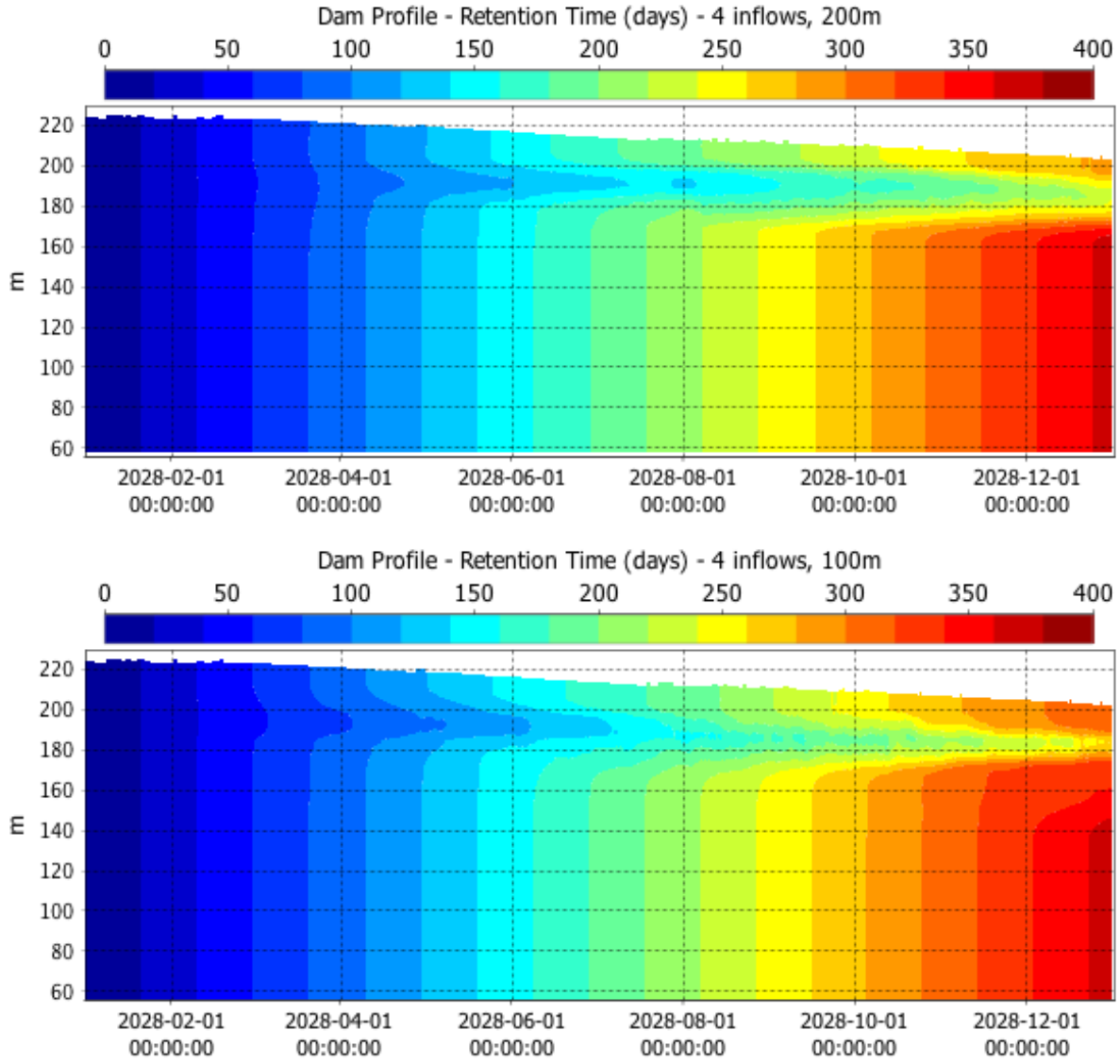

Figure 3.3 Simulated water age from the 200 m x 200 m grid model (top panel) compared to the 100 x 100 m grid model (bottom panel).

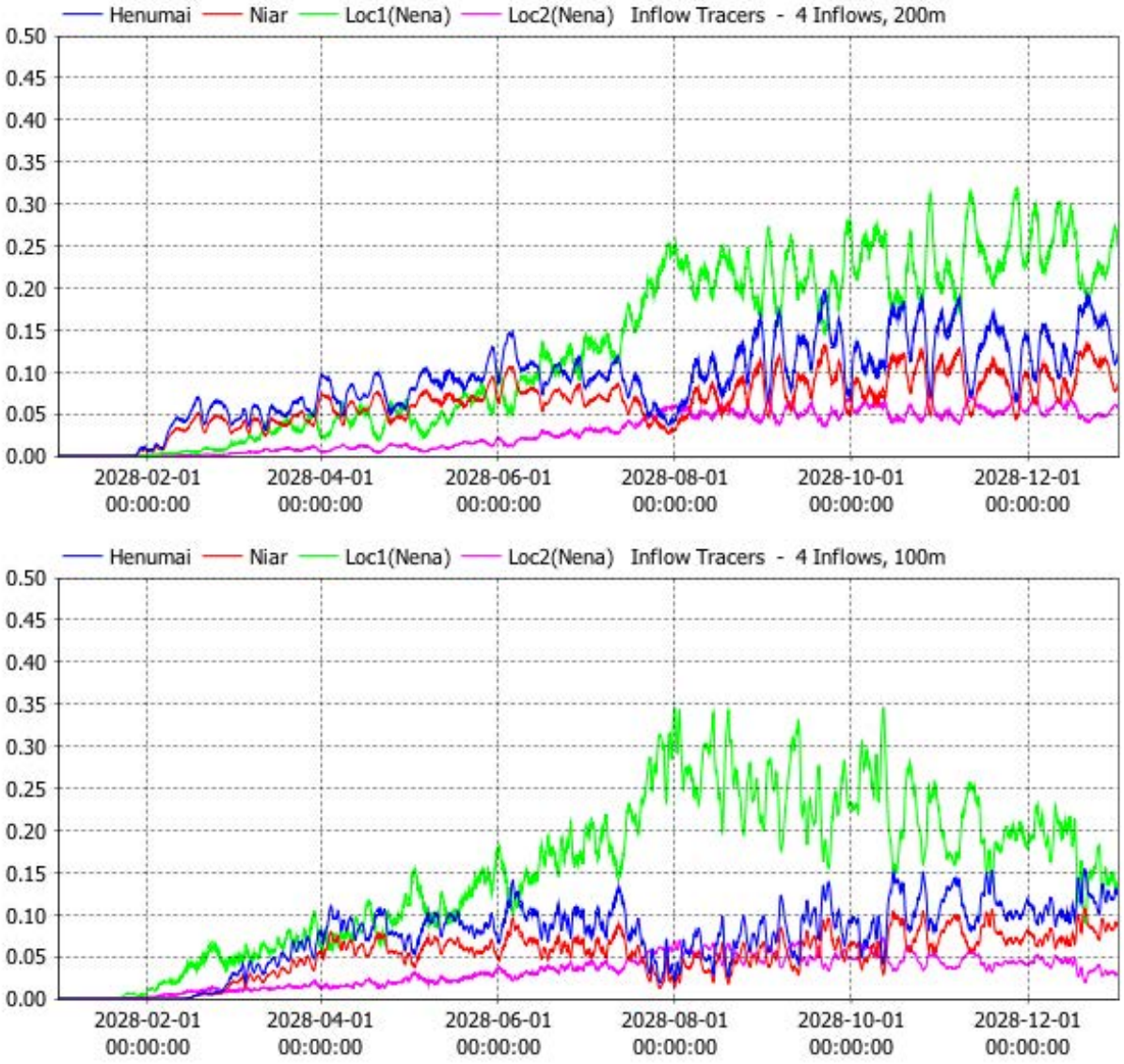

Figure 3.4 Simulated inflow tracer in the HEP intake water from the 200 m x 200 m grid model (top panel) compared to the 100 x 100 m grid model (bottom panel).

3.1.4 Hydrograph Period

Daily inflow rates provided by Golders Associates (2018) were compressed into 6-hour duration hydrographs to assess changes to the simulated limnology that arise from shorter period, higher rate inflows. The shape of each daily hydrographs was extracted from the peak flow assessments (SRK, 2017c).

The results illustrate that the short period hydrographs lead to negligible change in the simulated temperature (Figure 3.5); however, there are considerable changes to the vertical distribution of inflow tracers at the embankment (Figure 3.6). The results illustrate greater variation in the intrusion depths and concentrations, which indicate that the faster flow rates, matched with more varied ambient water conditions, change the entrainment and intrusion mechanisms that alter the inflows at the confluence of the reservoir arms.

Simulated HEP intake concentrations for the Nena River tracer and the Henumai River tracer (Figure 3.7) illustrate that while the range and mean concentrations are comparable, the phase of the contributions changes significantly between the cases of daily average flow and 6- hour hydrograph duration.

The test illustrates that the simulated fine clay extracted by the HEP intake is lowered in the case of the short-period hydrograph (Figure 3.8). The reasons for this may be varied and depend on a number of factors that are modified by the shorter period hydrograph and operate concurrently or in isolation. These include: i) deeper plunging of the faster inflows (because of higher momentum) that delivers more sediment load below the HEP intake level; ii) increased entrainment with surface waters due to faster flow; iii) more complex vertical layering of different inflows at the junction of the major arms (some have higher concentrations than others); and, iv) discontinuous flow that changes sediment deposition patterns.

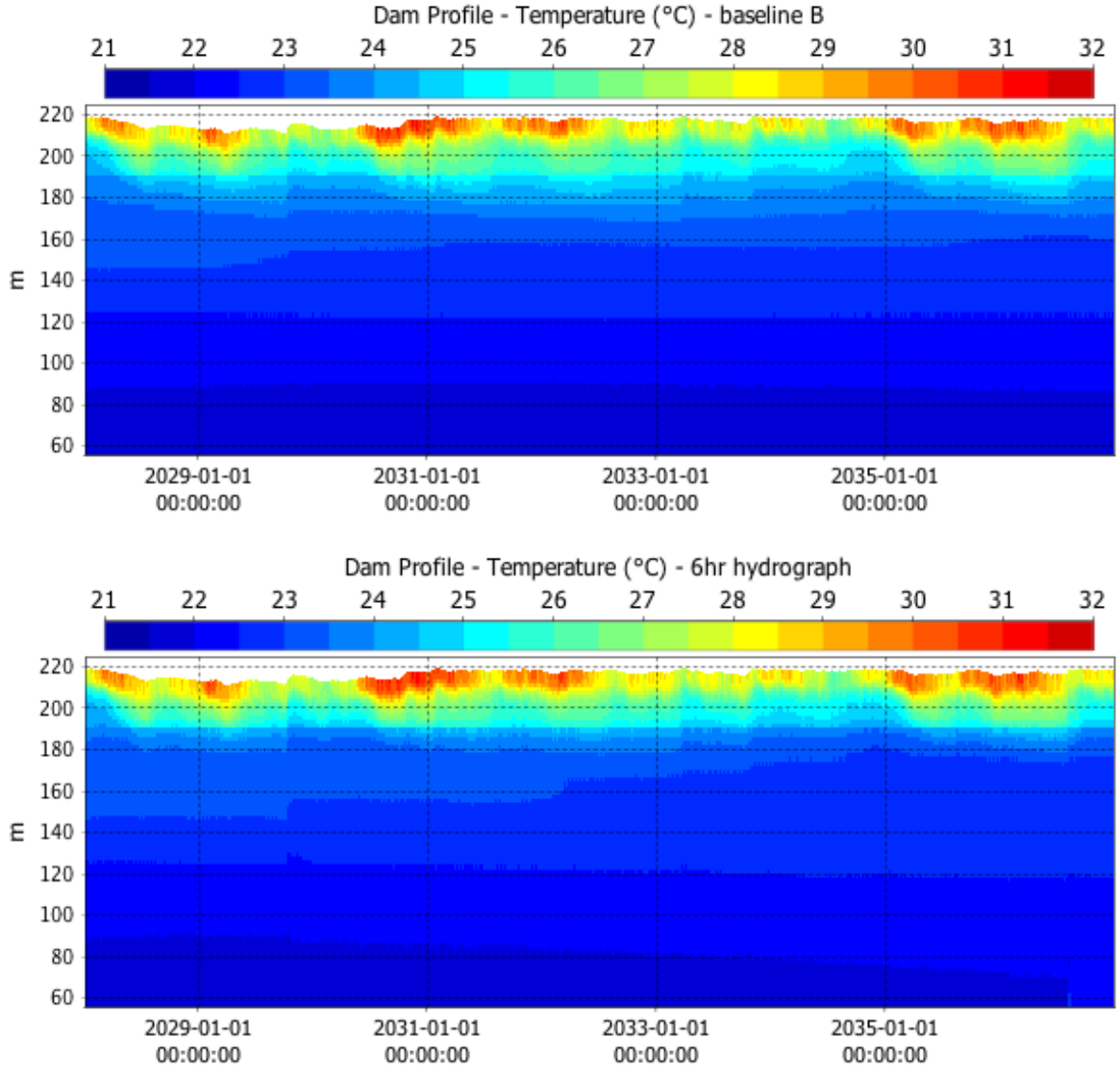

Figure 3.5 Simulated temperature at the embankment for daily average inflow (top panel) and 6- hour duration hydrographs (bottom panel).

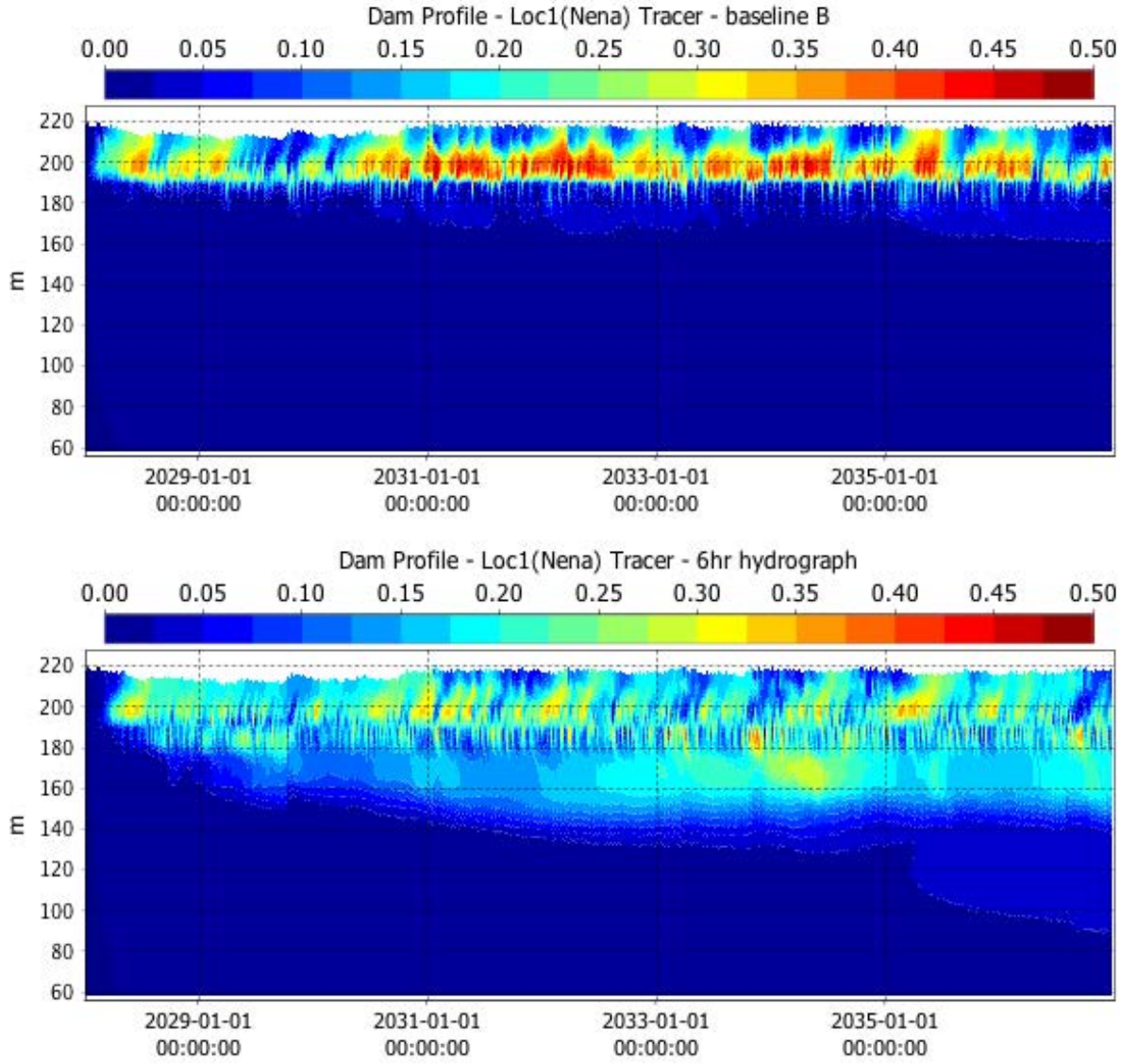

Figure 3.6 Simulated Nena tracer concentration at the embankment for daily average inflow (top panel) and 6-hour duration hydrographs (bottom panel).

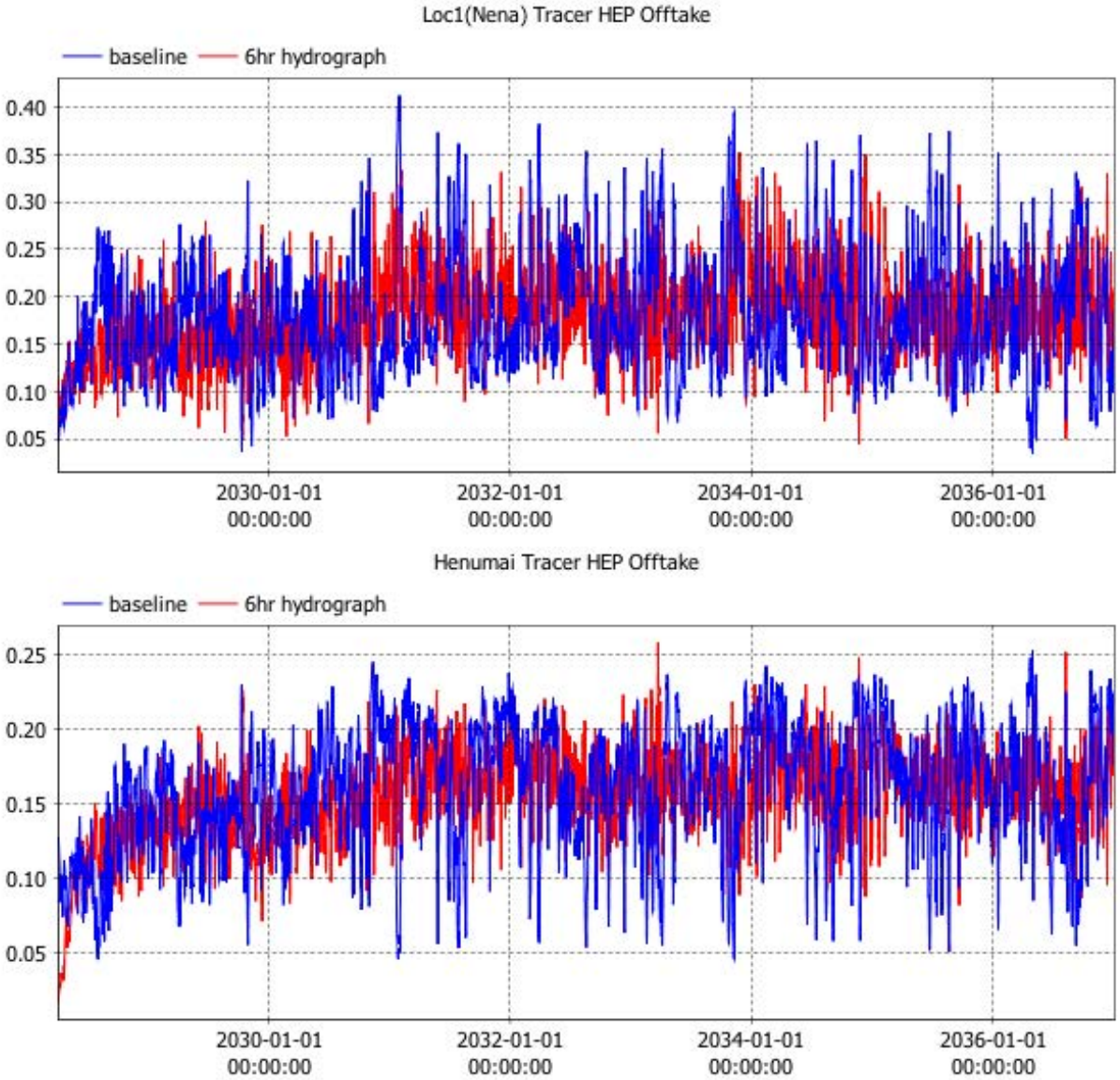

Figure 3.7 Simulated HEP intake concentrations of the Nena River tracer (top panel) and Henumai River tracer (bottom panel) for daily flow rates (blue) and 6-hour hydrographs (red).

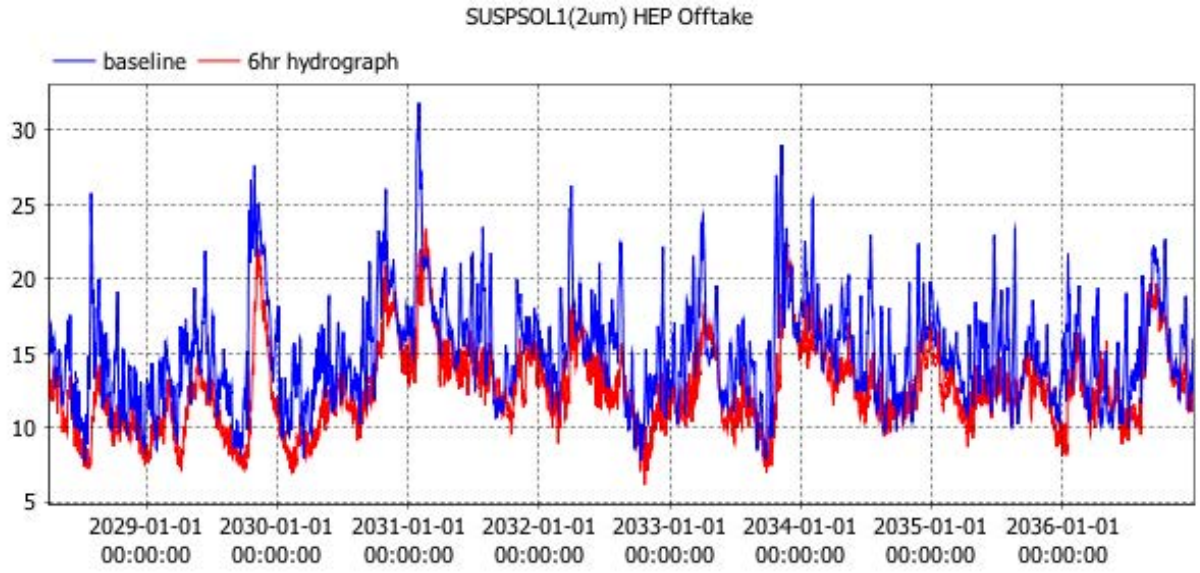

Figure 3.8 Simulated HEP intake concentrations of the 2-micron particles for daily flow rates (blue) and 6-hour hydrographs (red).

3.1.5 Inflow Temperature

Meteorological observations demonstrate a significant spatial gradient in air temperature in the region; air temperatures at Moraupi AWS are on average 4 ^{o}C warmer than at the Nena AWS. In addition, water quality data received from SRK (2017d) include some surface water temperature observations in the rivers made at different times of day, which suggest diurnal and spatial variation in river temperatures.

To test the sensitivity of the model to inflow temperature, two tests where undertaken with inflow temperatures 2 ^{o}C above and below the temperatures assigned to the inflows.

Simulated profiles of temperature (Figure 3.9) demonstrate that despite a shift in the inflow temperature, the thermal structure is maintained and is strongest for the cooler inflow test. The fate and dilution of tracers and sediments and the water age (see also Table 3.1) are modified by 5 to10%.

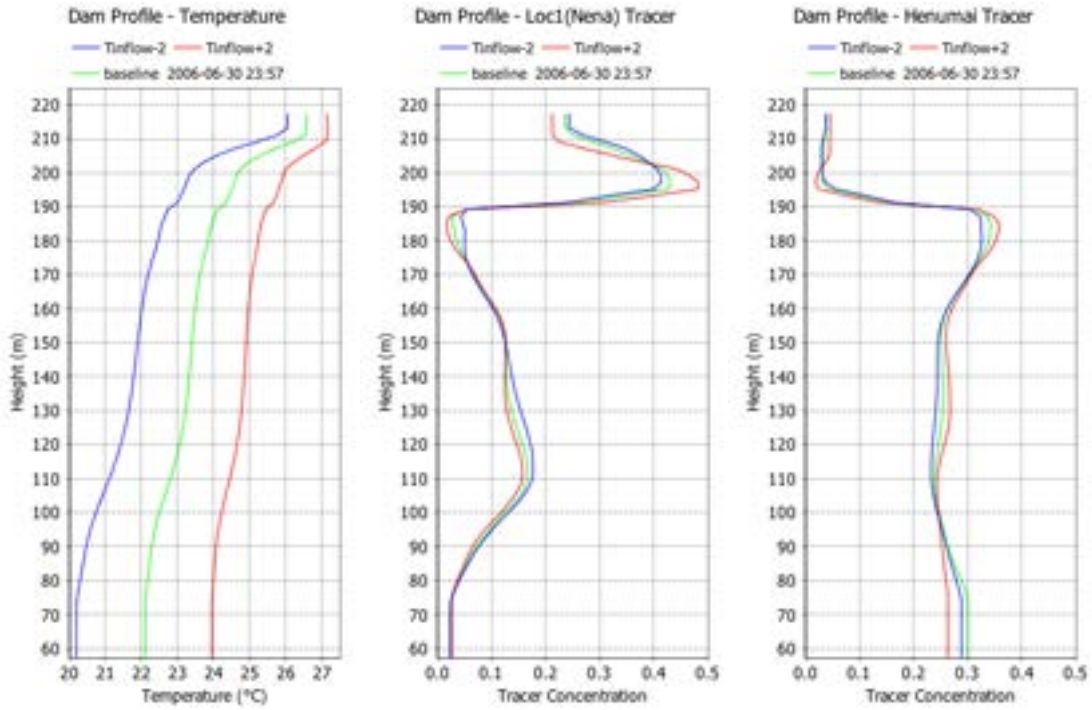

Figure 3.9 Simulated temperature (left), Nena tracer (middle) and Henumai tracer (right) at the embankment for the baseline (a) (green lines), T_{inflow} – 2°C (blue line) and T_{inflow} + 2°C (red line) sensitivity tests.

Table 3.1. Average values at the HEP intake for the base case and T_{inflow} +/- 2 °C test simulations.

Test	Period	Temperature (°C)	Henumai tracer	Nena tracer	2 micron	Age
Base case	2002-2006	24.8	0.19	0.20	32.5	318
T_{inflow}-2 °C	2002-2006	23.5	0.19	0.20	33.1	315
T_{inflow}+2 °C	2002-2006	26.0	0.18	0.21	31.4	328

3.1.6 Meteorological Data

Modifying the meteorological data to consist of Moraupi AWS observations in-filled with Nena AWS data (where required) produced a warmer overall temperature profile with similar stratification characteristics. As a result, change to the HEP intake waters remains limited (Figure 3.11).

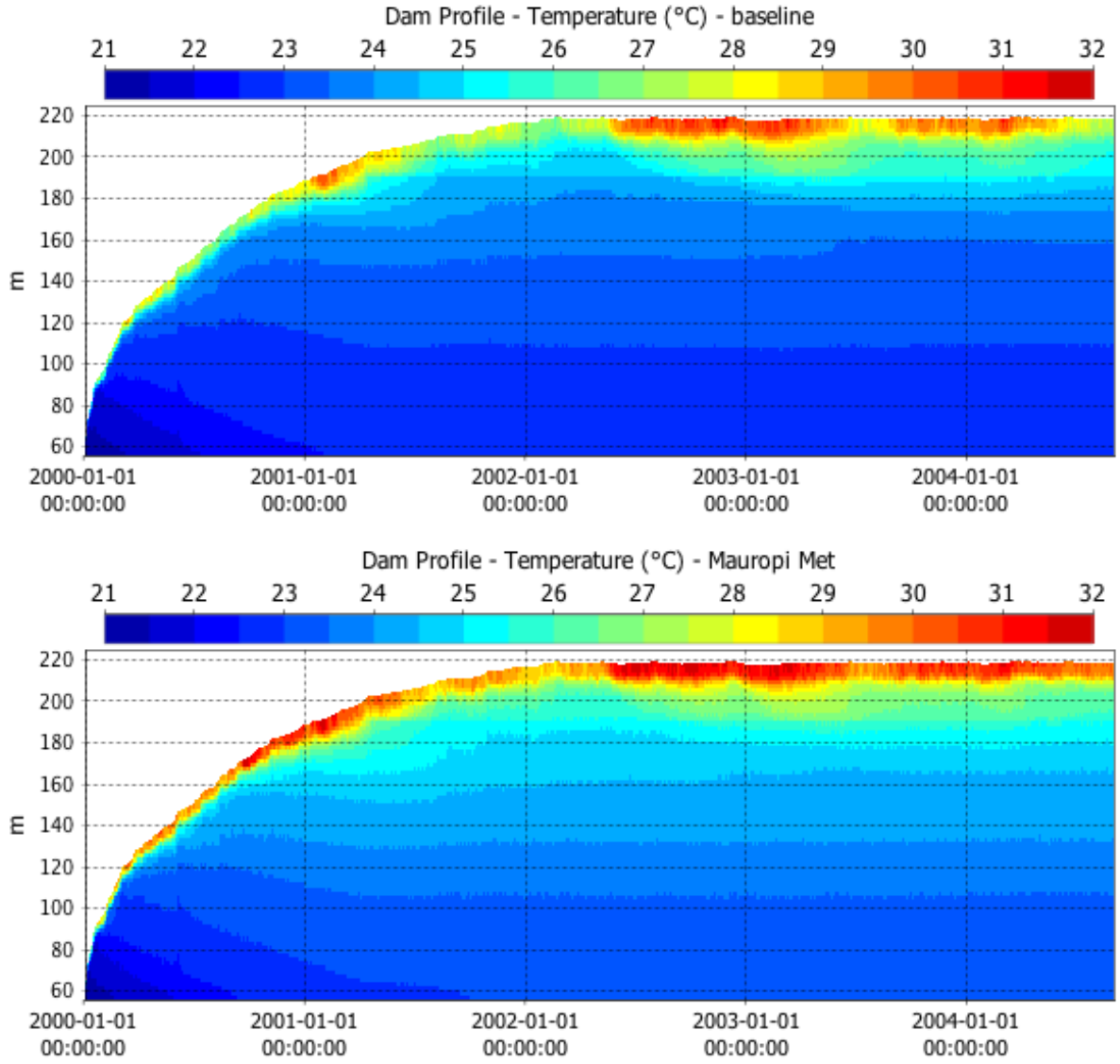

Figure 3.10 Simulated temperature at the embankment for baseline simulation (a) with Nena AWS meteorological data (top panel) and baseline simulation (a) with Moraupi meteorological data (bottom panel).

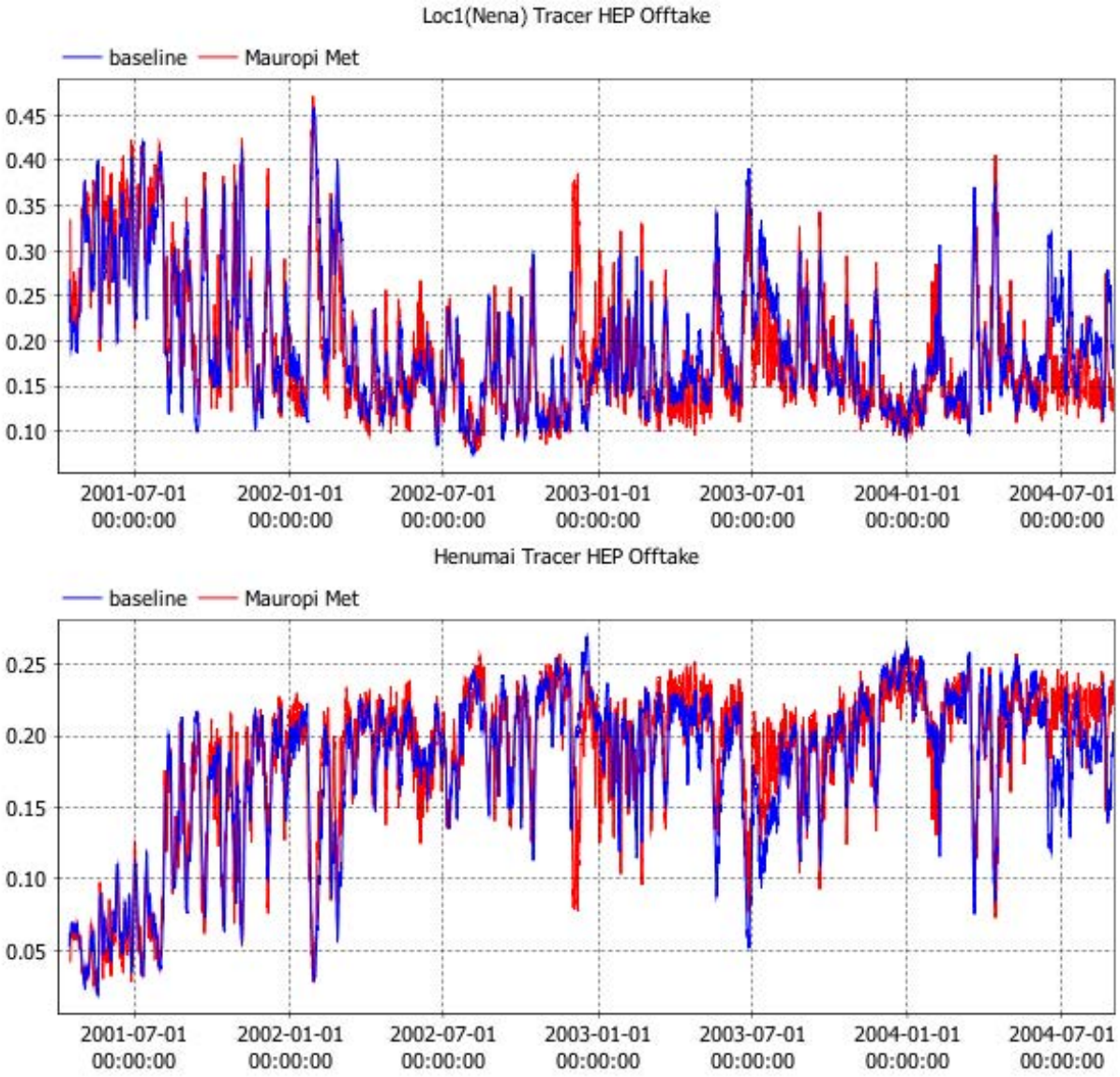

Figure 3.11 Simulated HEP intake concentrations of the Nena River inflow (top panel) and the Henumai River inflow (bottom pane) for baseline simulation (a) with Nena AWS meteorological data (blue lines) and Moraupi meteorological data (red lines).

3.1.7 HEP Operation

The influence of the HEP extraction on the thermal structure of the reservoir was examined by running a test case that was configured with the spillway as the sole downstream release, as would be the post-closure FRHEP case (Figure 3.12 to Figure 3.15). The model results indicate a significant shift in the temperature profile in which the metalimnion lifts to only several metres below the surface, and compresses to less than ten metres thick, with a uniformly strong gradient.

The lower portion of the metalimnion is very weakly stratified (perhaps now better described as part of the hypolimnion) with demarcation between metalimnion and hypolimnion (based on temperature gradients in the HEP operation case) becoming poorly defined. As a result of the change in thermal structure, the fate of the large river inflows is significantly altered. The Nena River flow reaches the embankment higher in the water column, reaching a peak beneath the shallower epilimnion, and makes a larger contribution to the epilimnion water itself. The Henumai is spread over a greater vertical range at lower concentrations. The distinctly layered structure in the baseline case becomes less defined in the spillway-only case as the

temperature gradients weaken significantly below 10 m depth. Despite the thin epilimnion that results and the week gradients beneath 10 m the simulations do no indicate that there are periods of where the stratification breaks down and complete mixing occurs between the epilimnion and hypolimnion.

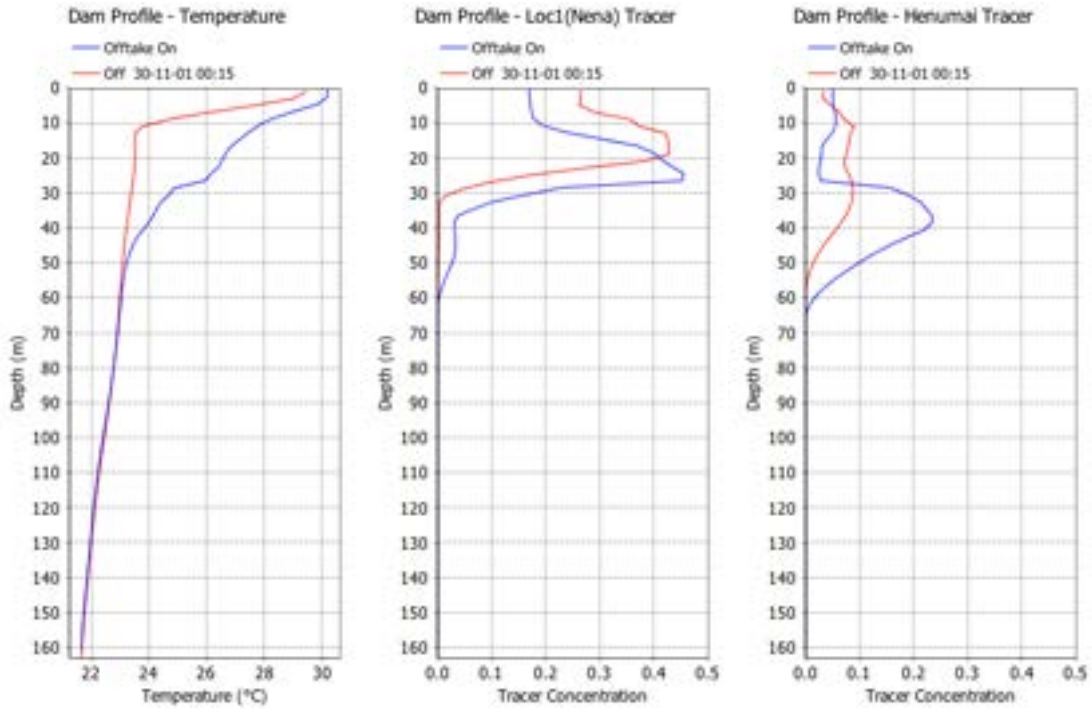

Figure 3.12 Simulated temperature (left panel), Nena tracer concentration (middle) and Henumai tracer concentrations (right panel) at the embankment for HEP operating (blue lines) and spillway-only test case (red line).

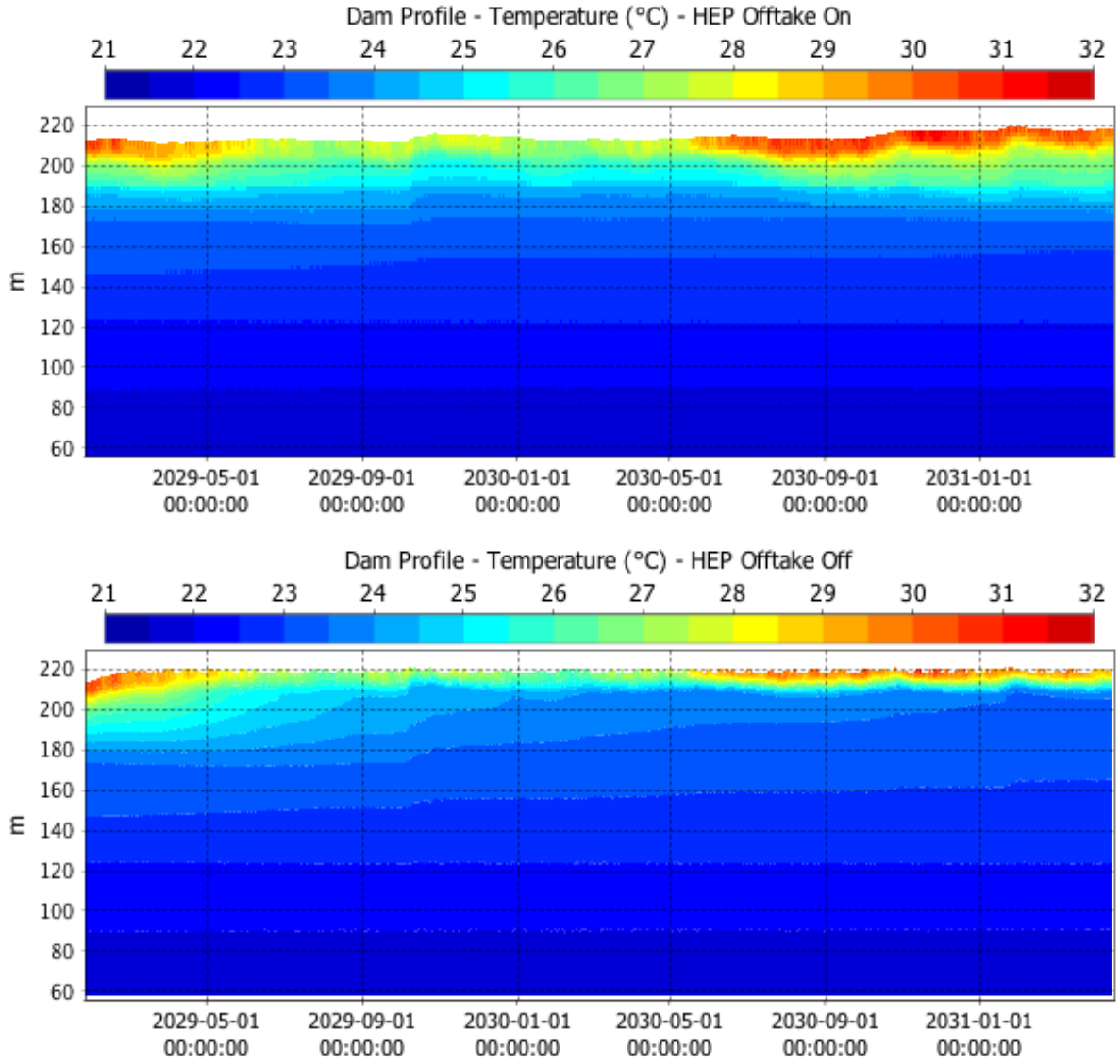

Figure 3.13 Simulated temperature at the embankment for HEP intake on (top panel) and HEP intake off (bottom panel).

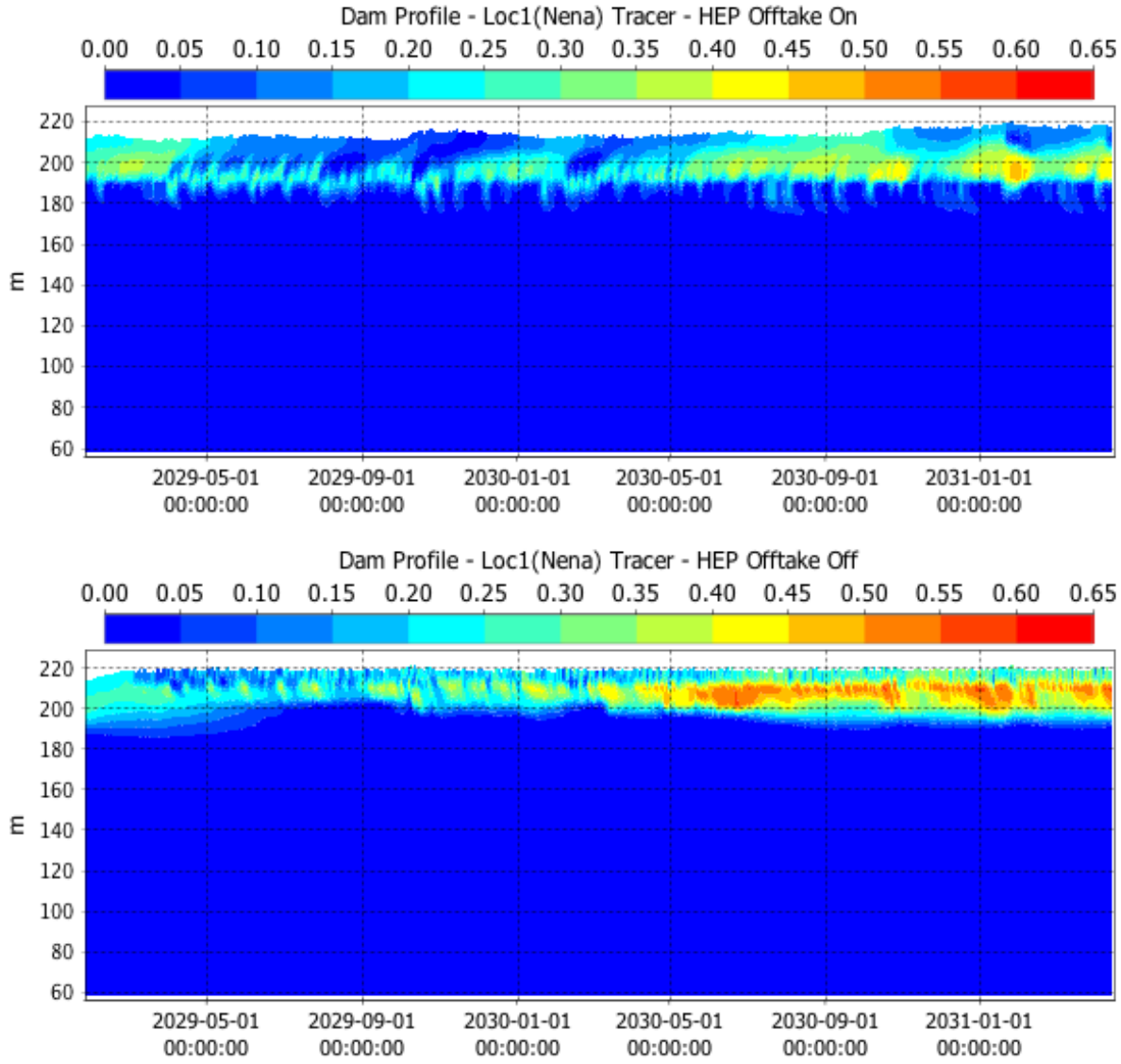

Figure 3.14 Simulated Nena River tracer at the embankment for HEP intake on (top panel) and HEP intake off (bottom panel).

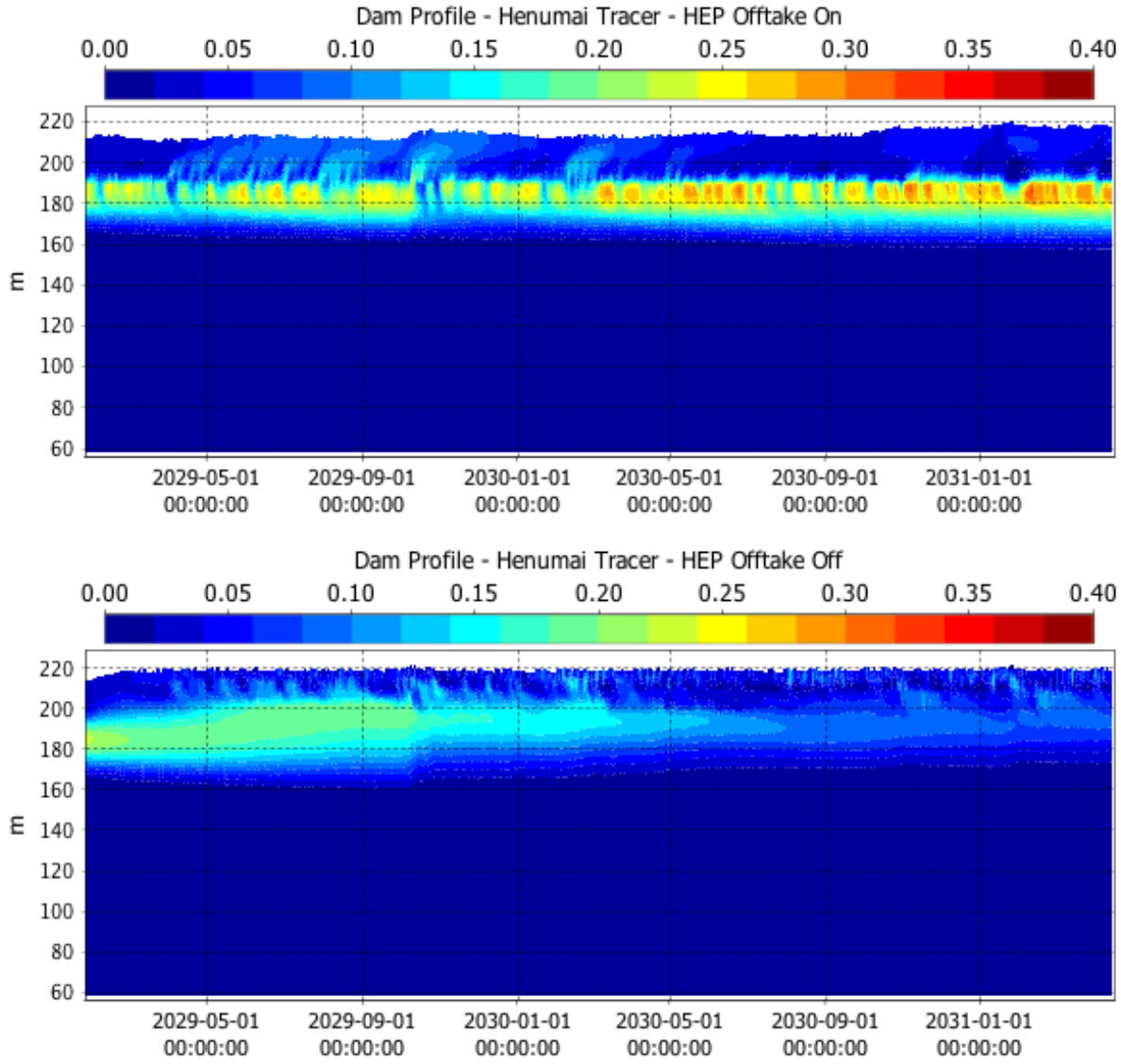

Figure 3.15 Simulated Henumai River tracer at the embankment for HEP intake on (top panel) and HEP intake off (bottom panel).

3.1.8 Waste Rock and Tailings Mobility

Incipient mobility of the waste rock and tailings is dependent on the extent to which bed stress exceeds a critical shear stress for the waste rock or tailings. The critical shear stress for the waste rock and tailings in this application are unknown and any estimate carries significant uncertainty. The maximum simulated bed stress over the duration of operations simulation (with 6-hour hydrograph) (see Figure 3.16) indicates that only near the headwaters of the large rivers does bed stress reach or exceed critical values of over 0.1 Pa. Moreover, time series of water level and bed stress at locations 3 km downstream of the Nena River headwaters (Figure 3.17) and 14 km downstream of the Henumai River headwaters (Figure 3.18) show only brief intermittent peaks of elevated bed stress that occur during the passage of inflows (when water level increases).

An assessment of potential exposure to stress above a critical value is summarised for the preliminary model in Figure 3.19 and Figure 3.19. These figures illustrate that for base case conditions material stored in the Nena arm (solely waste rock in the preliminary project description) with a critical stress for resuspension of greater than 0.1 Pa is unlikely to mobilise. However for a critical shear stress of 0.01 Pa there is likely to be up to fortnightly resuspension

events during high flow. For critical shear stresses less than 0.01 Pa the frequency of resuspension events increases rapidly. For storage of tailings from the mid-Niar arm down to the embankment (as was the case in the preliminary project description) mobility starts when the critical stresses are less than approximately 0.01 Pa. Below 0.01 Pa there is a rapid increase in the frequency of occurrence of events that will lead to mobilisation.

Storage or migration of waste rock and tailings upstream of the mid-Niar will expose the deposits to significantly more bed stress (as indicated by the grey line in Figure 3.19). In this region, material with a critical bed stress of less than 0.06 Pa is likely to mobilise, with frequent mobilisation (approximately fortnightly on average) for material with a critical stress less than 0.01 Pa. This result suggests that storage or migration of fine material upstream of the mid-Niar is likely to increase the frequency of resuspension. The increased likelihood of mobilisation of stored or migrated tailings further upstream of the mid-Niar arm is also compounded by significantly larger areas that are exposed to sufficient shear stress to trigger resuspension (see Figure 3.20), therefore increasing the potential resuspended load.

Simulated tailings deposition maps after 4.5 years (Figure 3.21) show that after initial transport some of the suspended tailings are re-deposited both upstream of the storage area in the Niar arm and throughout the Nena arm; the finer sediments are transported and re-deposited further away from the initial tailings deposition site because of their slower settling rates. Over time these re-deposited tailings will be more susceptible to ongoing resuspension, transport and re-deposition because of increased exposure the higher bottom shear in the upper reaches. In addition, re-deposition of tailings that are entrained higher into the water column may re-settle in shallow littoral zones with the potential to impact on riparian growth.

The re-deposited tailings will be subjected to some burial (or at least intermixing) with the catchment sediments that settle to the bed. Figure 3.22 illustrates that there is significant settling of all sizes of the catchment sediments that overlaps with the distribution of the tailings. The extent to which the deposited catchment sediment may provide additional stability to tailings so as to reduce potential resuspension is not known.

In addition to the uncertainly that is associated with the mobility of the stored waste rock and tailings, the bed stress derived by the model is also subject to uncertainty. An additional test was performed to assess the impacts bottom drag may have on the resolved bed stress. Within the model set-up, drag has been applied as a constant drag coefficient of 5×10^{-3} (taken from the range cited in Parker et al. 1987). The model uses the drag to then remove momentum from inflows as they propagate through the model domain.

In a test case where no momentum loss due to drag was imposed during flow (a so-called ‘free-slip’ condition) maximum simulated bottom stress increased (Figure 3.23) so that more of the bed was exposed to higher critical shear stress. However, this did not lead to any notable increase in the TSS in the HEP extraction due to the confined flow path of the re-suspended material described above (Figure 3.24). Furthermore, consistency in the TSS in the HEP intake indicates that the free-slip drag conditions did not substantially alter the overall dynamics of the inflows. Moreover, a low drag condition that approaches the free-slip assumption is unlikely given the drag that will be imposed on the flow by remnants of drowned vegetation that remain unburied by waste rock and tailings storage.

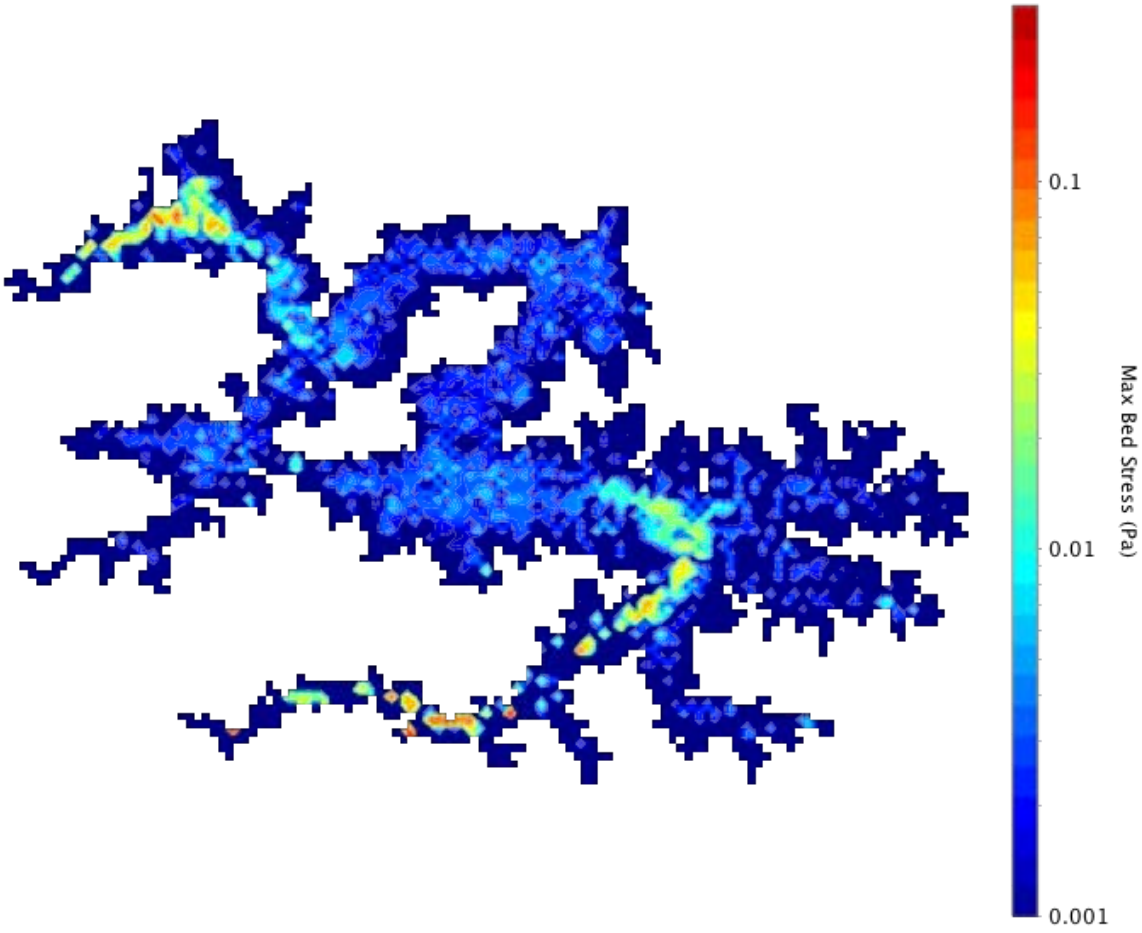

Figure 3.16 Simulated maximum bed stress during case of waste rock and tailings storage.

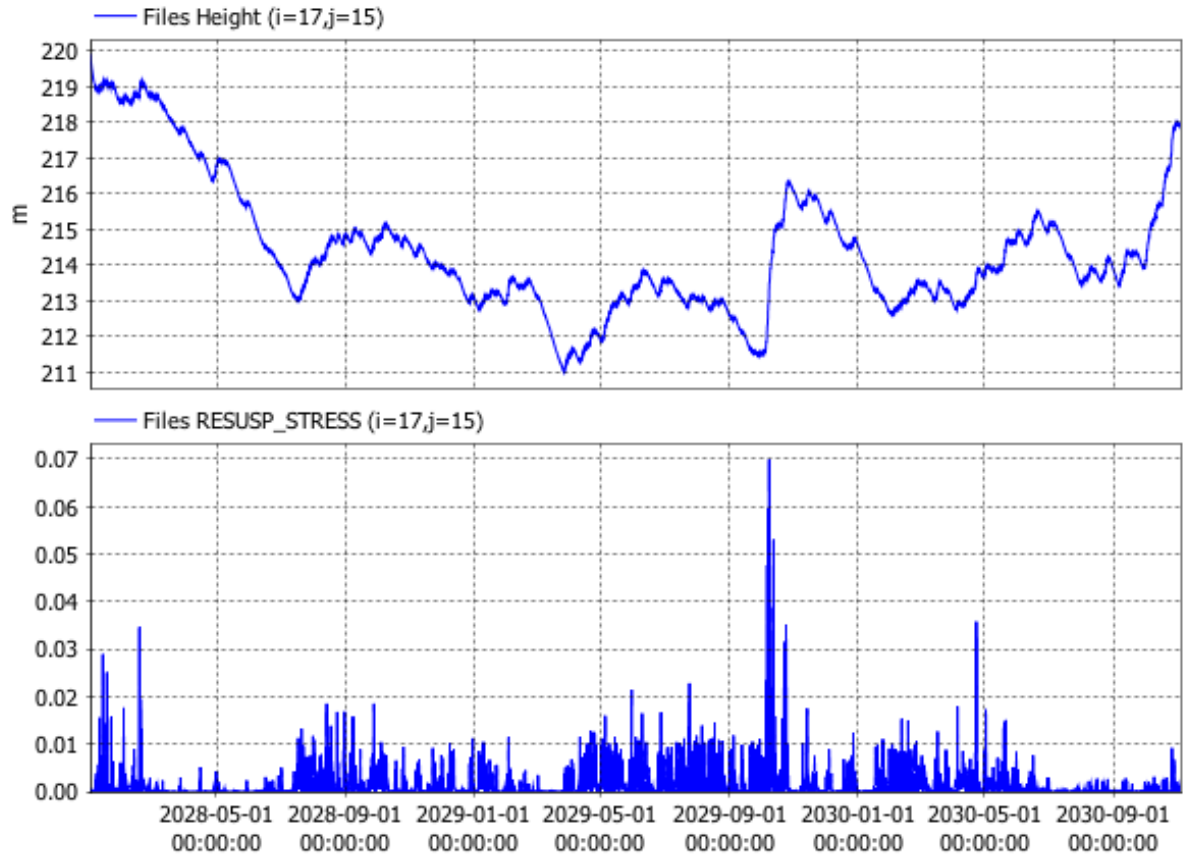

Figure 3.17 Time series of simulated water level (top panel) and bed stress (bottom panel) 3 km downstream of the Nena River headwaters.

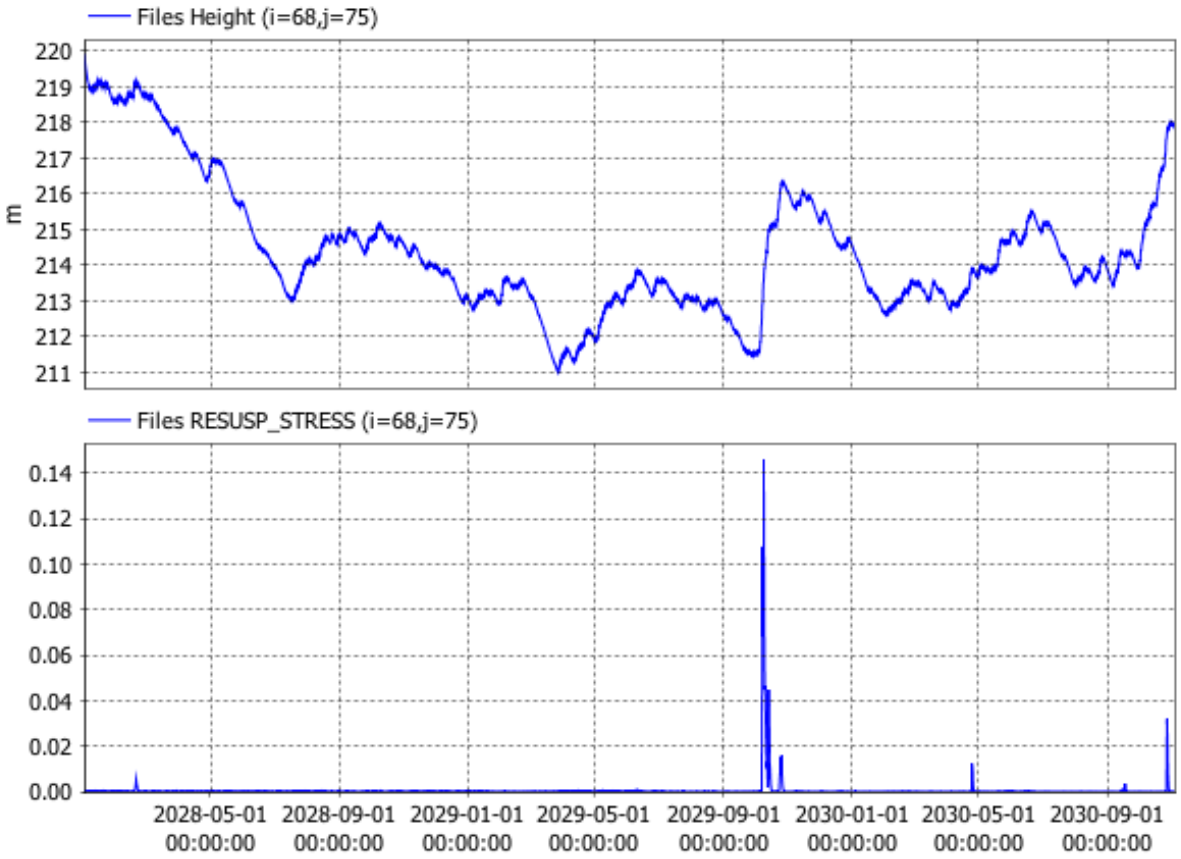

Figure 3.18 Time series of simulated water level (top panel) and bed stress (bottom panel) 14 km downstream of the Henumai River headwaters.

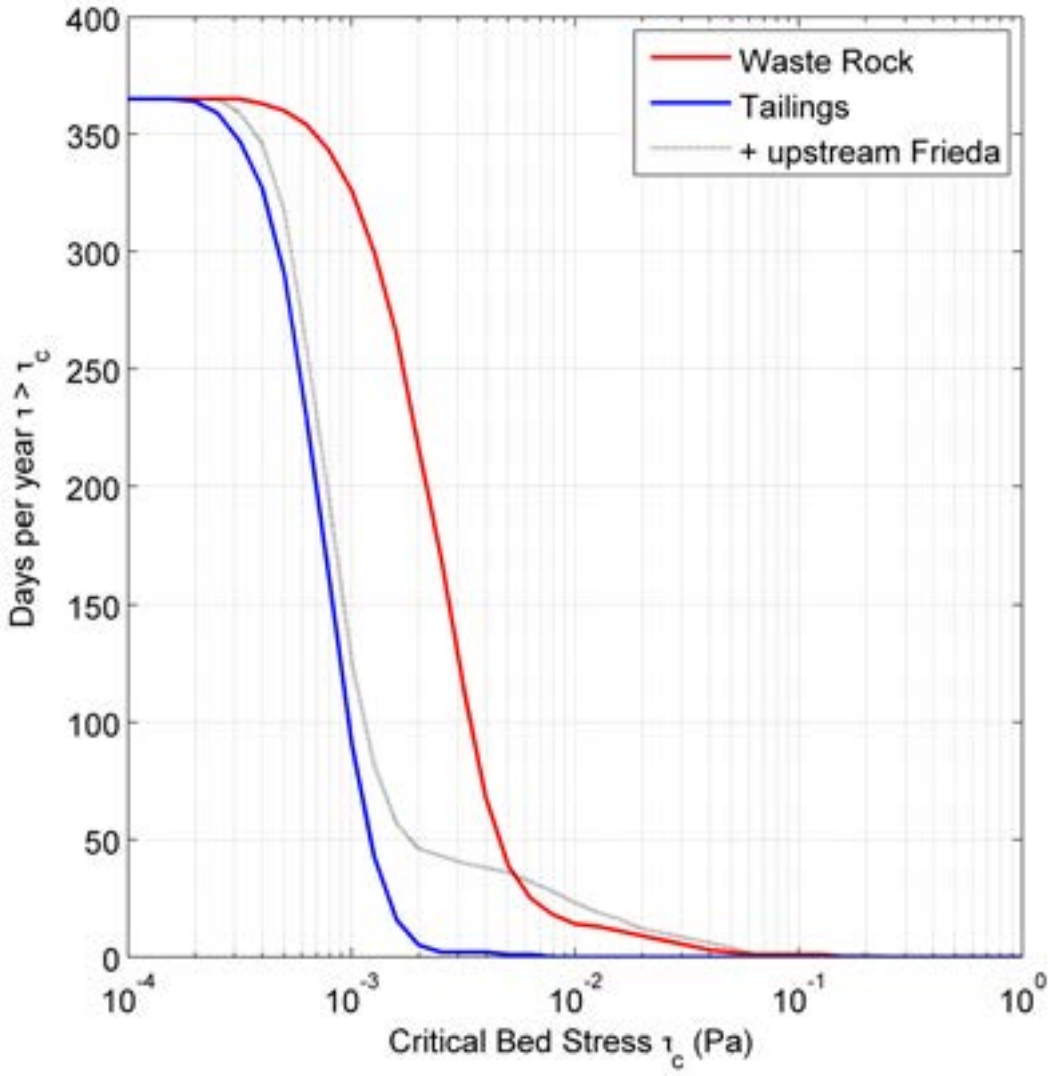

Figure 3.19 Average days per year bed stress exceeds critical (x-axis) over waste rock (red), and tailings (blue). The grey line indicates tailings deposition area plus upstream of the designated storage footprint to 162.5 m RL.

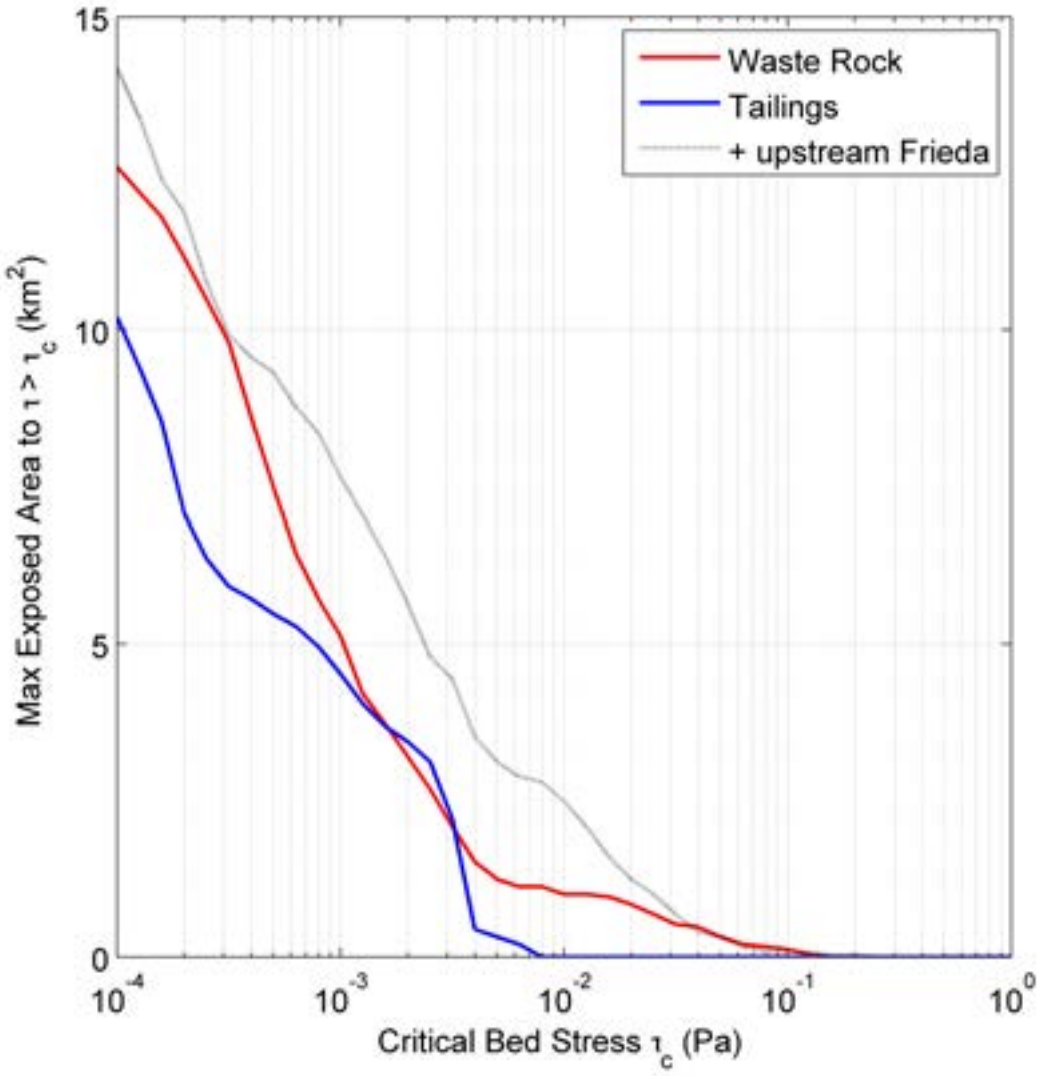

Figure 3.20 Maximum area over which bed stress exceeds critical (x-axis) over waste rock (red), and tailings (blue). The grey line indicates tailings deposition plus upstream to 162.5 m RL.

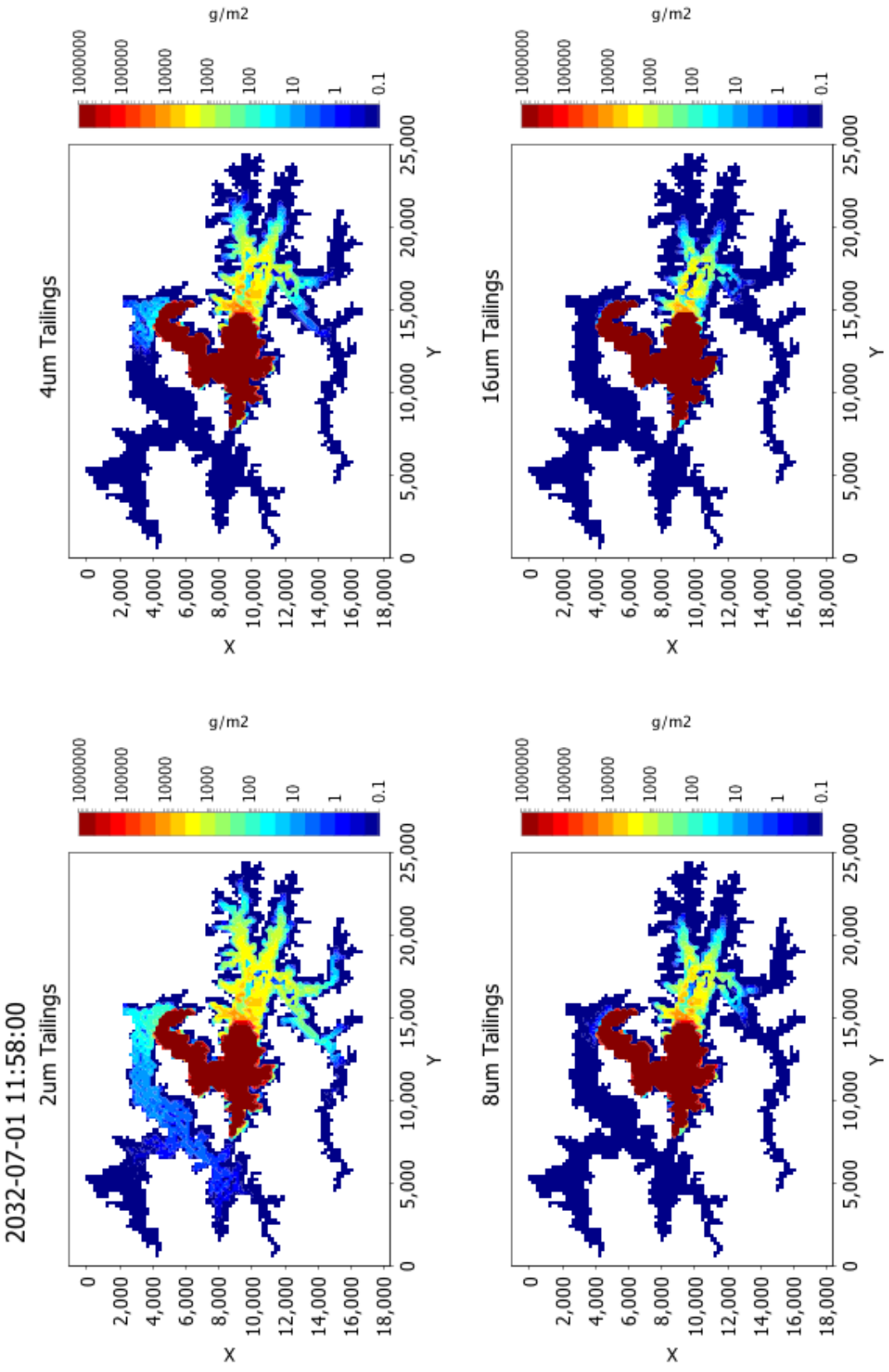

Figure 3.21 Simulated sediment deposition maps (in g m^{-2}) the four particle sizes in the tailings after 4.5 years of simulation.

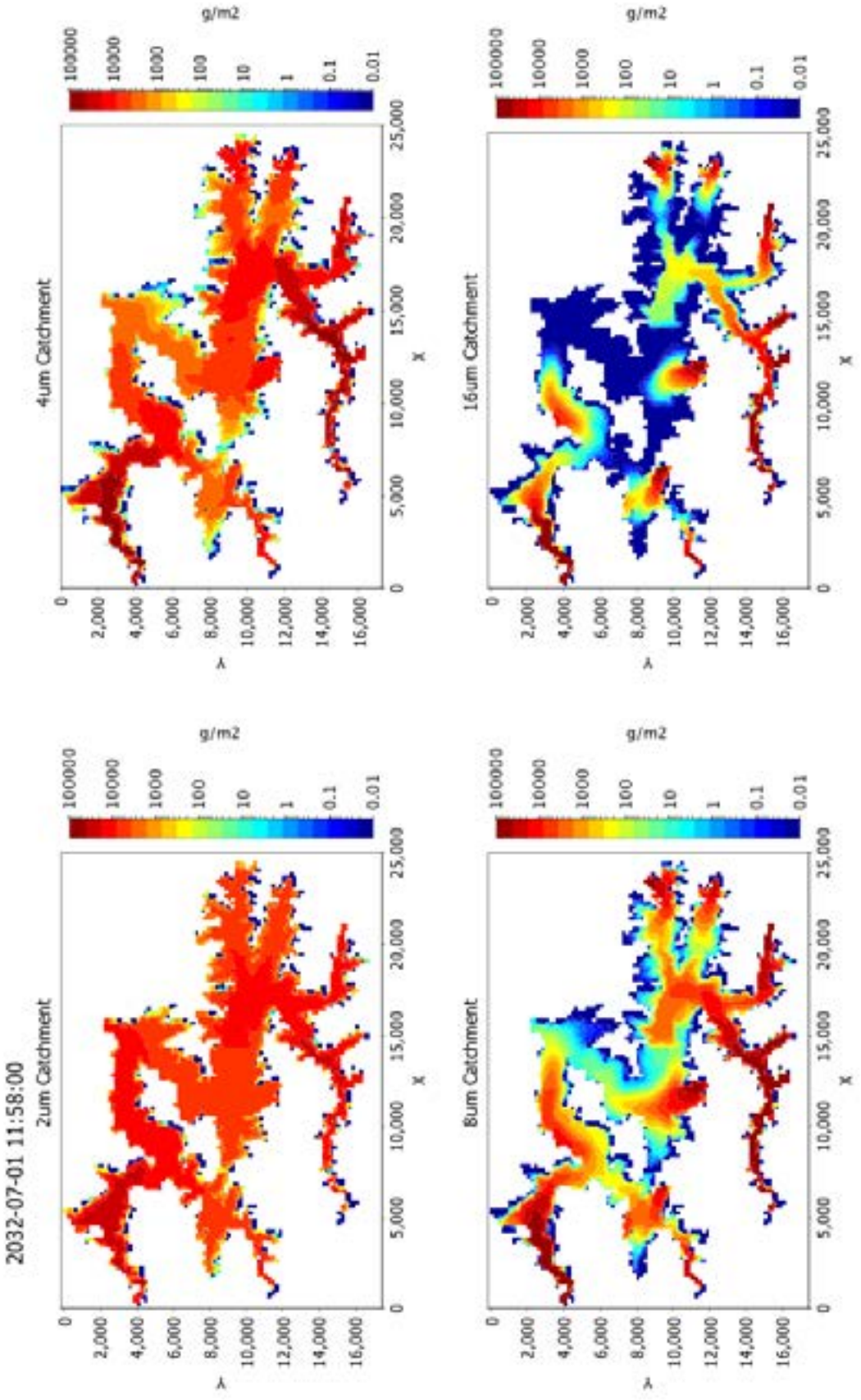

Figure 3.22 Simulated sediment deposition maps (in g m^{-2}) for the four particle sizes of catchment sediments after 4.5 years of simulation.

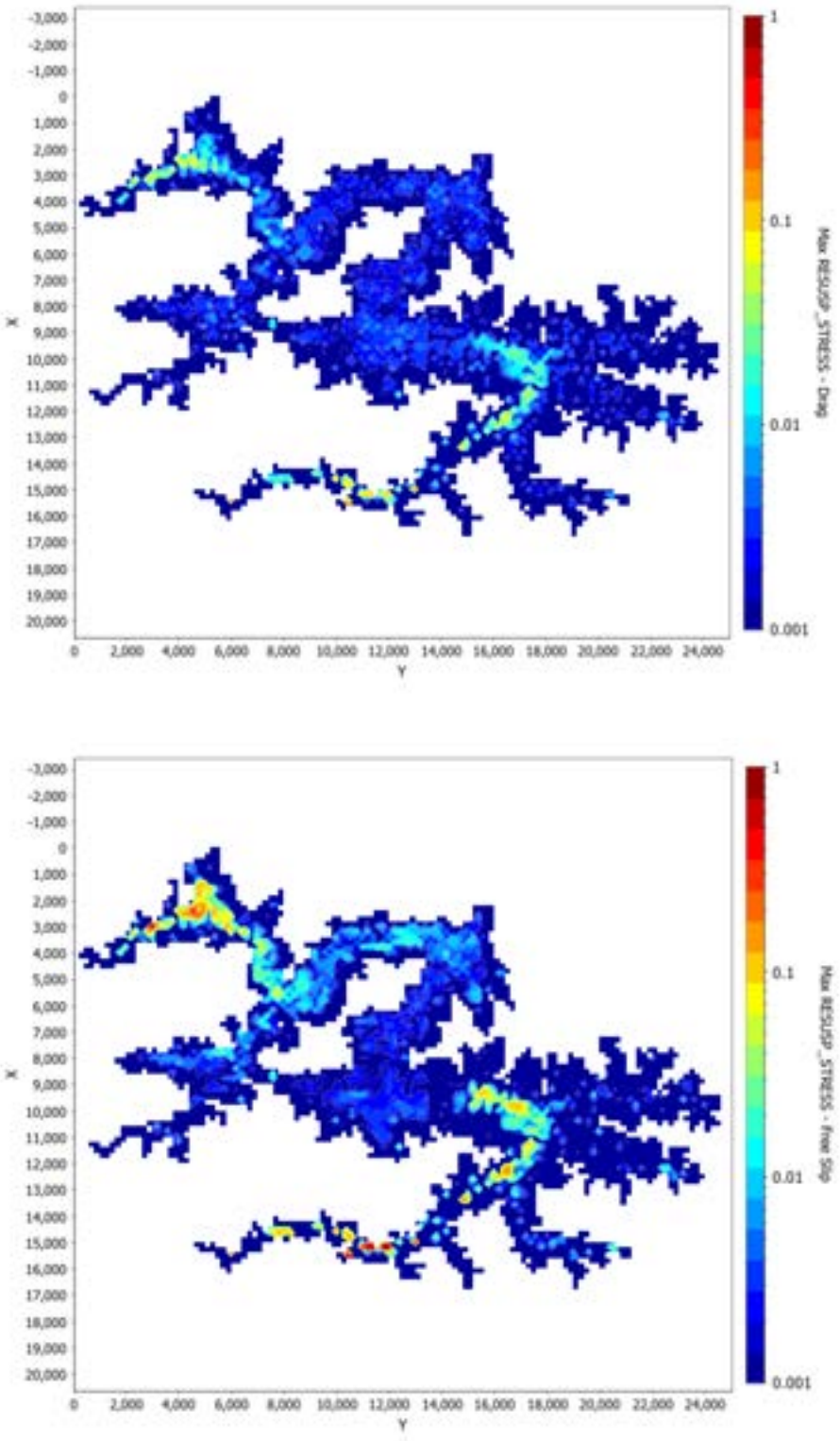

Figure 3.23 Maximum bottom shear stress (Pa) in waste rock and tailings storage simulations with drag bottom (top panel) and free-slip bottom (bottom panel) during 2028-2033.

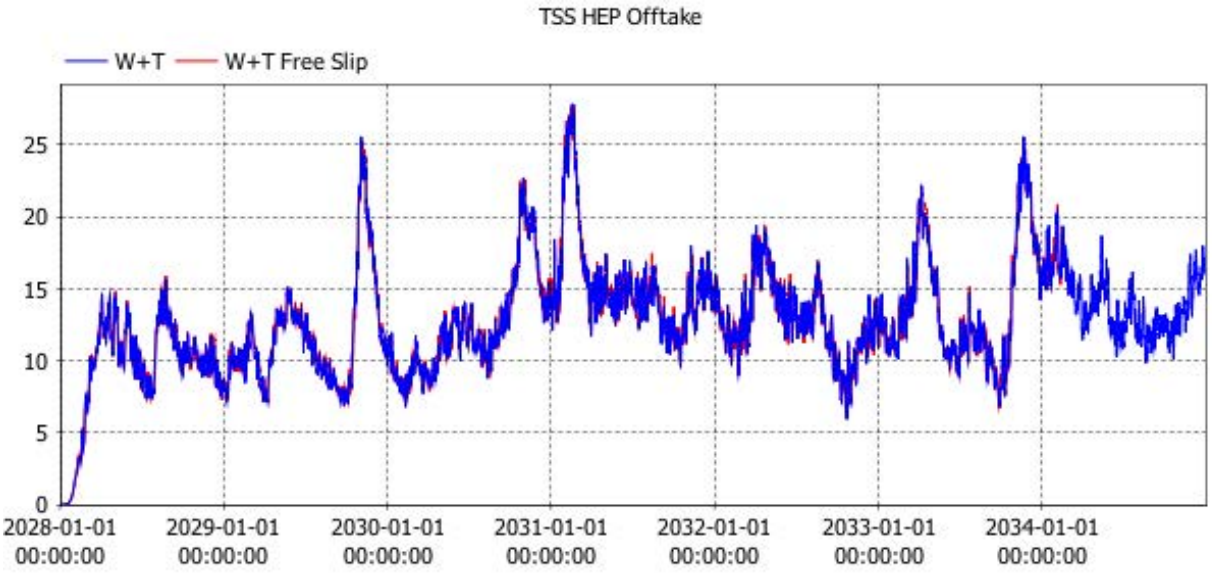

Figure 3.24 TSS in HEP intake (mg/L) for waste rock and tailings simulations with drag bottom (blue) and free-slip bottom (red).

3.1.9 Flow Events

Three large flow events were simulated with waste rock and tailings storage (at final height of 162.5 m RL) with 6-hour hydrographs. On 7 July 2030 a 1:1000 year ARI 6-hour duration hydrograph (SRK, 2017c) was applied to the Nena, Henumai and all rivers as three separate scenarios. The temperature and suspended solids concentrations of the large flow events remained the same as in the base case simulation. Although it is expected that the concentrations of suspended solids will increase during flood events, and there will be an increased contribution from larger grain sizes, at the time of undertaking the model assessment no information was available on the increased sediment load of modified PSD during flood flows.

For the combined large flows scenario, the tracers for flows from the Nena arm show a rapid increase in concentrations from the Nena tributaries in the HEP intake water in the 2-3 days that follow the inflow event (Figure 3.25) followed by a rapid decline. The rapid decline in concentrations of tributaries from the Nena arms coincides with a delayed but then a rapid increase in the contribution to the extracted water from the Niar arm inflows (Figure 3.26). The longer travel distance and the broader expanse of the Niar arm extends the travel time, compared to flows from the Nena arm. However, once it has arrived, the elevated flow contribution from the Niar arm at the HEP intake is prolonged compared to the early peak in Nena arm contributions.

Suspended sediments reaching the HEP intake peak from day 2 to 3 after the event (Figure 3.27), increasing by approximately two-fold, before a rapid return to pre-event concentrations. The simulations show that the catchment fines dominate total suspended solids; there is negligible contribution from the waste rock and tailings (see below for further discussion regarding resuspension of waste rock and tailings). Considering a Nena River and Henumai River 1:1000 flow event in isolation (Figure 3.28 and Figure 3.29, respectively) demonstrates that the Nena River is the major contributor to the peak suspended solids concentrations during high flow events. High flow events in the Nena River are likely to lead to peak concentrations extracted in the HEP intake owing to a shortened travel time and reduced dilution of the Nena River flow that delivers elevated concentrations of suspended solids to the embankment.

A map of maximum bed stress during the combined inflow event (Figure 3.30) illustrates an increase in the predicted area of the bed that is exposed to near-critical bed stress compared

to base case conditions consider in Section 3.1.8. This leads to considerable but localised resuspension of the fine fraction in the waste rock deposits in the upper Nena arm (Figure 3.31). Rapid settling of the resuspended waste rock (owning owing to its large size) confines the resuspended plume to a limited area and over a short duration (hours) during the passage of the large Nena River flow when bed stress temporarily exceeds critical (> 0.12 Pa for this simulation).

The simulated maximum bed stress map illustrates that the tailings in the mid-Niar are exposed to higher, but still sub-critical, bed stress and no resuspension results.

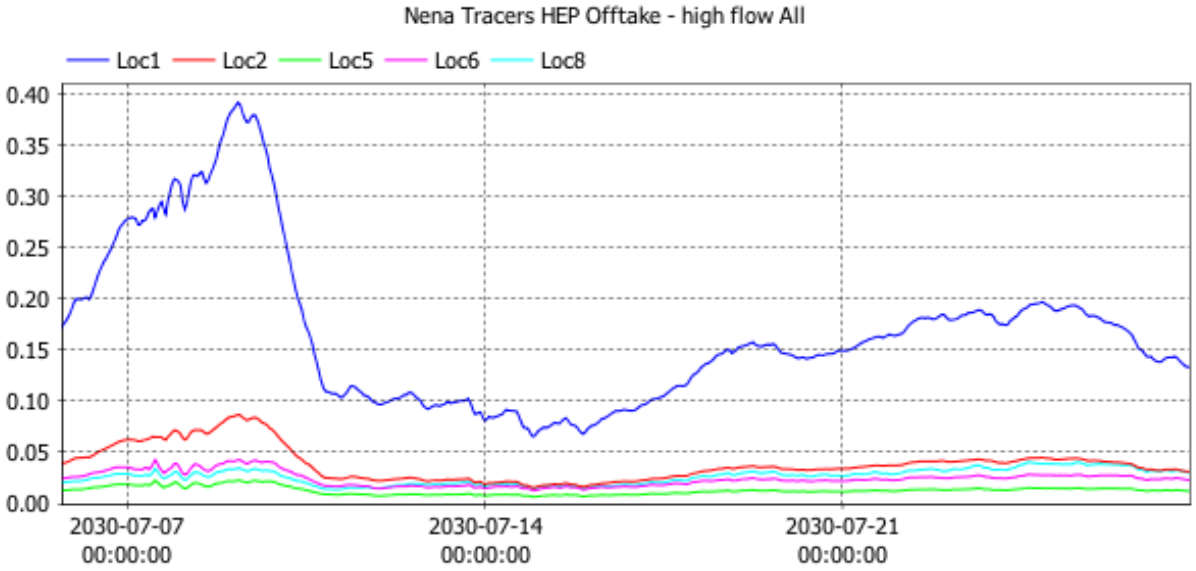

Figure 3.25 Simulated contribution from inflows in Nena arm to the HEP intake water during and after combined 1:1000 ARI flow event.

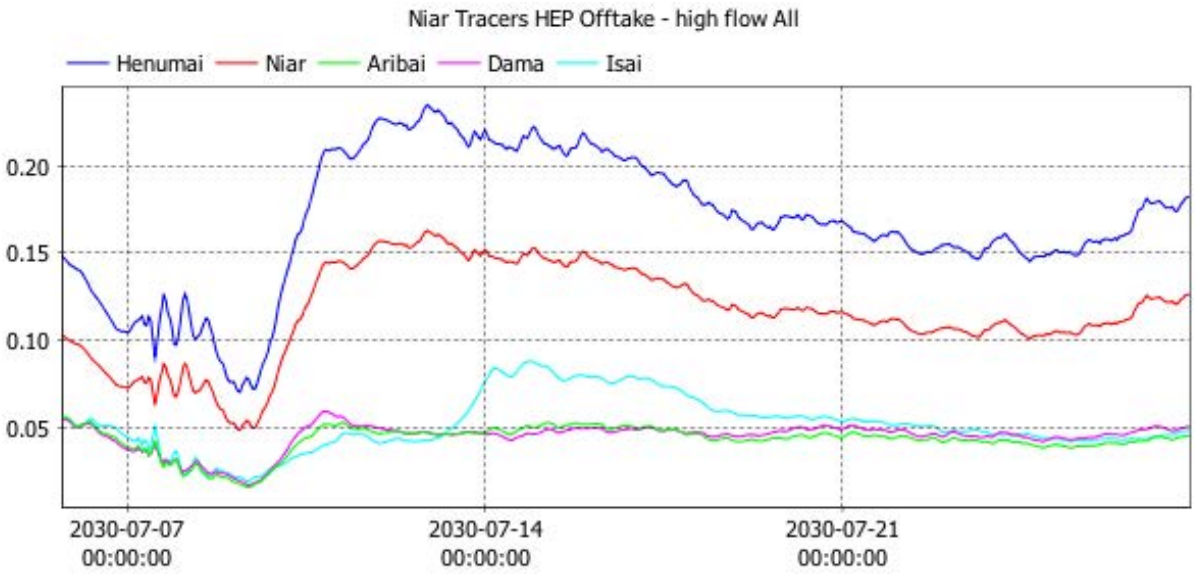

Figure 3.26 Simulated contribution from inflows in the Frieda arm to the HEP intake water during and after combined 1:1000 ARI flow event.

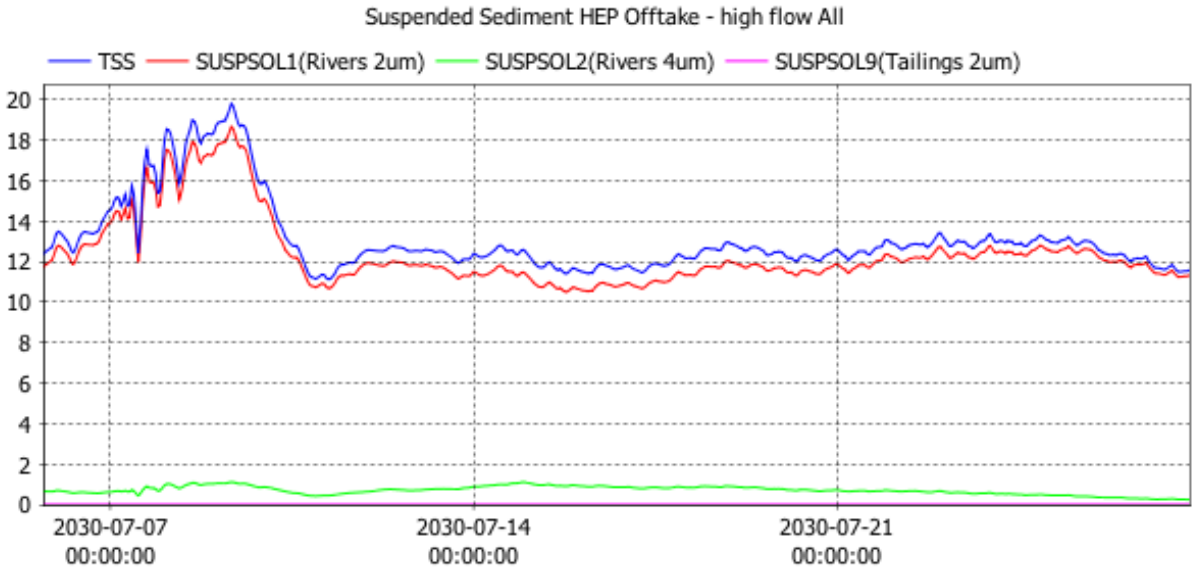

Figure 3.27 Simulated concentrations for suspended solids (total in blue; 2 micron river sediment in red; 4 micron river sediment in green and 2 micron tailings in magenta) in the HEP intake water during and after combined 1:1000 ARI flow event.

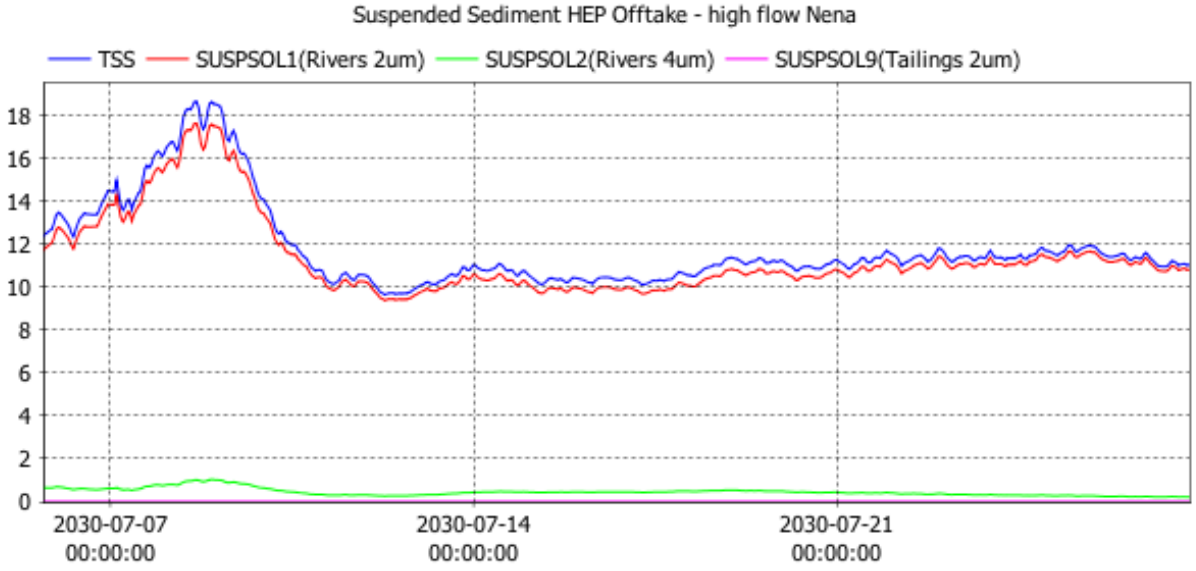

Figure 3.28 Concentrations for suspended solids (total in blue; 2 micron river sediment in red; 4 micron river sediment in green and 2 micron tailings in magenta) in the HEP intake water during and after 1:1000 ARI in the Nena River.

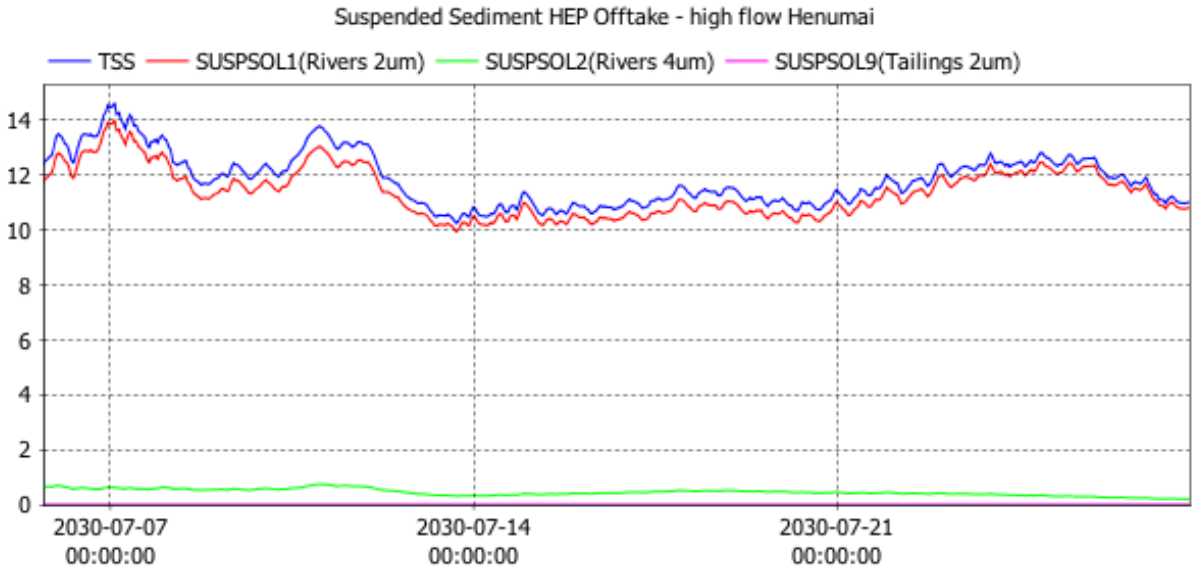

Figure 3.29 Concentrations for suspended solids (total in blue; 2 micron river sediment in red; 4 micron river sediment in green and 2 micron tailings in magenta) in the HEP intake water during and after 1:1000 ARI in the Henumai River.

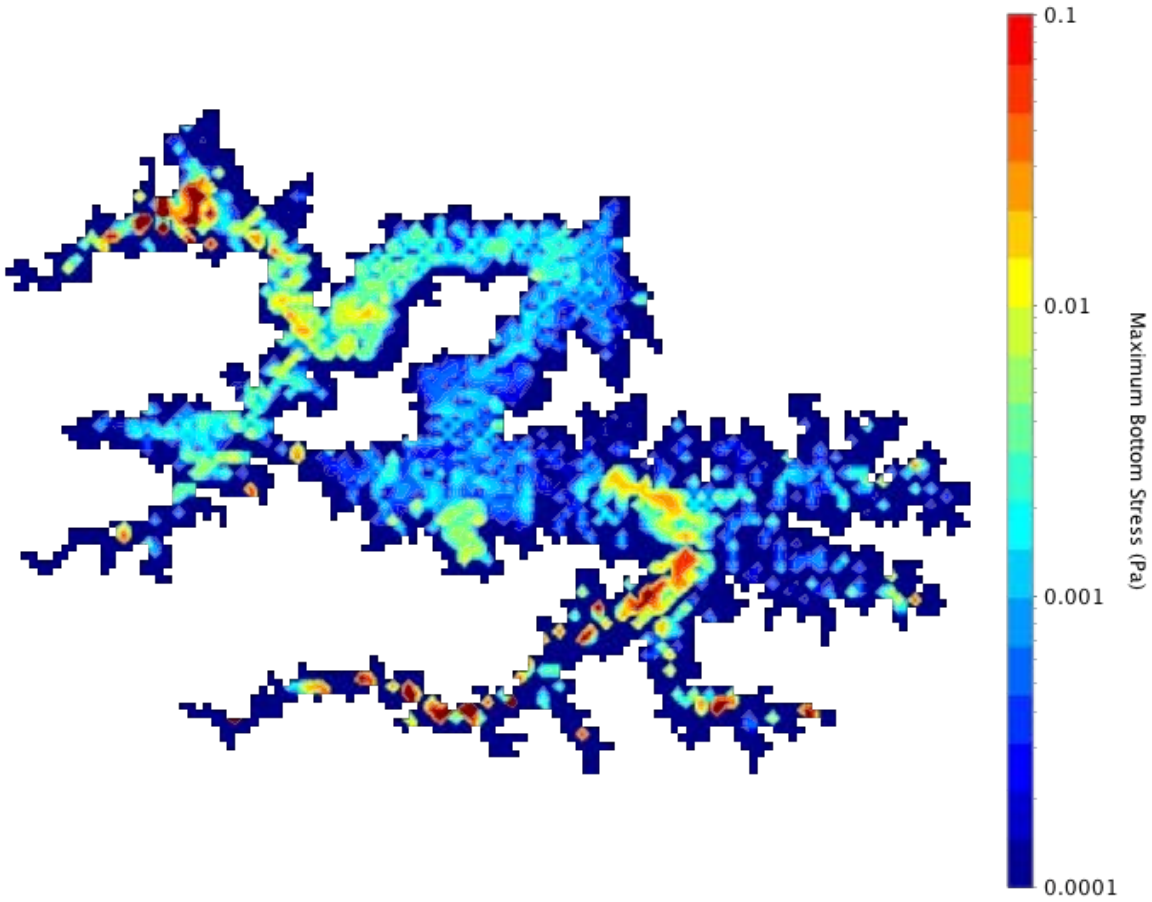

Figure 3.30 Simulated maximum bed stress during combined large flow event for waste rock and tailings storage case.

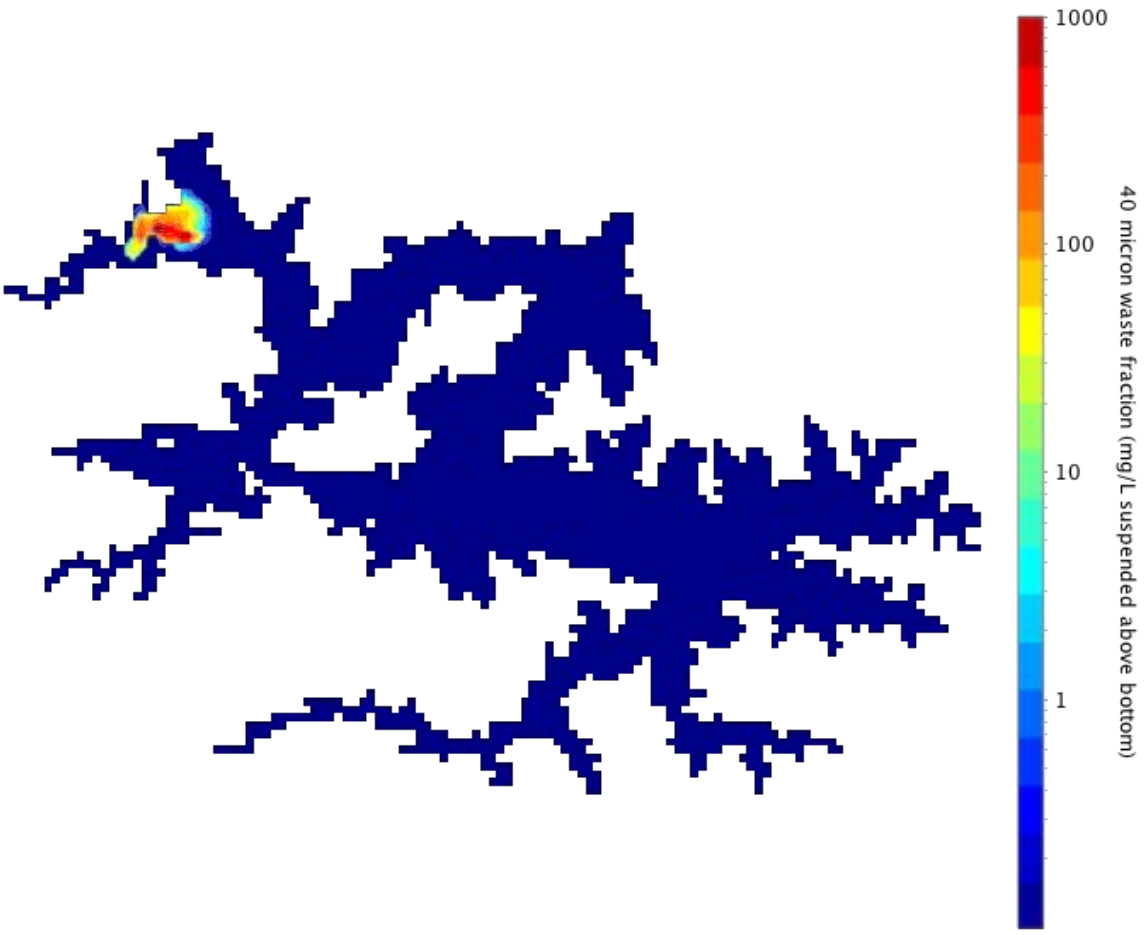

Figure 3.31 Simulated maximum concentration of suspended 40-micron waste rock fraction above the bed for combined large flow event with waste rock and tailings deposited in the reservoir to 162.5 m RL.

3.1.10 Storm Conditions

A synthesized one-day storm event on the 8 August 2029 was applied to the baseline (b) simulation with waste rock and tailings storage. The storm conditions were extreme and consisted of sustained cool temperature of 15 ^{o}C, prevailing wind speed of 10 ms^{-1} from the west and no direct solar radiation.

Simulated temperature at the embankment shows significant cooling and deepening of the epilimnion to approximately 190 m RL but no complete mixing (Figure 3.32). Furthermore, the thermal stratification is quickly re-established with no evidence of lasting impact as the simulation progresses.

A series of reservoir ‘curtains’ along the Niar arm illustrate that during and immediately after the storm (one day), there is complex detail in the isotherm distribution. This occurs because of differences in fetch (in relation to the prevailing wind direction) along of the reservoir, which leads to heterogeneity in the mixing, currents and tilting of the isotherms during the event. When the wind ceases the isotherms relax creating internal seiching and associated currents (Figure 3.34). These complex motions lead to rapid changes in the water quality at the HEP intake (see for example suspended solids time series in Figure 3.35) as water masses with different properties move vertically into and out of the HEP intake withdrawal window.

The currents generated by the storm move over the tailings (Figure 3.34), therefore increasing the bed stress (Figure 3.36). Although the stress remains sub-critical, there is a notable increase in maximum bed stress and the area exposed to higher bed stress as a result of the simulated storm.

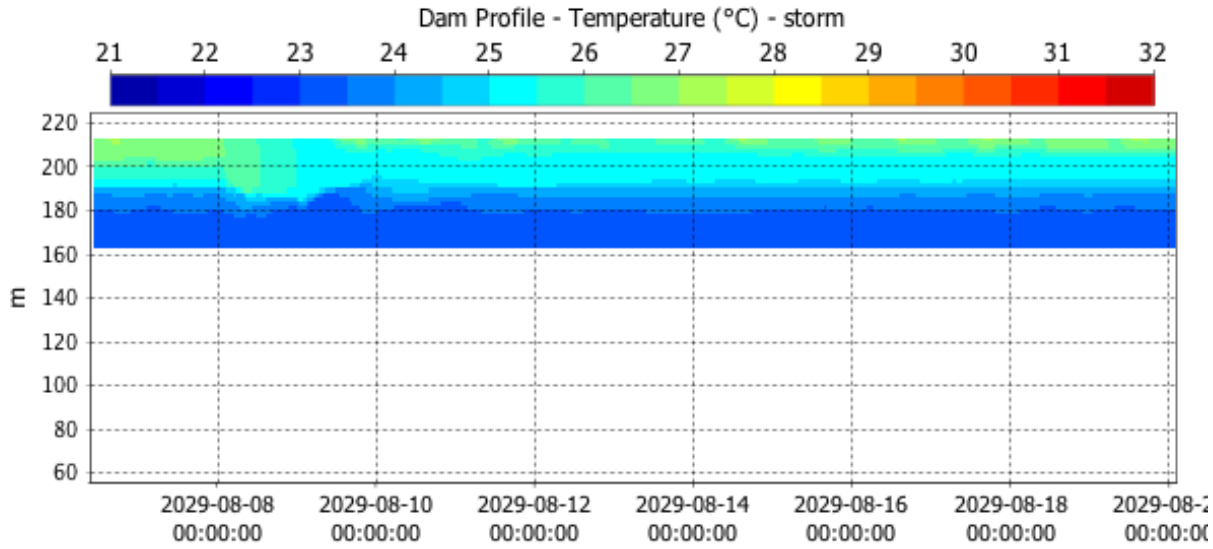

Figure 3.32 Simulated temperature at the embankment before, during and after a storm event on the 8 August 2029.

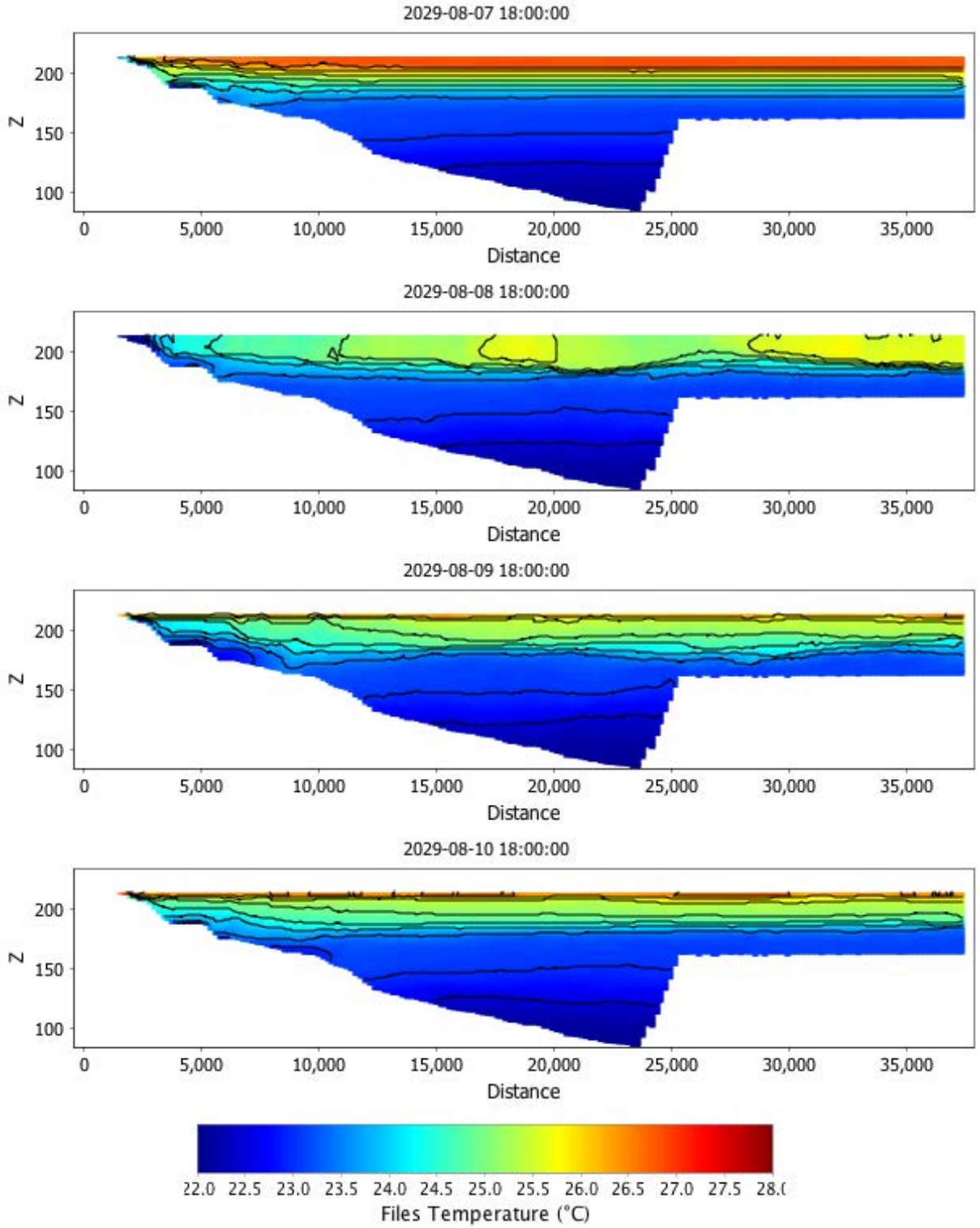

Figure 3.33 Simulated temperature along the Niar arm 6 hours before (first panel), during (second panel), and 18 and 36 hours after (third and fourth panel, respectively) a simulated storm event. The left of each panel is the Henumai headwaters, the right of each panel is the embankment. The ramp in the bathymetry in the mid-Niar is the tailings storage to 162.5 m RL.

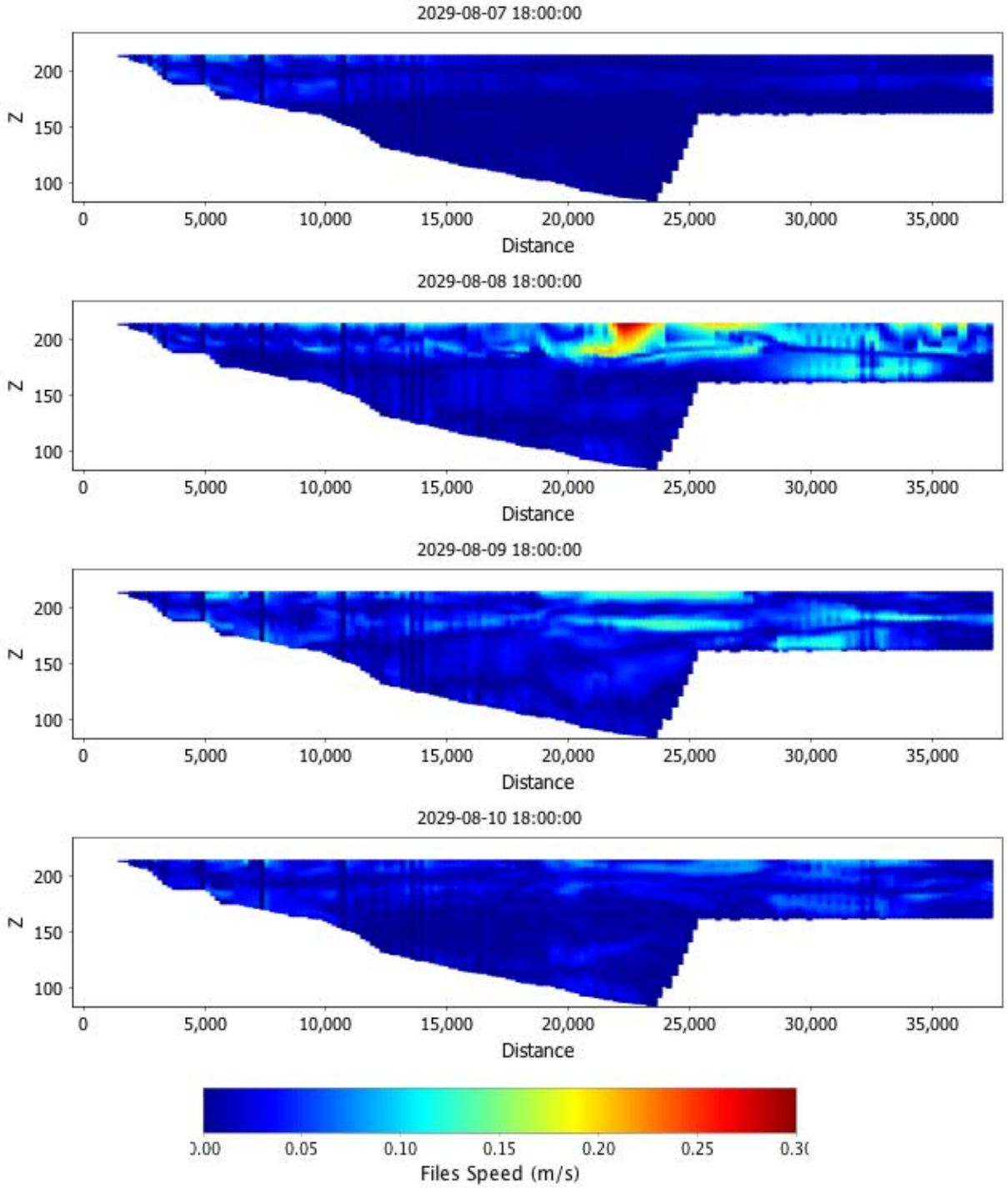

Figure 3.34 Simulated water current speed (m/s) along the Niar arm 6 hours before (first panel), during (second panel), and 18 and 36 hours after (third and fourth panel, respectively) a simulated storm event. The left of each panel is the Henumai headwaters, the right of each panel is the embankment. The ramp in the bathymetry in the mid-Niar arm is the tailings storage to 162.5 m RL.

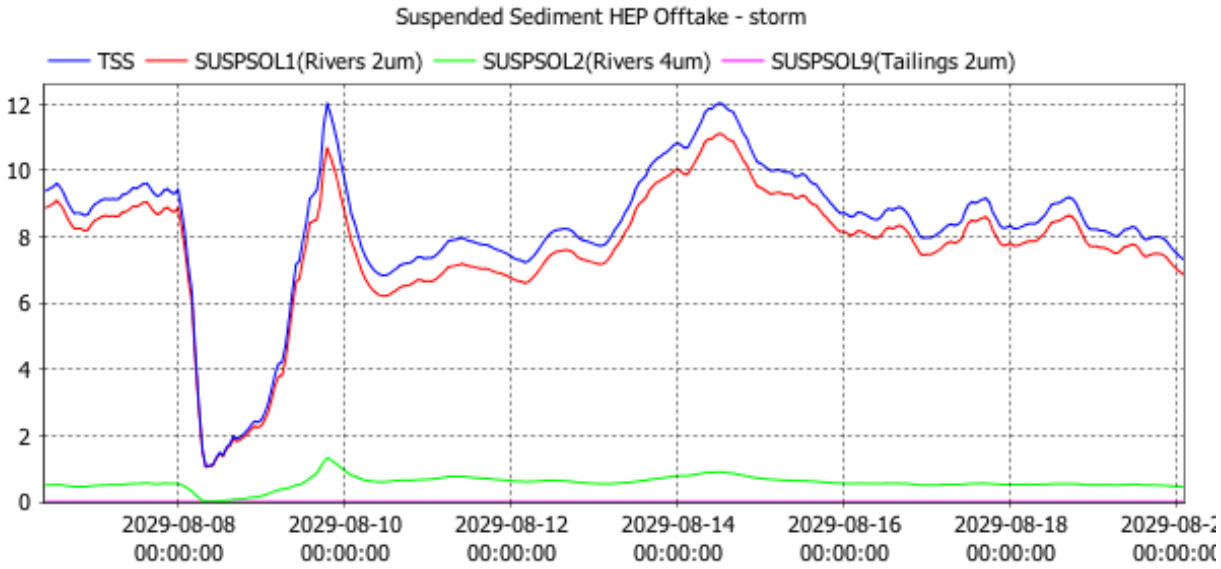

Figure 3.35 Concentrations for suspended solids (total in blue; 2 micron river sediment in red; 4 micron river sediment in green and 2 micron tailings in magenta) in the HEP intake water during and after a storm event on the 8 August 2029.

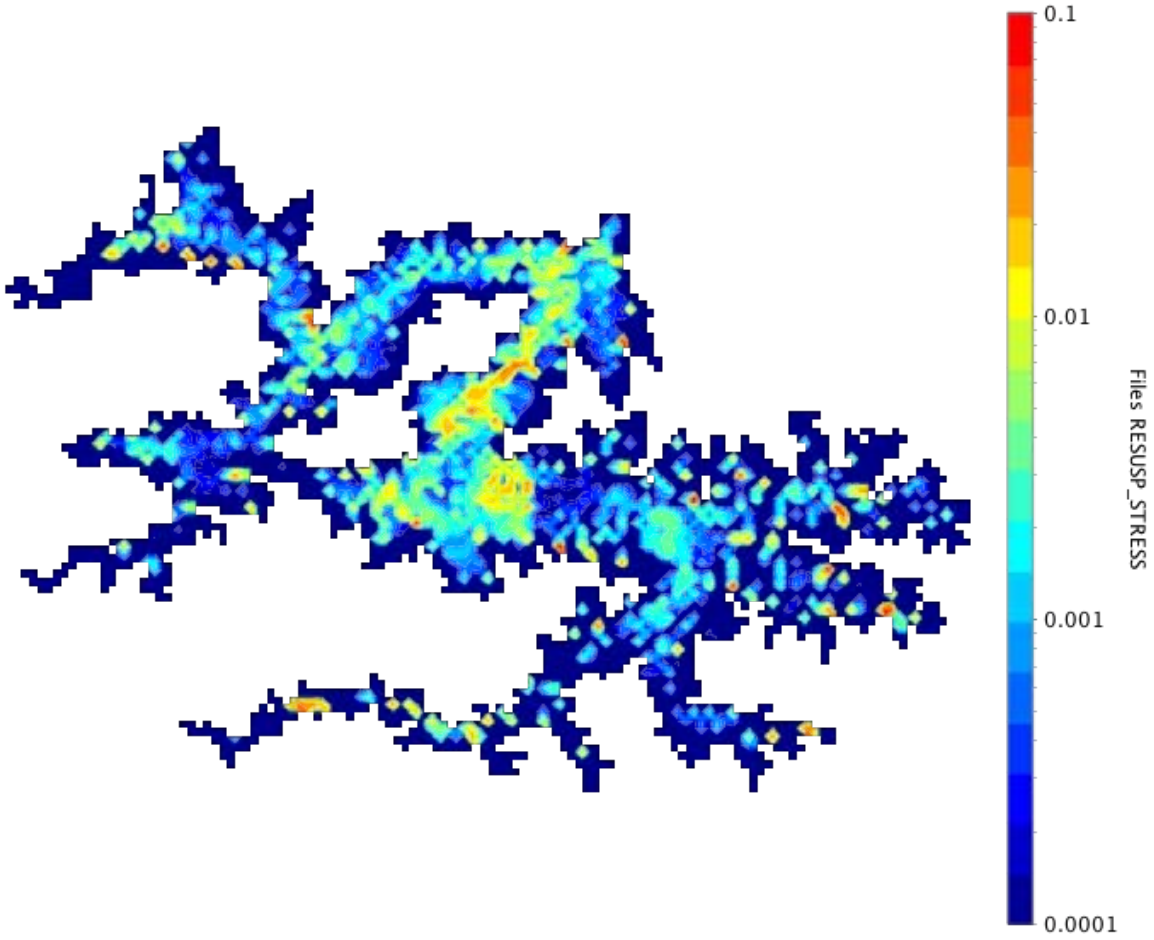

Figure 3.36 Simulated maximum bottom stress during storm event with waste rock and tailings deposited in the reservoir to 162.5 m RL.

3.1.11 Low Water Level

A simulation with an initial height of 202 m RL (i.e., 39.5 m below above the waste rock and tailings deposition depth) on 1 July 2029 was undertaken. The simulation began just prior to a period of drawdown and continued for 6 months, which included a large inflow event in October 2029. The maximum bottom stress was extracted from the model to determine the extent to which bottom shear may increase and potentially lead to resuspension. Results from the model suggest that the bed shear remains below critical values for resuspension above the tailings (Figure 3.37).

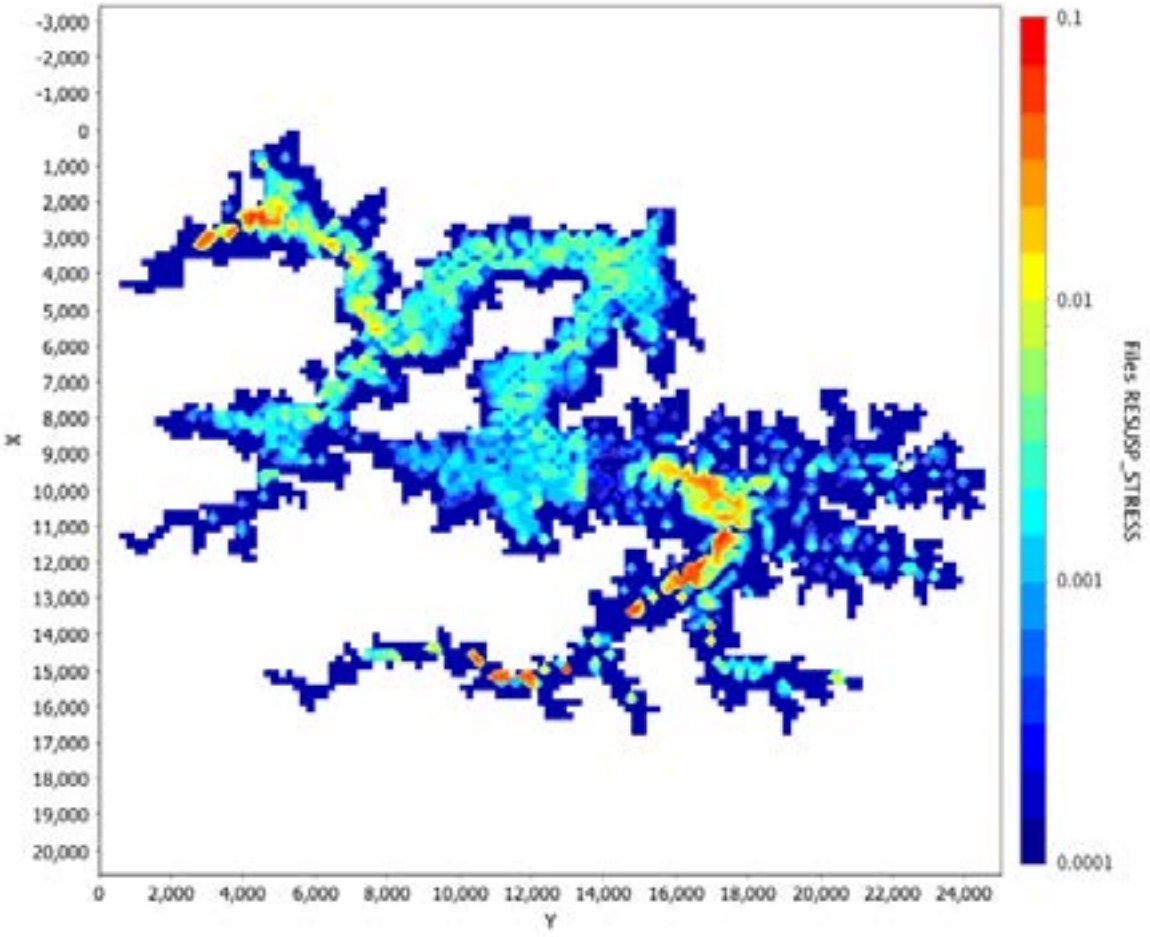

Figure 3.37 Simulated maximum bottom stress during low water level simulation with waste rock and tailings deposited in the reservoir to 162.5 m RL.

3.1.12 Leachate Release

A simple test of the fate of a leachate from the waste rock and tailings storage was undertaken. A nominal 1 g m^{-2} day^{-1} release of separate tracers from the waste rock and tailings was incorporated into the model. The results in Figure 3.38 indicate that the leachate release accumulates between the deposits at the bottom and approximately 180 m RL. The results also indicate that the leachate is periodically partially mixed into the waters above. However, the waters above 180 m RL have very low concentrations of leachate because the leachate is typically confined to near the bottom and when partial mixing does occur there is the a large dilution of the leachate. During partial mixing, there is elevated release of leachate through the

HEP intake (see Figure 3.39) and a corresponding reduction in concentrations above the sediments (Figure 3.38). During the mixing events in 2029 and 2033 the concentration in the HEP intake peak to 0.35 (up from 0.05 mg L^{-1}) and 0.4 mg L^{-1}(up from 0.1 mg L^{-1}) respectively. Prior to these peaks concentrations in near to the bottom at the embankment reached approximately 1.4 and 3.2 mg L^{-1}, respectively. This indicates a dilution of bottom concentrations of approximately 4 and 7 times prior to reaching the HEP intake. The results also indicate that the event in 2029 was more significant in terms of disturbance of the bottom waters as indicated by the near complete renewal (i.e. concentrations approaching zero) of the bottom waters. In the period from 2030 to 2033 there is no major disturbance of the leachate at the bottom and the concentrations above the storage material increase over time. Over this period HEP intake concentrations are relatively steady at approximately 0.1 mg L^{-1}, which is about 30 times more diluted than the bottom waters at the end of this period.

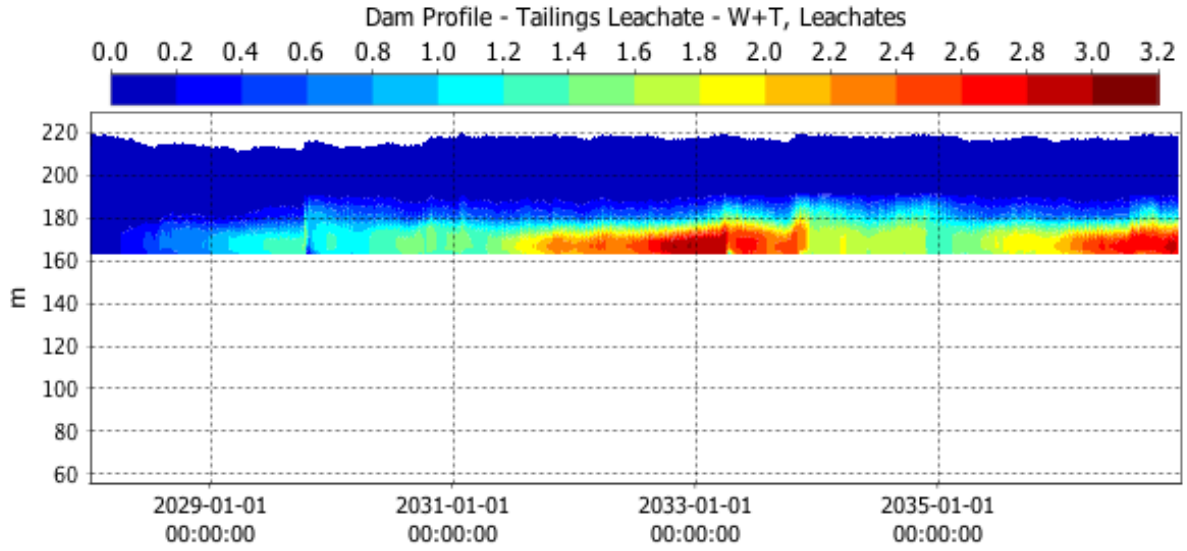

Figure 3.38 Concentrations of leachate (in mg/L) released from the tailings during base case simulation.

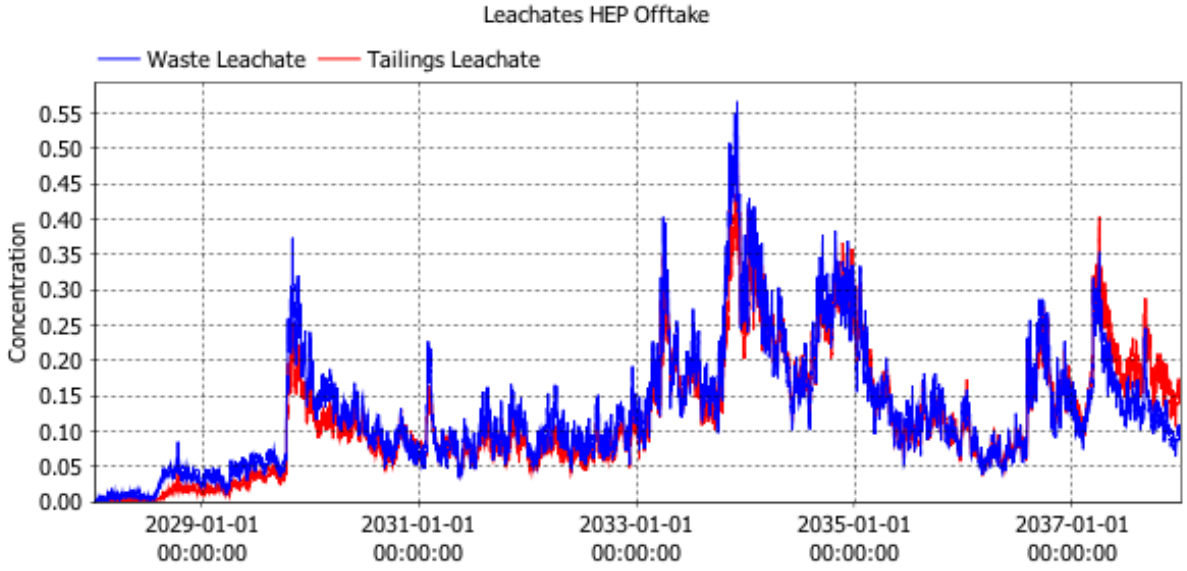

Figure 3.39 Concentrations of leachate in (mg L^{-1}) released from HEP during base case simulation.

4 Initial Condition Test

The operations simulation was initialised with the temperature structure at the embankment at 5 years into the filling simulation (2 years after the reservoir filled and the HEP intake shifted from 143.5 to 185.6 m RL). As the filling simulation progresses the temperature structure evolves over time, as shown in temperature profiles at 5 years and 10 years into the filling simulation (Figure 4.1). At 10 years there is a stronger thermocline at 10 m depth with cooler water below and a weaker temperature gradient below the HEP intake (when compared to the 5 year initial condition).

An operations simulation initialised with the temperature structure that evolved over 10 years before the influence of waste rock and tailings deposition changes the response to the October 2029 inflow event. In this simulation the peak catchment sediment load arrives at the embankment at a higher elevation increasing the TSS of the HEP intake (Figure 4.2). The cooler temperatures below 180 m RL promote a larger proportion of the inflow TSS to travel to the embankment in the intrusion at 180 m RL, rather than in the underflow across the top of the waste rock and tailings deposition (Figure 4.3). For the remainder of the operations simulations the results with different initial temperature structure are comparable.

For the derived mobility operations simulation the amount of tailings entrained into the waters that reach the HEP intake is less for the cooler initial condition (Figure 4.4) because there is less underflow over the stored waste rock and tailings to trigger resuspension.

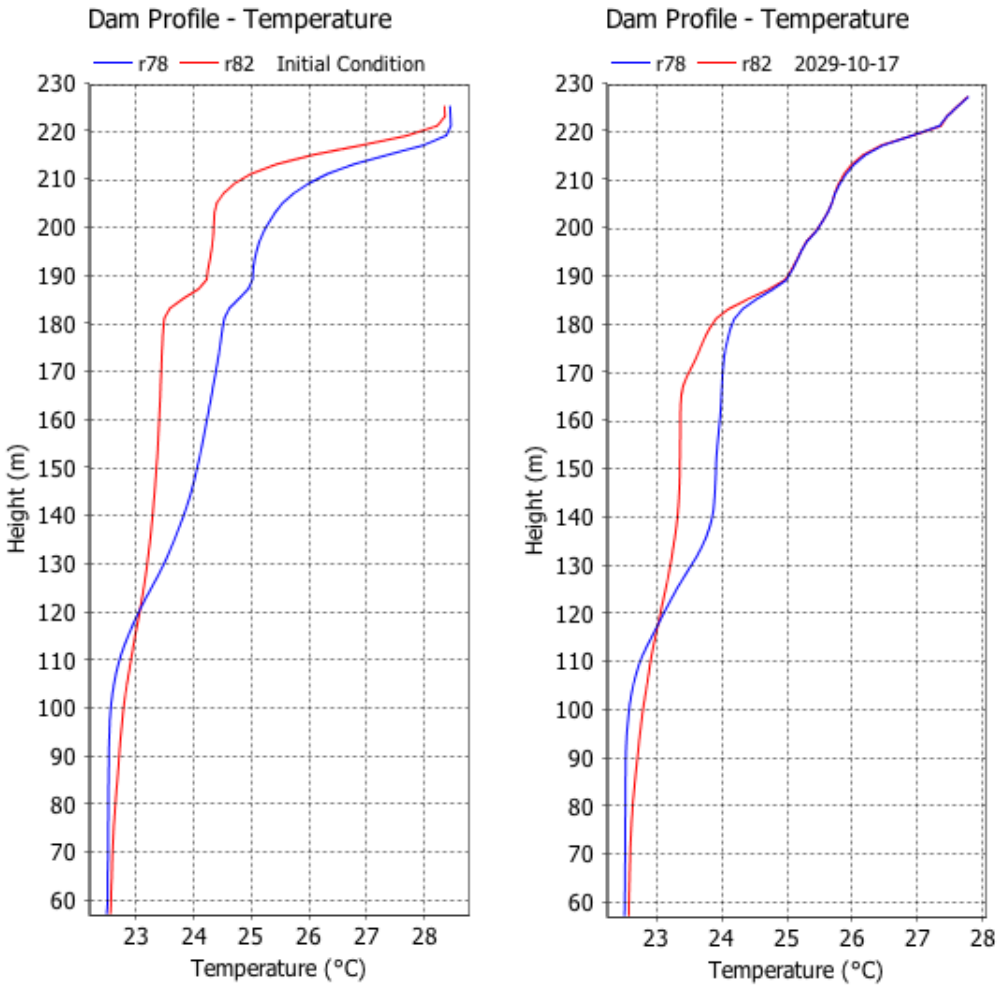

Figure 4.1 Temperature profile at the embankment at 5 years (blue) and 10 years (red) during the filling simulation (left panel), and temperature profile at the embankment in October 2029 of operations simulations with 5-year (blue) and 10-year (red) initial condition (right panel).

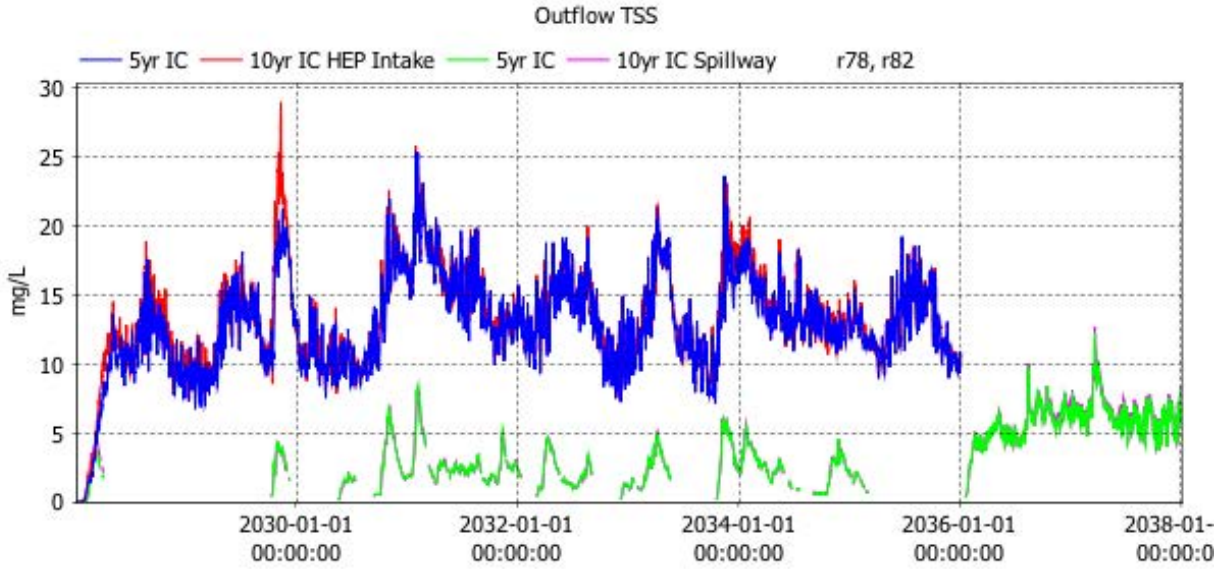

Figure 4.2 Concentrations of TSS in HEP intake and spillway during simulations with different initial temperature profiles.

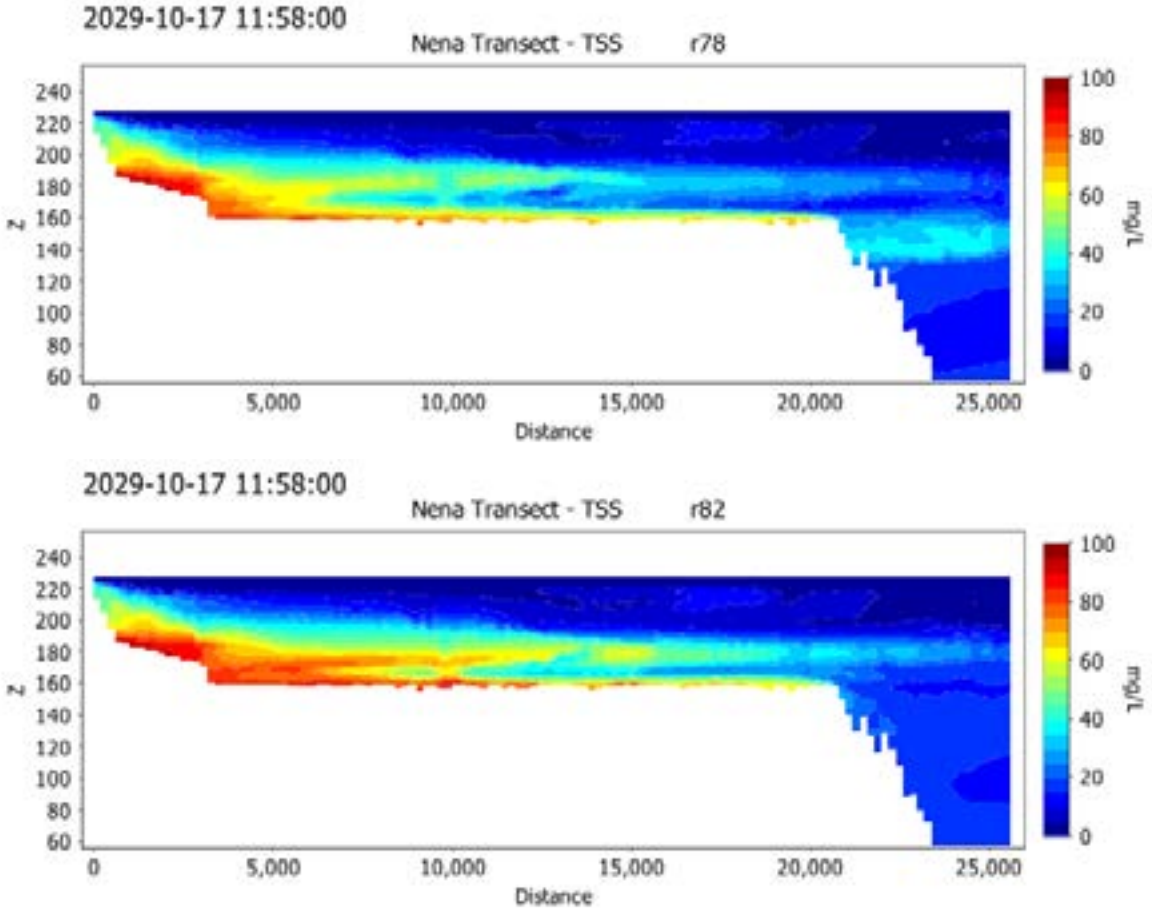

Figure 4.3 Simulated TSS from the headwaters of the Nena River (on the left of the figure) to the embankment (on the right) in October 2029 for simulation initialised with 5-year (top panel) and 10-year (bottom panel) temperature profiles.

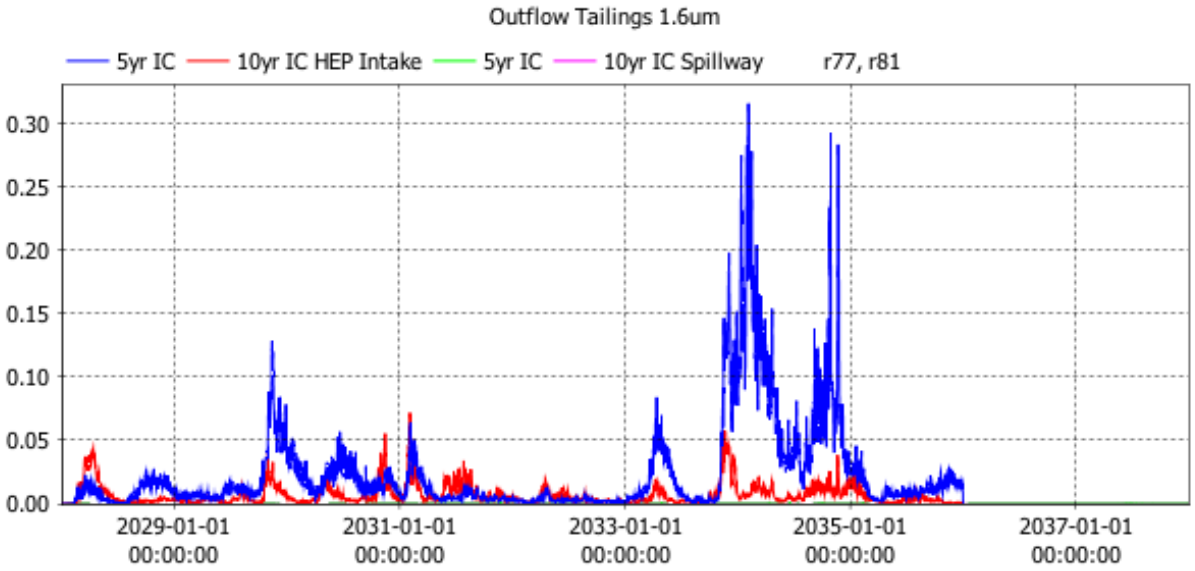

Figure 4.4 Concentrations of 1.6-micron tailings in HEP intake and spillway during simulations with different initial temperature profiles.

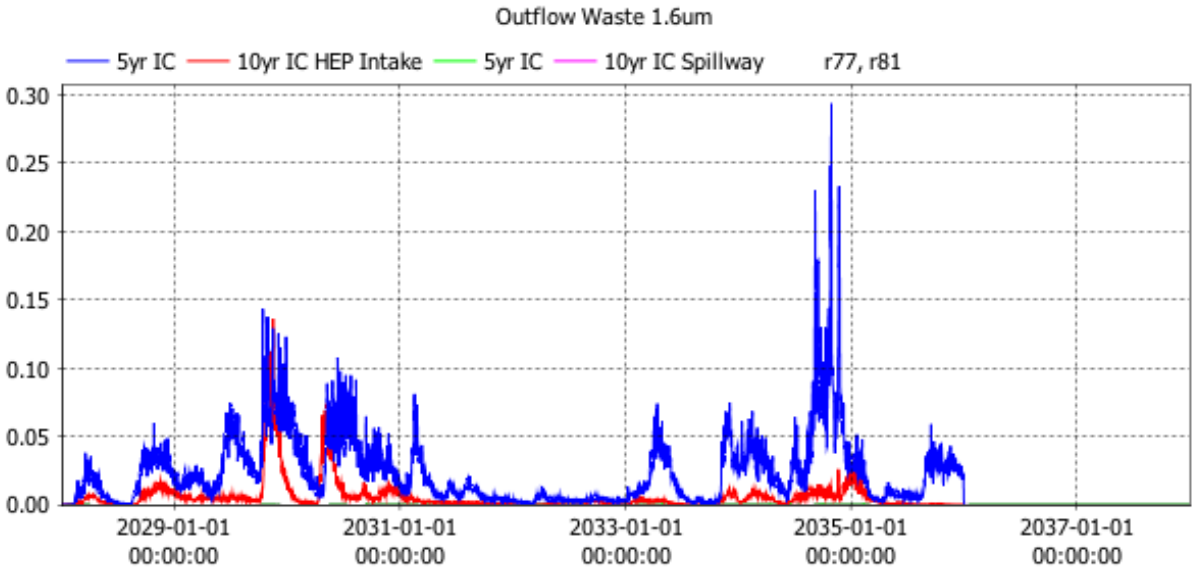

Figure 4.5 Concentrations of 1.6-micron waste rock in HEP intake and spillway during simulations with different initial temperature profiles.